DIELECTRIC BREAKDOWN OF HEAVY METAL AZIDES

by

Tong Bor Tang

A dissertation submitted to the University of Cambridge for the degree of Doctor of Philosophy

April 1979

St. John's College, Cambridge

DIELECTRIC BREAKDOWN OF HEAVY METAL AZIDES

Tong Bor Tang

The breakdown of single crystals of heavy metal azides has been investigated. In silver azide, the low-field conduction is by mobile interstitial cations and their enthalpies of formation and hopping have been determined from the Arrhenius plot of the conductivity. Based on AC conductivity measurements and the observed time dependence of the current, it is shown that ionic polarisations occur at the electrode interfaces. With fields higher than 15 $kV.m^{-1}$ (for silver or carbon electrodes) bipolar field injection is thought to take place. These fields can lead to dielectric breakdown, although the incubation period may last up to several days - but less than a second if the field is 0.4 $MV.m^{-1}$ or higher. Evolution of nitrogen has been measured by mass spectrometry under this condition. Based on a comparison with the *thermal* decomposition of AgN_3, the following mechanism is proposed for the 'electrical decomposition'. Holes injected from the anode combine bi-molecularly via traps and produce N_2. Some of the electrons from the cathode are localised at impurity centres or defects. The discharge of mobile Ag^+ at the electron traps results in silver atoms which, if formed on the surface, may migrate as well as aggregate because of their high diffusivity even at room temperature. By optical and electron microscopy silver nuclei have been detected on the surface of a crystal to which a strong field is applied through conducting contacts. It has also been observed that post-breakdown disruption in the form of an explosion occurs. The breakdown is explained as due to the formation on the crystal surface of filamentlike silver films, and the initiation of deflagration and subsequent detonation, to the appearance along the metallic conduction path of 'hot spots' arising from Joule heating and leading to *thermal* decomposition and self-heating. This explanation is supported by evidence such as initiation locality.

In the comprehensive study on the thermal decomposition of AgN_3, new methods have been proposed for the analysis of kinetic data, both isothermal and dynamic, from solid state reactions.

Parallel observations, in less detail, suggest that dielectric breakdown and explosion initiation by similar mechanisms occur in thallous and probably in lead azides. It is a possibility that breakdown of long incubation period can be brought about by analogous 'electrical decomposition' processes in certain metal halides, oxides, hydrides, alkali azides and other ionic metal compounds, although in substances which are not highly exothermic no explosion will follow the breakdown.

PREFACE

The work described in this dissertation was carried out between October 1974 and March 1978 in the Physics and Chemistry of Solids Group, Cavendish Laboratory, Cambridge, under the supervision of Dr. M.M. Chaudhri. I am indebted to Dr. Chaudhri for his interest, advice and, not least importantly, sustaining encouragement. On numerous occasions he has provided me with insights as well as foresights, academic and otherwise.

It gives me pleasure to take this opportunity to thank Professor D. Tabor, F.R.S., Drs. E.A. Davies, J.E. Field and A.D. Yoffe, and Dr. D.A. Young of Imperial College, London, for inspiring discussions, commenting on preprints, or generosity and kindness in many ways.

I am also grateful to many other members, both past and present, of the 'Fracture/Explosive Group' within P.C.S., with whom I have enjoyed working and from whom I have received much help. To name them all would invite the danger of possible omission. However, Drs. S.R. Elliott, D.A. Gorham, J.T. Hagan, H.M. Hauser, R.G. Patel, Mr. R.T. Phillips, and Mr. P.H. Pope are colleagues in P.C.S. whose assistance on several concrete matters are appreciated.

My gratitude goes to Mr. D. Allan, Mr. P. Stephens, and all the staff in the P.C.S. workshop and the P.C.S. electronics section for patient and expert cooperation. Thanks are due to Mr. A.H. Peck for the skilled preparation of the photographs used in this dissertation and elsewhere. I would like to record my thought that each of them is wiser than me in one way or another.

I acknowledge P.E.R.M.E. and R.A.R.D.E., Procurement Executive, Ministry of Defense (U.K.), for a research studentship, the Science ReSearch Council for equipment grants, and the Institution of Electrical Engineers for a J.R. Beard travel grant.

This dissertation is the product of my own work and includes nothing which is the outcome of work done in collaboration. All results presented in it are original except where reference is specifically given. It has not been submitted for a degree or any other qualification at any other University. It exceeds the regulation limit in length, but prior permission of the Degree Committee has been obtained.

April 1979 St. John's College, Cambridge

SYNOPSIS

The heavy metal azides and in particular silver azide are of great scientific and technological interest. The aim of this work is to investigate the mechanisms responsible for the dielectric breakdown and the subsequent initiation of explosion in these materials. To achieve this end, a number of experiments were performed and interpreted. In the first series of experiments I determined the electrical conduction processes in a single crystal of silver azide in low AC and DC fields. The conduction was found to be by mobile interstitial cations, in agreement with others' work on compacted samples. The activation energies of formation and hopping of these interstitials were found to be 1.2 ± 0.3 eV and 0.5 ± 0.2 eV, respectively. Strong time dependences of the DC conductivity were observed at both low and high fields, and explained by the polarisation due to ionic space charges and the double injection of holes and electrons from the electrodes, respectively.

In the next series of experiments, I examined whether any chemical activity occurs during the pre-breakdown period. The first set of these experiments was made in an ultra high vacuum apparatus to which a mass spectrometer was attached. At moderate and high DC fields, evolution of nitrogen gas was detected, indicative of chemical decomposition. The molecular rate of evolution was ca. 0.3 of the total flux of current carriers. The second set of experiments consisted of applying

similar fields to a crystal which was continuously examined in situ with an optical microscope. Metallic silver was observed to form on the surface throughout the length of the crystal between the two electrodes.

These experiments were followed by the third series, in which conducting contact was made at only one end of the crystal. No fast decomposition took place for fields up to three times the value at which it would within 1 s, had contacts been made at both ends. The sites at which the initiation occurred were then determined under two-contact conditions, by studying traces of the residue on the substrate. It was established that the site was usually away from the electrodes. These were important results, since they cannot easily be explained by many of the usual theories of breakdown.

The occurrence of decomposition led me to study the basic mechanisms involved in this phenomenon. A comprehensive study (which included developing new methods for the analysis of kinetic data) was therefore made of the thermal decomposition of silver azide. According to the model I suggest, the rate controlling step is the emission of an electron from the valence band to the fermi level of silver which has been formed.

On the basis of all the above experiments, the following mechanisms are proposed for the dielectric breakdown and explosion initiation of a single crystal of silver azide.

Under a DC field interstitial silver ions move towards the cathode, but cation and anion vacancies are immobile, and space charges are formed as the contacts are partially blocking. When the applied field is considerable, the magnitude of the accumulation and the depletion space charge fields at the cathode and the anode are sufficiently high to cause field injection of electrons into the conduction band of the crystal at the cathode. At the anode, this is accompanied by the injection of holes into the valence band, and the crystal remains electrically neutral. Nitrogen is evolved due to the combination of pairs of holes (i.e. azide radicals). Some of the injected electrons are localised at traps to which interstital cations are attracted. The ions discharge and silver atoms are produced, which have high diffusivity on the crystal surface. With the passage of time more and more silver accumulates on the surface and eventually paths of low electrical resistance are formed. Joule heating of these paths creates 'hot spots' where thermal decomposition and then initiation of fast decomposition occur.

The above model is based mainly on results from the work on silver azide and its validity for thallous and lead azides needs to be confirmed. Preliminary experiments show, however, that these two other heavy metal azides have rather similar electrical and breakdown characteristics. The model may, indeed, be applicable to many other ionic metal compounds.

CONTENTS

LIST OF SYMBOLS

[This list is meant to be neither exhaustive nor restrictive.]

u (prefixing physical units) ≡ μ

10En ≡ 10^n

log ≡ $\log_{10}$

ln ≡ $\log_e$

1 eV /molecule ≡ 1.60x10E-19 J /molecule ≡ 96.5 kJ /mole

a molar fraction of conversion of a reacting solid

e dielectric constant of silver azide

e* vacuum permittivity, 8.85x10E-12 F/m

f(1 - a) functional dependence on a of reaction velocity da/dt

h Planck's constant, 6.63x10E-34 J.s

k Boltzmann's constant, 1.38x10E-23 J/K

m (rest) mass of electron, 9.11x10E-31 kg

m* effective mass of electron in the solid under discussion

q quantum of charge of electron, 1.60x10E-19 C;
--- of the ion under consideration

t time

t* time over which the field has been applied to the crystal before dielectric breakdown is completed

<t> time constant (used in various contexts)

u drift mobility in silver azide of interstitial cations;
----- of electrons; ----- of holes

v velocity of sound in silver azide

w angular frequency of electric field

x electronegativity (Pauling's definition)

A sample cross-sectional area

E activation energy of a reaction;
-- of the pyrolysis of silver azide

Eg the band gap in electronic energy structure

F electric field

F* in silver azide, field at which current starts to fluctuate

H (constant) heating rate in a solid-state reaction, dT/dt

J electrical current density

L sample length

R (da/dt)/f(1-a)

R* pre-exponential factor in R

T temperature

$\underline{T}$ Debye temperature

U linear reaction speed in the pyrolysis of silver azide

U* pre-exponential factor in U

W energy barrier (used in various situations)

Wf work function

X electron affinity

$\angle\Delta S$ entropy change (used in various contexts)

$\angle\Delta H$ enthalpy change (used in various contexts)

6 electrical conductivity of silver azide

CHAPTER I

INTRODUCTION

1.1 DIELECTRIC BREAKDOWN

The work described in this thesis is concerned with dielectric breakdown of a type which is very interesting but which hitherto appears not to have received much attention. Any dielectric undergoes a failure in its electrical insulating properties when a sufficiently strong electric field is applied through conducting electrodes. For a given solid insulator at a certain temperature, once the field is increased beyond a normally more or less unique value, the current conducted by the material rises continously without any further increase of the field across it. The time taken for this monotonic rise is, depending on the mechanism responsible, either on the order of us or less, or (in practice) not more than a minute or so. This is followed eventually by localised or propagating post-breakdown disruptions (structural or compositional) in the material, unless, before they happen, the current is limited by the external circuitry.

This class of phenomena, referred to as 'dielectric breakdown', has obvious scientific as well as technological significance. The experimental works, carried out by von Hippel, Cooper, Klein and many others, and which aim at identifying the various mechanisms of breakdown in different materials under different conditions, constitute a major concern of physical laboratories and the electrical and

electronic industries. There has also been a great deal of theoretical effort, by authors like Frohlich and O'Dwyer; detailed calculations are available for many proposed models of current instability. However, in more cases than not, the empirical data do not fit very well any of the plausible models or are not exact and specific enough to identify one out of them. The subject is difficult and challenging, in comparison with breakdown in gases, in homogeneous semiconductors (called 'switching' if the collapse is not followed by irreversible material change), and in inhomogeneous semiconductors (junction breakdown), whose nature is known with fair certainty in the majority of cases.

For certain inorganic azides there are additional complications. When subjected to a variety of excitations these chemicals explode. The explosion starts at localised spots and propagates to all other parts. Such an explosion is found to follow the dielectric breakdown in heavy metal azides. Here additional questions arise as to whether their chemical instability plays a part in their breakdown and how exactly the explosion initiates. The objective of this work is to establish the mechanisms responsible for breakdown and subsequent initiation of explosion in the heavy metal azides, especially in silver azide. Such fundamental investigations are important for both theoretical and practical reasons made clear in the following sections.

1.2 HEAVY METAL AZIDES

The metal azides represent a step in complexity beyond the metal halides which, along with pure metals and elemental semiconductors, dominated the minds of the earlier generations of solid-state physicists. The normal azides formed by metals fall into two main groups, according to their stabilities. The 'explosive' group may broadly be sub-classified into the covalent and the 'heavy metal' (silver, thallous, lead) azides. The non-explosive group contains the alkali and some of the alkaline earth azides. The three azides classified under the heavy metal group are essentially ionic and, among the pseudohalogens, the azide ion with its $D_{\infty h}$ symmetry (the highest that any polyatomic species can possess) is the simplest. (More details will be given in Section 2.1.) Azido derivatives such as azidothiocarbonate and azidocarbondisulphide, cyanate and derivatives like thiocyanate and selenocyanate, cyanide, and cyanamide all have structures of lower symmetries. Fulminates, permanganates and oxalates, whose decomposition are also commonly studied, all have greater molecular complexity. Now, while the heavy metal azides are exothermic and their decomposition can become self-sustained (i.e. 'explosive'), the metal halides as well as the alkali metal azides are endothermic or at most slightly exothermic and do not explode. The research on breakdown in heavy metal azides may, therefore, provide a model theory for breakdown in

those ionic (crystalline) insulators whose chemical reactivities are important.

Historically, sodium azide and from it, hydrazoic acid, were first prepared in 1890 by T. Curtius. Following this, he made a prominent contribution to the isolation and characterisation of many of the other metal salts, including silver azide in 1891. By now, much is known of the chemistry of azides, both inorganic and organic; for a recent review see Patai 1971. (Unfortunately, the same cannot be said of their physics.) Very early on two structual formulae were proposed for the azide ion/group: a cyclic structure by Curtis in the 1890 paper and a linear configuration by J. Thiele in the following year. The advent of physical crystalographic methods saw the verification of the linear structure in both ionic (Hendricks and Pauling 1925) and covalent (Brockway and Pauling 1933) azides, with and without a centre of two-fold symetry, respectively (see Section 2.1). Also, since the earlier decades of the present century the pyrolysis of these azides has been the subject of investigation, both experimental and theoretical, by Garner, Mott, Yoffe, Gray, Tompkins, Young, Prout, Boldyrev, Zakharov and others. On the other hand, their dielectric breakdown was not investigated until much later and, probably, was up to now studied only as one of the means of initiating explosion.

1.3 BREAKDOWN IN SILVER AZIDE

In 1957, McLaren and Rogers of this Laboratory, observed, when experimenting with silver azide single crystals at room temperature, that these crystals exploded when a moderately high electric field was applied to them (Bowden & McLaren 1958). A breakdown in insulation was seen to precede the explosion. In the following twenty years, further works were done and extended to the breakdown in some other metal azides, mainly by a group under Zakharov in Kirov Tomskogo Polytechnic Institute, U.S.S.R., and another group connected with the Energetic Materials Division of the Armament Research and Development Command (formerly Picatinny Arsenal) in U.S.A.

Below we summarise the electrical properties of those explosive metal azides whose breakdowns have been studied:

Table 1.1 Dielectric Breakdown

Compound	Room-temp. low-field conductivity /$S.m^{-1}$	Breakdown field /$MV.m^{-1}$	Notes
AgN_3	3x10E-7	0.4	a
TlN_3	10E-10	1.2 1.1, 1.4, 1.5	a b
α-$Pb(N_3)_2$	10E-11	1.8	a
CuN_3	see text	ca. 0.2	c
$Cu(N_3)_2$	?	38, 50, 68	b
$Hg(N_3)_2$	6x10E-9	ca. 10	c
$Hg_2(N_3)_2$	low	very large	c

a = this work; b = Zakharov & Sukhushin 1970; c = Yoffe 1966
a = needle-shape single crystal, Ag electrodes
b = pellet 0.2 mm thick, Zn, Cu, W electrodes respectively
a & b : field values correspond to 50% probability of breakdown within ca. 1 s of application

We see that, with the exception of cuprous azide which has a complex conductance characteristic (Yoffe 1966), silver azide has the lowest value of breakdown field strength, followed by thallous and lead azides. This is remarkable (and will be given an explanation in Section 8.2) since in almost any other aspects, it will be the copper and mercury azides which are the least stable, because they are covalent while silver, thallous and lead azides are essentially ionic (Section 2.1). In this work, we have concentrated on the study of silver azide, although some experiments have also been carried out on thallous and lead azides. Their remarkably low breakdown

strengths are strongly suggestive of unusual mechanisms for their dielectric breakdown. Other insulators as well as homogeneous semiconductors generally have strengths of the order 100MV/m.

Our work has shown, among other things, that dielectric breakdown takes place in silver azide at even lower fields than the normal value given in Table 1.1, provided these moderate fields are maintained for long periods of time (Sections 2.5 & 3.3). This phenonenon, namely, a breakdown at a 'sub-critical' field with an extremely long 'wait time' (or, 'incubation' or 'induction' period) during which reversible current instabilities occur, is remarkable but has not been extensively studied before. Silver azide, because of its chemical reactivity, exhibited this behaviour quite distinctively. Preliminary observations suggested that the process occurs also in thallous (and sodium) azides. It may be that the phenomenon is a common, but hitherto neglected, process in many ionic metal compounds. It may also be that, although the detailed mechanisms vary among different classes of materials, they are all electrochemical in nature, as is (we are going to argue in this work) the case for silver azide.

1.4 PRACTICAL RELEVANCE

A study of the breakdown properties of the heavy metal azides and silver azide in particular has practical significance. The electrical initiation of explosion can be exploited in certain advanced engineering applications. An example is the designing of electrically compatible explosive-actuated devices such as the miniature explosive bolt and the detonating fuse lead (See e.g. Benedict 1965). On the other hand, without going to explosion, the azides may be used to generate nitrogen in novel situations. In the case of thermal decomposition, this has already been suggested (Breazeale 1976). Gas generation is also attained by decomposition under an electric field; this possibly useful application is a 'spin-off' from one of the results in this work. Thirdly, their electro-photolytic decomposition may be utilised in a one-step photographic process (Schaffert 1967; Schuttevaer 1969); in which exposure can be controlled by the switching of electric field instead of by a mechanical shutter.

The heavy metal azides are more stable than the covalent ones and, along with some other chemicals, have been exploited as primary explosives (detonants). Of the three, thallous azide is not very useful because, when unconfined, single crystals of it up to 200 um in diameter do not support a propagating explosion (see Table 1.2 later on). In contrast, fast decomposition once initiated is sustained in crystals down

to 20 to 30 um in diameter of the other two. Current utilisation in mining and in the military relies mostly on lead azide. Owing to its inherent hydrolytic instability and incompatibility with many polymeric materials used in fuze design, however, an alternative compound with longer service life has long been sought after. Very early on, silver azide was recognised as the potential substitute (Taylor & Rinkenbach 1925). Two years after its isolation by Curtius, in 1893, it was tried in the field by the Prussian government; the British has kept faith in it up to the present day. It is more powerful, but at the same time more stable than lead azide: it does not hydrolyse. Although it still is more expensive, methods exist for its factory production (Taylor 1957, Fiechowicz 1974). Unfortunately, it too suffers from incompatibility problems notably with any sulphur bearing substances -- a behaviour, incidentally, which was made evident when we embedded crystals in potting epoxies like araldite and found them turning black in colour after a week. The explosion initiation of these azides by high-dose radiation will then be an important problem for people concerned with the effects of thermonuclear explosion on nearby triggerable devices containing detonants. The initiation, in lead azide at least, is generally attributed to the generation of intense electric field within the azide dielectrics, due to the separation of charge produced by electron or photon irradiation, and the

subsequent breakdown by this radiation induced field (Brown et al. 1972; Zimmeerschied & Davies 1974, Hays and Seay 1976).

There is one last aspect which is connected to the problem of safety. The major hazard in the manufacturing and handling of the azides is their accidental explosion initiated by electrostatic spark discharge (Pollock 1974). Under the conditions of both metal/metal contact discharges and long-duration (>10 ms) unidirectional air sparks, the initiation mechanism is thought to be thermal (Moore 1958; Mel'nikov et al. 1970; Stengach 1972). That is, the energy of the discharge or the spark is degraded to heat, and explosion propagates from a 'hot spot' so created. For oscillatory or short-duration sparks (<1 us), however, the mechanism is not clear and dielectric breakdown under a high transient field may play an important part.

1.5 DECOMPOSITION, AND INITIATION & PROPAGATION OF EXPLOSION

We have said that the heavy metal azides are explosive. This aspect of their chemical reactivity is considered here in greater detail. One of the followng steady processes may occur in a decomposing solid:

i) Slow decomposition

ii) Deflagration } fast decomposition or 'explosion'

iii) High-velocity detonation }

The heavy metal azides decompose as ionic azides (Section 2.1).

Their decomposition has this broad scheme:

(a) $N_3^- \rightarrow N_3 + e$

(b) $e + M^+ \rightarrow M$

(c) $2\ N_3 \rightarrow 3\ N_2$

where N_3 is an azide radical, e an electron, and M the metal. The detailed mechanism, however, depends both on the azide concerned and on the means by which the decomposition is brought about. Step (a) is endothermic, while (b) and (c) are exothermic; the energetics of the overall decomposition process in various azides can be found later in this section, in Table 1.2.

All condensed matter, when subjected to sufficiently high temperatures, are unstable and will decompose. The reaction may be slow (meaning not self-accelerating), taking minutes or even days to reach virtual completion. Outstanding contributions towards its understanding have been made by the schools of Bowden and Yoffe at this laboratory, Tompkins and Young at Imperial College London, and Erofeev and Boldyrev in the U.S.S.R., among many others. Explosions, on the other hand, happen only if the decomposition is highly exothermic. In this case, once a local region of the material is made to decompose at a fast rate, a condition called 'initiation', the process becomes self-sustained and spreads to other parts. In a single crystal such as that of silver or lead azide, the speed of propagation may initially be of the order m/s,

accelerating then to a steady value of up to several km/s after the reaction front has travelled some distance. This limiting speed is dependent on the diameter of the crystal but will be below the velocity of sound in the material, and this stage is called deflagration. If the crystal is very thick, however, the final stage is high-velocity detonation when the speed stays constant at 5 to 8 km/s. In single crystals, the transition from deflagration to this supersonic regime is very rapid (ca. 1 us), and there is no intermediate stage of low-velocity detonation (Chaudhri et al. 1977).

Slow decomposition can be brought about by a number of means. So far, the agents which have been more thoroughly investigated are heat, light, and ionising radiations (pyrolysis or thermal decomposition, photolysis or photolytic decomposition, and radiolysis, respectively). For certain azides, we have found that slow decomposition may also occur when an electrical current is conducted; 'electrical decomposition' will be discussed in Section 3.3. Explosion is initiated, under appropriate conditions, by these agents as well as by hot spots arising out of friction between rubbing surfaces (Bowden & Tabor 1954, pp.33-57 & 317-8), by low-velocity (a few m/s) impact (ibid., pp. 270-1 & 318-9), by focused shock waves, localised adiabatic shear during mechanical failure of the crystal, atomic or nuclear particles irradiation, electric spark, and of course by dielectric

breakdown. A recent review on the subject has been given by Chaudhri & Field (in Fair & Walker 1977). In most cases, the mechanism of initiation is believed to be ultimately thermal, as is in gaseous explosions. This is the hot-spot theory developed by Bowden and Yoffe (see their book 1958) and later extended by their students as well as by other workers. The mechanism suggested for deflagration in single crystals which do not have gas-filled voids is the conduction of heat from decomposing layers to neighbouring fresh layers (Chaudhri & Field 1970). Other mechanisms have been put forward in which the propagation is by the mechanical activation, in one way or another, of reactant molecules (Taylor & Weale 1938; Carl 1940; Ubbelohde 1948; Fox 1970). These alternative explanations do not, however, seem to be supported by much experimental evidence to date. On the other hand, it is obvious that a high-velocity detonation, which is supersonic, cannot be purely thermal in nature. It is probably sustained by compresional heating of the crystal by the high pressures in the detonation front (Chaudhri et al. 1977), but no detailed theory for its mechanism has yet been worked out. However, the hydrodynamic theory of Chapman and Jouget has had many successes in describing it on the phenomenological level.

With the exception of the high-velocity detonation, therefore, the processes of initiation (when its mechanism is thermal directly or ultimately) and deflagration may be

regarded as extrapolations of the slow pyrolysis, involving basically not much more then a change of the decomposition rate. To illustrate this conception, we have compiled Table 1.2.

Table 1.2 Decomposition & Deflagration

	KN_3	NaN_3	LiN_3	TlN_3	AgN_3	α-$Pb(N_3)_2$	$Hg_2(N_3)_2$
Exothermicity of decomposition/eV, per molecule (a)	-0.013	0.22	0.11	2.42	3.21	5.01	6.14
Deflagration velocities/$m.s^{-1}$:					*		
1 single crystal 168 um thick(b)	0	0	0	0	1000	>1200	?
2 unconfined powder layer(c)	0	0	0	0	1500	2100	?
3 powder, steel block confinement (c)	0	0	0	1500	1700	>2100	?
4 film ca.100 um thick (d)	0	0	0	1500	2200	2300	2400
Ionisation potential (metal)/eV	4.34	5.14	5.39	6.11	7.57	7.42(Pb) 15.0(Pb)	10.43

(a) = data calculated from (Fedoroff et al.1960) where original references are given; (b) = Chaudhri & Field 1977; (c) = Bowden & Williams 1951; (d) = Boddington 1963
* velocity of sound in silver azide is v=2100 to 2900 m/s, according to Chaudhri 1969

Although data on deflagration velocities are unfortunately scarce, it may be seen from the Table that a consistent trend exists among the azides ordered by their enthalpies of decomposition, the effects due to variations in molecular density, thermal conductivity, and any other relevant properties being relatively insignificant. The alkali azides, which decompose endothermically or only slightly exothermically, do not support propagation, while for the heavy

metal azides, there is a positive correlation between the velocity and the heat of reaction. The ionisation potentials have been included in Table 1.2 for reference, but their correlation with the properties of the azides will be discussed later (Section 2.1).

In this dissertation, we are not concerned with the propagation, whether or not a part is still played by the electric field in this stage. Our attention is confined to the preceding two events of dielectric breakdown and subsequent explosion initiation. However, the conception that a continuity exists between slow and fast decomposition has influenced our experimental approach to the problem. This approach will be justified if, in the case of the application of electric field, there is also a direct link between the moderate-field and the high-field (breakdown) effects. Indeed, such a link is established by this work.

1.6 OUTLINE OF THIS WORK

Scientific and technological interest in the dielectric breakdown of the heavy metal azides in general and silver azide in particular have been explained in Sections 1.1-1.3 above. A research program was started with the aim of elucidating the mechanisms responsible for their breakdown and, because of the close connection, also that for the explosion initiation; the results so far obtained form the subject of this dissertation.

Our basic viewpoint in this investigation is that their unusually low breakdown strengths strongly suggest a dominant role played by their chemical reactivity. The outcomes of our study tend to confirm this view. Indeed, because of this connection, we found it necessary to make a detailed study on their thermal decomposition. Our approach has been through first doing experiments at pre-breakdown fields. Low- and moderate-field phenomena occur on long time scales and thus can be followed by a variety of techniques.

The experimental program began with an investigation of the conduction processes in silver azide at low fields. Relatively large single crystals having fairly perfect surfaces, which we had succeeded in growing from solution (see Appendix A), were used as samples in these and other experiments. The first systematic measurement was on the variation of their AC conductivity with frequency. The result was interpreted in terms of interfacial polarisations at the electrodes (a brief review of the theory used was given in Appendix B). Other authors had previously established that the conduction in compacted microcrystalline silver azide is predominantly ionic, with interstitial cations as the main carriers. Our suggestion was therefore that contacts of the single crystals with the metals used as electrodes (namely colloidal silver and carbon, and tantalum) were, to various degrees, partially blocking to the passage of Ag^+. Next, the temperature variation of the DC

conductivity was determined, from which the enthalpy of formation and the activation energy of hopping of interstitial Ag^+ in silver azide were tentatively identified as 1.2 ± 0.3 and 0.5 ± 0.2 eV, respectively.

The voltage-current characteristic was found to be no longer linear when a moderate field exceeding ca. 15 kV/m was applied; at the same time, the current started to display fluctuations. An explanation of these phenomena was offered in Chapter 3. By eliminating many other possible mechanisms and based on a calculation of the interfacial fields at the polarised electrodes, according to the Maxwell-Wagner model, it was conjectured that the conditions indicated the onset of electron and hole injections from the cathode and the anode, respectively, into the insulating crystal. Then, a probable consequence of creating a non-equilibrium concentration of free electrons is their capture in the crystal by traps, to which interstials are attracted resulting in the production of silver atoms, while the bimolecular combination of the injected holes (= azido radicals) drifting away from the anode generates nitrogen gas. The production of silver may therefore be expected along the crystal, though only on the surface because, in the bulk, a silver atom is not sufficiently mobile due to its size. At low fields, the discharge of anions may still take place at the anode but that of Ag^+ will be, in the absence of injection, confined to the cathode interface (electrolysis).

The prediction of electrical decomposition was tested by two experiments: [1] Samples were placed inside an ultrahigh vacuum chamber, to which a mass spectrometer was attached. When a current was passed through the crystal under study, evolution of nitrogen was detected. [2] Samples were mounted under an optical microscope and made to conduct a current. Tree-like formations were observed to grow at a number of places along the crystal surface, if only if the applied field was so strong that the current fluctuated. The formations were resolved, under the scanning electron microscope, into clusters of 'pebbles' protruding out from the surface.

The sequence of observations and deductions outlined above strongly suggests that the chemical reactivity of silver azide plays an important role in the dielectric breakdown. To study the reactivity, the simplest approach is to utilise heat as the reaction stimulus. Experiments were therefore carried out on the slow thermal decomposition, using several thermoanalytical techniques as well as electron microscopy. The results and our deductions form the subject of Chapter 6. The reaction rate was determined, by thermogravimetry, as a function of the extent of decomposition and the temperature, and a model calculation proved that this functional form was predicted if the decomposition started on the surface and advanced into the bulk at a constant speed. Electron microscopy showed that it was indeed the case. The pyrolysis

product, silver, was observed to be in the form of 'pebbles' projecting out of the decomposing surface. A reaction scheme was proposed, in which the rate-limiting step was taken to be the thermionic emission of electrons from the reactant silver azide into the product silver. According to this assumption, the reaction is autocatalytic. This gave theoretical values of the pre-exponential factor and the activation energy of the decompostion speed which were in good agreement with the experimental results of 10E2.5 to 10E3.4 m/s and 1.23±0.2 eV, respectively. Furthermore, the scheme of elementary steps is consistent with the observation of electrical decomposition descibed above. In view of the proportionality of the thermal decomposition rate to the surface area and the nature of the rate-limiting step, it was thought that a polycrystalline film of silver covered the decomposing surface. The 'pebbles' were formed by accretion in this film.

In the course of the work described in the last paragraph, it was realised that the methods currently available for the analysis of kinetic data from solid-state reactions in general were unsatisfactory. We have therefore attempted to develop a more reliable method of data analysis. A method was proposed in Chapter 4, in which the reaction rate is first determined, by a systematic procedure, as a function of the degree of chemical conversion, and then the temperature dependent part is calculated. The results given in the last

paragraph had been obtained by its use. We have also considered dynamic experiments, in which the reaction under study proceeded non-isothermally. It was again suggested that the current methods of data reduction and analysis have many limitations, including the insensitivity to the function just mentioned. An approach free from these limitations was put forward in Chapter 5, where a case study has been included.

From the electrical and the thermal decompositions experiments, it seemed clear that metallic silver was produced in both cases by rather similar mechanisms. In the earliest stages of both processes, interstitial cations drifted towards impurity centres or defects which had trapped electrons and discharged. Once a certain number of neutral atoms had agglomerated, the nucleus so formed would grow steadily, because metallic silver in silver azide acted as electron traps of large capture cross-sections. That is, during the later stages the growth of surface silver was self-sustained or 'autocatalytic'. However, one difference remained. In pyrolysis, valence electrons were emitted into silver which had been produced (thus generating holes at the same time), by electron-phonon interaction (thermal injection), whereas in electrical decomposition, operating at room temperature but under the action of intense interfacial fields set up by ionic polarisations, electrons were injected from the fermi level of the cathode and then got trapped. Further, the accompanying

generation of nitrogen was quite distinct mechanistically in the two processes. In the electrical case, valence electrons were separately extracted into the anode from the anode by field injection, so that the combination of holes was concentrated towards the anode side.

The explanation of dielectric breakdown was then put forward that electrical decomposition led, as in pyrolysis, to the growth of filamentlike patches of thin silver film on the crystal surface. Their gradual increase in number and thus in connectivity resulted in a more and more conductive path between the electrodes, corresponding to the onset of dielectric breakdown. The process continued until, because of the (non-uniform) temperature increase due to Joule heating, the rate of thermal decomposition at some region ('hot spot') became so fast that explosion was initiated which propagated to other parts of the crystal. Experiments described in Chapter 7 showed, consistent with the above hypothesis, that the explosion following a breakdown caused by a strong field was initiated fairly randomly and not necessarily at the cathode or the anode. When the applied field was decreased to moderate values it was found that, as long as injections remained operative, dielectric breakdown would still be possible (this was observed in the optical microscopy work described in Chapter 3) only that the time taken became much longer, up to many hours. These and other experiments (corona discharge, indentation, and

piezoelectricity measurement) eliminated several possible alternative mechanisms and tended to support our proposal, namely, that the dielectric breakdown is electrochemical and the subsequent explosion initiation thermal in nature.

The remarkable feature of the dielectric breakdown in silver azide is that it can be brought about by a moderate field, in which situation there is a long induction period when the current rises and falls reversibly, before the current increases steadily (onset of breakdown). Its mechanism is not, however, thermal aging or any environmental degradation, but rather is an example of what we call 'secondary processes' breakdown. Only upon the application of a 'high' field (upwards of ca. 0.1 MV/m) does the current tend to rise monotonically from the very beginning, similar in this respect to the breakdown normally studied in other crystalline insulators. The oustanding difference remains that in the normal breakdown, for a given sample there is a sharp value of the field below which it does not occur. Moreover, for a dielectric which is homogeneous in composition, the critical field is generally of the order 100 MV/m.

Some experiments have also been performed on thallous and lead azides, and the results suggest a certain similarity with the case of silver azide. Furthermore, it is possible that dielectric breakdown of long induction periods may also be found in many other ionic metal compounds.

CHAPTER II

ELECTRONIC STRUCTURE & ELECTRICAL PROPERTIES

2.1 IONISATION POTENTIAL

In studies of the electronic structure and other properties of a substance, insights may often be gained through a comparison of these properties with those of the others in the same chemical series. In the case of metallic azides, a systematic ordering of their behaviour will result if these can be shown to be highly correlated with a fundamental physical parameter of the metals. And indeed, the ionisation potential I of the metal has been found to provide a usually adequate criterion in the construction of consistent trends in the characteristics of the azides (See, e.g., Bowden & Yoffe 1958, Ch. 4).

One of the properties most obviously dependent on I is the ionicity (percentage ionic character) of the metal-azide bond. As I increases, the electron transfer from the metal to the azido ion or group will be less and less complete, and the covalent character of the bond may therefore be expected to increase. On this basis, the azides listed in Table 1.2 of last chapter may be classified into the alkali azides which are ionic, the heavy metal azides TlN_3, AgN_3 and $Pb(N_3)_2$ which are substantially ionic (polar), and the covalent azides which include $Cu(N_3)_2$, $Cd(N_3)_2$ and $Hg_2(N_3)_2$. This differentiation corresponds closely with the trend in chemical stability, the covalent azides being generally speaking the most liable to explode. The correlation of 'sensitities' (which have a

number of specific definitions) with increasing I, a proposal of Bowden and Yoffe , was the first quantitative attempt to understand the wide range of sensitivities found in the inorganic azides, and it still has validity today. The one exception in the trends, as we have said in Section 1.3, is that the dielectric strengths of the heavy metal azides are lower. In the concluding chapter of this work, we shall suggest that this exception may, ironically, be explained by the same property, namely their ionicity.

In this section, a semi-quantitative relation between I and ionicities will be described for the case of monovalent azides. Pauling (1960) has defined the electronegativity x of an atom (or a group of atoms) within a stable molecule as its power to attract electrons to itself, and relate the nature of the chemical bond in a binary compound to the difference in x of the two constituents. In fact, on his scale the single-bond energies and the standard enthalpies of formation in a series of binary compounds are used to calculate x. Mulliken (1934, 1935) proposed, instead, that the arithmetic mean of I and the electron affinity is a measure of x. However, in the case of monovalent atoms (groups), with suitable scaling this value of the mean is nearly identical to Pauling's x. For mixed-valency atoms they cannot be simply equated because of the complication due to different oxidation states.

Other scales of ionicity have more recently been

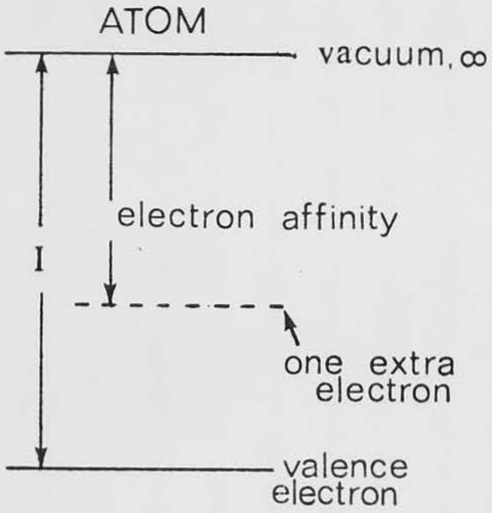

Fig. 2.1

IONISATION POTENTIAL
AND ELECTRON AFFINITY OF
AN ATOM

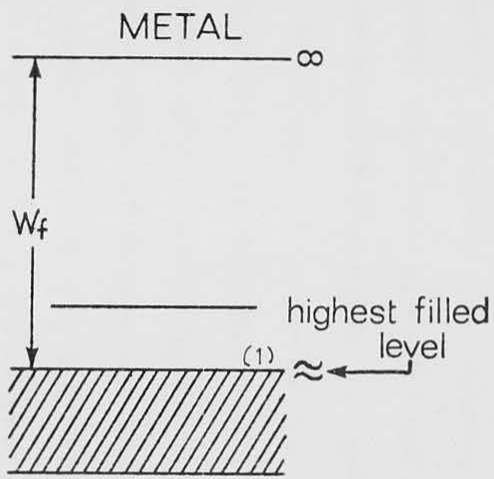

Fig. 2.2

WORK FUNCTION
OF
A METAL

(1) fermi level

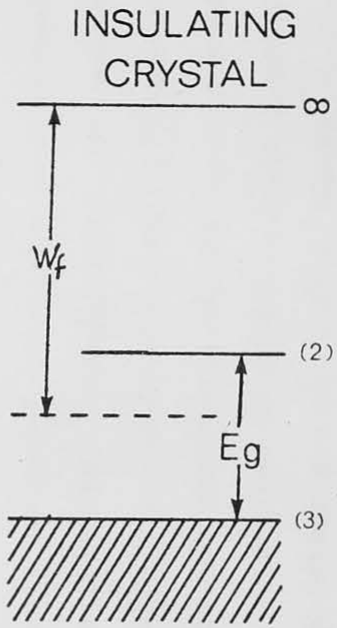

Fig. 2.3

WORK FUNCTION
AND BAND GAP OF
AN INSULATOR

(2) conduction band edge
(3) valence band edge

proposed. Notable among these is that due to J.C. Phillips (1970). In his scheme, the ionicity of a bond is defined in terms of spectroscopically obtained transition energies between bonding and antibonding states of the crystal. However, since the absorption spectra of even the simpler azides are far from well understood, we cannot use in the following discussions this modern and perhaps more true scale of ionic character.

Restricting ourselves to metals, we expect that there will be a high positive correlation between their I and electron affinities: when one energy level goes 'deeper' (Fig. 2.1) so will the other. Thus it may be expected that x, which apart from a scaling factor is given by (I+electron affinity)/2, increses with I. Indeed, we find that x changes monotonically along the series of metals in the following table.

Table 2.1 Metal

	K	Na	Li	Tl	Ag	Pb	Hg
I/eV	4.34	5.14	5.39	6.11	7.57	-	10.43
x (a)	0.8	0.9	1.0	1.8	1.9	-	2.0
Wf/eV (b)	2.24	2.28	2.35	3.68	(c)	4.0	4.53

(a) = from (Pauling 1960); (b) = 'preferred values' from (Weast 1974), determined photoelectrically;
(c) = 4.64±0.12 : see Table 3.1

It has been suggested that a reasonably linear correlation exists between x and the work function, Wf (Fig. 2.2), of the solid formed by the atoms (Gordy & Thomas 1956). The best

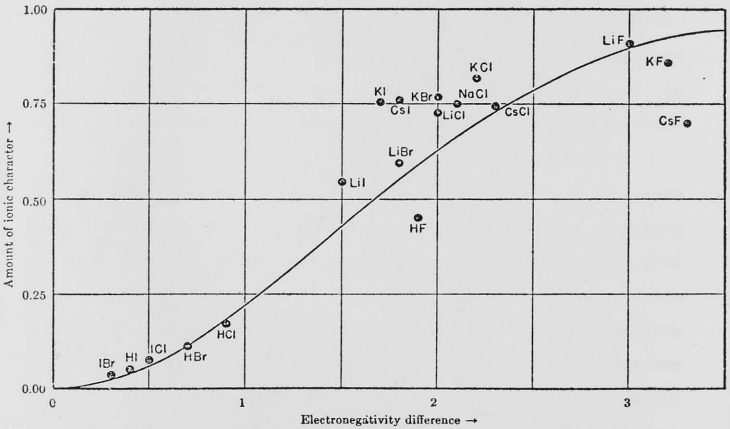

FIG. 2. 4

Semi-empirical relation between electronegativity difference and percentage ionic character of the bond formed (after Pauling 1960)

available values of the work functions, included in Table 2.1, do show a consistent trend, although their relationship with x is not quite linear. (In Chapter 6 we shall see that the magnitude of Wf may have a bearing on the mechanism of thermal decomposition in an azide.)

The electronegativity of the azide radical has been put at 2.71 (Gray 1963) or 2.95 (Herber & Cheng 1969). The difference between x(radical) and x(metal) will reflect the degree of charge transfer in the azide molecule, and Pauling has given a semi-empirical curve relating this quantity, Δx, and the percentage ionic character of the metal-azide bond. Using this approximate relation (Fig. 2.4), we can fix the ionicity of the silver azide bond as 23%. When silver azide molecules form into a crystal, which is of the orthorhombic body-centred type, each silver and each azide has eight nearest neighbours. The two molecular-type bonding will then be 'time-shared' by the eight resonating bonds, so that the crystalline ionicity comes out as 1 - (2/8)(1-23%) = 80%. The ionicities of the azide crystals, listed in Table 2.2 overfeaf, have been calculated by us in this way.

It has just been said that Δx relates to the degree of charge transfer within a binary molecule in the free state. In fact, by Pauling's definition Δx is numerically identical to the permanent dipole moment of the molecule in debyes. In the case of silver azide, its molecular dipolar strength is

therefore ca. 1.05x3.34x10E-30 C.m. In its crystalline state, the dipole moment will be of similar magnitude and will contribute to the polarisability, and is, we suppose, one of the reasons for its rather high dielectric constant of 9.5. A material of large band gap, if covalent, often has a low dielectric constant (cf. Madelung 1978, p.349).

Table 2.2 - Ionicity

	KN_3	NaN_3	LiN_3	TlN_3	AgN_3	α-$Pb(N_3)_2$	$Hg_2(N_3)_2$
Single-bond ionicity / % (a)	70	65	60	25	23	-	21
Crystal: coordination number (b)	8	6	6	8	8	8	4
ionicity / % (c)	93	88	86	81	80	-	61

(a) = calculated from Table 2.1 and Fig. 2.1;
(b) = from (Yoffe 1966); (c) = calculated from (a) and (b)

The gap in crystal ionicity values between the covalent and the heavy metal azides turns out to be about four times bigger than that between the alkali azides and the latters. The physico-chemical characterisation of the latters are still far from complete and many of their properties remain undetermined. When the need arises, therefore, one can with some confidence treat them as more similar to the alkali azides and use those ionic azides as their best available analogies. This is fortunate, since the alkali azides constitute perhaps the best-known group among inorganic azides.

In many aspects the heavy-metal azides indeed behave as predominantly ionic rather than covalent. In ionic azides, the

azide ion is linear and has $D_{\infty h}$ symmetry, with an N-N bond length of 0.116 to 0.119 nm. In covalent azides, on the other hand, the azido group has the lower aymmetry of $C_{\infty v}$. Thallous and silver azides both have azide units with $D_{\infty h}$ symmetry, with bond lengths of 0.118 and 0.116 nm respectively, while in α-$Pb(N_3)_2$ there are four crystallographically distinct units, three of which have equal or nearly equal bond lengths (C.S. Choi, in Fair & Walker 1977). The configeration symmetry of the azide unit, which affects the crystal field, has in turn been correlated with the stability of the chemical compound (see e.g. Yoganarasimhan 1976). Also there is, not surprisingly, a close relation between crystallographic structure and stability, but we shall not go into the details here. It suffices to note that the high coordination number (8:8) of silver azide, which crystallises in the orthorhombic CsCl structure, and of thallous azide, which is isostructural with potassium azide, (Choi, op.cit.), is another reflection of their ionicity. In contradistinction, a tetrahedrally coordinated structure of the zinc blende or the wurtzite type is a sign of covalent bonding (see e.g. Aschroft & Mermin 1976, pp. 380 & 387).

The differentiation of bond types may be correlated with still more properties of the azides. Before ending this section, we shall mention one further example. When heated, covalent azides such as mercurous azide decompose to give

nitrides. The initial step is the fission of the longest bond in the azide radical. In contrast, the decomposition of an ionic azide involves the electron transfer from the azide ion to the cation, either in one step or through intermediate stages, and only the metal is formed (Yoffe 1966; Section 1.5 this work). Nitrides are found during the decompositions of lithium azide and some alkaline earth azides, but they result in fact from secondary reactions between reactive metals and nitrogen. For lead or thallous azides, nitride formation has not been observed (e.g. Hitchinson et al. 1973); in the case of silver azide, a minute amount of nitride may have been detected by X-ray photoelectron spectroscopy (Sharma et al. 1975).

2.2 ELECTRONIC STRUCTURE

The band structure of an azide contains basic parameters for describing many processes which may be involved in the dielectric breakdown and/or the thermal decompositon of the substance. For this reason, its knowledge is of immediate interest to us and will be discussed here.

The ionisation potential of the metal has again some correlation with the band gap Eg of the corresponding azide (Fig. 2.3). A method has been proposed by de Boer, van Geel and Mott (see Mott & Gurney 1948, pp. 95-8) for calculating Eg in alkali halides, which we have simplified so that it can be

extended to the case of a monovalent metal azide. In this approach, the excitation of an electron from the valence band to the conduction band (at 273 K) is approximated by the following cycle :

1. An ion pair is removed to infinity and separated. With the relaxation of surrounding ions ignored, the work done on the crystal is U, its lattice energy per molecule;
2. The azide ion frees an electron to form a radical. The energy required is the electron affinity of the radical which, from appearance-potential measurements, is deduced to be ca. 3 eV (Franklin et al. 1958);
3. The electron and the cation combine to form an atom. The work done by the system is I, the ionisation potential of the metal;
4. The neutral pair is put back into the lattice. A valence electron of the metal goes into the crystal conduction band (arising usually from the overlap of neutral cation states), the 'hole' on the radical goes into the valence band (arising normally from the overlap of anion states), and the electron-hole pair is dissociated. The energy involved are difficult to estimate, but the net sum will be assumed zero.

This gives us the zeroth order approximation:

$$Eg' = U - I + 3eV$$

which have been calculated for the monovalent azides and are

shown in the following Table.

Table 2.3 Band Gap

	KN_3	NaN_3	LiN_3	TlN_3	AgN_3	α-$Pb(N_3)_2$	$Hg_2(N_3)_2$
U /eV (a)	7.03	8.63	?	7.09	8.88	23.4	?
Eg'/eV	5.7	6.5	?	4.0	4.3	-	?
Eg /eV (b)	8.55	8.46	?	4.1	4(c)	3.9	?

(a) = from (Gray & Waddington 1956) and (Gora 1971);
(b) = experimental values from (Deb 1961,1967); (c)=see later

We see that, in the case of an alkaline azide, Eg' is a gross underestimate compared to the experimental value. This is due to polarisation and any effect of band broadening, which have been ignored in formulationg Eg'. On the other hand, it is gratifying to note that the agreement is close for both thallous and silver azide; being less ionic, they have larger dielectric constants and these effects are much smaller. The experimental values used in Table 2.3 all appear reasonable, although we are aware that the interpretation of the optical absorption spectra is complicated and does not lead to unambiguous values of Eg (cf. Young 1971). Nevertheless, once again a high (negative) correlation is seen between I and Eg. A partial explanation is offered by Eg', which decreases with increase in I if the corresponding variation in U is less significant.

The expression derived above for Eg' contains the three dominant terms appearing in the Born-Haber equation for the

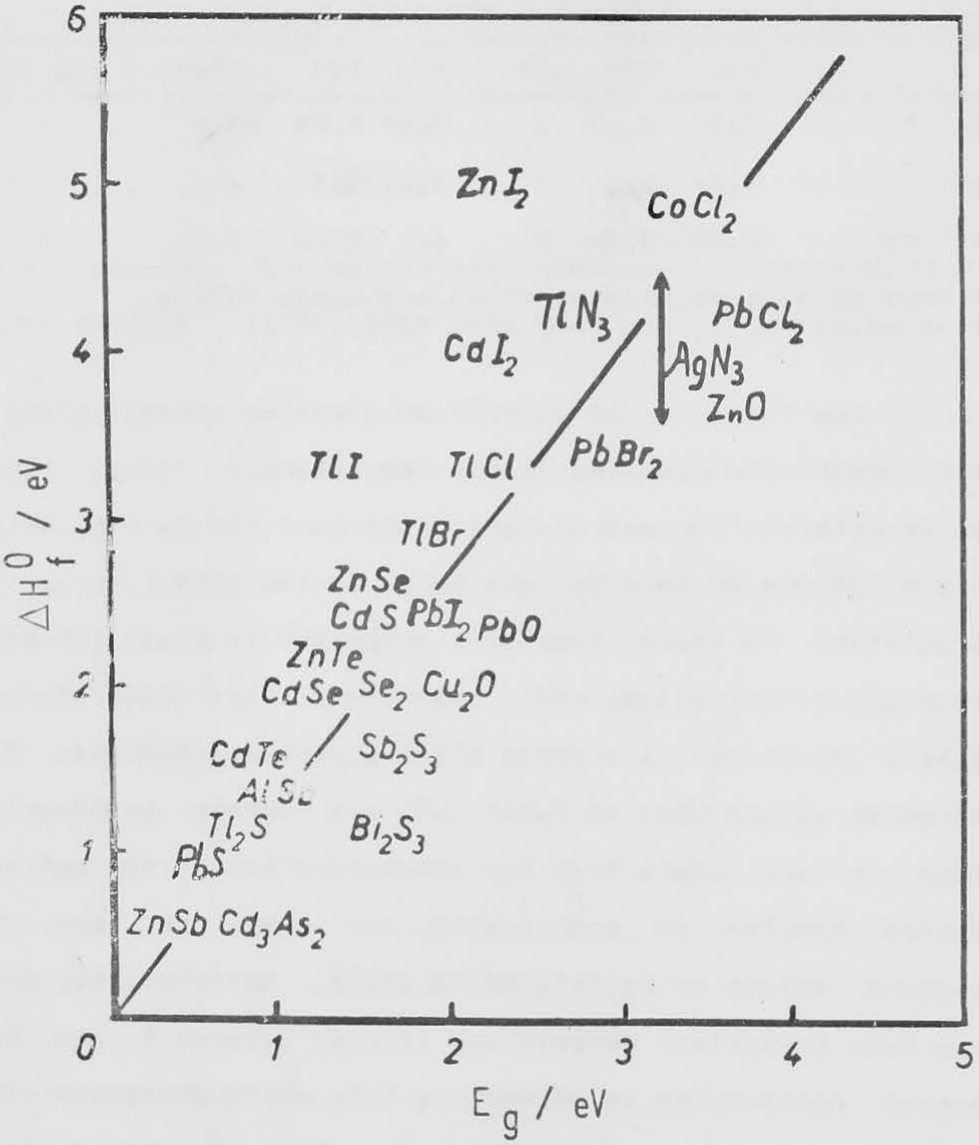

FIG. 2.5 CORRELATION BETWEEN ENTHALPY OF FORMATION AND BAND GAP

standard enthalpy of formation ΔH_f^0. We may therefore expect a rough equality between Eg and ΔH_f^0. Ruppel et al. (1957) have studied empirically the correlation between these two quantities in semiconductors. Using their data as well as those from more recent literature, we have plotted Fig. 2.5 which indicates that, indeed, ΔH_f^0 / Eg is roughly constant with an average value of ca. 1.3. However, data we have collected but not shown in Fig. 2.5 show that this does not hold for many strongly ionic compounds, whose Eg are all greater than 5 eV while their ΔH_f^0 are less.

From here onwards, our attention will be primarilly devoted to silver azide. Several experimental band gap values for it have been reported. McLaren & Regers (1957) investigated both the absorption spectrum and photoconductivity of plate-like samples. At 98 K, a polarisation-dependent band was found centred at 359 nm (Fig. 2.6). Since at that temperature no photoconduction was observed, they attributed that absorption band to an exciton formation. They obtained the activation energies of photoconductivity from 163 to 318 K of two samples as 0.31 eV and 0.45 eV, giving a mean value of 0.38 eV. Using the ratio of the high and low frequecy dielectric constants to convert this thermal energy into the equivalent optical value (Mott & Gurney 1948, pp. 160-2), they estimated Eg to be (hc/359nm) + (9.35/4.06)0.38 eV = 3.44 eV + 0.88 eV = 4.32 eV.

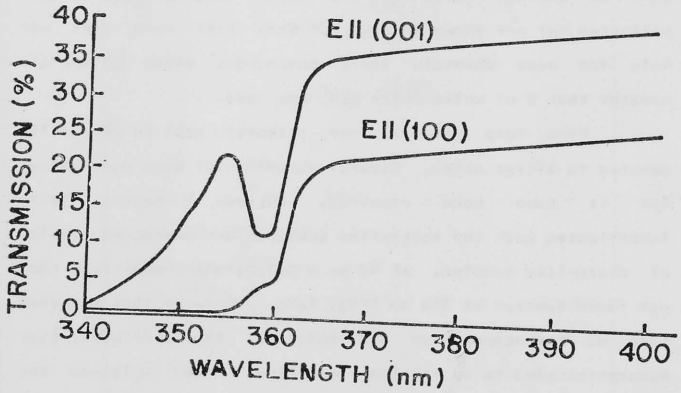

FIG. 2.6 ABSORPTION SPECTRA OF AgN_3 AT 98 K FOR POLARISED LIGHT VIBRATING IN THE [001] AND THE [100] DIRECTIONS; from (McLaren & Roger 1957)

Evans & Yoffe (1959) measured the spectral distribution of photocurrent. They observed a maximum at 375 nm, in close agreement with the result of McLaren & Roger which is 380 nm for both polarised and unpolarised light. Using the value of the high frequency dielectric constant for silver azide obtained earlier (Evans & Yoffe 1957), they calculate that the optical energy to dissociate an n=1 Wannier exciton is 0.77 eV. At around room temperature, nearly all excitions with $n \geq 2$ will be dissociated so that this value of 0.77 eV should be the activation energy of photoconduction. The agreement of this theorectical value with the experimental figure of McLaren & Rogers (0.88 eV) is thought to be excellent. A slightly different Eg is deduced: (hc/375nm) + 0.77 eV = 4.27 eV.

One may perhaps feel confident in assigning the value of 4.3 ± 0.1 eV to the band gap of silver azide, but unfortunately there are serious objections. The two activation energies that McLaren & Rogers have measured differ very widely, and probably represent not some intrinsic properties of pure silver azide but rather the thermal activations of electrons from certain impurity levels such as surface silver (Young 1964). In the calculation of Evan & Yoffe, the exciton radius is computed to be 0.2 to 0.5 nm (T. Gora et al., in Fair & Walker 1977), which is too small to be treated in the Wannier formalism, so that there appears to be an internal inconsistency.

Later, Deb & Yoffe (1960) resolved the 359 nm absorption band into two peaks at 359 and 360.8 nm, the measurement being at a bandwidth of 1 nm and with unpolarised light. The first one they tentatively assign to n = 4 excitons, and the second to n = 3 excitons. This leads to reasonable exciton radii (T. Gora et al., op. cit.). They further explained that, the values of both the low fequency dielectric constant and the reduced effective mass of the excitons being uncertain, one could not rule out the possibility that the 375 nm or 380 nm peak is the n = 1 exciton level. The dissociation energy of an n = 1 exciton will be 0.36 eV if its effective mass equals the electron mass m, or 0.18 eV if it is m/2. These values may be compared with 'mean' value of photoconduction activation energy obtained by McLaren & Rogers, 0.38 eV, and with the photolysis activation energy estimated by Bartlett (quoted in Young 1966), 0.26 eV.

However, there are still difficulties. The absence of the n = 2 exciton peak remains unexplained. Moreover, the validity of identifying the n = 1 level by extrapolating from higher states is highly questionable (Young 1966). The n = 3 and 4 states may fit well a hydrogenic series ($E_n = E_1/n^2$), but the radius of the n = 1 exciton is only a few lattice spacings so that the Wannier treatment necessarily fails.

Bartlett, Tompkins & Young (1958) measured photoconduction in freshly prepared, annealed microcrystalline silver

azide. The spectral response curve shows a sharp rise at 313 nm with no fine structure (exciton bands) before the threshold frequecy (cf. Fig. 2.5). According to this result therefore Eg = 3.9 eV. It is surprising, however, that this response was not seen in the single-crystal work described above. On the other hand, Young (1964) detected the same 359 nm absorption band in these polycrystalline samples from reflectance measurement. Bartlett et al. found that the photoconductive response shifts to the visible at ca. 2.75 eV when the samples are partially decomposed by heat. In addition, a new band of photosensitivity appears, at 1.65 eV for the low temperature form of silver azide and at 1.48 eV for the high temperature allotrope. (We have mentioned in Appendix A the crystallographic change at ca. 461 K). The latter two values are interpreted as the optical energy required to excite electrons into the conduction band, from (colloidal) silver which is formed during the pyrolysis. The presence of colloidal silver is also inferred from the absorption spectrum, which furthermore contains several more bands if the decomposition has been by UV light. Bartlett et al. ascribed these bands to the presence of R'- and F- or β- centres. (An R'-centre is a pair of adjacent cation vacancies sharing an electron. A cation vacancy with a trapped electron is called an F-centre, but a β-centre if it is near a lattice imperfection.) These colour centres as well as (colloidal) silver are, however, possibly not formed in the

pyrolysis of grain-free single crystals, which we think proceeds by an interfacial mechanism directly giving compact silver nuclei (see Chapter 6).

Recently, Dubovitskii et al. (1976) in their investigation of the photolysis of silver azide reported that a well-developed absorption band is found at 305 nm. If this corresponds to the band-to-band transition, then the value of Eg they have obtained is 4.1 eV.

Zakharov and co-workers published an electron energy scheme for silver azide which they specified had been prepared from sodium azide and silver nitrate solutions (Zakharov et al. 1976). It was based on photoelectric and other measurements (see Zakharov et al. 1975), but no details were given. However, it is the most complete band 'structure' reported in the literature. The band gap is given as 3.7 eV, a low figure compared to the values we have discussed above. The fermi level is ΔE = 0.8 to 0.9 eV above the filled band, which is confirmed to have originated from the 2p levels of nitrogen. It is slightly surprising that the fermi level is so much nearer to the valence band than to the conduction band; in ionic insulators, the impurity levels are usually very deep inside the band gap, so that the fermi level is more or less at the centre (the difference between the effective masses of the electrons and holes generally does not shift it appreciably). The fermi level according to Zakharov et al. implies that holes

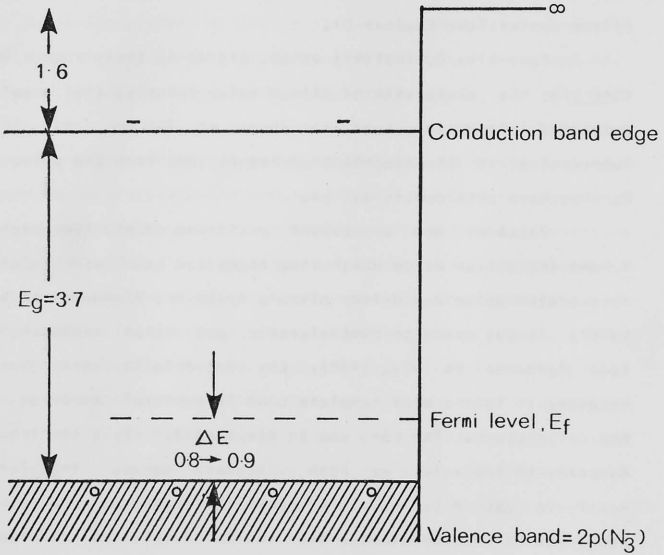

Fig. 2.7

Electron energy levels in Silver Azide according to Zakharov et al. (1976); the energies are given in eV

are much more numerous than electrons in silver azide, though even their concentration will be less than the minority carrier density normally encountered in a semiconductor (Fig. 2.7). The electron affinity has also been determined as 1.6 eV. The work function thus comes out as 1.6 eV + 3.7 eV - ΔE = 4.4 to 4.5 eV. Zakharov et al. found that doping with Cu++ up to ca. 0.01 mol% does not appreciably change the work function.

In summary, we have in the literature come across the following room-temperature values of the band gap: 4.32, 4.27, 4.1, 3.9 and 3.7 eV. The best conclusion seems to be that Eg = 4 eV ±10%. This average value, incidentally, does not contradict the trend depicted in Table 2.3, namely a fall in the band gap as the ionisation potential of the metal increases. The position regarding exciton energy levels is in greater confusion. Not being concerned with photolysis, however, we shall not have to decide on a likely set of their spacings.

There are two final points. In silver azide, which is significantly ionic, a conduction electron will be strongly coupled to phonons (forming a 'polaron'). The energy Et required to promote thermally an electron from the valence band edge to the conduction band edge is less than Eg, since the lattice can relax during the thermal process. Mott & Gurney (1948, pp. 160-2) have derived the approximate relationship that Et/Eg = ratio of high- to low- frequency dielectric

constants. This ratio is 0.45, according to McLaren & Rogers (1957) and Evans & Yoffe (1959). However, they have calculated the high frequency dielectric constant from the refractive index whose large anisotropy they had not taken into account. If we use the value of specific refractivity of nitrogen atoms in silver azide computed by Lewis (1966), we find that the ratio becomes 0.60±0.03.

Secondly, the Eg values have all been measured on the low-temperature allotrope of silver azide. In our dielectric breakdown work, no problems arise: when the transition temperature is reached, the onset of disruptive processes will be so imminent that any crystallographical change will not be significant. In the study of thermal decomposition, however, the samples will necessarily be heated to above 461 K in order that the reaction proceeds at convenient rates. It would be very difficult to measure Eg in the high temperature phase because of the formation of silver due to decomposition. It seems likely, on the other hand, that Eg will not change greatly. The ratio Et/Eg for this allotrope has been directly determined as 0.38, from the values of the optical and the thermal energies required to excite an electron from colloidal centres in microcrystalline samples (Bartlett et al. 1958). The first value was inferred from the 1.48 eV photoconductivity band (see above), and the second by interpreting it as twice the thermal activation energy measured for the electronic

conduction, which is 0.28 eV.

The band gap values of thallous and lead azides have been given in Table 2.3. As in the case of silver azide, however, the interpretation of their absorption spectra is not without ambiguities and thus the values should be viewed with caution. More recently, the Picatinny group has developed various methods for preparing thin films of these azides and has measured their spectra. Their results are in rough agreement with our values (Fair & Downs 1971; Fair & Forsyth 1969, Gora 1971). The electron affinity of thallous azide has been estimated as ca. 3 eV (Gray 1963) but to us it appears unreliable (cf. Section 6.6.1). That of lead azide has been said to be ca. 1.2 eV (K. Hunter & F. Williams, private communication quoted in Downs et al. 1975).

2.3 ELECTRICAL CONDUCTION

From the band structure just described and given that silver azide as an ionic solid also has the usual parabolic density of states, it is obvious that the concentration of holes in the valence band, evaluated approximately as 10E24 exp(-ΔE/kT) /cubic-m, (see e.g. Ashcroft & Mermin 1976, pp. 572-4), is insufficient to account for the relatively high electrical conductivity of ca. 10E-7 S/m at room T, unless the holes have an extraordinarily high mobility. Indeed, near room temperatures the activation energy of conduction (at low

fields: see Section 2.5.2) is found to be 1.1 eV (see 2.6.2). If the conduction process involves the drift of electrons or holes, which exist because of the presence of shallow donor or acceptor levels, this activation energy should be of the order 0.1 eV, otherwise their concentration is no greater than that of band-to-band excited carriers. The conductivity is therefore more probably ionic; the formation energy of ions is, of course, not directly related to the electron energy band gap. Now, the enthalpy of formation of an Ag^+ vacancy should be much smaller than that of an azide ion vacancy, in view of the sizes involved. Together with the high dielectric constant and close packing (coordination number 8:8) of silver azide, it suggests that Frenkel defects in the form of cation interstitials and vacancies predominate over the Schottky type. This is unlike the situation in the alkali halides but the same as in silver oxalate (Boldyrev et al. 1963; Zakharov et al. 1965) and in the silver halides. Indeed, strong experimental evidence has been gathered suggesting that the dark conduction in compacted powders of the pure material is mainly ionic and is due to interstitial silver ions.

Bartlett, Tompkins & Young (1958) and Young (1964) measured the conductivity and the thermoelectric power of polycrystalline samples. Microscopic examination suggested that intergranular cohesion occurred at around 450 K, and they found that when an originally uncompacted sample was slowly

heated and then cooled, the conductivity rose abruptly at this temperature if the sample was confined, but fell if it was unconfined. Their understanding is that the difference is due to the ionic conductivity of the high temperature phase, which makes a larger contribution in the pellet because of more effective compaction.

This interpretation is supported by the p-type of thermoelectric power measured in powder where sintering is complete. In partially decomposed samples, just before the temperature at which this takes place, a sharp n-type peak is observed. The explanation is that the intergranular adhesion is at first lost due to volume reduction accompanying the formation of the high temperature allotrope. The electronic contribution presists, since electrons can still flow across the loose contacts, while the ionic part is eliminated. At these temperatures and pressures, however, the crystallites rapidly sinter together again, so that the thermoelectric power returns to p-type. The authors concluded that in undecomposed silver azide, the main charge carriers are ions, and may be either interstitial cations or anion vacancies. The geometry of the crystal structure and the small size of silver ions (0.126 nm) suggest that the former alternative is more likely and, further, that the collinear interstitial migration in the <001> directions would involve the least strain energy. In partially decomposed samples, electrons donated by metallic

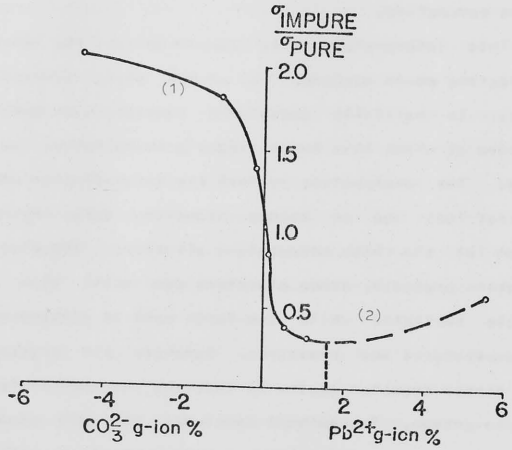

FIG. 2.8 ISOTHERMS FOR THE RELATIVE ELECTRICAL CONDUCTIVITIES OF AgN_3 CONTAINING (1) CO_3^{2-} AND (2) Pb^{2+}; from (Zakharov & Kabanov 1964)
NOTE : rising branch of Isotherm (2) consists of a single experimental point and is therefore tentative

silver will also conduct electricity; the electronic and the ionic parts are reckoned to be about equal at decomposition temperatures.

The investigations by Zakharov and co-workers confirm the role of the interstitial cation as the main current carriers. Their measurements of dielectric constant and dielectric losses on pellets of silver azide co-precipitated with lead azide and with silver carbonate show that substitutional solid solutions are formed in this way (Zakharov & Kabanov 1964). They also found (ibid.; Zakharov et al. 1964) that electrical conductivity is lowered by the Pb++ doping, but becomes higher with the carbonate doping: see Fig. 2.8. Over the temperature range of 293 to 388 K, the same activation energy is determined for the pure substance and both of the doped materials; any change is confined to the pre-exponential factor. The hypothesis of interstitial cation being the dominant charged defect system explains these observations. The enhancement of conductivity upon the (substitutional) incorporation of carbonate ions follows from its increased concentration needed to compensate the extra negative charge on these ions at anion sites. The decrease in the other case is due to its reduced concentration following combination with the excess cation vacancies generated to compensate the extra positive charge on the Pb++ ions. The gradual recovery of conductivity when the doping by Pb++ exceeds 2 mol% (Fig. 2.8)

is due to the increased number of cation vacancies. The relative slopes of the two branches of the isotherm serve to confirm that the silver ion in silver azide is much more mobile by an interstitial than by a vacancy mechanism.

Before ending this section, we review briefly results which are available, concerning the identification of charge carriers in other azides. The conductions in potassium and sodium azides are also ionic, but the responsible species are cation vacancies. On the other hand, lead azide conducts by anion vacancy motion. The main evidence is as follows. In potassium azide, Maycock & Pai Verneker (1969) found that the incorporation of Ba^{++} increases the conductivity. Sharma & Laskar (1973) measured self-diffusion of K by the radioactive tracer technique and showed that the migration activation energy, 0.80 ± 0.06 eV, is nearly identical to the activation energy of defect migration experimentally deduced by Maycock & Pai Verneker. In the case of sodium azide, diffusion measurement together with a calculation of polarisation energy suggest that Schottky defects predominate with Na^{+} most mobile by a vacancy mechanism (Torkar & Herzog 1966). The various activation energies for these azides will be given later in Table 2.5, Section 2.6.2. For lead azide, it was found that doping with Ag^{+} increases the conductivity, while the addition of Cu^{++} has the opposite effects. The interpretation is that Ag^{+} doping leads to the formation of compensating anion vacancies,

whereas Cu++ ions, which enter the lattice interstitially, decrease the anion vacancy concentration. The activation energy of conductivity is 1.0±0.1 eV according to Savel'ev et al. (1967), or 1.39 eV according to Sheckhov & Zakharov (1969).

2.4 AC CONDUCTIVITY MEASUREMENT

In an attempt to learn more about the conduction processes, we carried out measurements on the conductivity as a function of frequency. Its characteristic in the frequency domain may provide information concerning the azide-electrode interface and, as we shall describe in Section 2.5.2, ionic polarisation is suspected to accompany the application of the voltage.

All the experiments described here and elsewhere in this work have been on relatively large single crystals; the way in which we had grown them is recorded in Appendix A. This sample form offers advantages over pressed pellets or compacted powder. Its preparation involves no pressing which may result in plastic deformation, so that any strain-induced changes in electrical properties are avoided (see Chapter 8). It minimises the surface to bulk ratio, so that one can be more certain of measuring the bulk rather than the surface properties. The boundary conditions of density, powder particle size distribution, and properties of the interstitial gas are also eliminated. The drawback is that the geometry and

dimensions of the sample are restricted to those of the as-grown crystal. Nevertheless, the use of single crystals make data reduction and interpretation much less ambiguous.

2.4.1 Experimental

The needle-shape single crystals were mounted on microscope slides made of Corning 7059 glass. This glass at room temperature is stated to have a volume resistivity of greater than 10E12 ohm.m, a breakdown strength in excess of 1 MV/m, and a low frequency dielectric constant of 5.9 with the loss tangent being ca. 10E-3. Electrical contacts were made to each end of the crystal under study by applying a conductive paint with a wire (Driver-Harris 'T.2 Alloy' 0.0076-inch wire was found convenient: it is resilient and picks up the paint easily). Fine copper wires were then held on the glass surface, again with the use of the paint, and the line of the paint from the crystal end was extended to complete the connection. The conductive paint used in this particular series of experiments was DAG 915 (colloidal silver plus binder in methyl isobutyl ketone). Each sample was dried in an evacuated dessicators for at least 16 hours before use.

Measurements were performed on a General Radio 1621 System, containing the Type 1616 capacitance bridge, the Type 1310 oscillator, and the Type 1236 detector. The bridge gives five digits in its conductance readout but, for our samples, adjustments of the third significant figure and downwards often

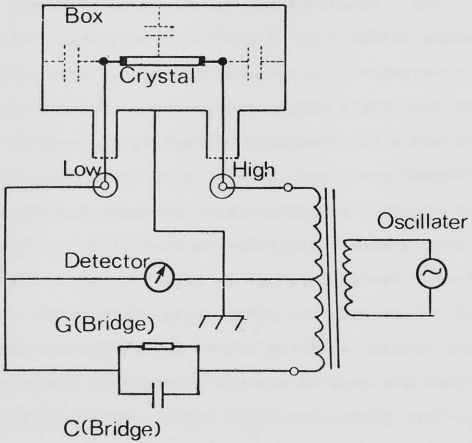

Fig. 2·9

SCHEMATIC DIAGRAM OF A C MEASUREMENTS

have no apparent effect on the null detection, so that the random error in the calculated conductivity is about 2%. (Systematic error due to the error in the microscopic measurement of crystal dimensions is estimated as 15%). The error due to temperature variation is unknown but should be small. The frequency accuracy of the oscillator is specified as 1%. The range provided covers four decades, from 10 Hz to 100 kHz. For some samples the upper limit was at 60 kHz, above which instability occurred and the bridge could not be balanced.

Measurements were in the 3-terminal configuration. The sample was enclosed in a die-cast box, with the copper wires from its two ends soldered onto GR874 connectors (locking type) which were mounted on one side of the box. These connectors could be plugged directly into the HIGH and LOW terminals of the bridge, to minimise leads resistance and leads-to-earth capacitance. The box was thus earthed, but either end of the crystal was floating with respect to earth. In this way, the capacitances to earth of the crystal and the copper wires were excluded from the measurement so long as they are not exceedingly large (Fig. 2.9).

Measurements on each sample consisted of balancing the bridge at selected frequencies of increasing values; this was then repeated, with the frequency going downwards and the connections of the box to the bridge terminals reversed. No significant discrepancies in corresponding pairs in the values

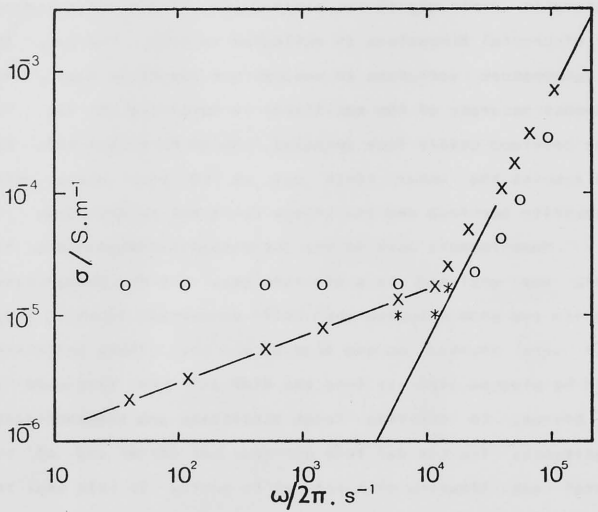

Fig. 2·10

FREQUENCY DEPENDENCE OF CONDUCTIVITY OF AgN_3

X : FRESH SAMPLE, * : CORRECTED BY SUBTRACTING EXTRAPOLATED VALUES FROM THE SECOND SEGMENT; O : SAME SAMPLE AFTER HEAT TREATMENT

of the conductance in the 'up' and 'down' runs were observed. The signal voltage used was 5V peak-to-peak, corresponding to an applied field of between 0.5 to 2 kV/m for different samples.

Measurements were done on three samples. One of the three samples was then heated at 413 K for twenty minutes but subsequently found to have cracked. The other two were heated at 383 K for sixty minutes. After the treatment, they were seen under the microscope to be still transparent but to have turned brownish in colour, suggesting a small degree of decomposition. Their conductivities were measured once more.

2.4.2 Results and Discussion

The spectral characteristics of conductivities of the three samples all display the same shape, and for clarity only one set of data has been given in Fig. 2.10. The capacitances which were also recorded are of the order of 0.1 pF and decrease monotonically with frequency. The dielectric constant of silver azide is about 9.5, but the smallness of the crystal cross-sectional area makes it likely that the relatively large capacitance of 0.1 pF is due almost entirely to electrodes and the glass substrate, and does not represent the crystal capacitance. We were thus unable to calculate the real part of the complex permittivity (see Appendix B) nor to generate complex impedance plots ('Cole-Cole' diagrams). The results for the slightly decomposed samples are also shown in Fig. 2.10.

but will be discussed later.

Let us consider first the leading segment in $\delta(w)$ of the 'fresh' sample. The slope is measured to be 0.4 ± 0.02, i.e. $\delta \propto w^{0.4}$ where w is the angular frequency. No frequency dependence should be seen in band conduction (see end of this Section). Several other conduction mechanisms do predict a power law relation between δ and w, and they are considered below:

[a] Hopping Conduction

When the charge carriers have with very low mobility (< 10E-4 $m^2/(V.s)$; cf. Section 3.2) and energies near the fermi level, they move by tunnelling between localised states, and

$$\delta = Aq^2d^{-5}N^2kT\ w\ \ln^4(1/<t>w) \qquad (2.1).$$

Here A is a numerical constant, q the electronic charge, 1/d the spatial extent of the localised state wavefunction exp(-dr), N the density of states at the fermi energy, k Boltzmann's constant, T the temperature, and <t> the relaxation time associated with the hopping between the localised states. The last parameter may have a fairly broad distribution. The constant A has different values as derived by various authors: $\pi/3$ (Austin & Mott 1969), $\pi^2/96$ (Pollak 1971), and $3.66\,\pi^2/6$ (Butcher & Hayden 1977). At constant temperature and with the observation that $<t>w >> 10$, so that $\ln\ln(1/<t>w) << 4$, (2.1) leads to

$$\delta \propto w^z \qquad (2.2).$$

where

$$z \equiv 1 - 4/\ln(1/\langle t\rangle w)$$

If $\langle t\rangle$ is ca. 10E-13 s, then for w between say 0.1 and 10 kHz, z is essentially constant and equal to about 0.8. For (2.2) to approach our measured slope, however, $\langle t\rangle$ has to be as large as ca. 10E-6 s and in this case z will vary from 0.55 to 0.14 when w changes from 0.1 to 10 kHz. This model of conduction process can therefore be rejected.

[b] Impurity Conduction

If the current transport is again by charged defect centres which have sufficiently low mobility for them to be considered as localised states, then, by analogy to the results due to Pollak & Knotek (1979) for disordered solids,

$$6 = (\pi \ln 2 / 192) q^2 d^5 N^2 kT\, w \ln^4(1/\langle t\rangle w) \exp(-\Delta E/kT) \quad (2.3),$$

where ΔE stands for the energy difference between the fermi level and their energy levels. At constant temperature, this again leads to (2.2) and the model can be rejected for the reason as above.

[c] Ionic Conduction

This we shall see is the most plausible conduction mechanism -- in agreement with the deduction for polycrystalline samples in Section 2.3. A monotonic increase of 6 with w will arise if polarisation occurs at the electrodes which are partially blocking to the discharges of cations and/or anions (Appendix B). In the case of complete blocking,

$$6 = G w^2\langle t\rangle^2/(1 + w^2\langle T\rangle^2) \quad (2.4),$$

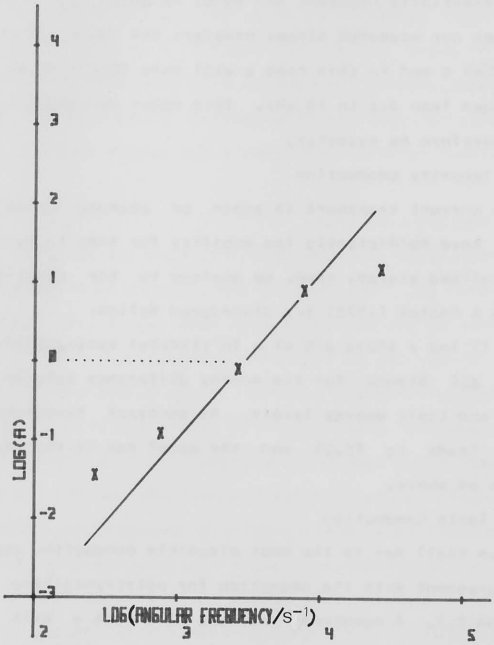

FIG. 2.11 PLOT OF $\text{LOG}(\frac{\sigma}{G-\sigma})$ VS. LOG ω FOR FIRST FIVE X POINTS IN FIG.2.10

where G is the high frequency limiting conductivity and <t> here is the Debye relaxation time. We plot in Fig. 2.11 the log of 6/(G-6) against log w. An expression of the form (2.4) will give a slope of 2; the x-intercept will be $\log(\langle t \rangle^{-2})$, or equivalently <t> is the reciprocal of w at which y = 0 (6 = G/2). From Fig. 2.8, G is estimated as about 0.95 x 10E-5 S/m, the conductivity at 8 kHz being corrected by subtracting from it the extrapolation from the second, sharply rising segment. Shown as the second * point in Fig. 2.8, it appears to corresponding to the saturated value of 6(corrected). Using this value in Fig. 2.9, we find that the plot does approach a straight line of slope 2 for w between 10E3/s and 10E4/s. The Debye relaxation time so obtained is ca. 0.3 ms, a reasonable value. In practice, of course, a distribution of relaxation times occurs, and this value will correspond to their 'average'. The drop in 6 as w is reduced is, however, slower than in (2.4). Our conclusion therefore is that the electrodes are only partially blocking but, when the silver azide crystal is made to conduct electricity, ionic polarisations occur (possibly in addition to a polarisation at the anode due to the generation there of nitrogen gas).

We now consider the second segment, in which a square law dependence of 6 on w is apparent. Such dependence may, in amorphous semiconductors, be an evidence of charges hopping under thermal excitation between pairs of potential wells. In

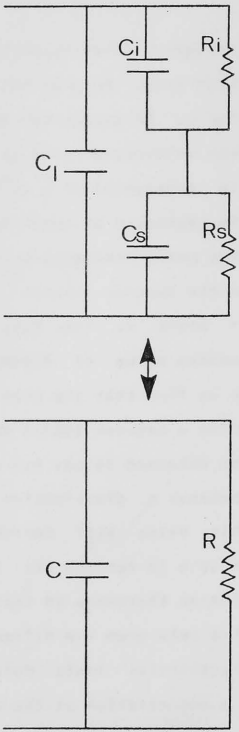

FIG. 2.12 EQUIVALENT CIRCUIT OF A CRYSTAL WITH ELECTRODES; Ci AND Ri REPRESENT THE INTERFACIAL, AND Cs AND Rs THE BULK, CAPACITANCE AND RESISTANCE RESPECTIVELY.

C_1 IS THE CAPACITANCE BETWEEN LEADS. C AND R ARE MEASURED VALUES

our case, however, it is most probably due to a contact resistance between the electrodes and the crystal. Referring to Fig. 2.12, we see that the measured resistance

$$R = Ri + Rs/(1 + w \langle t \rangle) \qquad (2.5),$$

where $\langle t \rangle \equiv Cs\ Rs\ [Rs/(Ri+Rs)]^{1/2} \approx Cs(Rs\ Ri)^{1/2}$, it having been assumed that $Ci = 0$ and $Ri \ll Rs$. The behaviour of R may be broadly divided into three frequency regimes:

Low frequency region

$$w^2 < 1/Cs^2\ RsRi \qquad R = Rs \qquad (2.6),$$

Mid frequency region

$$1/Cs^2\ RsRi < w^2 < 1/Cs^2\ Ri^2 \qquad R = 1/w\ CsRi \qquad (2.7),$$

High frequency region

$$1/Cs^2Ri^2 < w^2 \qquad R = Ri \qquad (2.8).$$

The relation (2.7) shows that $\delta \propto 1/R \propto w^2$, when the quantity Rs^2Ri is reasonably constant. Street et al. (1971) have derived these relations to explain the apparent w^2 dependence of δ in Se, As_2Se_3 and As_4S_4 films. In Fig. 2.8, we can find the x-intercept by extrapolation and obtain Cs^2Ri =ca. 10E-21 s.F. If we assume that Cs remains approximately equal to the product of dielectric constant, vacuum permittivity, and area divided by length, then Cs is ca. 10E-15 F and Ri about 10E9 Ω. Taking Rs to be 10E11 Ω, the resistance of the sample at $w = 2\pi(4 \times 10E3)/s$, we find that the frequency range for Relation (2.7) will be 10E5 /s < w < 10E6 /s. This agrees with the actual range so that our

explanation of $\sigma(w)$ by (2.7) is self-consistent.

Lastly, we consider the data shown as circles in Fig. 2.8, which were measured on the same sample after heating at 383 K for thirty minutes. The w^2 part is nearly identical to that seen before the heating, and may be ascribed to the same cause, i.e., contact resistance. The flat section, we tentatively explain as a higher conductivity arising from a free electron concentration due to silver produced in the pyrolysis. These mobile electrons conduct either in a metallic region on the surface of the crystal or by being thermally excited into silver azide from the silver (see Chapter 6). The electronic conductivity will classically obey Drude's law

$$\sigma = \sigma(0)/(1 + w^2\langle t\rangle^2) \qquad (2.9),$$

in which $\langle t\rangle$ is now the mean free time of the mobile electrons, and $\sigma(0)$ the DC conductivity. $\sigma(0)$ is given by $Nq^2\langle t\rangle/m$, in which N is the concentration of free electrons and m their mass. Since $\langle t\rangle$ is expected to be of the order of 10E-15 s, no frequency dependence should be exhibited by σ for w going up to only 10E7 /s.

2.5 FIELD DEPENDENCE & TIME VARIATION OF DC CONDUCTION

The conduction of single crystals of silver azide when subjected to a steady voltage has rather unusual characteristics. We have carried out experiments to investigate the conduction as functions of time and of the

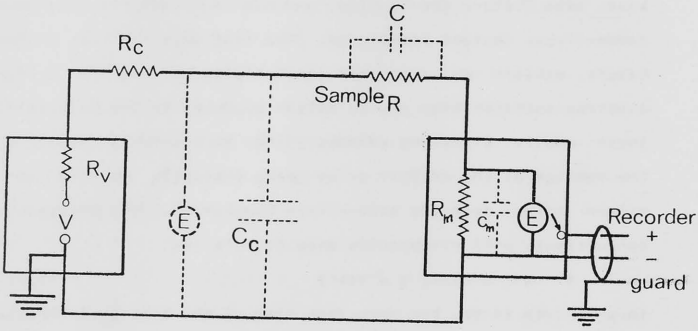

Fig. 2-13

SCHEMATIC DIAGRAM OF D C MEASUREMENTS (see text for description)

field. Also, in other experiments designed to study different phenomena, the DC current was often monitored as well. Our observations from all these experiments are summarised here.

2.5.1 Experimental

The general arrangement for DC measurements is shown in Fig. 2.13. The power supply used was in most cases a Fluke 412B. It is capable of supply a voltage from true zero to 2.1 kV, and a current of up to 30 mA. From the measurement of its load regulation, we found that its equivalent resistance Rv is less than an ohm within the rated current and thus could be ignored. The output voltage is selected by digital dials. Rc is a chain of resistors in a die cast box. Its function is to protect the electrometer E in the event of the sample breaking down, by limiting the short circuit current to below an appropriate value. In low field measurements, it was taken out of the circuitry. From time to time, the output voltage of the power supply was re-calibrated by connecting the electrometer in parallel. Cc represents the total capacitance due to the power supply, the resistance box, and the relevant sections of coaxial cables (100 pF per meter length). It has, however, no effect on our current measurement.

The sample, mounted on a slide, was shielded in a die cast box or a vacuum chamber, except in some breakdown measurements (Chapter 7) when it was placed in front of a camera. The cable connecting it and the electrometer was always kept short.

A Keithley 616 (3 1/2)-digit electrometer was used. In the current-measuring mode, it displays the voltage across a precision resistor shunting its input. The maximum sensitivity of 10 mV full scale 'deflection' was generally selected; in this way the shunt resistance was kept to the minimum value appropriate to the magnitude of the current being measured. In measurements over extended periods, the electrometer was periodically zero-checked to correct for its zero-drift. Its input capacitance is specified as 20 pF, so that Cm, which includes the capacitance of the cable connecting it to the sample, would be about 70 pF.

The analog output of the electrometer may be monitored by a chart recorder. The recorder, when used, was often a Rikadenki B281. Care was taken, especially in those situations when the measurement circuitry being set up was complicated, to avoid earth loops which could lead to reference voltage differentials or magnetic pickups. The connecting coaxial cables in every part of the circuitry were, as far as practical, taped down on rigid surfaces to reduce triboelectrostatic and microphonic effects. Attention was paid to the isolation of nearby vibration sources, in particular the rotary pump when used. Measurements were performed only after the power supply and the electrometer had warmed up for an hour.

The practice was adapted that, as far as possible, the

two ends of the sample were shorted for a period lasting at least half an hour between one measurement and the next. This was done to faciliate the relaxation of any ionic polarisation at the electrode interfaces. Note that higher-than-room-temperature cycling cannot be applied, for fear of changing the crystal through decomposition.

2.5.2 Results and Discussion

We found that, at room temperature, when a constant voltage is maintained across a single crystal of silver azide, the current through the crystal generally changes with time. The time-domain behaviour of current falls into three categories, depending on the magnitude of the field applied:

[a] Low fields

The current decays slowly, at an initial rate of ca. 5%/min. A steady state, non-zero, current is obtained eventually. The time taken for the current to drop by 0.63 of the final amount of decrease is of the order 10E3 s and shorter when the applied field is higher, but no detailed analysis of the current-time behaviour has been attempted. A constant field as small as the peak-to-peak value used in AC experiments discussed in the last section would lead to this behaviour.

[b] Moderate fields

The current fluctuates. If the field has a value that is at the lower end of this range, an initial period can be distinguished during which the average value of the current

is seen to decay. Eventually, however, after some minutes or a few tens of minutes, the current shows non-periodic rises and falls. Just before the onset, there is sometimes a distinct rise in the average level of the current, and the power density conducted by the crystal immediately after the onset is generally of the order 10E2 W/cubic-m. If the field has a larger value, the current fluctuations start sooner and the initial decay period is no longer apparent; at the same time, the fluctuation amplitudes expressed as percentages of the average value of the current seem to become smaller. After a further period of time, the non-steady character of the current changes, but we shall not discuss this part of current behaviour until Section 3.3. In all cases, although a unique value cannot be assigned to the magnitude of the current, it is obvious that its approximate average increases supralinearly with the applied field. The range of fields within which such a behaviour is observed varies from crystal to crystal and/or with the electrode material; its lower limit, F*, will be given below for those experimental conditions we have investigated.

[c] High fields

The current fluctuates but at the same time its average value increases steadily with time. Dielectric breakdown and explosion initiation will occur eventually unless the field is removed or unless an current is limited by an external

FIG. 2.14 (b)

FIG. 2.14 (a)

1min
50 pA
5 pA
3
2
1
L=30mm, A=(180μm)²
CONDITIONS AS IN Fig.14(a)
200V - 3
40V - 2
10V - 1

FIG. 2.15(a)

0
0.2
0.4
0.6
0.8 nA
20 s
40 s
60 s
80 s
100 s
1
2
2'
L = 6.78 mm,
A = (255 μm)²
CONDITIONS
AS IN Fig. 14(b)
125 V - 2'
100 V - 2
50 V - 1

FIG. 15(b)

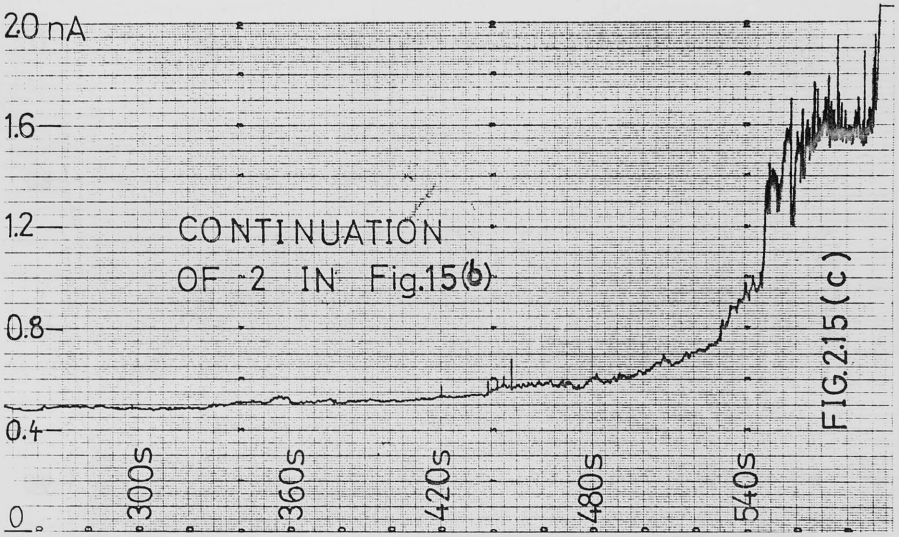
2.0 nA
1.6
1.2
0.8
0.4
0
300s
360s
420s
480s
540s
CONTINUATION
OF -2 IN Fig.15(b)

FIG.2.15(c)

circuitry. The lowest fields F** at which this behaviour were found will be given later in this section.

A 'memory effect' has also been observed. If the field is removed and then applied again, the current has the same starting value but its rate of rise is faster than in the previous application. This increase is more noticeable if the former application of voltage has lasted longer (the current reached has been higher), and if the interval between the two applications is shorter. Such a memory effect was detected after intervals as long as an hour, in some samples which had previously been subjected to electric fields so high and for periods so long that, had the fields not been removed in time, the breakdown would have occurred. Our attempted explanation of the high-field phenomena will have to wait until Section 7.8.

Chart recordings illustrating [a], [b] and [c] are given in Figs. 2.14 & 15. The five experimental conditions under which these phenomena have been studied are:

1) silverdag-painted electrodes, 1 mPa vacuum;

2) same electrodes, but in air;

3) tantalum wedge pressure-contacted electrodes, 10E-6 Pa UHV;

4) same electrodes, in air; and

5) carbon-dag painted electrodes, in air.

The silverdag was prepared by suspending colloidal silver in methyl iso-butyl ketone, and carbon-dag was colloidal carbon in

ethanol. The situations of asymmetrical electrodes have not been fully investigated. However, a few measurements with mixed Ag- and C-electrodes were carried out, and in either polarity the same phenomena were observed. It should also be mentioned that we could not embed a crystal in a potting epoxy so that different metals may be pressed against the ends and serve as electrodes, the reason being chemical reactivity as already mentioned in Section 1.4. Among the materials tried, only 'Celloidin Wool' (made by Hopkin and Williams) was found to be adequately inert to silver azide, but its electrical properties are not suitable. We have not used metallic thin films as electrodes; both evaporation and sputtering were found to cause decomposition which produces silver (cf. Section 6.2).

The non-steady-state characters of the current are qualitatively the same whether the electrodes are of siverdag or of the other materials. In particular, the initial values of conductivity measured at low fields show no systematic variation significant compared to the estimated experimental error. The conduction seems therefore to be bulk-limited, at least before the field has been applied for long and the current has significantly decayed -- see later. This implication is consistent with the picture offered in Section 2.3 that it proceeds by the movement of interstitial cations present in the crystal. Further, it is more likely to involve the discharge of azide ions leading to electrolytic decomposition,

at a silver anode as at an 'inert' anode, and not the oxidation of silver which leaves the anode and 'dissolves' into the crystal as ions. Also, under low and medium fields the current is not noticeably affected by the ambient gas, water vapour excepted, as can be observed when the vacuum system was gradually pumped down. However, the rise of current under high fields is faster for a crystal in vacuum than in air. Secondly, it is a preliminary observation that the use of tantalum rather than silver or carbon electrodes leads to lower values of both F* and F**. These values are, for both Ag- and C-dag, 15±2 and 170±50 kV/m. For tantulum electrodes there are greater variations between samples, and the values are 12±5 and 120±55 kV/m, respectively.

More charts illustrating behaviours [b] may be found in Chapters 3, and [c] in Chapter 7 where suggestions will be put forward for the explanations of both.

Current instabilities and the subsequent breakdown resulting from the application, over extended periods, of fields significantly less than 100 MV/m, have, if effects due to electrolysis are excluded, hitherto received little attention. Cornelis (1974) descibed a similar 'memory effect' in the electrical conduction of lead azide, but gave no correlation with other properties and offered no interpretation of the effect. Independently, we have also noted this effect in lead azide; it is almost certain that it has the expanation that we

shall propose for that in silver azide. Very recently, a paper (Narayan et al. 1978) appeared which reported that dielectric breakdown occurred in MgO at 1300 K after being subjected to 100 kV/m for over 100 h; this work we shall discuss in Section 7.6.

A third piece of work was due to Thoma (1975, 1976), who measured the time and voltage dependence of currents in insulators and semiconductors, and proposed that very generally there are two critical values for the power density. When it exceeds 10 kW/cubic-m, eventual breakdown due to localised melting is unavoidable. If it is less, but greater than ca. 10 W/cubic-m, dischargelike instabilities do not occur but the current may display flunctuations as well as have long-period (several minutes) rise and fall (with a more or less rectangular time dependence, and a maximum amplitude of about three times the normal level). At even smaller power density, the typical instability is a very infrequent (seen after ca. 300 h) step-like irreversible increase of the current by a factor of ca. 1.5. These observations are most easilly explained by current density inhomogeneities in the solid, which lead to local structural changes. One evidence for this mechanism is the fact that a strong magnetic field reduces the 'induction time' for a step-like increase to ca. 24 h (Thoma 1973). In intrinsic semiconductors, the inhomogeneous current density distribution is thought to be due to Joule heating and

insufficient heat transfer between different parts and should not occur until the upper critical power density is approached, while in wide-gap semiconductors and insulators it is proposed to occur at lower power densities, arising out of extended defect regions which are present in the crystal before the field is applied. It will be seen that the model we have indenpendently arrived at for the breakdown of silver and thallous azides may be regarded as a specific and more definite example of the current filament (thermal breakdown) theory but, because of the particularity of the azides, namely their chemical reactivity, our proposal include a hitherto neglected mechanism for the formation of conductive filaments.

Here we shall only discuss probable explanations for the decay of current in [a] and in the initial part of [b]. Such a behaviour indicates in general some relaxation process or a slow build-up of non-equilibrium space charges, and the possible mechanisms, in silver azide, are:-

1 charging of the geometrical capacitance;

2 electronic (or optical) polarisation -- the negative electron clouds of the atoms or ions in the crystal are displaced with respect to the positive cores;

3 dipolar (or atomic) polarisation -- the relaxation of the electric dipoles formed by pairs of the anion and the cation (see Section 2.1);

4 interfacial polarisation -- due to the electrodes being par-

tially blocking to cations, and to electrons for the discharge of anions;

5 trapping of certain charge carriers which are injected from one of the electrodes, when the field is switched on.

Carrier tunnelling to empty traps and hopping through localised states are two other processes which can be responsible (Das Gupta & Brockley 1977), but they are probably unlikely to occur in crystalline insulators.

The time constant of the current decay is, as we have mentioned, of the order 10E3 s. Referring to Fig. 2.13, we expect C to be small (except in the rare circumstance when long parallel-running leads have to be connected to the two ends of the sample). A typical situation will be that C =ca. 10 pF and Rm = 10E10 ohm, so that the transient voltage across Rm when a step voltage V is applied will fall with a time constant of ca. 0.1 s, which is so small that the transient will not be recorded on the chart. Indeed, we see from Fig. 2.15(b) that in the first few seconds after the application of V, the voltage across Rm rises slowly instead. This we interpret as the charging of Cm, with a time constant of Cm(R + Rc), or approximately Cm R which is of the order 1 s at room temperature.

Mechanisms 2 and 3 may be dismissed for the similar reason that they are expected to be fast. Carrier trapping, the last in the list above, may play a part but no data are

available. In any case, ionic polarisation must be the dominant contribution, on the strength of the results described in the last section. Thus, when V is first applied, the current density is uniform along the length of the crystal; the conduction is bulk-limited but not steady-state. As time increases, positive ionic charges accumulate in front of the cathode and, at the anode, there forms a negatively charged depletion layer possibly in addition to a region accomodating nitrogen atoms resulting from the discharge of azide ions. The electric field and therefore the current flow in the bulk thereby decrease. Eventually, when the current through the interfacial layers equals that in the bulk, the system has reached steady state, but the current is now electrode-limited. This eventual current is non-zero, consistent with the deduction in Section 2.4.2 that the electrodes are only partially blocking.

We shall see in Section 3.2 that the fluctuating current of [b] or [c] is probably also electrode-limited. The crucial effect of the interfacial polarisation is that the field along the crystal becomes inhomogeneous, so that the maximum value of local fields is enhanced. All the other relaxation processes, including charge carrier trapping (unless for some reasons the traps are grossly non-uniformly distributed), do not lead to a non-linearity in the field.

Using the Maxwell-Wagner model of the two-layer

capacitor, the time constant for the process is (see Adamec & Calderwood 1978):

$$\langle t \rangle = (e/6)(L/d) \qquad (2.10),$$

where e is the dielectric constant of silver azide, 6 its conductivity, L the length of the sample, and d the combined effective thickness of the interfacial layers. Relations (2.10) is approximate in that the interfacial layers are assumed to have zero conductivity: the electrodes are totally blocking. As an order of magnitude, however, <t> = (10 x 8.9 (pF/m)/100 (nS/m))(1 cm/d) = 10E3 s, if d is ca. 10 nm.

Without access to a highly automated measuring system, we found it not worthwhile to investigate the changes of <t> with voltage and temperature. A few preliminary observations showed, however, that <t> increases when T is lowered. We have determined also that the zero-time conductivity obtained by extrapolation (Fig. 2.15(a)) is constant at low fields, i.e., the V-I characteristic is ohmic (cf. the discussion on Eq. (2.14) in the next section). Above F* the data, unfortunately, are not reproducible, one reason being the uncertainty in estimating the average value of the current. Nevertheless, the characteristic is obviously supralinear; its possible form is I proportional to V squared, log(I) to V to the power 1/4, or to the power 1/2. We shall discuss this nonlinearity again in Chapter 3.

A phenomenon we have observed which is also

irreproducible from one sample to another is an occasional decrease in the low field conductivity after a voltage has been applied to the crystal once. About a day after the first application of voltage, the initial value of the conductivity obtained in any subsequent measurement becomes constant, and this irrespective of the polarity of the applied voltage and whether the voltage is maintained for all or only parts of the period. The ratio between the initial and the final conductivities has been found to be : i] ca. 1, i.e. no significant difference, for fifteen samples (with silverdag electrodes nine in air and two in 1 mPa; with tantalum electrodes one in air and three in UHV), ii] ca. 5 for two samples (one with silverdag electrodes in 1 mPa, one tantalum electrode in UHV), and iii] ca. 10 for one sample (tantalum electrodes in UHV). One possible explanation for the phenomenon is the capture of electrons by mixed-valency impurity ions which constitue deep trapping centres. In our samples they can be ions of transition metals such as iron (Appendix A; Section 2.6.2). Very recently (December 1978), we found that a similar decrease of conductivity has been observed by Sonder et al. (1978) in MgO single crystals. These authors suggested a slightly different mechanism, in which the impurities move to nearby dislocations along where they, or their charges, are transferred to the cathode. The result, the reduction of aliovalent impurities, is the same.


TBT 11

2.6 TEMPERATURE DEPENDENCE OF CONDUCTIVITY

In the low-field regime the conductance in AgN is ohmic and is attributed chiefly to the drift of interstitial cations. The bulk-limited conductivity, σ, is therefore determined by their equilibrium concentration n and their mobility u. The magnitudes of both n and u are themselves controlled by thermally activated processes, namely, the thermodynamic formation of Frenkel disorders and the hopping over interatomic energy barriers by the ionic defects formed, respectively. By studying $\sigma(T) = q\, n(T)\, u(T)$, we can therefore estimate the physical parameters describing these two processes.

2.6.1 Experimental

The arrangement for current measurements was identical to that described in the last section, except that the glass slide on which the crystal was mounted was glued to a copper cold finger with Dow Corning 340 heat-sink compound. The copper block was welded to a Kovar disc which formed the bottom of the inside wall of a vacuum Dewar (Fig. 2.16). The specimen was cooled by introducing water+ice or methanol+dry ice into the Dewar. A silvered glass socket-and-cone (not shown in the photograph) formed an outside wall of the Dewar, enclosing the copper block. The Dewar was evacuated to 1 mPa by an oil

<<--

FIG. 2.16
Dewar system for conductivity measurements

diffusion pump backed by a rotary pump. Electrical connections between the sample and the power supply as well as the electrometer were made via a multipin feedthrough.

A Eurotherm 072 temperature controller was used. A copper-constantan thermocouple was held by heat-sink compound on the glass slide next to the crystal. It was connected to a DVM and, in parallel, to the Eurotherm which controlled the current into a soldering-iron heater (1.9 k-ohm) mounted on the copper block. The stability of temperature achieved, as monitored by the DVM, was ± 1 K. When the initial values of conductivities at different temperatures were measured, the glass slide was heated to a chosen temperature and then the Eurotherm output power reduced to zero. This was to avoid mains pickup by the electrometer circuit, and the change in temperature while the reading was quickly taken was checked to be not more than 1 K.

The offset and the noise levels in the electrometer add up to 0.01 pA. In our particular system, however, the limit of measurement was set by the leakage current through the glass slide and the feedthrough and some residual pickups, which was ca. 0.1 pA at 100 V. Current measurement commenced at low temperatures, and the electric field applied was about 20 kV/m below 273 K, 1 kV/m above 323 K, and 5 kV/m in between. Between each measurement, while the temperature was raised to a new setting, the ends of the crystal were kept shorted.

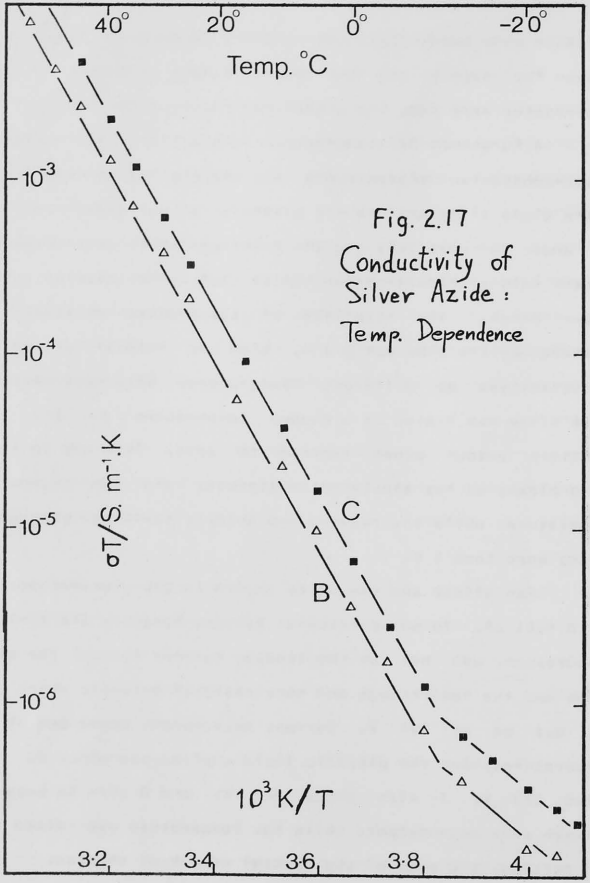

Fig. 2.17
Conductivity of Silver Azide: Temp. Dependence

2.6.2 Results and Discussion

Measurements were carried out on three samples. Each was 'formed' by having five volts applied to it for an hour and then its ends shorted for a day. The conductivities of samples A and B were unchanged, but that of C afterwards was reduced by a factor of 4.3. Sample A was broken when liquid nitrogen was introduced into the Dewar. The Arrhenius plot of the conductivities of the other two specimens is shown in Fig.2.17. Let us first consider the high temperature part. Our results, as well as those obtained by other workers, all of which have been in this temperature region, are compared in the following table:

Table 2.4 Activation Energy of Conductivity

Sample form	Electrodes	Slope/eV	Temp./K	References
pellet	?	0.46	453-523	Gray & Waddington 1957
sintered powder	?	1.09	433-453	Bartlett et al. 1958
pellet (in vacuum)	graphite	0.82 ± 0.05	293-388	Zakharov & Kabanov 1964; Zakharov et al. 1964
sintered powder (in vacuum)	silver wire pressure contact	1.08	293-453	Young 1964
pellet? (in 1 mPa vacuum)	?	1.08	293- ?	Sheckhov & Zakharov 1969
pellet	sputtered silver	0.80 ± 0.08	293 - ca.388	Gas'maev & Zakharov 1972
"	"	ca. 1.87	ca.388 - 430	Zakharov et al. 1976
single crystal (in 1 mPa vacuum)	silverdag	1.11 ± 0.05	262-343	this work

Note to Table 2.4 : The result of Gray & Waddington probably applies to electronic conduction in decomposed samples, in view of the very high temperatures they have used. They stated that a discontinuous change in the conductivity was observed below 453 K. Zakharov et al. (1976) thought that the conduction is electronic when the temperature exceeds ca. 388 K. Young (1964), however, has shown that when his specimens were cooled from 453 K down to room temperature, the conductivity did not change its slope and could be attributed entirely to ions.

The low temperature part of our plot gives a smaller slope of 0.5±0.2 eV. It appears to correspond to the extrinsic conductivity region, in which the majority of free ions are not thermally generated but exist because of the presence of uncompensated multivalent impurities in the crystal. We may therefore consider the approximate value of 0.5 eV to be the activation energy for motion of the ionic carrier, Wv.

The high temperature part then corresponds to the intrinsic region. Applying the law of mass action to the reaction :

occupied lattice site + unoccupied interstitial site

<---> cation vacancy + interstitial cation

at constat pressure, we see that the density of interstitial cations, n, is given by :

$$((Ni-n)/n)((N-n')/n') = \exp(\Delta S /k - Wc /kT) \qquad (2.11),$$

where Ni is the density of possible interstitial sites, n' that of cation vacancies, N that of cation lattice sites, and ΔS and Wc are respectively the entropy and the enthalpy of formation of a pair of cation interstitial and vacancy. (The case

being considered is where the charge carriers are interstitial cations, as it is in silver azide.) Since Ni is nearly the same as N, n << Ni, n' << N and, in the intrinsic region, n' is about equal to n, (2.11) reduces to :

$$n = p\,N \exp(-Wc/2kT) \qquad (2.12),$$

where $p \equiv \exp(\triangle S/k)$ is usually not very different from unity. When an electric field F is applied, the motion of the ions exhibits a net drift because of the created difference in the inter-site barrier heights, with a velocity

$$V(drift) = v\,d \exp(-Wv/kT)\, 2\sinh(qFd/2kT) \qquad (2.13),$$

where v is the jump frequency, d the jump distance, and q the charge on the ion. The change in potential due to F from one interstitial site to another is small compared to thermal fluctuations: $qFd << kT$, so that $\sinh(qFd/2kT)$ can be approximated by $qFd/2kT$. The ionic mobility is then

$$u \equiv V(drift)/F = (qvd/kT) \exp(-Wv/kT) \qquad (2.14),$$

and is proportional to $(1/T)\exp(-Wv/kT)$, V and d having only mild temperature dependences. Since $6 = nqu$, the conduction characteristic is ohmic, and the slope of the plot of 6T vs. 1/T should be Wc/2 + Wv. Hence Wc is obtained as ca. 2(1.11-0.5) or 1.2 eV.

Using crystallographic data to evaluate N, we find from (2.12) that at room temperature n is ca. p(2x10E18)/cubic-m. At room temperature therefore, approximately

$$u = (1/nq)\ 10E\text{-}7\ S/m = (1/p)\ 10E\text{-}7\ (m/s)(V/m).$$

This results seems to be rather too large unless p is exceptionally large; the typical mobility of the interstitial silver ion in silver halides is of the order 10E-13 (m/s)(V/m). On the other hand, the value estimated by Zakharov & Kabanov (1964) is definitely too small. From the conductivity isotherm of silver azide containing Pb++ (Fig. 2.8), they calculated that u =ca. 4x10E-16 (m/s)(V/m). This corresponds to n/N =ca. 0.1, which is quite impossible except in a superionic solid-electrolyte. The authors did, in fact, point out that the assumptions made in their calculations were unlikely all to be satisfied. Our conclusion is that from one interpretation of the conductivity plot, values have been found for the free energies of formation and of motion for the dominant charge carrier in silver azide at low fields. These values can, however, at present be regarded as tentative only. They can be independently checked by, for example, self-diffusion measurements. Considering the geometry of our single crystals, however, we decided that the effort likely to be required to make the experiment work was not justifiable in view of the secondary importance of the result to the present research programme.

Corresponding values for the other heavy metal azides are totally unknown. Nevertheless, it is plausible that in monovalent metallic azides they will show a consistent trend with I, the ionisation potentials of the metals. We may expect

that as I increases in the series K, Na, Tl and Ag, the ionicity of the corresponding azide bond decreases, so that in the crystalline state the energies required to create defects and for the charged defects to move are reduced. As a result of both of these effects the conductivity will increase. Our expectation is not contradicted by experimental results which are summarised in the following table:

Table 2.5 Conduction in the Azides

	Potassium	Sodium	Thallous	Silver
Conduction species	cation vacancy(a)	cation vacancy(a)	?	interstitial cation (a)
Wc/ eV	1.43 (b)	1.91 (c)	?	(1.2)
Wv/ eV	0.80 (a)	0.87 (c)	?	(0.5)
Activation Energy of intrinsic conductivity /eV (d)	1.52	1.83	?	1.11
Room-temperature conductivity/(S/m)	10E-12(b)	-	10E-10	3x10E-7

Results from this work unless otherwise specified
(a) as discussed in Section 2.3
(b) Maycock & Pai Verneker (1969)
(c) Tonkar & Herzog (1966)
(d) equal to Wc/2 + Wv

CHAPTER III

CURRENT INSTABILITY & CHEMICAL DECOMPOSITION

3.1 POSSIBLE MECHANISMS OF NON-OHMIC CONDUCTION

In Section 2.5.2 we have described the observation that in silver azide, when the applied electric field exceeds a certain critical value F*, the current displays fluctuations. Also, the approximate average value of the current increased superlinearly with the field. In this and the next section, we shall attempt to identify, through plausibility arguments, the processes responsible for the non-steady-state and non-ohmic behaviours.

First, we examine here the spectrum of mechanisms which may explain non-linear current-voltage characteristics in ionic crystals. These mechanisms can be classified according to whether they take place in the bulk or at the electrodes. They lead to an increase of the conductance either by enhancing the ionic mobility or the density of mobile ions, in the bulk, or by generating new current carriers in the bulk or at the electrodes.

3.1.1 Bulk Effects

(a) A field-dependent mobility of ionic defects can be derived in a straight-forward manner, without the postulation of any new processes. Referring to Eq. (2.13), we see that u is constant given by (2.14) only if $qFd \ll kT$, where q is the ionic charge, F the field, d the distance over which the ion hops, and kT has the usual significance. In the case that this condition does not hold, but that qFd is still sufficiently

small in relation to kT so that it is adequate to take only the first two terms in the series expansion of the sinh factor, we obtain

$$u(F) = u(0)\,[1 + (qFd/2kT)^2/3] \qquad (3.1),$$

in which $u(0)$ is the low-field mobility given by (2.14). At room temperature, kT is approximately 1/40 eV so that the field-dependence in (3.1) is significant only for $Fd \geq 1/20$ V. Since d is typically of the order 1 nm, this implies the condition that F >ca. 100 MV/m.

(b) When the field is applied, the density of mobile ions may be increased because of the lowering of the potential barrier for an ion to leave its normal lattice position. Bean et al. (1956) have analysed the ionic conductivity data of tantalum oxide, and suggested that the density is given by

$$N(F) = N(0)\exp(-qFd/2kT) \qquad (3.2),$$

where N(0) is the thermal equilibrium density, and d here is a parameter which itself depends on F but is generally 1 nm or less. Relation (3.2) has further been applied to the data of some other oxides (Young 1961). Like (3.1), it implies that at room temperature F > 100 MV/m before the field-assisted generation of ionic defects can become important.

(c) The density of free electrons or holes is, in the intrinsic region, governed by the thermal process of exciting electrons from the valence to the conduction band. If the band-to-band energy gap is Eg, this number is the effective

density of states times exp(-Eg/2kT). For a material such as silver azide with Eg ca. 4 eV, the exponential factor will be so small that, although the electrons or holes or both may have much higher mobility than the ionic defects, their contribution to the conductivity is utterly negligible. Alternatively they may, of course, be derived from donor or acceptor impurity atoms contained in the material, but usually the impurity levels are so deep inside the energy gap that at room temperature, most of the impurity centres remain un-ionised. However, if the applied field is high resulting in significant lowering of the ionisation energy barrier, then thermionic emission from these electron or hole traps may become important. If the trapping potential has the Coulombic profile $-q^2/4\pi ex$, then the barrier reduction is $\Delta W = (q^3F/\pi e)^{1/2}$ and the density of conduction electrons or holes is

$$n(F) = n(0)\exp(\Delta W/kT)$$
$$= n(0)\exp[q(qF/\pi e)^{1/2}/kT] \qquad (3.3).$$

Here q is the electronic charge, e the static permittivity of the material, and n(0) the original density in the absence of the field. At room temperature, n(F)/n(0) is not large enough unless $F^{1/2}(q/\pi e)^{1/2} > 1/40$ V. For silver azide whose e is $9.5/36\pi$ nF/m this condition means that F > 100 MV/m.

Eq. (3.3) was first derived by Frenkel (1938) and based upon the earlier experimental work of Poole (1916, 1917). Various refinements have been proposed to this Poole-Frenkel

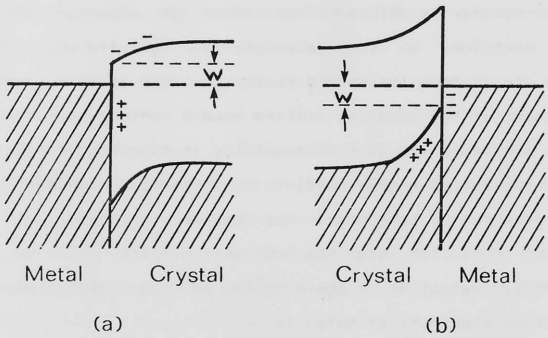

Fig. 3·1

MOTT BARRIER AT (a) ELECTRON- OR (b) HOLE-INJECTING CONTACT

expression (Jonscher 1967; Idea et al. 1971; Hill 1971). In all these modifications, however, the factor which varies most rapidly with F is of the same form as that in (3.3), so that the condition remains valid.

3.1.2 Electrode Effects

The electrodes, being metals, have electron energy bands which are only partially filled. The density of free electrons is therefore orders of magnitude higher than that in the crystal. By thermionic emission, electrons may be injected by the electrode into the conduction band of the crystal, or extracted from (i.e. injection of holes into) the valence band. Since the electrons and holes have small effective masses, tunnelling is also possible across an interfacial energy barrier. Below, we consider these processes in greater detail.

[a] Electrons or holes can 'boil off' from the metal into the crystal just as they do from the heated metal into vacuum. Depending on the particular crystal surface and metal, it may be that the activation energy W for the process is substantially smaller than the corresponding work function for the metal-vacuum interface (Fig. 3.1). If W is not very much larger than kT (1/40 eV, at room temperature), then a vapour of electrons or holes is maintained in the crystal. In the absence of compensating charges, a space charge will then exist in the crystal, accompanied by an equal and opposite charge on the surface of the metal. This is the case of thermal injec-

tion, and has been studied by Mott & Gurney (1948, pp.168-73), Rose (1953) and Lampert & Mark (1970). The carrier density in the crystal immediately near to the interface is, with generally valid approximations,

$$n = 2(2\pi m^* kT/h^2)^{3/2} \exp(-W/kT) \qquad (3.4),$$

where m^* is the effective mass of the charge carrier and h the Planck's constant. The pre-exponential factor is typically of the order 10E19. If the applied voltage V is very large, the current density in the crystal will be

$$J = qnu(V/L) \qquad (3.5),$$

in which L is the length of the crystal. The conduction is therefore ohmic, and it is said to be emission or temperature limited, with an activation energy equal to W. However when V is less than qnL^2/e (but still much larger than 1/40 eV), the rate of carrier injection from the electrode exceeds the rate at which the carriers can be transported across the bulk of the crystal, and a space charge is maintained near the boundary. The current density under this space charge limited (or voltage limited) condition is

$$J = (9/32\pi)eu V^2/L^3 \qquad (3.6),$$

if the bulk is trap-free. This case is in many ways similar to the situation in the thermionic vacuum diode, where Child's law gives $J = (4\sqrt{2}/9)e^* (q/m)^{1/2} V^{3/2}/L^2$; the difference is that in vacuum the charge moves with constant acceleration instead of at the constant velocity uV/L. Eq. (3.6) is modified if the

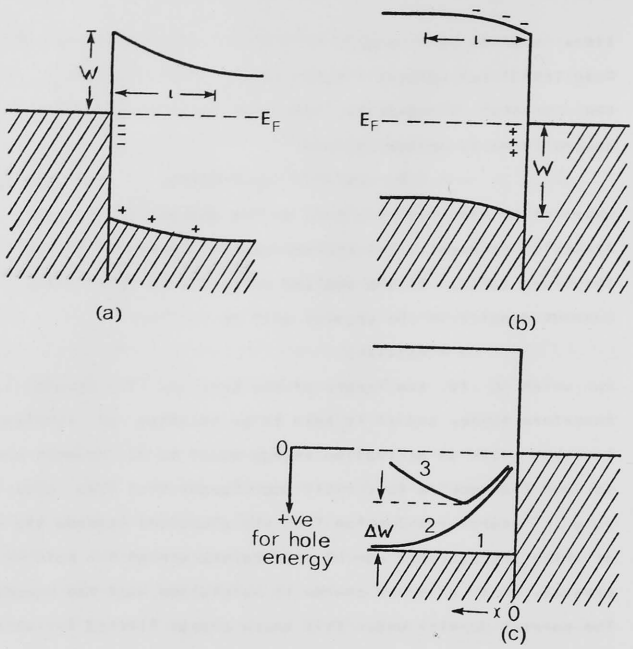

Fig.32

SCHOTTKY BARRIERS TO (a) ELECTRONS, (b) HOLES ; (c) : see text

carriers are trapped; the various cases corresponding to different trap distributions and the situation that the drift mobility may become itself field-dependent have been considered by Caserta et al. (1969) and Murgatroyd (1971).

[b] In the case of space charge limited conduction discussed above, W is assumed small. This in fact is not the common situation. More often, a blocking contact is formed, where W is large, forming an energy barrier which not many carriers can surmount to get into the crystal (Fig. 3.2 (a) & (b)). Still, when the applied field is high enough, the barrier height may be so much reduced that significant emission is obtained and an appreciable current flows. This case of field-injecting electrodes has been considered by Schottky (1938). (Note: Some authors, e.g. Mark & Gora (1974), do not refer to field-assisted emission as injection, reserving the term for what we have called thermal injection. This distinction will not be made here; it is unnecessarilly restrictive and apparently seldom recognised.) The model is shown in Fig. 3.2 (c) for the case of hole injection; the situation of electron injection is completely analogous. Band-bendings are ignored (see below) so that the valence band edge is approximated by the straight line labelled '1'. When a hole is emitted into the crystal, it induces a negative charge in the metal. Hence, it does not have the full potential energy W until its distance from the interface, x, is infinite. With

the image force included in consideration, the barrier profile is modified to '2': $W=q^2/(4\pi ex)$. Finally, when a field F is applied to the electrode, which is made positive relative to the counter electrode, the voltage is assumed to drop uniformly inside the crystal. The barrier profile is then

$$W' = W - qFx - q^2/(4\pi ex) \qquad (3.7).$$

The minimum can be found at once to be

$$W - \Delta W = W - (q^3F/4\pi e)^{1/2} \qquad (3.8).$$

The field-assisted thermionic emission current density is

$$J = [PT^2\exp(-W/kT)]\ \exp[q(qF/\pi e)^{1/2}/2kT] \qquad (3.9),$$

where P, the Richardson-Dushman constant, is $4\pi(m*/m)qk^2/h^3$ = ca. $1.2(m*/m)$ 10E4 A/m^2K^2, where m* is the effective mass of the electron in the metal.

Let us now examine the effect of the actual bending of the band edge. In the crystal adjacent to the interface, there is a region where free electrons have flowed into the metal to allow the fermi levels on both sides to align. The length of the resulting electronic depletion layer is (Simmons 1968) :

$$l = (2eW/q^2n)^{1/2} \qquad (3.10).$$

Here n is the density of conduction electrons in the crystal. As we have mentioned before, in ionic solids which have large band gaps and deep impurity levels, n will be small. Hence l may be of considerable magnitude. If e.g. W = 1 eV, n = 10E15 /cubic-m and if the crystal has a dielectric constant of 10, then l is ca. 1 mm. The condition that l, the space-

charge length before application of external field, is large guarantees that the straight line approximation, 1, used in deriving (3.7) is perfectly adequate, even if F is not very large. (On the other hand, the fact that n is so large in metals underlines our implicit assumption that the metal side of a contact can be considered free of any space charge.)

[c] Charge carriers may tunnel from the fermi level of the electrode into the conduction band of the crystal. The process can be either thermally-assisted, or field-assisted alone (i.e. field emission). The tunnelling may also be directly to the fermi level of the counter-electrode, but this mechanism is important only if the insulator is an ultra-thin film and will not be considered here. A unified theory for thermally-assisted tunnelling (TAT), field emission and over-the-barrier thermionic emission (which we have described already as (b) in the above) has been presented by Tantraporn (1964). In this approach it becomes possible to identify discrete regions on a temperature-field plot in which each of the three mechanisms is predominant. The field emission, governed by a modified form of the Fowler-Nordheim Equation, will not be discussed because of its relative insignificance at room temperature for fields less than about 300 MV/m, given the usual orders of magnitude of W, e, and m. It remains necessary to consider the TAT emission, which has been calculated by Roberts and Polanco (1970) by a W.K.B. approximation. Although

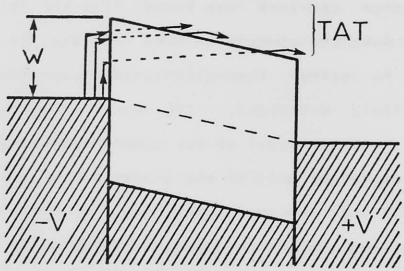

Fig.33

THERMALLY-ASSISTED TUNELLING OF ELECTRONS

FROM A METAL INTO AN INSULATOR

the appropriate equations cannot be solved analytically to give the current density, they found that the following empirical relation fitted within 3% of the computer-generated results:

$$J = B \exp(-W/kT) \exp[(C+D/kT)F^{1/2}] \qquad (3.11).$$

Here $B = 7 \times 10E11$ A/square-m, $C = 10E-4$ $m^{1/2}/V^{1/2}$, and $D = 10E-5$ $eV.m^{1/2}/V^{1/2}$. This relation applies, however, only for the ideal case of a trapezoidal potential hill (Fig. 3.3), in which band-bending and image forces are neglected.

3.2 SUGGESTED MECHANISM OF CONDUCTION IN SILVER AZIDE UNDER STRONG FIELDS

In the preceeding pages we have presented a brief review of the various mechanisms by which current may be carried in an ionic crystal, besides that of ohmic ionic conduction. In the present case of silver azide, all those three which take place in the bulk may be rejected at once. They are unimportant until F approaches at least 100 MV/m, more than three orders of magnitude higher than F* (Section 2.5.2) which is a globally averaged value. The bulk effects can therefore be ruled out. Incidentally, at a bulk field of such magnitude, some processes which lead to dielectric breakdown are already feasible (see Section 7.3.2).

As to the electrode effects, space charge limited conduction appears unlikely since [1] at low fields, the current has been established by several authors as mainly ionic

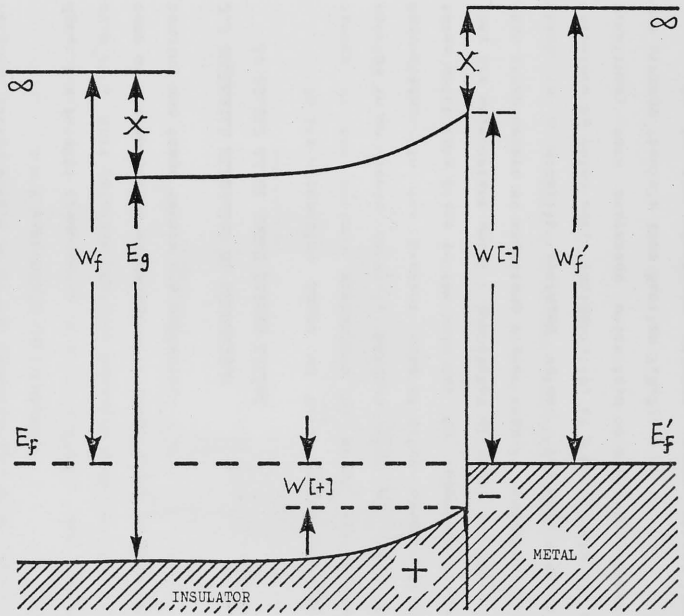

Fig.3.4 IDEALISTIC ENERGY DIAGRAM FOR A METAL-INSULATOR CONTACT ($\phi<\phi'$)

(Section 2.3), and [2] the activation energy (1.1 eV) of low-field conductivity which we have measured is relatively high. If this activation energy is identified as W (and not as in Section 2.6), then from (3.4) n is about 10, an utterly negligible space charge density. Indeed, from general experience with semiconductors we will be quite surprised if thermally injecting contacts to an azide have been achieved without elaborate treatment of its surface and careful choice of electrode materials. For Schottky (field-) emission we may, considering a silver azide crystal of cross-section (150 um) and at room temperature, calculate from (3.9) that the current is, in A,

$$I[S] \approx \exp(-40W + 0.015F^{1/2}) \qquad (3.12),$$

if W is in eV and F in kV/m. Here F is the local field near the electrode and may be different from the bulk value. Similarly, from (3.11) the TAT current is numerically

$$I[TAT] \approx (10E4)\exp(-40W + 0.016F^{1/2}) \qquad (3.13).$$

Let us now consider the likely values of W. The electron energy diagram for a metal-insulator interface, after thermal equilibrium has been attained by the electrons on the insulator side, is shown in Fig. 3.4 where the bands of the insulator bend up to take up the contact potential between the insulator and the metal. The contact potential arises from the difference between the work function Wf of the insulator and that of the metal, Wf', both of which are measured from the

corresponding fermi levels to the vacuum level. The electron affinity, X, of the insulator is the minimum energy that has to be given to an electron in the conduction band for it to escape to infinity. The diagram has been drawn for the case Wf < Wf', so that a Mott barrier exists for holes and a Schottky barrier for electrons. If Wf > Wf', then the bands bend downwards and the reverse situation applies. Experimental values of the work functions of silver, tantalum, and aquadag are listed in Table 3.1 below. For silver azide, Wf = 1.6 + 3.7 - (0.8 to 0.9) = 4.4 to 4.5 eV, according to Fig. 2.7. Since silver azide crystal is an essentially ionic solid, it should have a density of surface states less than 10E14 /square-m (Kurtin et al. 1969), so that the real contact will not behave very differently from the limiting situation depicted in Fig. 3.4. (This argument, incidentally, will be invoked again in Section 6.6.1)

Table 3.1 Work Function

Conductor	Face	Wf'/eV	Reference
Ag	(100)	4.64	Dweydari & Mee 1975
	(110)	4.52	Dweydari & Mee 1975
	(111)	4.74	Dweydari & Mee 1973
Ta	(100)	4.15	Protopopov et al. 1966
	(110)	4.80	Protopopov et al. 1966
	(111)	4.00	Protopopov et al. 1966
C(dag)	polycrystalline	5.0	Robrieux et al. 1974

The values for Ag were all measured photoelectrically, those of Ta by thermionic emission, and that of C by contact potential difference.

It will be seen from Fig. 3.4 that the theoretical values of the energy barriers for holes and for electrons are, respectively, $W[+] = Eg + X - Wf'$ and $W[-] = Wf' - X$. In the case of the silver-silver azide contact, $Wf' = 4.52$ to 4.74 eV (Table 3.1), $X = 1.6$ eV, and $Eg = 3.9$ to 4.3 eV (Section 2.2). Thus $W[+] = 1.1 \pm 0.3$ eV and $W[-] = 3.0 \pm 0.1$ eV. With the bands bending up at the contact, hole injection (from the anode) may occur by Schottky emission, and electron injection (from the cathode) by TAT.

When we substitute the above values of $W[+]$ and $W[-]$ into (3.12) and (3.13) respectively, the currents are seen to be negligibly small, if the fields at the electrodes are taken to be the bulk average so that $F \leq$ ca. 100 kV/m. However, the energy barrier values are actually applicable only in the condition when there is no externally applied field. Otherwise, when a current flows, ionic space charges will be set up as we have argued in Sections 2.4.2 and 2.5.2. In front of the anode, there will be a region depleted of silver interstitial ions, and thus a negative space charge arises out of the under-compensation of immobile cation vacancies, accompanied by an induced positive charge of the same magnitude on the anode surface. Adjacent to the cathode, the accumulation of interstitial cations gives rise to a positive space charge, and the cathode surface acquires a negative charge. The presence of such double layers leads to a reduction in $W[+]$

and in W[-]. This phenomenon has been referred to by Pollack (1963) in his investigation of Schottky current in the (Pb - Aluminium oxide - Pb) system. Using the macroscopic average value of E, he found for the emission energy threshold W[-] = 0.64 eV. This value is lower than expected, and he attributed the reduction to the formation of a space charge in the oxide adjacent to the cathode, due to a migration of either Al+++ to vacant nearby interstices in the oxide lattice, or anion vacancies (oxygen deficiencies). In a study on the relationship between time lag and applied field in the breakdown of NaCl, Watson and Heyes (1970) have also postulated the formation of ionic space charge (see Section 7.6).

Let us admit at the outset that we have few accurate data accumulated, but nevertheless we may attempt a semi-quantitative assessment of the plausibility of this picture. Take that the crystal is 1 cm long, and the voltage applied is 300 V (i.e. F ≥ca. F*). It seems reasonable to suppose that a total of 5% drop of the voltage occurs at the interfaces with the two partially blocking electrodes. Assuming a total effective thickness of the interfacial layers of 10 nm, the same as the low-field value deduced in Section 2.5.2, the effective local fields in each layer will be ca. 1.5x10E6 kV/m if they are equal. Putting this value of F into (3.12) and (3.13), we get I[S] about 1 nA and I[TAT] roughly 1 uA. These values are obtained in a speculative way, but nevertheless are in the

expected range within one or two powers of ten. An interfacial field of ca. 1500 MV/m looks excessive, but it applies over a very short distance. In a calculation of field emission in alkali halide crystals due to space charge build-up by photo-excitation, von Hippel et al. (1953) have estimated a field strength of ca. 250 MV/m in cathode regions. These regions were estimated to be effectively about 8 um deep; the crystals in the calculation were 1 cm long to which 1 kV was applied.

An alternative way of looking at the effect of the accumulation or the depletion of interstitial cations is to consider that it reduces the distance over which the band-bending occurs, according to (3.10). The local carrier density is enhanced, so that l becomes so small that the flat-band approximation invoked in the derivation of relations (3.9) and (3.11) leads to gross over-estimation of the energy barriers.

According to our suggestion, therefore, bipolar injections take place at the two electrodes, whenever the applied field is strong enough to cause a large interfacial space charges within a narrow distance. A bipolar injection leads to a much larger current increase than if it is unipolar, since holes and electrons are injected into the crystal at the same time whose overall charge neutrality is maintained. Moreover, the field injection of holes probably automatically creates the conditions for that of electrons, because the holes or azide radicals may combine leading to a non-stoichiometric excess of

Ag^+. It is possible, then, that the non-steady-state behaviour (Section 2.5.2) of the current is due to a fluctuation in the heights of the interfacial energy barriers. This fluctuation can be caused by a number of factors. Those which have been studied are non-equilibrium polarisation (Marcus 1956) and lattice vibrations (Dogonadze et al. 1965). Neither effect seems large enough to account for the observed fluctuations in the current. However, we propose a new mechanism, which may be important in our case because the interfacial layers have been supposed to be very narrow.

When emission or tunnelling occurs, the electron or hole concentration in silver azide is increased to higher than the thermal equilibrium value. The localisation of some of the injected charges at some of the impurity centres and defect systems existing in the interfacial region gives rise to a trap space charge whose polarity is opposite to that of the ionic space charge. (We assume that, near the electrode under consideration, the trap space charge due to carriers injected from the other electrode is negligible since their flux here has been greatly attenuated through recombination and/or combination.) It is possible, in fact, that the interstitial Ag^+ themselves constituting the ionic space charge in front of the cathode can act as electron traps, and the Ag^+ vacancies near the anode as hole traps. A steady-state value, if permitted, of the cathodic or the anodic field will be

determined by the algebraic sum of the ionic and the trap space charges. However, carriers are continually released thermally from the traps, after which they drift outside the interfacial region, and re-set traps are continually refilled by fresh carriers. In the case of ions and vacancies acting as traps, re-setting may similarly take place, except that if they are on the surface (either external or 'internal') then the accretion of neutral Ag, and the combination either of two holes (azide radicals) may occur instead -- cf. Sections 6.5.1 and 6.5.2. There is, therefore, a statistical fluctuation in the length of time, t, that a particular trap remains empty. Such a Δt leads to a corresponding fluctuation in the number of trapped charges, ΔZ. Since the trapping and detrapping events can to a close approximation be treated as causally independent of one another, we may consider that the fractional fluctuation $\Delta Z/Z$ has a mean value of the order of $1/Z^{1/2}$. The net charge density in the interfacial region is $Q = q(N - Z/lA)$, where N is the ion density, if the filled electron or hole traps are all singly-charged.

The relaxation of the ionic space charge should be a slow process so that, when Z varies, N will be assumed to remain constant. By Poisson's equation, the average fractional fluctuation of the interfacial field $\Delta F/F \approx \Delta Q/Q$. Denoting the thickness of the interfacial region by l and the cross-section area by A, let N and Z/lA be given the guessed values of

10E22/cubic-m and 9x10F21/cubic-m respectively, corresponding to a concentration of about 1 ppm which seems a reasonable magnitude. With l = 10 nm and A = $(150\ um)^2$, we then find that $\Delta Z = Z^{1/2} = 1.5x10E3$ and therefore $\Delta F/F = 6.7x10E-3$. Using Eq. (3.12) and the good approximation that $(F\pm\Delta F)^{1/2} = (1\pm\Delta F/2F)F^{1/2}$, we deduce that the current is modulated by the factor $\exp(0.15 \times 3.4x10E-3 \times (1.5x10F4)^{1/2}) = 1.07$. The calculation is speculative, but the average magnitudes of current fluctuations which have been observed do range from a few percent to (occasionally) a few tens of percent, so that the model may appear feasible. However, more investigations are obviously needed to test the model. One way is to study the power spectrum of the fluctuations and its variation with temperature. To be able to give them independent interpretation one need, however, to know the exact nature of the traps and the distributions of the most probable trap time among the different kinds of trap in the crystal. Such knowledge may be gained by, e.g., subjecting the crystal to a low-energy electron beam or to a corona discharge. Cf. the experiments on Myler by Monteith & Hauser (1967) and by Seiwatz & Brophy (1965), respectively.

Lastly, we may mention that Young (1964) has measured the Hall coefficient of well-annealed, compacted, partially decomposed powder. Assuming that the ionic contribution is insignificant in comparison, he deduced for the mobility of

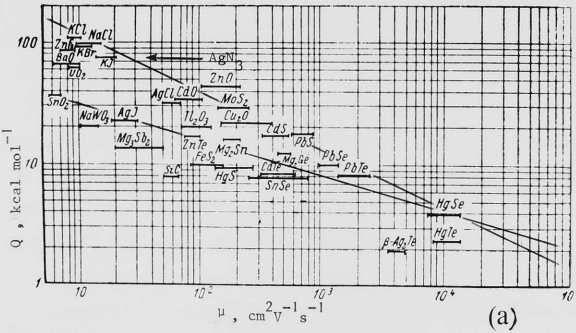

FIG. 3.5

Semi-empirical relations between electron mobility and (a) enthalpy of formation; (b) electronegativity difference (Zhuze 1955)

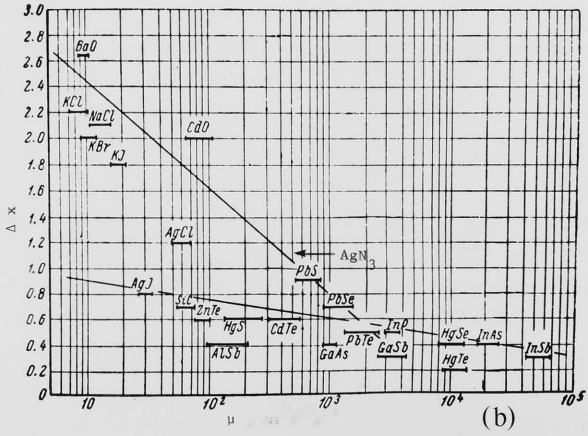

electrons in silver azide a value of (1±0.8) 10E-2 (m/s)/(V/m) at 373 K. We argue here that this seems a reasonable result. To the degree of accuracy appropriate here, the Hall mobility is of course identical to the drift mobility. Now, Zhuze (1955) has found the following semi-empirical relations between the electron mobility u in (cm/s)/(V/cm) and the enthalpy of formation $\angle\Delta H_f$ in kcal/mol, both measured at room temperature

$$u = (1.56 \times 10E5)\ \angle\Delta H_f^{-2}$$
$$u = (1.56 \times 10E6)\ \angle\Delta H_f^{-3.5} \qquad (3.14)$$

for crystals of NaCl and ZnS structures, respectively (Fig. 3.5(a); note non-S.I. units). Silver azide is body-centred, and the electron mobility data for materials of this structure are scarce in the literature. However, silver azide is to a large extent ionic, and the body-centred structure is much closer to the NaCl type than the covalent ZnS structure (Section 2.1). Using the first relation, then, we obtain the tentative assignment that u is about 30 (cm/s)/(V/cm) = 0.3x10E-2 (m/s)/(V/m). Zhuze has also found correlations between u and the difference in electronegativity between the compound constituents, and his diagram is reproduced in Fig. 3.5(b). Using again the NaCl curve, we find u to be around 4x10E-2 (m/s)/(V/m) for silver azide. (The values of its $\angle\Delta H_f^0$ and $\angle\Delta x$ have been discussed in Section 2.1.) The room temperature electron mobility probably has a value intermediate between the two rough estimations. Since the mobility usually

varies inversely with a modest power (0.5 to 1.5) of temperature, this deduction is consistent with the experimental result of Young. Incidentally, the relatively small value of the electron mobility implies a narrow conduction band, but it is not so small that the band picture becomes inapplicable (Section 2.4.2 [a]; O'Dwyer 1973, p.48).

The mobility of holes may be assumed to be some orders of magnitude smaller than that of electrons. They are often trapped fairly deeply in the band gap, and to drift they have to be thermally excited into non-localised states (cf. Klein 1978). With a trap depth of merely a few tenths of a eV, the trap-controlled mobility at room temperature falls to a tiny fraction of the band mobility.

More exact knowledge of the transport parameters is obviously needed to achieve a quantitative understanding of the strong-field conduction in silver azide. It may be recorded that we have attempted to measure, using single crystals, the electron drift mobility by transit time experiments. However, the current waveforms obtained using photo-injection as well as electron beam excitation were all different in structure, and no transit time could be determined. Hall effect experiments were also carried out, again without success; the samples used were fresh crystals illuminated with mercury arc lamp.

FIG. 3.6

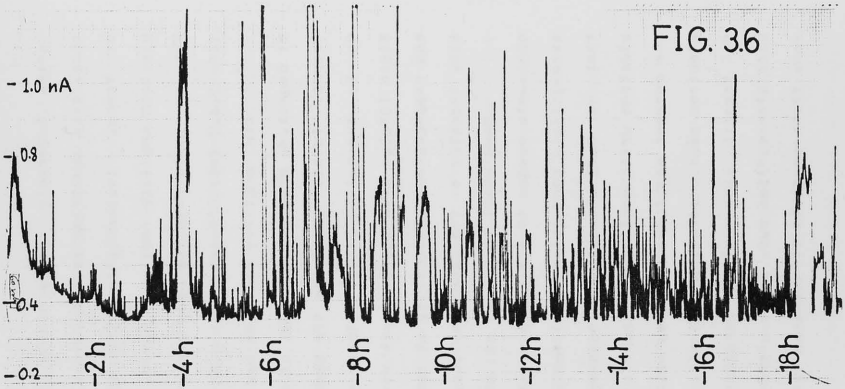

FIG. 3.8

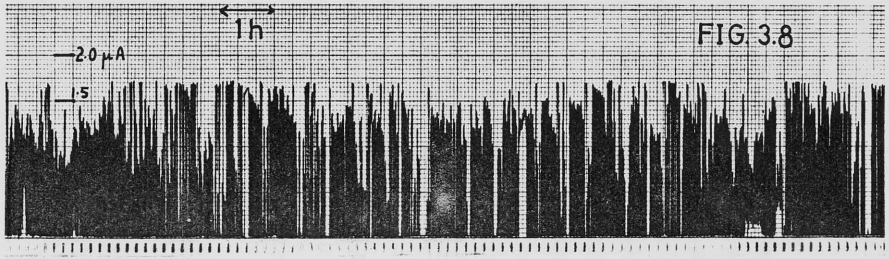

(a)
(b)

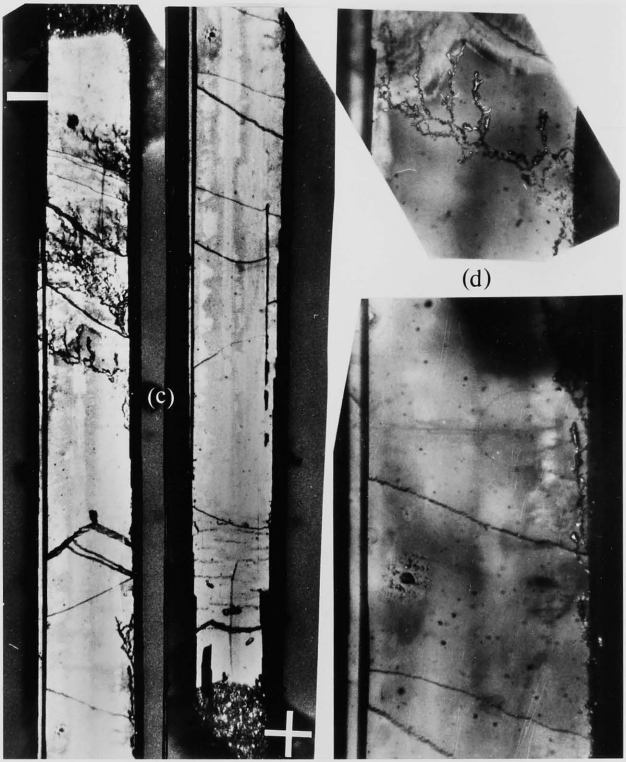
(c)
(d)

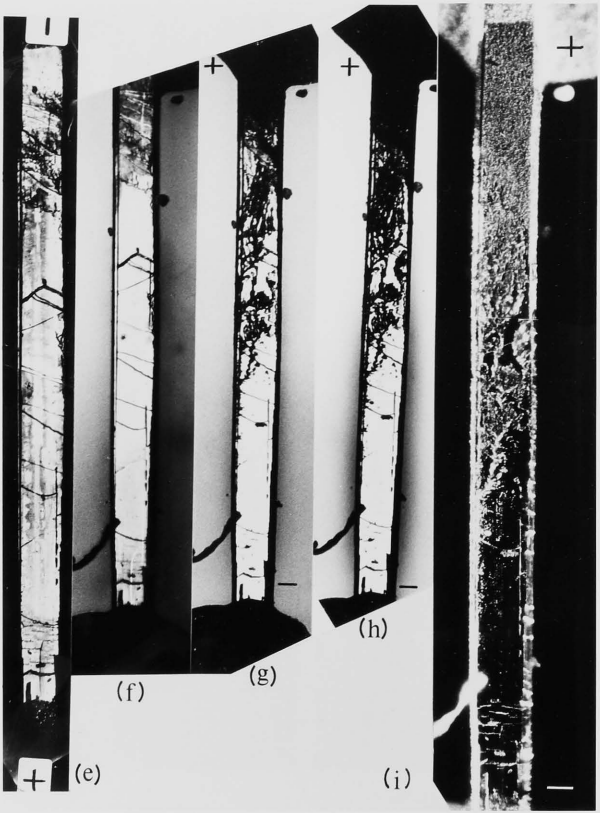
+
(e)
+
(f)
+
−
(g)
+
−
(h)
+
−
(i)

(j)

3.3 DECOMPOSITION UNDER CONDITIONS OF CURRENT INJECTION

3.3.1 Observations

In the above we have outlined, as a plausible postulate, an explanation of the current instability in silver azide conducting under a moderate or strong field. However, it was observed (Section 2.5.2) that with the application of a moderate field, the non-steady character of the current changes after a period of time. Fig. 3.6 shows the current-time behaviour when 60 V was applied to a crystal, the inter-electrode (silverdag) distance being 1.8 mm , so that the field is 33 kV/m > F*. It is seen that the current, in addition to fluctuating, displayed 'blips' (large jumps) after 4 h. The 'blips' are reversible changes, so that there remains a steady 'dormant' current level, but their amplitudes are distinctly larger than the fluctuations we have so far discussed.

The sample was observed under an optical microscope, this being the simplest way to find out if the remarkable current behaviour is accompanied by any structural changes of the crystal. In Fig. 3.7(a) are transmission micrographs of its two ends before any voltage was applied. Fig. 3.7(b) was taken after it has conducted for 19 h, (c) shows the same specimen in reflected light, and (d) gives the details. It is

<<--

FIG. 3.7
Refer to text for descriptions of micrographs;
scale: visual width of the crystal is 135 um

apparent that some tree-like formations have grown out on the crystal surface, their protrusion being suggested by the bright reflections seen in (d). These formations appear to have spreaded from the cathode. Near the anode, the bulk has apparently suffered some fractures (transmission micrograph (b)) and on the surface are found lines of 'dots' ((c)).

The crystal was then left in an evacuated dessicator and kept in the dark for 28 days. As seen in Fig. 3.7(f), the surface formations did not disappear and are thus permanent. A voltage of 60 V was applied again but in opposite polarity to that before. The current displayed fluctuations as well as 'blips' right from the beginning. Figs. 3.7(g) & (h) show the crystal after 5 and 10.2 h, and (i) & (j) are the same as (h), except that (i) was taken in oblique reflected light and (j) at a higher magnification. The tree-like formations are seen to continue growing on what had become the anode side, but on which now are also found the 'dots'.

After the appearance of the tree-like formations, the crystal became strongly photoconductive in a He-Ne laser light (photon energy 1.96 eV). This probably indicates the presence of metallic silver, which gives donor levels. Also, averaged over a period of an hour or so, the 'dormant' current level rose gradually and, more dramatically, the 'blips' increased in amplitude. At (h) dielectric breakdown seemed imminent. To prevent this, a current-limiting resistor was added in series

(a) (b) (c)

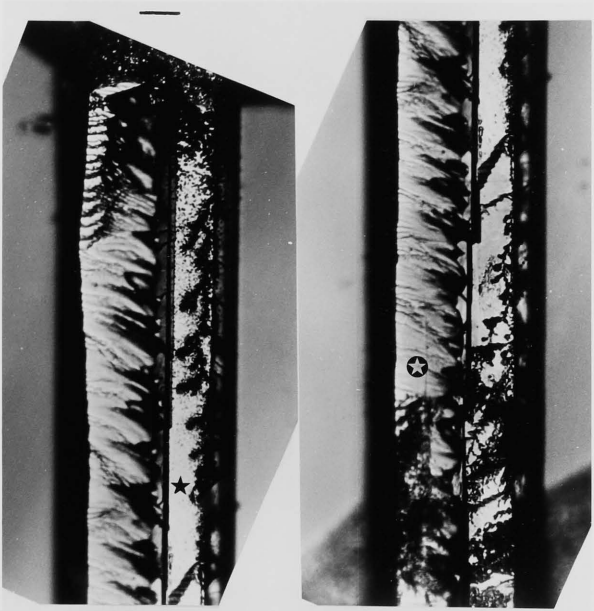

(d)

(e)

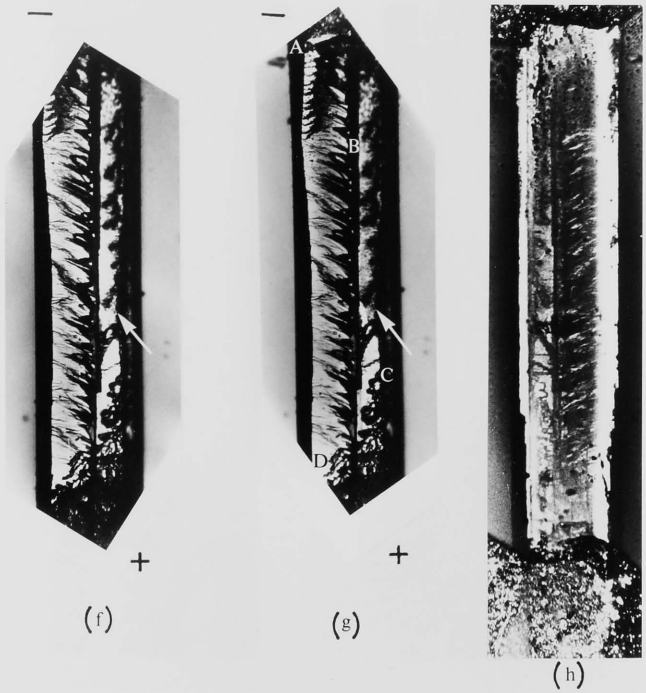
—
+
(f)
—
A
B
C
D
+
(g)
(h)

in the external circuitry. It was then found, by using different voltages and different series resistances, that fields as low as 5.5 kV/m would also lead to breakdown and that at the peak of a 'blip' the crystal resistance could have dropped to as small as 10E5 ohm. Fig. 3.8 illustrates the case of applied voltage being 10 V and series resistance 5.5 M-ohm.

Fig. 3.9(a) shows another crystal, where the silverdag electrodes are separated by a distance of 0.70 mm. Alternating voltages were applied for 16 h (at 20 kHz) and for 23 h (at 2 kHz), both of 30 V peak-to-peak. Fig. 3.9(b) indicates that little or no changes have taken place on the crystal surface. A DC field F of 129 kV/m $\geq$ F** was then applied through a series resistance of 29.5 M-ohm. Figs. 3.9(c) to (g) are photomicrographs taken at 5-minute intervals; the arrows and stars there mark areas where new features were formed during each stage. In (g) a whole area, from the cathode to where the white arrow points, has gone distinctively brownish in colour. Micrograph (h) shows the reverse sides of the crystal, where much less changes have occurred.

Fig. 3.10(a) to (f) are scanning electron micrographs taken with a Cambridge Stereoscan S4-10. (See Section 6.2 for more details of micrography by S.E.M., which was extensively

<<--
FIG. 3.9
Refer to text for descriptions of micrographs;
scale: visual width of the crystal is 143 um

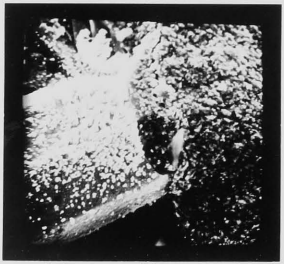

(a) 150

(d) 300

(b) 75

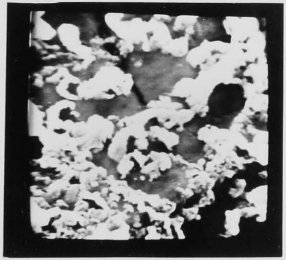

(e) 30

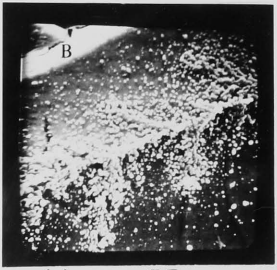

(c) 75

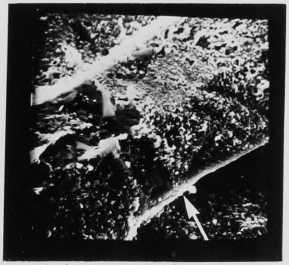

(f) 150

used in the study of silver azide pyrolysis.) The tree-like formations were resolved into clusters of 'pebbles' projecting out of the surface. In addition, an evaporated carbon film mounted on a transmission electron microscope grid was pressed against them so that some adhered to the film. In this way, they were shown to contain silver by energy dispersive X-ray analysis, for which a Link System incorporating a Kever series 3000 Li-drifted Si detector with a 1 mil beryllium window has been used. They are observed to be inert under the electron beam and, therefore, are metallic silver.

The amount of silver on the surface has been estimated visually at different times and, although such a measurement is obviously highly approximate, it suggested that the rate of production greatly decreased towards the later stages. The experiments to be described in Section 3.4 were more quantitative in nature and supported this observation.

The 'pebbles' found on the anode side (Fig. 3.10(d)) have a 'hillock' shape like that of surface mass accumulations produced in the electromigration of aluminium (Gangulee & d'Heurle 1975). However, an electrotransport of materials from the electrode through the crystal over distances of the order

<<--
FIG. 3.10
Electron micrographs of surface formations in Fig. 3.9(g), the letters indicating correspondence;
The arrow in (f) points to the extent of the silver-dag painted electrode on the lower side;
The number beneath each micrograph gives its width in um

mm, whether by a lattice or surface diffusion or by a dislocation migration process, can safely be ruled out in our case where the temperature is low and current density small. This is confirmed by a short experiment on a sample having C-dag electrodes, which after being subjected a field of 165 kV/m for 5 min, also produce silver 'pebbles'. On the other hand, we shall find that silver atoms do have a significant surface diffusivity enabling them to migrate at room temperature, a point we shall shortly consider.

3.3.2 Discussions

As we have said in Section 1.5, when a heavy metal azide decomposes the solid product is the metal. It requires therefore little imagination to infer that decomposition may be occurring in silver azide when a moderate to high field is applied to the crystal through conducting electrodes. We supported this conjecture by looking for the other end product, namely nitrogen gas. This result, to be described in the next section, also serves to confirm that the silver aggregates do not come from any ions injected from a silver anode. Harris (1968) has shown that dislocations and subgrain boundaries in KBr were decorated with silver, after a prolong application of a strong field through silver electrodes to the crystal.

It may be seen at once that the decomposition is not electrolytic, because the silver formed would then be confined to the cathodic interface (cf. von Hippel 1937). Moreover, as

we have just argued in Section 3.2, most of the current in the present situation is carried by injected electrons and holes. Using the low-field conductivity to predict the ionic part of the strong-field fluctuating current, we estimate that the rate of silver concurrently formed by electrolysis is insignificant compared to that observed, the more so the higher the field.

It is natural to guess that the the underlying processes in the phenomenon, which we shall call 'electrical decompositon', are closely related to the condition of bipolar injection: they appear not to occur at low DC fields (Fig. 2.14), nor under high frequency fields (Fig. 3.9(b)) when field enhancement by ionic polarisation is absent. To examine the actual mechanism involved and to explain the current 'blips' observed (which we shall do in Sections 7.1 & 8) require, however, an understanding of the detailed course of the decomposition; this we shall offer in Chapter 6, where our kinetics experiments and their interpretations will be described. Here we confine the discussion to the topographical features of the phenomenon. Surface 'pebbles' appear to initially grow more on the cathode side, where electrons are injected, but at later stages can be found throughout the crystal. Their distribution is non-uniform between different crystal surfaces. On the anode side, internal cracks are formed. Holes are injected from the anode and, if they are responsible for the formation of the cracks which in contrast

seem not to spread towards the cathode as time goes on, the process must be one which mainly occurs near where the holes are generated. If the polarity of the applied voltage is changed (Fig. 3.7(e) to (j)), cracks are apparently formed on the new anode side but most of the additional pebbles are produced where they are already concentrated, i.e., on the original cathode side.

We have also observed, and Fig. 3.9(g) shows this most clearly, that, at later stages, the crystal face on which pebbles are distributed becomes uniformly coloured. We shall take this to imply the permanent existence of a relatively thick silver film. We can show here that the presence of silver films as well as pebbles has a unified origin. That silver evaporated on alkali halide crystal surfaces have large surface diffusivities at temperatures not much higher than half the melting point of the halide, has long been known (e.g., Grigorovici et al. 1961). By taking transmission electron micrographs of extraction replica of a silver azide surface on which silver has been evaporated, McAuslan (1957) argued that the silver atoms migrate very fast on the surface and will aggregate at little above room temperature. The situation in which silver is continuously condensing from vapour may be analogous to the generation of silver by electrical decomposition. Montagu-Pollock (1962) in his study on the surface decomposition of silver cyanamide, has also put forward the

concept of a mobile film of silver existing on the cyanamide. We conclude, therefore, that the production of silver atoms is initially distributed, the formation of compact pebbles being by the secondary process of accretion. A patch of continuous and thick (permanent) silver film appears only when a very large number of atoms have been produced in that area.

Our discussion here ends with a review of two earlier works reported in the literature, which have a bearing on electrical decomposition. In the experiments of Sukhushin et al. (1973), single crystals of silver, thallous and lead azides (average dimensions 1.5 x 0.25 x 0.1 mm) were placed between two gallium electrodes, put in cells filled with paraffin oil, and observed under the microscope. After the application of a voltage, the crystal was removed, washed free from oil with benzene, and then placed in another cell where it was slowly etched (by 0.1 N solution of ammonium hydroxide, distilled water at 320 K, and mono-ethanolamine for silver, thallous and lead azides, respectively).

Beginning with a field strength amounting to about half the 'breakdown value' (meaning, as we judge from the published graphs, 0.15 and 0.5 MV/m for silver and lead azides respectively), they noted irreversible changes consisting of specifically distributed gas formation and separation of solid products. The observations (Fig. 3.13) agree on the whole with ours, which are more detailed. However, our approach has been

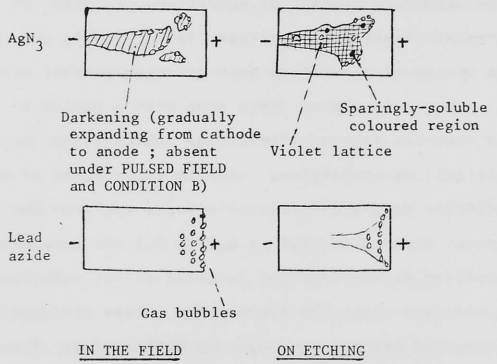

FIG. 3.13

Observations by Sukhushin et al. (1973) on changes in silver and lead azides crystals after conducting under strong fields (case of thallous azide investigated but not shown in the original paper)

to begin the investigation by looking at the effects of moderate fields over extended periods of time. Thus, we showed that silver is produced at fields as low as F* =ca. 15 kV/m, a tenth of the critical value according to Sukhushin et al. More importantly, but probably also consequently, the mechanism they proposed to explain the decomposition in a strong field involved electronic avalanche that somehow developes, and is very different from ours. The question of mechanism will be discussed in Section 7.1, after a case has been built up for the one we shall put forward.

In a later publication, but apparently unaware of the closely related work of Sukhushin et al., de Panafieu et al. (1976) reported that placing an electric field across a heated potassium azide crystal led to additional decomposition. The experimental temperature range was 500 - 540 K, and stainless steel grids were used as the electrodes. They interpreted the phenomenon as field enhancement of the pyrolysis and suggested a mechanism based on the polarisation of azide ions by the surface dipole layer, which reduces their stability and which is increased by the application of a field. We agree that such a field effect should exist but think that its magnitude is insignificant, at experimental ranges of the applied field, in potassium azide and in the case we are interested in.

The case of silver azide will be considered in Chapter 7. For potassium azide, from the published data concerning the

vacuum system and a graph showing the effect when 300 V was applied, we calculate that nitrogen evolution rate was ca. 2x10E11 molecules/s and that the (single-)charge carrier flow rate was 3.5x10E11 /s. The calculated ratio of the two rates being so close to the value of 2/3, it appears highly probable that the phenomenon is purely a classical solid-electrolyte process, in which azide ions are discharged at the anode to produce nitrogen and their rate of arrival was recorded as a conduction current. The authors reported that an increased pyrolysis rate was observed for both polarities of the applied field when one electrode was a thick evaporated gold film, but the enhancement was larger when the grid electrode was positive. Our explanation (which they also have briefly considered) for the effect when the grid was negative is that anion vacancies are being moved away from this region and the surface thus obtains an excess of K adatoms. This increases the rate of pyrolysis due to 'autocatalysis' (Section 6.6.1) -- it has been shown that potassium azide decomposes faster when a vapour of K is maintained over the surface (Garner & Marke 1936; Jacobs & Tompkins 1952; Young 1966).

To return to our investigation of electrical decomposition we describe, in the following section, the detection by mass spectrometers of the other end product of decomposition, i.e. nitrogen. Measuring decomposition rate in this way is obviously more sensitive and exact than the semi-quantitative

technique of estimating the volume of silver produced at different times.

3.4 MASS SPECTROMETRIC STUDY OF ELECTRICAL DECOMPOSITION

NOTE : Due to the calibration of our measuring instruments, pressures and partial pressures are given here in Torrs.
1 Torr ≡ 101325/760 Pa =ca. 10E2 Pa.

3.4.1 Experimental

Two ultrahigh vacuum (UHV) systems have been used. One incorporates a quadrupole mass spectrometer (Varian R.G.A. model 974-0002), the other, a time-of-flight mass spectrometer (Bendix RGA-1A) with an ion flight tube 0.2 m in length. To both systems are attached a molecular sieve sorption and a sputter-ion pump, whose operations are contamination-free, and the latter of which need no vapour trap that has to be periodically filled with liquid nitrogen. Also fitted in both systems are a pirani and an ionisation gauge (Vacuum Generators IGP 3), for measuring the total pressure, and a leak valve. Compared with conventional manometry, the UHV technique offers higher sensitivity and, by allowing the use of residual gas analysers, specificity in the measurement of gas evolution; these advantages have been mentioned by Walker (1967). The operations of the quadrupole and the time-of-flight R.G.A. have been described in ibid. and (Patel 1978), and in (Hauser 1977),

respectively.

In previous quantitative works (Walker et al. 1966, Soria Ruiz 1968, Fox 1970, Patel 1978) using these mass spectrometers, thermal decomposition was investigated so that the maximum partial pressure increase in each experimental run could be assumed to correspond to 100 % decomposition of the crystal under study. In our runs, the (electrical) decomposition did not proceed to completion and the final pressure attained had no special significance. Therefore, the current outputs of the the spectrometer-electron multipliers required calibration so that the sensitivities (in say amps/Torr) would be known.

We had at first calculated the sensitivity by operating the spectrometer in the scanning mode and then dividing the sum of peak heights in the output by the total pressure as read from the ionisation gauge. However, in either case the results obtained at different pressures, as the UHV system was gradually pumped down, were found to vary by a factor of up to 5. This we decided was due to the changing gas compositions together with the dependence of the sensitivity on specific gas species both for the spectrometer and for the gauge. We therefore next measured particularly the spectrometer sensitivity to N_2^+, at the chosen operational conditions like the setting of the electron multiplier gain, and at a total pressure inside the UHV system between 5x10E-9 and 10E-7 Torr.

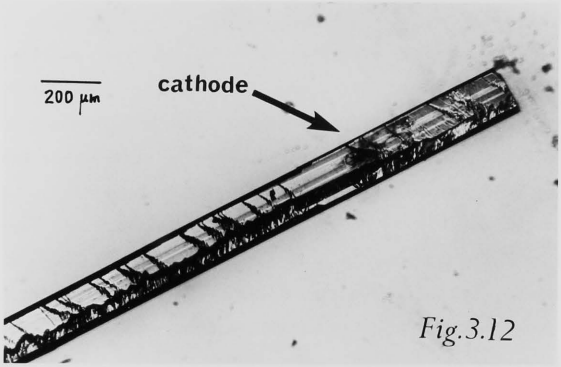

Fig.3.12

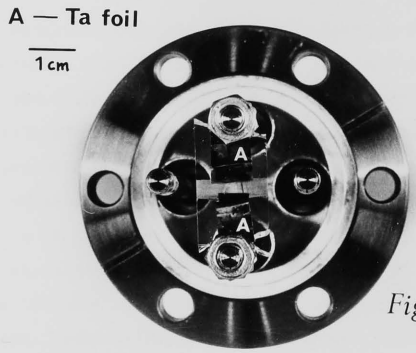

Fig.3.11

This was done by introducing through the leak valve a small quantity of nitrogen (British Oxygen, spectrometrically pure grade) and then correlating the m/e=28 peak height with the ionisation gauge reading. The spectrometer sensitivity so obtained was constant (and presumed accurate) to within 25%; the gauge sensitivity to N_2^+ had been accurately specified by the manufacturer. Within the same system pressure range, the resolution of nitrogen partial pressure was found to be ca. 10E-9 Torr for both spectrometers.

The crystal under study was placed across a grove cut on a quartz plate, each of whose ends were fixed in position by two nuts screwed onto a conductor rod of an electrical feedthrough. (Alumina plates had been tried but were found to have less satisfactory electrical and vacuum properties.) A third nut on the top held a tantalum foil which made a mechanical pressure contact to one end of the crystal and served as an electrode. (See Fig. 3.11.) The whole assembly fitted into either of the UHV systems, with the crystal within 5 cm of the ion source of the spectrometer.

In all, three samples have been studied. The experimental procedure was as follows. With the sample put inside, the UHV system was evacuated. When the vacuum levelled off at a pressure of the order 10E-7 Torr, the system was baked with heating tapes for periods of about 6 h each. Longer periods of continuous heating were avoided, to prevent

decomposition of the crystal despite its thermal insulation. In the case of the quadrupole spectrometer, the ionising filament was degassed simultaneously in the later periods of baking; this was sparingly done for that in the time-of-flight spectrometer, because of its much shorter rated life. The final working pressure attained, after 5 or 6 bakings, was generally about 5x10E-9 Torr.

During decomposition, when a voltage was applied across the sample, the evolution of nitrogen was followed by monitoring the increase of the 28 a.m.u. peak with an electrometer (Keithley 610B) which in turn drove a chart recorder. (That peak is of course also attributable to CO+ due to the coincidence of mass to charge ratio, but its possible contribution may safely be ignored in our situation.) The monitoring was carried out in two ways. In the earlier series of experimental runs, the sputter-ion pump was first isolated from the UHV system. The parts of the partial pressure-time curve before and after the application of the voltage were observed to be linear and quite parallel to each other. Therefore, any evolution of nitrogen immediately after the removal of the voltage must be at very low rates. Also, the net background pressure rise in nitrogen due to filament outgassing, leaks from the atmosphere and to the sputter-ion pump, and pumping of the ionisation gauge and the spectrometer ion source could therefore be assumed given by the extrapola-

tion of the initial part of the pressure-time curve, and subtracted from the second part obtained when the voltage was on. The adsorption of nitrogen on the walls must have been proportionally quite insignificant, so that its pressure dependence was not passed on to the background rise rate, which was thus virtually a constant throughout. On the other hand, it was necessary to estimate the background rise individually in each experimental run, since the closing (manually) of the isolation valve to apparently the same position did not always lead to the same background rate.

The drawback in the above procedure is that, because of the accumulative rise of pressure, the usuable length of experimental time was limited to 4 or 5 minutes. The later series of experimental runs were therefore carried out under the condition of non-zero pumping speeds, when the isolation valve between the ion pump and the UHV system was left in a half-open position. The resulting base pressure was then higher, about 1 to 5x10E-8 Torr. In the next section we shall describe how we derive the decomposition rate from the pressure-time curves so obtained.

In the first few runs on a fresh sample, the rates of nitrogen evolution were generally found to be greater by up to an order of magnitude than those in subsequent runs at the same voltages, the rates of which were quite consistent -- unless the crystal became highly decomposed, when they dropped (see

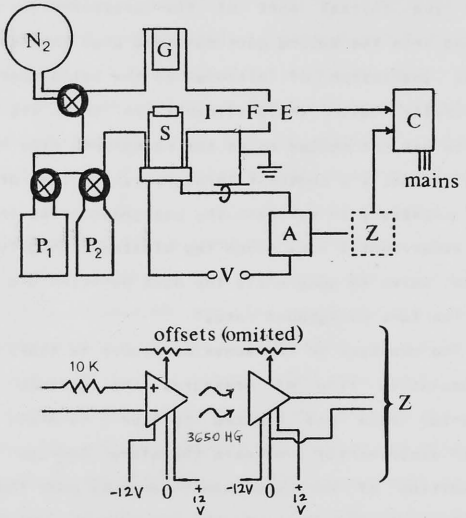

Fig. 3.14

P_1 Sorption pump; P_2 Sputter-ion pump; S Sample;
G Ionisation pressure gauge; I Ion sourse;
F Filter; E Electron multiplier;
V Power supply; A Nanoammeter;
Z Isolation amplifier; C Chart recorder

later). It may be recalled that the low-field electrical conductivity also decreases initially (Section 2.5), and the two phenomena may be related. Otherwise, a possible explanation is that the additional evolution is due to desorption of nitrogen on the crystal surface. The quantitative results, to be given in Fig. 3.16 below, were obtained from subsequent runs made consecutively within a few hours.

There was one final complication. We discovered that the quadrupole spectrometer induced a current of the order 1 nA in the specimen circuit and, more importantly, its electric fields interacted with the one applied across the specimen resulting in spurious increases of all peaks (N_2^+, H_2^+, CO_2^+, etc.) in its output. These interference effects were virtually eliminated when the specimen voltage was floated, so that no electrical connection existed between the two circuits through earth. This was achieved by using a battery bank for the voltage source, a battery-operated DVM (Keithley 160B) to monitor the specimen current, and an isolation amplifier for the DVM analogue output to eliminate earthing through transformer coupling in chart recorder. (See Fig. 3.14.) There was no problem of interferences in the case of the time-of-flight spectrometer, which was, however, slightly less sensitive and accurate because of its bigger volume.

3.4.2 Results and Discussions

After the passage of currents, the crystals were taken

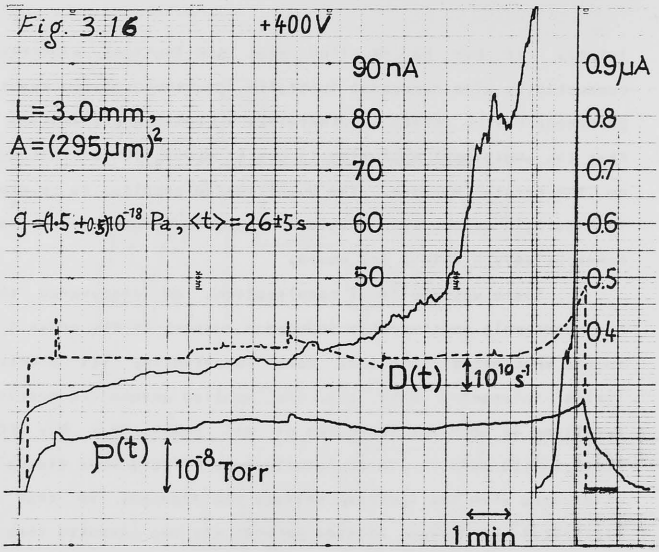
Fig. 3.16
+400V
L = 3.0 mm,
A = (295 μm)²
g = (1.5 ± 0.5) 10⁻¹⁸ Pa, ⟨t⟩ = 26 ± 5 s
90 nA
80
70
60
50
0.9 μA
0.8
0.7
0.6
0.5
0.4
D(t) ↕ 10¹⁰ s⁻¹
p(t) ↕ 10⁻⁸ Torr
↔ 1 min

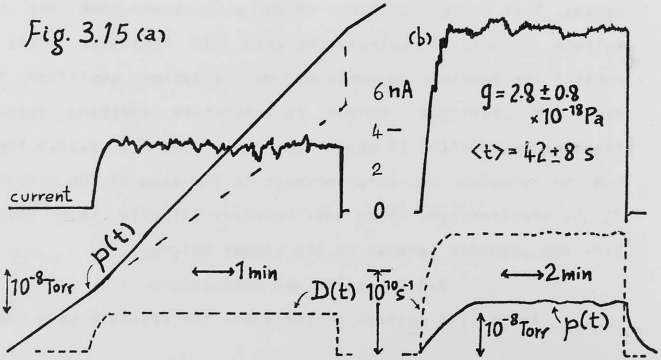
Fig. 3.15 (a)
(b)
6 nA
4
2
0
current
g = 2.8 ± 0.8 × 10⁻¹⁸ Pa
⟨t⟩ = 42 ± 8 s
10⁻⁸ Torr
p(t)
↔ 1 min
D(t) 10¹⁰ s⁻¹
↔ 2 min
10⁻⁸ Torr
p(t)

out and brownish-coloured regions were clearly visible especially towards the cathode sides. Fig. 3.12 is a typical micrograph, showing similarities of these physical changes to those discussed already in Section 3.3.1.

The analysis of pressure-time curves measured with the valve closed is straight-forward. It will be assumed that the gas is uniformly at the constant room temperature T. By calculating geometrically the volume V of each of the UHV system-spectrometer assembly and using the universal gas law, we can convert an increase of partial pressure, Δp, into that of nitrogen molecules, ΔN (table below).

Table 3.2 Conversion Factors

System	V / 10E-3 cubic-m	Δp / 10E-9 Torr	ΔN / 10E10 molecules *
Quadrupole	1.5 ± 0.1	1 ±0.25 **	5 ±1.5
Time-of-flight	2.6 ± 0.3	1 ±0.25 **	9 ±3

* : $\Delta N = (V/kT)\,\Delta p$ see below;
** : estimated error of spectrometer readings

A typical pressure-time curve and its interpretation are given in Fig. 3.15(a), which shows also the current through the crystal; this particular measurement has been obtained with the quadrupole system, as was also the case for Fig. 3.15(b) which will shortly be discussed. A general observation from these curves is that although the decomposition rate appears to take a significant length of time in reaching its steady value after

the application of a voltage step, it ceases essentially abruptly the moment the voltage is removed.

Our analysis of curves obtained with the valve partially open, illustrated by Fig. 3.15(b), is as follows. Denoting the number of nitrogen molecules in the whole system by N, we consider all its sources and sinks and write its rate of change as:

$$dN/dt = B + D(t) - p'(t)\,P/kT \qquad (3.15),$$

where B is the net background rate of nitrogen evolution and as before assumed to be a constant throughput, D, the additional evolution rate from the crystal, p' the partial pressure measured of nitrogen, and P, the pumping speed through the valve and should be a constant volumetric flow rate. Now, before any voltage is applied, the base pressure p* is steady and from (3.15),

$$0 = B + 0 - p^*\,P/kT \qquad (3.16),$$

so that B is readily obtained as p* P/kT. Substituting this back into (3.15) and introducing the experimentally more direct variable, namely, the pressure rise $p \equiv p'-p^*$, we have

$$(V/kT)\,dp/dt = D(t) - pP/kT \qquad (3.17).$$

This may be written in the commonly recognised form of first-order linear differential equation with constant coefficient:

$$dp/dt + p/\langle t\rangle = g\,D(t) \qquad (3.18),$$

where $\langle t\rangle \equiv V/P$ and $g \equiv kT/V$. In the case that $P \to 0$ so that $\langle t\rangle \to \infty$, this equation reduces to the situation in

Table 3.2. Its solution, when P is finite, is elementary:

$$p = g \exp(-t/\langle t\rangle) \int_0^t D \exp(t/\langle t\rangle)\, dt \qquad (3.19),$$

and if D equals a constant d between t = 0 and t* but is zero afterwards, then for $t \leq t^*$:

$$p(t) = g\, d \langle t\rangle [1 - \exp(-t/\langle t\rangle)] \qquad (3.20a),$$

and for $t = t^* + t'$, $0 \leq t'$:

$$p(t) = p(t^*) \exp(-t'/\langle t\rangle) \qquad (3.20b).$$

Eqs. (3.20) show that p rises to the asymptotic value of $gd\langle t\rangle$ on a step increase of D, and decays when D switches to zero, both processes being exponential with the same time-constant $\langle t\rangle$. The pumping speed can be adjusted to obtain different $\langle t\rangle$, but if $\langle t\rangle$ is smaller so that the response becomes faster, then the sensitivity of p to D is less, and vice versa. In fact, we may perhaps, with significance, define a 'gain-bandwidth' product as $g\langle t\rangle(1/\langle t\rangle) = kT/V$ which shows, however, that a higher T or, more relevantly, a smaller V will decrease the lower limit of D which can be detected experimentally. This is expected, since reducing V leads to a larger density of gas for a given number of gas molecules present, and raising T, to a greater p for a given density.

Our analysis of p(t) proceeds according to Eq. (3.18), which may be rendered as

$$D(t) = (1/g)\,(\Delta p/\Delta t + p/\langle t\rangle) \qquad (3.19),$$

in which Δt is the resolved time in which an experimentally

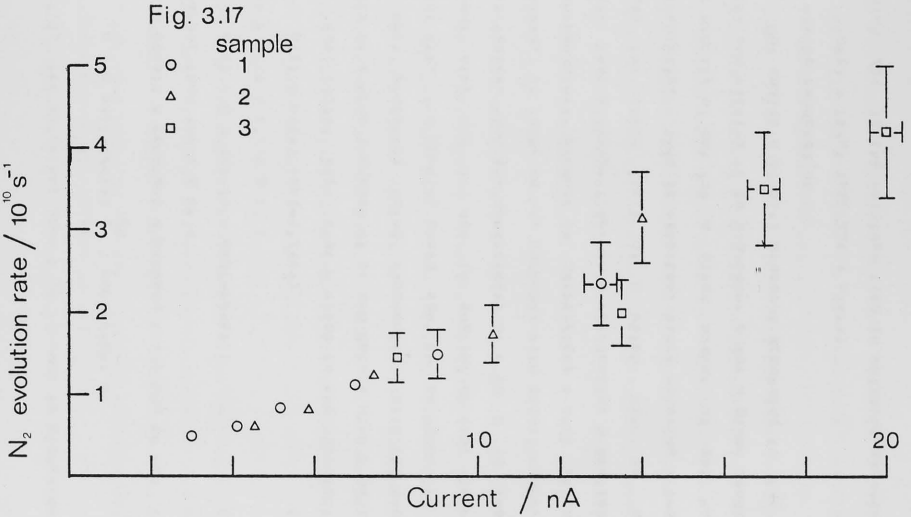
Fig. 3.17
sample
1
2
3
5
4
3
2
1
N_2 evolution rate / 10^{-10} s^{-1}
10
20
Current / nA

significant Δp occurs. If $\Delta t \rightarrow 0$ (a step change in p(t)), then by multiplying (3.19) throughout by Δt we see that it reduces to Table 3.2. On the other hand, if $\langle t \rangle$ is arranged so small that always $\Delta t \gg \langle t \rangle$, then the term $\Delta p/\Delta t$ may be omitted in (3.19). The last situation is the only one analysed (Redhead 1962) and commonly used (e.g., de Panafieu et al. 1976) in the literature. We believe that Eq. (3.19) which we have derived here is useful, since the minimum detectable D(t) may then be attained by adjusting $\langle t \rangle$ to be as great as the rise of base pressure (resulting from the reduction in P) allows, although the ultimate limit is set by g. Moreover, $\langle t \rangle$ in each case may itself be measured directly from the 'decay' part of p(t), according to Eq. (3.20b).

The quantitative results from our analyses are summarised in Fig. 3.17. The data for samples 1 and 2 were obtained by the quadrupole spectrometer, and 3, by the time-of-flight instrument. The systematic error in the evolution rate D is ca. 30 %, arising from the uncertainties in the UHV systems volumes, but for those obtained with non-zero pumping speeds (data points with vertical error bars) there is an additional random error of ca. 25 % propagated from the estimation of $\langle t \rangle$. The lower limit of detectable decomposition corresponded to an applied field of 30 kV/m; the highest point shown was at 133 kV/m. Between this range D changed by a factor of 9. However, if at fields above 75 to 90 kV/m the

initial values of the current are taken -- currents under these fields increased in general with time -- and these points are drawn with horizontal error bars, then a good correlation can be established between D and the current I. The ratio of D, in molecules/s, to I/q, where q is the electronic charge, comes out as ca. 0.3.

At high fields the followings have also been noted. Superimposed on the continuous decomposition were found sharp bursts of nitrogen evolution. Both their magnitudes and frequency increased with the field. On the other hand, as may be seen in Fig. 3.16, the decomposition rate did not increase proportionally to the current when the latter rose sharply. It was difficult to determine how large was the increase in the rate going to be if the current was allowed to proceed beyond the reversible limit. The reason was that the subsequent explosion would occur on a time scale of a microsecond, and the time resolution of the spectrometer would be inadequate to separate the pre-breakdown increase from the tremendous generation of nitrogen resulting from the fast decomposition, which moreover could damage both the ion source and the electron mutiplier. Nevertheless we may infer that, assuming a continuity in the mechanism underlying the current runaway, any large increase of D(t) that may finally occur is more likely to be a result rather the cause of the breakdown, since a major part of the rise in the current preceeds it. Explanations for

the above two observations will be put forward in Section 7.8, where we suggest a breakdown mechanism. Thirdly, when an external resistor was inserted in series to limit the current, the ratio of D to I/q was found to drop significantly with time slowly as the degree of decomposition of the crytal increased. This fact is consistent with the preliminary observation stated in Section 3.3.1 that the rate of production of surface silver decreased after repeated passages of fluctuating current.

The phenomena mentioned above will be further elucidated in Chapter 7, where mechanisms will be put forward for the electrical decomposition and for the dielectric breakdown. To end this chapter, however, we should point out that the work described here may have a practical relevance, namely, the controlled generation of nitrogen by the passage of an electrical current. The case where this is done by the application of heat has already been patented (Breazeale 1976).

We have now shown that the chemical reactivity of silver azide is a prominant factor in processes occurring under moderate and high fields. To study the reactivity, we carried out experiments on its slow thermal decomposition, and the next three chapters are concerned with the subject of this investigation.

CHAPTER IV

REACTION KINETICS: ISOTHERMAL METHOD

4.1 PREAMBLE

In this chapter we are going to discuss, firstly, the functional forms of the kinetics of solid state reactions and their theoretical interpretation. After this, a method is proposed for their determination from data obtained in isothermal experiments; its application to the pyrolysis (thermal decomposition) of silver azide will be presented in Chapter 6.

There are many reactions of interest in which one of the reactants is in the solid phase. These reactions can be classified variously as decomposition, dehydration, calcination, dehydroxylation, reduction, polymeric inversion and degradation, oxidation etc., and they occur in a wide range of substances from explosives to biological materials. Various discussions of the subject may be found in Garner (1955), Young (1966), Schmalzried (1974), and Harrison (1969), and recent reviews on the pyrolysis of metal azides in particular have been given by Fox & Hutchinson (in Fair & Walker 1977) and Yoganavasimhan (1976). In a solid-state reaction generally, the molar reaction velocity is given by $-d(1-a)/dt = da/dt$, where $a \equiv a(t)$ is the fraction of the solid reactant which has reacted by time t. The kinetics is solved if a is determined as a function of T, the temperature, and 1-a, the global amount of reactant left. This phenomenological knowledge is a necessary, though not sufficient, condition for elucidating the

reaction mechanism. It is necessary to formulate the reaction velocity in terms of the global variable a, because there is a continuous collapse of structure in the reactant; the local concentration of the reactant varies throughout the reaction volume and cannot be used as a state variable. In fact, unlike the case of a homogeneous reaction in the liquid or the gaseous phase, there is no real 'reaction order' with respect to any reactant in a reaction involving solids whose mechanism is usually of the heterogeneous type.

If the reaction proceeds isothermally, it is observed empirically that (a, t) curves corresponding to different temperatures T are isomorphic to one another, at least within a range of T, i.e., by a linear scale change in t, different curves can be superimposed (Young 1966). It follows that da/at is a separable function:-

$$da/dt = R(T)\, f(1 - a) \qquad (4.1).$$

Here f(1 - a) may change in different ranges of T or a, but for every f(1 - a), there corresponds a single R(T) which is characteristic to the reaction under study and indepedent of reacting sample geometry. It should be noted that experimental data may be adequately analysed by (4.1) only if the temperature distribution in the sample has been ensured sufficiently uniform and constant. Furthermore, the significance of R(T) and f(1 - a) determined from the data, regarding the class of mechanisms they independently indicate, should always be

examined for consistency. In the method we propose for determining f(1 - a) and R(T) from isothermal data, the interpretation of f(1 - a) forms the essential link between the experimental data and the functions.

4.2 PHYSICAL INTERPRETATIONS OF KINETIC LAWS

4.2.1 The Function f(1 - a)

Solid-state reactions are complex processes which proceed in several stages. These can be the delocalisation or transfer of electrons in chemical bonds in the case of non-metals, the diffusion of atoms, free radicals, or ions, the desorption of product molecules when they are in the gaseous phase, the heat transfer to reaction zones in the case of endothermic reactions, and the formation of a new solid structure (crystalline or amorphous) if one of the products is in the solid phase. The last step may often be further differentiated into nucleation, growth of nuclei at velocities which depend on sizes of nuclei (Young 1966), and sometimes the collapse of the lattice from a transitory one to the equilibrium structure (Sawkill 1955). Irrespective of the details of reaction mechanisms, however, under a given set of circumstances (T, a, sample history etc.) one of the stages will be the slowest. It then acts as the rate limiting step of the reaction, and it will determine the kinetics i.e., the rate law in (4.1).

Further, a solid-state reaction has, in contrast to a homogeneous reaction whose progress in independent of spatial coordinates, an additional controlling factor, namely topochemistry. This refers to the geometrical shape of the solid reactant and, in different cases, to its free surface area, its defect structure, the thickness of the product layer if solid, or to the product-reactant boundary etc.

The function f(1 - a) reflects the nature of the rate-limiting step and the topochemistry of the reaction. It may accordingly depend on certain sample conditions, such as whether the sample has been pre-irradiated or bleached, and whether the sample is in the form of a powder, or a large single-crystal of a different shape from the crystallites. It will vary in several ranges of T if in each of them a different elementary step becomes rate-limiting, as occurs in the decomposition of potassium azide (Jacobs & Tompkins 1952). At a given temperature, it may also change in different ranges of a, due to a switching of the rate-limiting step or to topochemical chages. This happens, for instance, in the oxidation of zirconium (Rozenband & Makarova 1977) and in most decomposition processes (Young 1966). An extreme case is the decomposition of ammonium perchlorate which, in the two temperature regimes below and above 620 K, has entirely different reaction mechanisms and in fact yields different reaction products (Galway & Jacobs 1960). In such cases there

	$f(1-\alpha) = \dot{\alpha}/K$	$F(\alpha)=Kt$	$m^{i)}$
A.	$\alpha^{1-1/n}$	$n\,\alpha^{1/n}$	$\approx 1.27n$
B.	α	$\ell n\alpha - C(T)$	ii)
C.	$\alpha(1-\alpha)$	$-\ell n\{-(1-1/\alpha)\} - C_o$	ii)
D.	$\{-\ell n(1-\alpha)\}^{1-1/n}\ (1-\alpha) \approx \alpha^{1-1/n}\ (1-\alpha)^b$	$n\{-\ell n(1-\alpha)\}^{1/n}$	n iii)
E.	$\alpha^{3/2}$	$2(\alpha_0^{-1/2} - \alpha^{-1/2})$	ii)
F.	1	α	1.24
G.	$(1-\alpha)^{1/2}$	$2\{1-(1-\alpha)^{1/2}\}$	1.11
H.	$(1-\alpha)^{2/3}$	$3\{1-(1-\alpha)^{1/3}\}$	1.07
I.	$1-\alpha$	$-\ell n(1-\alpha)$	1
J.	$1/\alpha$	$\alpha^2/2$	0.62
K.	$1/\{-\ell n(1-\alpha)\}$	$\alpha+(1-\alpha)\ell n(1-\alpha)$	0.57
L.	$1/\{(1-\alpha)^{-2/3} - (1-\alpha)^{-1/3}\} \approx 3(1-\alpha)^{1/3}/\{-\ell n(1-\alpha)\}$	$3\{1-(1-\alpha)^{1/3}\}^2/2$	0.54
	$1/\{(1-\alpha)^{-1/3}-1\} \approx 3/\{-\ell n(1-\alpha)\}$	$3\{1-(1-\alpha)^{2/3}\}/2 - \alpha$	0.57

i) Log $\{-\ell n(1-\alpha)\} \approx$ Constant + m log t, $0.15<\alpha< 0.5$

ii) Plot of L.H.S. in i) against log t distinctively concave upwards; C_0 and α_0 are constants

iii) b = 0.774, 0.700, 0664, 0.642, ..., 0.556 for n=2,3,4,5,... ∞

may be competing paths for the chemical reaction or it may in fact be followed by another chemical reaction whose 'onset temperature' is higher. In all possibilities, however, f(1 - a) should be independent of T (within a range) if it is to have more than only an empirical significance.

In Table 4.1, we have collected together the more common forms of f(1 - a) which have been used in the literature, and the corresponding integrated forms

$$\int_0^t dt\ (da/dt)/f(1-a) = \int_0^a da/f(1-a)$$

which we shall denote by F(a). Also, we write R instead of R(T) for simplicity. Note that F(a) = R (t-t') if the range of a for which it becomes applicable starts at a = a(t').

In many reactions, such as most decomposition and most dehydration processes, the rate-limiting step takes place at the interface between different phases as in sublimation. The speed at which the interface moves into the reactant is (at a given temperature) then either a constant, or a unique function of the interfacial area. This area therefore, from the kinetic point of view, plays the same role as that of concentration in homogeneous reactions. If the speed is constant, then the theoretical significance of f(1 - a) is clear: it gives the area expressed as a fraction of the original area at a = 0. This is the case of a reaction controlled by the movement of a coherent phase-boundary (Table 4.1 : F, G and H). In this

situation, the exact form of f(1 - a) will depend on the geometry of the reacting system, though generally the shape of the (a, t) curve is such that its slope is either constant or steadily decreasing.

If the reaction consists of the formation of compact nuclei of a solid product at localised places in the reactant followed by their relatively rapid growth, then, to express the total interfacial area, f(1 - a) is derived from the laws of nucleation and growth and the geometry of the reacting sample has no effect on f(1-a). This is the situation when the reaction is autocatalytic (Macdonald & Hinshelwood 1925): reactant molecules at a reactant-product interface react in preference to those at a reactant-'vacuum' surface. The preference is due to the existence of microstrains in the reactant at the interface, or due to the electrochemical potential of the product phase when the rate-limiting step is a redox process. The various possible forms of f(1 - a) for an autocatalytic reaction are listed in Table 4.1, A to E. Note that they have the general form log f(1 - a) = p log(a) + q log(1-a). In A, B and E, q is zero and da/dt increases monotonically with a. Such a situation is most unlikely to last up to a = 1. These types of f(1 - a) therefore may apply only to the acceleratory part, if it is present in the a-time curve and which will usually be followed by a decay part. In C and D, q is non-zero and these types give sigmoid-shape (a, t) curves, the infexion

point occurring at $a^* = p/(p + q)$. It is thus kinetically feasible for them to fit the complete experimental curve. There are, however, physical grounds to consider that even they should be used to analyse only the accelatory period (Young 1966).

In other reactions the rate-limiting step is not confined to, or does not only occur at, the reactant surface. For instance, in the unimolecular-decay type of reaction, all molecules whether on the surface or in the bulk have an equal probaility per unit time of reacting. The reaction therefore has a homogeneous mechanism. It has a true reaction order of the value of one, and $f(1 - a) = 1 - a$ irrespective of the geometry of the reacting sample: the reaction velocity is simply proportional to the amount unreacted. Many decomposition reactions tend to this limit at high a values. Another example is when the rate-limiting step is the migration of product ions along the dislocation network to form additional growth nuclei at dislocation nodes (Hill 1958). This leads to $f(1 - a) = a$, the same form as for branching nuclei (Hailes 1933). The slow process of 'ageing' in some explosives when they are stored at room temperature may be by such a nucleus-chain mechanism. A third category consists of reactions controlled by the diffusion of reactants across a solid product layer. The diffusion may proceed uniformly through the bulk of the layer and is thus structure-insensitive, or preferentially

along its gross lattice imperfections arising from product-reactant mismatch. In the case of uniform diffusion, the speed at which the product-reactant interface moves is a function only of the product thickness (and temperature), and the appropriate forms of f(1 - a) are included in Table 4.1 as J, K and L. The forms depend on the geometry of the reacting system. The oxidation of metals often follows diffusion-controlled kinetics; in sheet form these tarnish according to the parabolic law J. Exceptions are those metals in Groups Ia and IIa of the Periodic Table. Excluding beryllium, they all form oxide layers which are porous, so that the atoms of the metal do not have to diffuse through a coherent layer before coming into contact with oxygen.

4.2.2. The Function R(T)

It is almost always the case that the temperature-dependent part of (4.1) can be represented successfully by

$$R(T) = R^* \exp(-E/kT) \qquad (4.2),$$

in which the macro-kinetic constants E and R* do not depend on T (within the range), though they may take on different values when f(1 - a) changes.

If it is established that the reaction rate is limited by a diffusion or migration process, the interpretation of R(T) is complicated, but obviously it is proportional to the corresponding transport coefficient, which in general is an exponential function of T.

For a single-solid-reactant reaction which is controlled by a surface process, on the other hand, the simple theory of Shannon (1964) is often successful. This theory is a generalisation of the Polanyi-Wigner equation. Assuming the existence, in the reaction path, of some activated complex (defined as the transition state having the configuration of maximum potential energy) and that it can be treated as in thermodynamic equilibrium with the reactant, he related the pre-exponential factor R* to the rotational and other internal degrees of freedom of a reactant molecule in addition to the vibrational ones. Following Shannon we can set :-

$$R^* = (kT/h)\, \exp(\Delta S'/k)\, Sd/V \qquad (4.3),$$

and

$$\exp(-E/kT) = \exp(-\Delta H'/kT) \qquad (4.4).$$

Here the mean-frequency factor kT/h is usually in the region of 10E13 Hz (see later), $\Delta S'$ and $\Delta H'$ are respectively the entropy and the enthalpy of formation of the transition complex, d is the thickness of one monolayer and V the initial volume of the reactant, and S f(1 - a) gives the free surface or the product-reactant interface area when the degree of conversion is a. (Strictly speaking, it has been assumed that the reaction proceeds isobarically.)

Note that in this interpretation the empirical quantity R* contains the surface-to-volume ratio and so depends on the sample geometry. Also R* is proportional to T, apparently. In our opinion, if the vibrational modes are being considered then

only at low temperatures will the peak distribution of phonon frequencies lie at kT/h. In most substances (with the exceptions of Be, Cr and diamond) the Debye temperature Θ is less than 500 K, so that the frequency factor should stay constant at $k\Theta/h \leq 10E13$ Hz for all likely experimental temperatures.

For certain reaction mechanisms, nevertheless, R* may be predicted to have temperature dependence. (In gas reactions, R* is proportional to the square root of T.) An example can be found in Section 6.6. However, any variation of R* due to a modest power of T contained as a factor in it will be much smaller than that of exp(-E/kT). (cf. Section 5.2.)

The factor $\exp(\Delta S'/k)$ may alternatively be written in terms of partition functions as Q'/Q, which can be determined from spectroscopic data (Cagle & Eyring 1953). $\Delta S'$ usually cannot be larger than the reactant entropy of melting, and $\exp(\Delta S'/k)$ comes out normally between unity and 10E4. Occasionally $\exp(\Delta S'/k)$ is found to be less than unity, as it is for the steric factor in gas reactions. Such a negative value of $\Delta S'$ means that the activated complex is more ordered than the reactant (e.g., Mackenzie & Banerjee 1978). Experiments on some decomposition reactions have given R* which are abnormally high in comparison to the theoretical values of (4.3). Hypotheses put forward to explain such discrepancies include co-operative activation (Garner 1939), proton-delocalisation (Fripiat & Toussaint 1963), and a mobile layer

of molecules on the reactant surface (Shannon 1964).

4.3 KINETIC ANALYSIS

4.3.1 Current Practice

In determining the kinetics one wishes to find R*, E, and f(1 - a) or equivalently F(a) so that the reaction velocity can be predicted at any given T and a. This is commonly done by analysing a set of da/dt or equivalently a(t) values obtained by monitoring samples reacting isothermally at a number of temperatures. The consistency of the R* and E values with f(1 - a) should as far as possible be assessed, and correlated with, for instance, visual examination.

A quick method of calculating E was used by Haynes and Young (1961). Consider a set of (a, t) curves which have been found to be isomorphic. For any two curves (a', t') and (a", t") corresponding to temperatures T' and T" respectively, one can write

$$F(a') = t' R^* \exp(-E/kT') \qquad (4.5)$$

$$F(a") = t" R^* \exp(-E/kT")$$

By choosing points corresponding to the same a on the two curves so that F(a') = F(a"), E can be evaluated by plotting log t vs. 1/T. On the other hand, to determine F(a) the experimenter often relies on visual inspection of the general shape of the curves, and a trial-and-error method is resorted to. Conflicting forms of the function have sometimes been

asserted by several authors for the same material, like ammonium perchlorate (see Maycock & Pai Verneker 1968) and potassium permangante (see Ng 1975).

A conventional way of superimposing isothermal curves is to convert them into 'reduced-time plots' by individually scaling their t-axis with the factor $1/\langle t \rangle$, where $\langle t \rangle$ is the time when a is 0.5 on the i-th curve. In this way R(T) is absorbed into each scale factor, and all (a, t) = (0.5, 1) points coalesce, while other a(t) points may be plotted out to see if the curves are indeed isomorphic. Sharp et al. (1966) tabulated the theoretical values of a against $t/\langle t \rangle$ for some of the F(a) shown in Table 4.1. They proposed that by comparing experimental data with such master values the correct F(a) can be identified.

The above method may, however, result in ambiguity due to a number of aspects. Experimental data contain random errors, but no simple statistical analysis can be applied to the identification criterion it employs because no straight-line graphs are involved. Additionally, a general problem for all isothermal experiments is the zero-time uncertainty. The finite time taken by the sample to reach the designated temperature may be negligible relative to $\langle t \rangle$, yet may affect the comparison with the tabulated values (Hancock & Sharp 1972). Moreover, F(a) may change in different regimes of the a(t) curves, as mentioned earlier.

4.3.2 A New Method

Here we suggest a step-by-step approach to determine F(a). It was noted by Hancock and Sharp (1972) that for many forms of F(a), the plot of log[-ln(1 - a)] vs. log t is almost linear if a is restricted to between 0.15 and 0.5. Using a computer program (Appendix D) to generate artificial values and their log-ln plots (Fig. 4.1 (a) & (b)), we have found this true for all the theoretical forms listed in Table 4.1, with the exceptions of B, C, and F. The slope in each case is listed there under the Column 'm'. (In the figures, ln is to base e, log is to base 10, and t is normalised to t/<t>. The value of m is, of course, independent of these choices.)

Obviously a log-ln plot is not very sensitive. If we were to rely solely on it to discriminate between the functional forms of F(a), the experimental data would have to be of the highest quality. A slightly more sensitive way is to plot the m-th root of [-ln(1 - a)] vs. t, but then m can only be obtained iteratively. Fortunately, m does differ significantly between different groups of F(a), and the final discrimination is easily achieved by a further graphical step. There are three possible situations for this second step :-

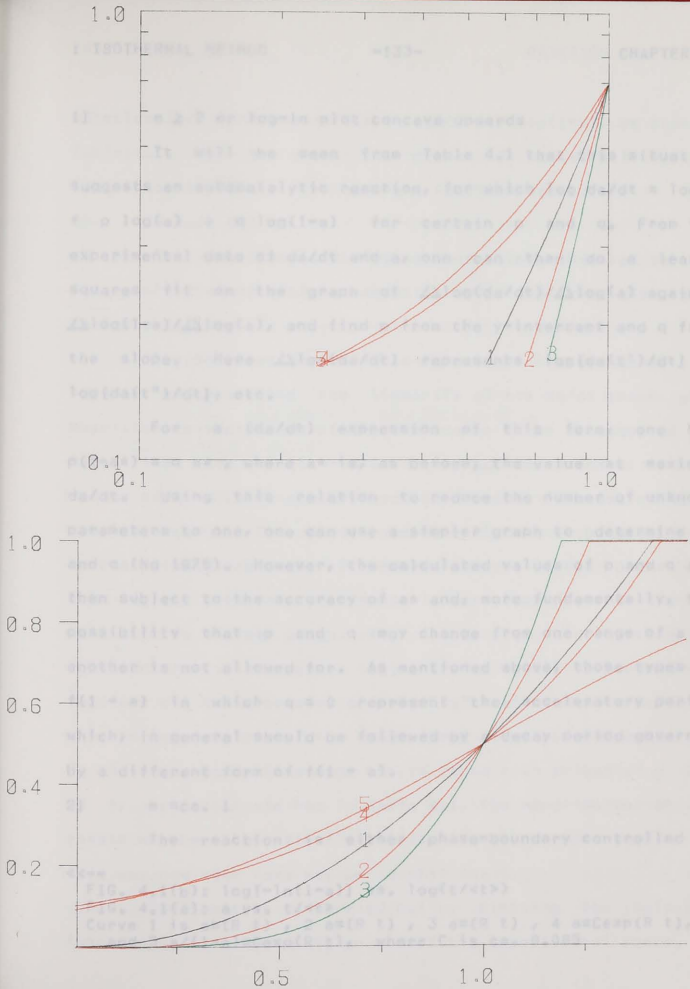
1.0
0.1
0.1
1.0
3
1
2
3
1.0
0.8
0.6
0.4
0.2
5
4
1
2
3
0.5
1.0

1] $m \geq 2$ or log-ln plot concave upwards

It will be seen from Table 4.1 that this situation suggests an autocatalytic reaction, for which $\log da/dt = \log R + p \log(a) + q \log(1-a)$ for certain p and q. From the experimental data of da/dt and a, one can then do a least-squares fit on the graph of $\Delta\log(da/dt)/\Delta\log(a)$ against $\Delta\log(1-a)/\Delta\log(a)$, and find p from the y-intercept and q from the slope. Here $\Delta\log(da/dt)$ represents $\log[da(t')/dt] - \log[da(t")/dt]$, etc.

For a (da/dt) expression of this form, one has $p(1-a*) = q\, a*$, where a* is, as before, the value at maximum da/dt. Using this relation to reduce the number of unknown parameters to one, one can use a simpler graph to determine p and q (Ng 1975). However, the calculated values of p and q are then subject to the accuracy of a* and, more fundamentally, the possibility that p and q may change from one range of a to another is not allowed for. As mentioned above, those types of f(1 - a) in which q = 0 represent the acceleratory period which, in general should be followed by a decay period governed by a different form of f(1 - a).

2] m =ca. 1

The reaction is either phase-boundary controlled or

<<--
FIG. 4.1(b): log[-ln(1-a)] vs. log(t/<t>)
FIG. 4.1(a): a vs. t/<t>
Curve 1 is a=(R t) , 2 a=(R t) , 3 a=(R t) , 4 a=Cexp(R t),
and 5 a/(1-a)=Cexp(R t), where C is ca. 0.085

unimolecular, and log(da/dt) = log(R) + r log(1-a), as seen in Table 4.1. One then draws the graph of log(da/dt) against log(1 - a) to find r, the apparent reaction order.

3] m =ca. 0.5

The reaction is diffusion controlled. One has to test separately whether a(t) is parabolic or of the other two forms in Table 4.1.

The correlation coefficient in the least-squares fit serves, by measuring the linearity of the da/dt graph, as a quantitative indication of the confidence to be attached to the identified form of f(1 - a). It may be that p and q, r, or s change once or twice as the reaction proceeds from beginning to completion, but the da/dt graphs will show it by displaying several linear segments. If however, a part of the graph say from (a', t') to (a", t") is non-linear, then F(a) has changed to a form in another group. The first step should then be repeated for that part: log[-ln(1 - a + a')] is plotted vs. log (t - t') for a between a' + 0.15(a" - a') and a' + 0.5(a" - a'), followed by one of the above three alternative procedures. On the other hand, if a good fit is found with values of p and q, r, or s that are not in Table 4.1, the experimenter should assess whether theoretical justification can be provided. In this way new rate laws may be identified.

Confirmation is carried out by plotting the selected functional form or forms on top of the experimental curve. A

slight misfit in the very early part (ca. 1 min, depending on the sample size and the environment) may be attributed to thermal lag-time and ignored. The da/dt graphs give R, and from a set of R values at different temperatures R* and E can be determined. Note that the determination of these macro-kinetic constants depends on the forms of f(1 - a) chosen (when there are more than one, applying to differences ranges of a), as it should be.

4.4 EXPERIMENTAL TECHIQUES & IMPLEMENTATION OF DATA REDUCTION METHOD

Experimentally, da/dt or a(t) values of a solid-state reaction may be obtained by a variety of techniques. They include dilatometry, quantitative infra-red spectroscopy, and quantitative X-ray diffraction. Measurements of electrical conductivity, dielectric constant, optical reflectivity, viscoelasticity, ultrasonic attenuation (Belomestnykh & Sharov 1978), chemi-luminescence, and evolved gas pressure (thermomanometry) are also used. In fact, the measurement may be of any physical property whose correlation with the change of chemical composition in the sample under study is well-defined. Most universally applicable, however, are the thermoanalytical techniques, namely thermogravimetry (TG) and the two differential methods of thermal analysis (DTA) and scanning calorimetry (DSC).

It may be added that we regard it as possible to have full automation in the acquisition and processing of data obtained by thermalanalytical techniques. The hardware can be under the control of micropossessors or dedicated minicomputers, and their output would go into a computer or the same minicomputer. A computer program can then reduce the data to a(t) or da(t)/dt values, which may be further analysed to identify f(1 - a) and so calculate R* and E, according to the method proposed here. For instance, a cubic spline fitting to a(t) curves can be used to generate da/dt or, in the reverse direction, the calculation can be by numerical quadrature (cf. Appendix F). The intermediate results from the first and the second steps can be stored on a disc or a floppy disc and the plots or graphs drawn on an interactive display console. The experimenter can then, after looking at the intermediate results, select the next step and, in the final stage, input the appropriate form(s) of f(1 - a) which are to be plotted on top of the original data. The whole procedure may thus be fast and efficient. Nevertheless, the physical interpretation of these results by the experimenter remains the crucial step.

The method we have proposed in this chapter has been applied to investigate the kinetics of slow thermal decomposition in silver azide single crystals. The results are described in Chapter 6.

CHAPTER V

REACTION KINETICS: DYNAMIC METHOD

5.1 PREAMBLE

The dynamic method of studying solid state reaction kinetics involves measuring the reaction rates under conditions of a continuous temperature change, in contrast to the situation discussed in the last chapter where the reaction proceeds isothermally. Originally proposed by Skramovsky (1932), the method is becoming popular, especially with the development of differential thermoanalytical techniques like DSC and DTA.

Since the initial temperature can be chosen so that the reaction rate is relatively insignificant to begin with, the method does not suffer from zero-time inaccuracy: a problem which exists in isothermal experiments where the temperature is raised rapidly and then held constant. A further advantage is that, provided the dynamic data have been unambiguously and correctly analysed, any changes in the kinetic constant will not be overlooked even within small temperature intervals. In contrast, the isothermal method only provides values averaged over discrete points in temperature. Also, when the data are so analysed that the kinetic constants are calculated from each dynamic curve then very few samples are required; only a milligram or so of the material is needed for its thermal characterisation. If many runs are indeed carried out, differences between individual samples can be determined. The last two advantages are particularly useful in single crystal

work.

On the other hand, intrinsic differences should be carefully distinguished from the effects of experimental conditions. Firstly, literature data have shown that experimental parameters such as the sample mass (Fong & Chen 1977) and shape, the particle size distribution in the case of powder samples, and the ambient atmosphere can affect significantly the calculated values of kinetic constants (see Simon 1973). If this happens, then whenever possible the empirical results should be extrapolated to refer to a 'standard' set of experimental conditions. Secondly, the heating rate very often affects the shape of the dynamic curve obtained; in particular, the temperature distribution in the sample may no longer be adequately uniform, but fuller discussion will be deferred to the next section. Lastly, the very fact that temperature is now a variable, in addition to time, complicates the analysis of data. If due care is not taken, either inaccurate or totally misleading values are obtained. In fact, a survey of the literature reveals several instances of high-quality experimental data being misinterpreted by methods beyond their ranges of validity. In this chapter we first describe various methods currently employed and point out their limitations. We then justify the approach in which use is made of both isothermal and dynamic experiments. The analysis of isothermal data yields $f(1-\alpha)$ unambiguously and, knowing $f(1-\alpha)$, one

can calculate individual values of the kinetic constants from each set of dynamic data. We may mention that, historically, isothermal experiments were the only ones carried out in the pioneering age of the twenties and thirties, when solid-state reactions began to be studied from the modern point of view, as distinct from that of Langmuir, Nernst and Tammann.

5.2 KINETIC EQUATION

As discussed in Chapter 4, the kinetics of a reaction proceeding isothermally can usually be described by the empirical relation:-

$$da/dt\ [\text{isothermal}] = R^* f(1-a) \exp(-E/kT) \qquad (5.1),$$

where the quantities explicitly written down on the L.H.S. are 'usefully' temperature-independent. That is, the function $f(1-a)$ may change in different ranges of a but is, for a given a, independent of T, at least within a range of T, and R^* and E should be the same for the same $f(1-a)$. If the rate-controlling step of the reaction occurs on the reactant free surface or on the reactant-product (solid) interface, then R^* will contain the surface-to-volume ratio. In other words, the reacting system should really be normalised per unit area rather than per unit size, and R^* be given in units such as molecules /(s.square-m).

Some authors have questioned the general validity of (5.1) on various grounds (Garn 1974, Barzukin 1974, Draper &

Steum 1970, Krug 1977). However, in the literature (5.1) is almost always successfully fitted to experimental data. Indeed, this empirical relation can be given mechanismic justification (see Chapter 4).

In dynamic experiments, it is commonly agreed that (5.1) may be adapted to describe the reaction rate:-

da/dt [non-isothermal] = R* f(1 - a) exp[-E/kT(t)] (5.2).

T(t) is controllable by the experimenter. Some temperature programs offer the mathematical advantage that exp[-E/kT]/(dT/dt) can be integrated analytically (see later discussion on integral methods of data analysis). Examples are the hyperbolic program where T = 1/(A - Bt), (Zsako 1970, Simmon & Debreczeny 1971); a parabolic program in which 1/(dT/dt) = 2AT + B, with B = AE/R* by iteration (Marcu & Segal 1978); and an exponential program so that dT/dt = exp(-B/T) with B = E/k by iteration (ibid.). For the sake of experimental convenience, however, the arrangement is usually that dT/dt = H. (A, C and H represent constants in a particular run of experiment.)

However, it has been taken by some authors who object to (5.2), that

da = (Da/Dt)dt + (Da/DT)dT + (Da/DH)dH (5.3),

where (Da/Dt) ≡ da/dt [isothermal] and D denotes partial differentiation. The argument is then that (5.2) is seen to be inadequate even in the case of dH = 0, since the second term on

the R.H.S. of (5.3) is non-zero but left out in it (see e.g. MacCallum & Tanner 1970, MacCallum 1971, Murant et al. 1977). The opinion has further been offerred (Norwisz 1978), by a derivation starting from (5.3), that (5.2) is correct only if it includes the extra factor

$$1 + (1 - T(0)/T)E/kT$$

But we believe that (5.3) is unsound. Given t, T and H, a is not uniquely determined and therefore not a function of these system variables; it cannot decrease even for negative dT and dH. Nevertheless, the inexact differential da can be integrated, if the dynamic process can be treated as the limiting case of a series of time intervals, during which the reaction proceeds isothermally according to (5.1) but at the end of each of which T is altered, in a time so short that during it the sample is unchanged. Along this path P the result is easily obtained (Simmons & Wendlandt 1972):

$$\int_0^a da/f(1-a) = \int_P R\,dt = \frac{R^*}{H}\int_{T(0)}^{T} \exp(-E/kT)\,dT \qquad (5.4),$$

where $R \equiv R^* \exp(-E/kT)$. We must emphasise that (5.4) is not logically self-evident, as is sometimes implied (Simmons & Wendlandt 1972) or argued by mathematical operations based on the presumption that $a = a(T,t)$ (Gorbatcher & Logvinenko 1972). Rather, it comes from the assumption that the reaction under study involves no slow processes, so that da/dt depends only on the present values of a and T (meaning that da/dt is a function

of state) and not on the history of the reacting system (c.f. Felder & Stahel 1970). Only by this assumption (absence of memory effects) can the dynamic process be treated as P. Experimentally, a temperature program with temperature jumps, which approximates P, has been realised on a thermobalance interactively controlled by computer (Dickens & Flynn 1976). Equations (5.2) and (5.4) are of course equivalent. Their validity has also been shown by 'rational' thermodynamic arguments, in which the functional relation da/dt = g(t, t dR/dt) is regarded as the 'constitutive equation' characterising the reaction system (Sestak & Kratochvil 1973).

On the other hand, experience shows that apparently (5.4) is not always followed exactly. Consider a reaction being investigated by a series of experiments conducted at different heating rates H but with the same initial temperature T(0). In (5.4) we see that the R.H.S., for a given upper temperature limit T, is directly proportional to 1/H. Plots of the L.H.S. vs. T should therefore all have the same shape. It may happen, however, that increasing departure from isomorphism is seen when experimental data obtained at higher H are so analysed. The most probable explanation is that the temperature change is too fast, causing the temperature distribution in the sample to become significantly non-uniform. In fact, thermal equilibrium is an underlying assumption when (5.4) is derived above; without it da/dt will depend on the thermal

history of the reacting system.

It may be that some other factor is at work. The reaction rate may be sensitive to the structure of the reactant, and a higher H can enhance the defect density or change the reaction activation energy at a defect site (Sosnovsky 1959). In branched-chain reactions, the speed of the progressive accumulation of active centres may vary with H (Azatyan 1977). If the reaction is a surface process, the distribution of reaction centres among corners, edges or faces of the sample may change with H (Constable 1925, Heuchamps & Duval 1966). The chemical system under study may have multiple reactions proceeding concurrently in it, and they have different E (Ozawa 1976). All these variations in the reaction activation energy may be accompanied by changes of R* in the same direction. Because of this coupling, a linear relation between E and log(R*) is sometimes observed. Called the 'compensation effect', this phenomenon does not necessarily mean, as was suggested (Garn 1974), that the Arrhenius expression in the R.H.S. of (5.4) is invalid. In all these cases, by varying H the experimenter can, in fact, gain additional insights into the mechanism of the reaction, or distinguish between the competitive reactions in the reacting systems (a situation usually, though not always, indicated by the presence of multiple peaks in the da/dt curves). This is possible if the method of data analysis employed is such that K and E are

determined from a single da/dt or a(t) curve, rather than from data at a number of heating rates. The method we suggest will be of this type.

It may also happen in (5.2) that R* is proportional to T, so that R* cannot be taken outside the integral sign in (5.4). Indeed, modifications have been suggested of some methods of data analysis (those that assume a reaction order for the reaction) to take this extra temperature dependence into consideration (Petty et al. 1977). However, even when theoretically required, the correction may for practical purposes be ignored, unless E is small or temperatures used are very high: $d(\ln R)/dT = (E + kT)/kT^2$. Likewise, any slight temperature dependence of E can usually be neglected. Furthermore, irrespective of this or the above complications the form of f(1 - a) in (5.2) and (5.4) is not affected. It should be the same as in (5.1), on the basis that the dynamic process can be treated as the limiting case of a series of isothermal intervals, an assumption already mentioned above.

5.3 CRITICAL EXAMINATION OF CURRENT METHODS OF ANALYSIS

Many methods of analysing da/dt or a(t) data have been proposed to calculate the kinetic constants E and R*, and sometimes also f(1 - a). Often they were originally formulated with reference to one particular instrumentation, but they may be made generally applicable to all techniques after quantities

measured on DSC, DTA, TG, etc., are all interpreted in terms of da/dt and a(t). On the other hand, their validity does depend on the particular reaction whose data are being analysed. Their limitations in this respect form the subject of our discussion below. They will be examined in three groups: peak-temperature, integral and derivative methods, in this order. Sophisticated instrumentation systems are coming into use, that incorporate computers to establish baselines or other null settings, to carry out automatic data acquisition, and to let the experimenter interactively analyse the data (e.g. Doelman et al. 1977, 1978). Such advances do not, however, remove the danger of uncritical choices of the method of data reduction.

5.3.1 Peak-Temperature Method

Kissinger (1957) considers reactions of the type $f(1-a) = (1-a)^n$. Differentiating (5.2) with respect to t, and setting the resulting expression to zero, he obtains

$$(da/dt)^* (E/k)H/T^{*2} = \exp(-E/kT^*)\, n(1-a^*)^{n-1} (da/dt)^* \qquad (5.5)$$

in which * signifies 'peak' quantities at the point of maximum (da/dt) where $d^2a/dt^2 = 0$. He next assumes that $n(1-a)^{n-1} \approx 1$; therefore

$$H/(T^*)^2 \propto \exp(-E/kT^*) \qquad (5.6),$$

regardless of n, which itself may be calculated from the shape of the a(t) curve. E and R*, on the other hand, are obtained by performing a series of experiments at different H. An aspect, which we regard as an inefficiency of Kissinger's

method, is that only one point on the curve is used although, in the case where multiple peaks occur signifying that different $f(1-a)$ and E govern different sections of the curve, the method should still be applicable to each peak.

There is, however, an important limitation. The 'a priori' condition that $f(1-a) = (1-a)^n$ is actually valid only in very special circumstances, namely when the rate-limiting step of the reaction is the inward movement at constant speed of the reactant-product interface, where n is 0, 1/2 or 2/3 for one-, two-, or three-dimensional movement respectively, or when the reaction is unimolecular so that $n = 1$. (See Table 4.1.) Even among these special cases, the other approximation that Kissinger uses is still conditional, since $n(1-a^*)^{n-1} \equiv 1$ only for $n = 1$. When n is 1/2 or 2/3, this expression varies with a^* approximately as $(n(1-n)/(1-a^*)^{2-n})\Delta a^* \geq 0.2\Delta a^*$, where Δa^* is the variation in a^* itself. In Appendix C we show that a^* changes with H in the general case. Hence, when an apparent reaction order exists and is 1/2 or 2/3, Kissinger's method can lead to a systematic deviation in (5.6) and thus generate a significant but hidden error in the calculated E and R*.

If no apparent reaction order exists, then it definitely should not be used, otherwise an approximately linear plot from (5.6) results in totally misleading values of the kinetic constants. An example is in the decomposition of

benzenediazonium chloride: it derives from DTA data a value of E that is 40% lower than the nearly identical values, obtained by applying other methods of analysis to the data from DTA as well as other techniques (Reed et al. 1965). Other examples are in the study of lithium aluminium hydride, where the Kissinger values are half of the isothermal result (McCarty et al. 1968), in RDX where it is again 40% lower than all the values calculated by other methods (Rogers & Smith 1970), and in urea nitrate, where it is 30% lower (Borham & Olson 1973).

5.3.2 Integral Methods

The L.H.S. of (5.4) is a function of the upper limit of the integral, a, only and will be denoted by F(a); the lower limit of integration in the R.H.S. can for practical purposes be taken as 0, since in experiments T(0) will be such that reaction velocity is negligible below it, i.e. $T \ll E/k$. In view of these considerations, many authors have proposed different methods of analysing a(T) data.

The temperature integral, $\int_0^T \exp(-E/kT)dT$, has no analytical solution in general. Only in the unusual case of a hyperbolic, parabolic or exponential temperature program, then $\exp(-E/kT)/(dT/dt)$ is integrable, but, as we have said in Section 5.2, normally T is experimentally arranged to rise linearly with t, and this is the sole case to be considered here. The numerical values of the integral have been compiled but, being a function of both E and T, are not directly useful

unless an iterative solution of (5.4) by trial-and-error is resorted to. For more efficient approaches, approximations to the integral are necessary. Thus, taking the first two terms in an asymptotic ($z \equiv E/kT \dashrightarrow \infty$) series of $\int_0^z t^{-2}\exp(-t)dt$ Coats and Redfearn (1964) obtain the linearised relation:

$$\ln(F(a)/T^2) = A - E/k(1/T) \qquad (5.7),$$

where $A \equiv \ln(R*k/EH)(1 - 2kT/E)$ is 'sensibly constant' if the range of temperature ΔT is small. They further assume that the reaction has a reaction order, n, so that $f(1 - a) = (1 - a)^n$, and thus F(a) can be calculated at each (a, T). Plotting (5.7) for several values of a thus gives E and R*, making use of only one set of data corresponding to a single H.

Several cautionary notes should again be made here. The assumption for f(1 - a) has already been discussed. Similar to the case of Kissinger's method, results obtained may be wrong and misleading if this functional form is not independently determined beforehand. Thus, in a study on the dehydroxylation of kaolinite (MacKensie 1973), straight lines over different ranges of (1/T) are given by (5.7) for a whole series of values of n, namely, 0, 0.5, 0.667, 1 and 2. In particular, plots using n = 1 and n = 2 are almost equally 'good'.

Secondly, the accuracy of the asymptotic approximation is rather low. By comparing its values with tabulated values of the integral (Doyle 1961, Biegen & Czanderna 1972), we find

its relative errors to be $\Delta T/I = 20\%$ at $z = 5$, 5% at $z = 10$, and 1.5% at $z = 20$. Thus, for example, if E is 1 eV, then for an accuracy of 98% the highest temperature reached in the experimental run should not be more than 600 K, a very low figure for most materials though it is higher for larger E. Additionally, expanding A into a power series shows that $\Delta A/A = 2k\Delta T/E$ approximately, so that at say 2% inaccuracy the range of temperature, ΔT, from which (a, T) points are selected should be less than 100 K (for E = 1 eV). The total possible deviations in the calculated E and R* are, to first approximation, the sum of the $\Delta T/I$ and $\Delta A/A$. It certainly is unsatisfactory if they are large and yet nowhere mentioned in the calculation.

Other approximations to the temperature integral have been suggested by van Krevelen et al. (1951) and by Horowitz and Metzger (1963), who made use of certain asymptotic expansions in the vicinity of T*, the temperature at peak reaction rate. Both have been shown (Zsako 1973) to be even less accurate than the Coats and Redfearn approach, and so will be left out in our discussion.

Amongst the integral methods, the best is probably the one due to Ozawa (1965), which requires data at different H but, in it f(1 - a) remains completely general. The approximation to the temperature integral is :

$$\int_0^T e^{-E/kT}\, dT = \frac{E}{k}\, 10^{(-2.32\, -\, 0.457\, E/kT)} \qquad (5.8),$$

so that from (5.4)

$$\log H_1 + 0.457(E/k)/T_1 = \log H_2 + 0.457(E/k)T_2 \qquad (5.9),$$

where the two T's are taken at an arbitrary but identical value of a in the two curves corresponding to the two different heating rates. Plotting log H vs. 1/T for selected values of a should therefore produce straight lines, the slopes of which give E.

Three comments are appropriate here. By comparing (5.8) with tabulated numerical values, we see that it is 7% out at z = 10 or T = 1170 K, and 3% and less only for T < 720 K (if E = 1 eV). These errors should be examined before Ozawa's method is applied. Secondly, the method has been modified (Krien 1973) to read, in place of (5.9),

$$\Delta \ln H / \Delta(1/T^*) = 0.457\, E/k \qquad (5.10),$$

in which * denotes peak quantities, as before. This relation may be compared with (5.6) but in general it does not hold since, as we show in Appendix C, a* varies with H. Lastly, like Kissinger's method, E cannot be determined from data at a single H, and in some cases this may be a disadvantage, as discussed in Section 5.1.

5.3.3 Derivative Methods

The derivative methods offer an advantage over those

described above in invoking no mathematical approximations. Unfortunately, they use da/dt data which, with present instrumentation, tend to be of lower quality whether they are obtained by numerically differentiating the a(t) data or are direct experimental read-outs.

The most straightforward, but as it stands relatively inefficient, of the derivative methods is to write (5.2) as :

$$\ln (da/dt)/f(1-a) = \ln R^* - E/kT \qquad (5.11),$$

and to substitute different forms of f(1 - a) until a linear plot appears (Sharp & Wentworth 1969). Later we shall argue, however, that even this 'labor omnia vincit' approach, like all dynamic methods in general, cannot guarantee correct values of E and R* (nor an unambiguous form of f(1 - a) in this specific case), although the labour it involves may be undertaken by the computer.

The earliest derivative method is probably that of Borchardt and Daniels, originally formulated for homogeneous reactions in the liquid phase (Borchardt & Daniels 1957) but later extended to solid-state reactions (Blumberg 1959) for which it is now frequently used. The method assumes a reaction order n, and substitutes f(1 - a) in (5.11) by the explicit expression with n given a guessed value. If a linear plot results then E and R* are obtained from it. Based on this method, Hauser and Field (1978) have developed a computer procedure, in which plots are generated for a series of values

of n incremented at discrete steps, and the 'best' one is then selected to yield E, R*, and n. An attraction of this method is that the correct n can be readily selected by eye. Alternatively, since in this case

$$\Delta\ln(da/dt)/\Delta\ln(1-a) = -E/k\ [\Delta(1/T)/\Delta\ln(1-a)] + n \quad (5.12),$$

a plot of the L.H.S. vs. the quantity in the square brackets gives E from the slope and n as the y-intercept (Freeman & Carroll 1958). If constant $\Delta\ln(da/dt)$, $\Delta\ln(1-a)$, or $\Delta(1/T)$ is selected, Eq. (5.12) can be further simplified (Segal & Fatu 1976). However, we have emphasised previously the fallibility in presuming such a convenient form of f(1 - a); Ozawa (1975) has commented on the possibility that this procedure, and the integral method of Coats and Refearn, may give false values of E and R*. In addition, since (5.12) involves the ratios of differences, the quality of data called for is even higher than that demanded alone by the use of da/dt. There is another method due to Roger and Morris (1966) in which $\Delta\ln(da/dt)$ is plotted against (1/T), and can be seen to be the special case of n = 0 in (5.12). An example of the general danger that very linear plots may sometimes appear even if the applied method is not valid is given by Patel and Chaudhri (1978). The Roger and Morris method was used to analyse DSC data on lead azide, and a straight line results although the calculated E turns out to be 180% larger than Ozawa value. Conversely, the coincidence of values calculated by various methods need not prove that these

methods are all applicable to the case in hand. A counter-example is provided by a DSC study on RDX (Rogers & Smith 1970), where the Roger and Morris value agrees well with other values but the complex decomposition is beyond doubt far from the n = 0 type.

On the other hand, David & Zelenyanszki (1973) plot ln [d ln(1-a)/dt]/(1-a) against (1/T); this amounts to assuming a reaction order n = 1. It serves as yet another example of the futility of linear plots, for their method gives such plots for the decomposition of 'a wide range of materials' including calcium oxalate and polyethylene which, most likely, are not of first or any other 'order'.

Some of the integral and derivative methods described in the foregoing have been compared by testing their accuracies on synthesised DTA data (exact as well as with artificial random error) for one E value and temperature range, the reaction considered being of the type with reaction order (Anderson et al. 1977). Among the methods not included there is that due to Friedman (1967). It probably is the most general among the derivative methods. Like Ozawa's procedure, it makes no assumption about f(1 - a), although it requires da/dt data which, furthermore, have to be at a number of H. Once again, from (5.2):

$$\ln (H\, da/dI) = \ln(R^* f(1-a)) - E/kT \qquad (5.13).$$

Since R*f(1-a) is identical for the same value of a, taking

da/dt and the corresponding T from several data sets at different H one can determine E.

It is our contention that even Friedman's method has one basic limitation which, more significantly, is shared by all dynamic methods described above. The point in question is that all of them have to presume the constancy of f(1 - a) as the temperature is changed. However, since mechanisms of solid-state reactions are generally complicated, there is no general justification for this presumption, though it may be true for particular reactions within specific temperature ranges. An illustration is the case where parallel reaction paths exist, each with values of R* and E such that a quantitative change of T will lead to a qualitative change in the dominating path. Another case is where the identification of the rate-limiting step depends on T. Methods have been proposed which, by the use of computers, try different forms of f(1 - a) in analysing the dynamic data (Skvara et al. 1974, Nolan & Lemay 1973, Chen & Fong 1977). However, the search is limited to functional forms which are already known.

More importantly, from our own experience with azides we have strong doubts as to the exactness in determining f(1 - a) or even its constancy from dynamic data. Likewise, in a study on the dehydration of manganese formate (Nolan & Lemay 1973) for instance, no unique form of f(1 - a) and correspondingly no unique values of E are identified even over

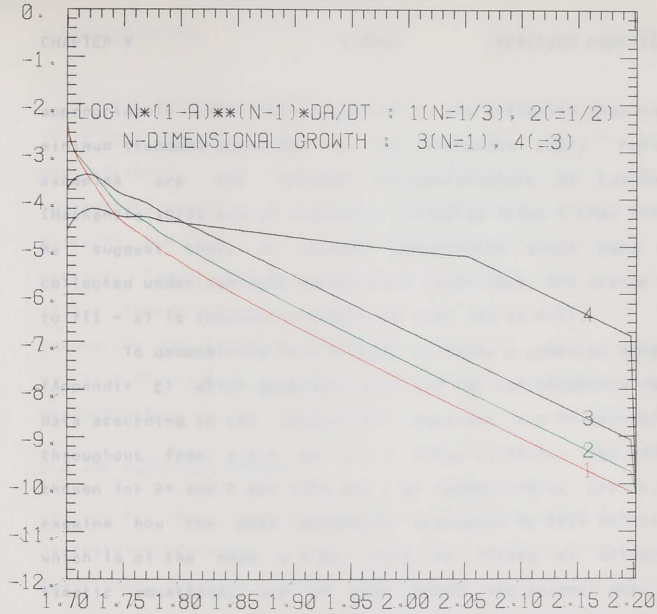

FORTRAN UNIT NUMBER 8

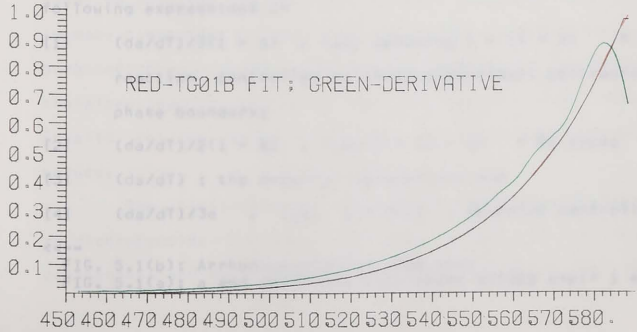

appropriately restricted ranges of a, the criterion used being minimum standard deviation in the Arrhenius plot. Further examples are the thermal dehydroxylations of kaolinite (MacKenzie 1973) and of magnesium hydroxide (Fong & Chen 1977). We suggest that, in dynamic experiments since data are collected under variable temperature conditions, the change due to f(1 - a) is inherently masked by that due to R(T).

To demonstrate this effect, we wrote a computer program (Appendix E) which generated a(T) and the corresponding da/dT data according to the theoretical equation a = R* exp(-E/kT) throughout from a = 0 to a = 1 (Fig. 5.1(a)). The values chosen for R* and E are 10E8 and 1 eV respectively. Let us now examine how the data generated according to this relation, which is of the type a = Rt, will be fitted by different kinetic equations, one of them being the correct one. In Fig 5.1(b) we plot against 10E3/T the natural logarithms of the following expressions :-

[1] (da/dT)/3(1 - a) , i.e. assuming 1 - (1 - a) = Rt : reaction controlled by three-dimensional contraction of phase boundary;

[2] (da/dT)/2(1 - a) , i.e. 1 - (1 - a) = Rt type;

[3] (da/dT) : the original assumption; and

[4] (da/dT)/3a , i.e. a = (Rt) : reaction controlled by

<<--
FIG. 5.1(b): Arrhenius plots -- see text
FIG. 5.1(a): a and da/dT vs. T/K, where a=10E8 exp(- 1 eV/kT)

e.g. three-dimensional growth of existing nuclei. It is seen that the incorrect f(1 - a) in [1] and [2] still give virtually linear plots, with slightly different slopes; interestingly, curve [4] is so misleading as to show two 'linear' segments with a seemingly significant transition in between. Experimentally, Guarini et al. (1973) have noted that it is impossible to ascertain from their DSC data whether the monomerisation of 9-Me-10-AcAD has an apparent reaction order of 1, 0.67, or 0.5, in all of which cases E has about the same derived value.

5.4 THE SUGGESTED APPROACH

In the foregoing sections, we have discussed the limitations regarding the applicability of various methods that have been used to analyse dynamic data. In many published works we find that often many apparently different methods are used to analyse the same set of data. However, we think that in many cases this procedure is of no real significance, when some of the methods used are mathematically equivalent and therefore lead to the same results, and/or when some are invalid in the given situation and thus lead to doubtful values.

The limitations of the methods express themselves both as discrepancies in the calculated values of the kinetic constants, and sometimes as fortuitous agreements when some of

the methods are certainly inapplicable. An extreme example of the second situation is that, for RDX, the Kissinger value (Rogers & Smith 1970) of E is near to that obtained (Maycock & Pai Verneker 1970) by plotting a vs 1/T, a procedure which has absolutely no theoretical justification. Accordingly, we suggest that the interpretation of dynamic data should as far as possible be based on results from isothermal experiments.

One can unambiguously determine f(1 - a) over the whole range of a and over the relevant temperature range, from the independent analysis of individual isothermal curves. A systematic method of efficiently implementing this identification has been proposed in Chapter 4. It may also be noted that thermoanalytical equipments are equally applicable in isothermal experiments (see Patel & Chaudhri 1977 and our work in Chapter 6) though they were more often used in the dynamic mode. The identified form(s) of f(1 - a) can then be substituted into either (5.2) or (5.4). In this way, from the dynamic a or da/dt data one can then determine accurately the non-average and single-sample values of E and R*: advantages which have been mentioned in the preamble of this Chapter. Moreover, the values will correspond individually to different heating rates.

We applied this approach to the spinel formation $ZnO + Cr_2O_3 \rightarrow ZnCr_2O_4$. A DTA curve (experimetal atmosphere: nitrogen at 300 mm mercury) was published in Ishii et al.

(1977), who have also monitored a(t) by chemical analysis when the reaction proceeded isothermally in nitrogen flowing at 50 ml/min, and showed that the isothermal data fit $[1 - (1 - a)^{1/3}]^2 = Rt$. We have measured R from experimental data points at t = 20 min in the published isothermal plots. From these values of R, given in Table 5.1, we calculate a value of 1.5 eV for E.

Table 5.1 Isothermal Data

T/K	R / arb. units	ln R
1073	1	0
1173	4	1.4
1273	23	3.1

Table 5.2 Dynamic Data

T/K	a	(da/dt) / arb. units	*
973	0.1	2	-2.6
1093	0.15	4	-1.4
1173	0.2	7	-0.54
1273	0.35	12	+0.76

$* \equiv \ln[(1 - a)^{-2/3} - (1 - a)^{-1/3} (da/dT)]$

In Table 5.2, da/dt values were measured from the published DTA curve whose heating rate was unspecified, and the a values were read off from the (a, T) graph which Ishii et al. have drawn presumably by integration. Now, from their analysis of the isothermal data the governing kinetic equation is, in

differential form, $da/dt = K/[(1 - a)^{-2/3} - (1 - a)^{-1/3}]$, at least within the ranges 1073 - 1273 K, and a from 0 to ca. 0.6 corresponding to Rt = 0 to ca. 0.07. The Arrhenius plot of $(da/dt)(1 - a)^{-1/3}[(1 - a)^{-1/3} - 1]$, for the four data points shown in Table 5.2, is indeed a good straight line. From the plot we obtain E = 1.3 eV. In view of the probable experimental errors and inaccuracies in obtaining data from the published graphs, we consider satisfactory the reasonable agreement between this value and the one calculated from the isothermal data.

The suggested approach has also been applied to dynamic TG data of the pyrolysis of silver azide. The results are given in Appendix C.

CHAPTER VI

DECOMPOSITION: KINETICS & MECHANISM

6.1 PREAMBLE

This chapter describes the results we have obtained on the pyrolysis of silver azide, using the thermogravimetric technique and the data reduction methods proposed in the two previous chapters. Some of its thermal properties have also been measured, using other techniques. From the kinetic results deductions have been made concerning the mechanism of the reaction, whose knowledge is relevant to our study of dielectric breakdown.

Several kinetic studies of the reaction have been reported in the literature. Audubert (1939) measured the extent of pyrolysis by monitoring the accompanying UV emission, Audubert (1952), Gray and Waddington (1957), and Bartlett et al. (1958) measured the pressure of the evolved gas, whereas Zakharov et al. (1964,1966) used a gravimetric method, the same technique as ours. These techniques of studying solid-state reactions have already been mentioned in Section 4.4. The approach of the 'English School' of Gray, Tompkins, Young, et al. in investigating decomposition reactions has mainly been by the fitting of sophisticated equations to the experimental rate curves, that of the 'Cavendish School' by (transmission, scanning and diffraction) electron microscope observation of decomposing single crystals, and that of the 'Russian School', by studying the catalytic effects of additives. However, there is still no general agreement on the reaction mechanism.

In all the previous works quoted above, the silver azide used was in the form of pressed pellets or fine powder. The disadvantages of using this sample form have already been discussed in Section 2.4. Here in particular, it introduces boundary conditions such as the packing density, the degree of sintering (if any), the particle size distribution (Bircumshaw & Newman 1955; Hitchinson et al. 1973) and the particle shapes. All of these influence inter-crystallite contact areas. Another experimental condition which may be important is the nature of the interstitial gas. Further, in experiments in which the nitrogen pressure is monitored, a complication may arise due to the possibility that the diffusion through the interstitial spaces may be so slow as to significantly distort experimental readings. As Yoffe (1966) commented sometime ago, the real difficulty in kinetic studies is in the interpretation of results and it is profitable to work with single crystals.

In this study, we have investigated the isothermal decomposition using the relatively large single crystals we have grown. Both reaction kinetics and related thermal quantities have been determined. The use of large crystals also made possible a study of the morphology of the decomposition surface utilizing scanning electron microscopy. A similar study has previously been undertaken by McAuslan (1957) at this laboratory and, although the conditions of our experiments were somewhat different, our main conclusions are in agreement (Sec-

tion 6.3.3). Unfortunately, the thickness of the crystals precluded in-situ electron diffraction studies of selected areas of the decomposed surface. However, as the decomposition end product consisted of an agglomerate of small particles, electron diffractograms of individual particles were taken.

We have also studied the pyrolysis kinetics by the dynamic method (Chapter 5) using thermogravimetry. The results are given in Appendix G.

6.2 EXPERIMENTAL PROCEDURES

In our kinetics experiments we have chosen TG, which involves following the weight of a sample as its reaction proceeds. Historically, isothermal studies of exothermic reactions by this technique were reported as early as 1956 (Cook and Abega), though dynamic studies appear not to be so commonly employed. The weight of a silver azide sample is an unambiguous function of its degree of decomposition since, unlike in the case of alkali metal azides, the vapour pressure of its metallic product is negligible at experimental temperatures. The classical method of thermomanometry, i.e., the measurement of the isochoric pressure of the evolved gas, has not been chosen because of its inherent non-isobaric conditions. In accordance with Le Chatelier's principle, an increase in the partial pressure of the product gas over the reactant should cause a decrease in the decomposition rate

(cf.Rouquerol 1973). If the effect is large enough, the interpretation of data becomes difficult.

To measure the specific heat and enthalpies and temperatures of phase transitions, the technique of DTA has been employed. The temperature of the sample was continuously compared with that of a reference, when both were heated by identical power inputs such that the temperature of the reference increased linearly. One DSC experiment was also carried out. The temperature of the reference was controlled to rise at a constant rate, and the change in the power required to maintain the sample at the same temperature as the reference was monitored.

A DuPont 990 Thermal Analyser was used to which a DTA module was fitted. The sample pan, 1 mm deep and 5 mm in diameter, was made of aluminium which was inert at experimental temperatures. The reference was an empty pan. The temperature difference was monitored with a chromel-alumel thermocouple and displayed in two sensitivites on an X-Y,Y' chart recorder. Dried argon flowing at 10 ml/min was used as the purge gas. This was to reduce further the small chance of side reactions occurring concurrently when oxygen and water vapour were present. Five experimental runs were made at a heating rate of 5 K/min, and sample weights ranged from 0.213 to 2.019 mg (1 to 8 crystals). For the DSC experiment, a Perkin-Elmer model DSC-2 was used. Temperature measurements were made with

platinum resistance thermometers and the sample weight was 4.019 mg; other conditions of operation were identical.

A Stanton Redcroft TG-750 electronic thermobalance was used at its maximum usable sensitivity of 50uV/2ug. A Solartron LM 1450 (3 1/2)-digit DVM was triggered by a sequential timer to read in the gravimetric output at regular time intervals, and a data logger recorded the digitised weight readings on tape. The timing circuit used was designed and built especially for the purpose and it has been described in (Tang 1978); it can generate short as well as unusually long gating pulses, is reliable in operation, and is much cheaper than commercially available instruments. The data logging system was set up as in (Hauser 1977). The furnace temperature was measured by a Pt-(Pt,13% Rh) thermocouple, and was displayed in deg.C by a linearising circuit. The sample pans were of the same type as before. Eight experimental runs were carried out at selected furnace temperatures between 513 and 558 K. Each sample comprised of two crystals. These selected crystals were of uniform cross-section ca. 100 um across, and of average weight about 250 ug. Using smaller crystals would reduce the uncertainty in the sample temperature due to exothermicity, but this was not possible because of the limited sensitivity of the thermobalance.

The thermobalance incorporated a programmer which, in the experiments reported in this chapter, controlled the

furnace temperature to stay within 0.5 K of a preset value. (For the calibration of a thermobalance, see Blazek 1973, Chapter 2.) In each run, the furnace was first pre-heated to the selected temperature and an empty pan was lowered into it. There would be an apparent weight increase followed by a slow decrease, the transient lasting a total of 2 to 4 minutes. This was recorded on tape and used to correct for the initial part of the weight-loss curve, obtained when the pan was again lowered, this time with the sample in it. The correction was by simple subtraction and, consequently, the very early parts of our decomposition curves are not reliable. The pyrolysis took place in a dynamic atmosphere similar to that in the DTA and DSC experiments.

A Cambridge Stereoscan S4-10 was operated at 27 kV for the microscopy work. Sample pans containing crystals which had reached various degrees of decomposition were transferred from the thermobalance to the microscope stage. For a crystal in an early stage of decomposition, and especially when viewed at high magnifications (x1000 and above), photographs were taken 'blindly' by using an adjacent area for focusing. This was necessary because experience had shown that continuous scanning lasting many seconds produced electrostatic charge accumulation and radiation damage. The former led to fictitious contrast effects, and the latter was visible as cracks or small aggregates of silver on the surface (Figs. 6.1 & 6.2). We have

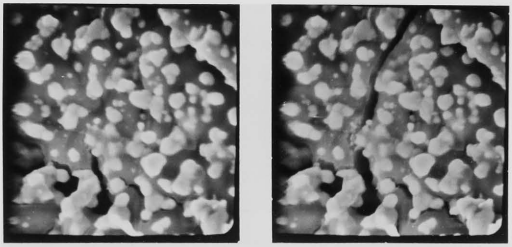

(a) FIG. 6.1 (b)

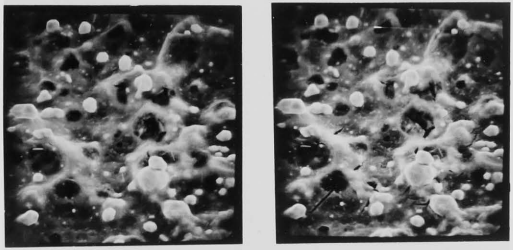

(a) FIG. 6.2 (b)

not found it necessary to evaporate a metallic film on such crystals or to prepare carbon replica: both processes seemed to cause extraneous decomposition. In his previous study, McAuslan (1957) maintained that the evaporation of a conducting film was required before the crystal could be photographed, while admitting that this practice complicated the interpretations of observations.

To take diffractograms of the decomposition product (particles of silver or 'pebbles' - see below), we used the 750-kV high voltage electron microscope (HVEM) designed and constructed by the Electron Microsopy Group of the Old Cavendish. An evaporated carbon film, mounted on a 200-mesh-per-inch copper grid, was pressed gently against a partially decomposed crystal so that some of the 'pebbles' adhered to the film. With the microscope operating at 600 kV in the transmission mode, a 'pebble' was located that was small enough to allow the electron beam to penetrate through it, and then a selected area diffraction pattern was taken. X-ray diffraction pictures were also taken of completely decomposed crystals by the Laue method, using a beam size of 0.4 mm.

<<--
FIG. 6.1(a) : partially decomposed crystal surface
(a =ca. 0.1); (b) : after irradiation for 10 s
FIG. 6.2(a) : silver azide melted and partially decomposed
(a =ca. 0.8); (b) : after irradiation for 20 s
In both cases the electron beam intensity was
ca. 1 pA/(100 square-nm) at 27 kV

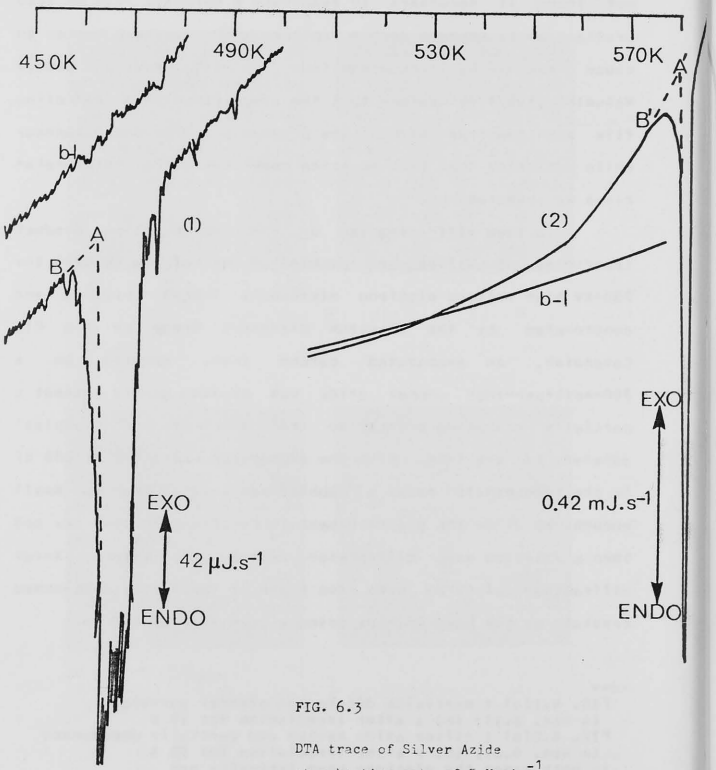

FIG. 6.3

DTA trace of Silver Azide
at a heating rate of 5 K.min^{-1}

6.3 RESULTS

6.3.1 DTA and DSC

Fig. 6.3 gives typical DTA traces, and results are summarised in Table 6.1. The specific heat was previously quoted as 490 J/kg/K at 523 K (Yuill 1953). Our lower value appears to be more reasonable. Since the temperatures of measurements are higher than the Debye temperature (see Section 6.6), the specific heat should approximate to the Dulong-Petit value of 2x3k per molecule or 335 J/kg/K. Another point concerns the critical temperatures given in the table. As extrapolated onset values marked A and A' in Fig.6.3, they are not necessarilly identical to the thermodynamic temperatures of the phase transitions but are, according to Garn (1976), more reproducible than the departure values B and B'.

Table 6.1 Calorimetric Values

Enthalpy change/(kJ/kg)	Temp. /K	Explanation
10.5 ± 0.8	461 ± 2	Crystallographic transformation
0.29 ± 0.04	465 to 530	Specific heat
104 ± 2	581 ± 2	Melting

The melting point was given as 524 K (Hitch 1918) and this is the value usually quoted in the literature. It is too low and may have been measured on impure silver azide. Using a Gallenkamp melting-point apparatus and a sample of four crystals, we observed that at ca. 553 K the crystals stuck to

FIG. 6.4 (a) (b)

one another and, at ca. 583 K, underwent a sharp transition into the liquid state which seemed to bubble, until completely decomposed (Fig. 6.4).

The DSC trace obtained is reproduced in Fig. 6.5. It shows that the slow pyrolysis developed into a fast decomposition before complete melting of the crystals. Previously, it had been thought that the minimum explosion temperature was 620 K which is appreciably higher than the melting point. To explain initiations of explosion by drop weight and particle impacts, the mechanism of localised adiabatic shear failure had been proposed (see Chaudhri & Field 1977). The present observation suggests that all that has to happen is for the impact to create hot spots so fast that they lose little heat to the bulk but which, however, need not somehow get hotter than the melting point.

6.3.2 TG

From the stoichiometric equation of the pyrolysis of silver azide, the molar fraction of decomposition , at time t, in a sample is:

$$a = 149.9/(149.9-107.9)\ W(t)/W(0) \qquad (6.1),$$

where W(t) is the sample weight, and 149.9 and 107.9 are the molecular weight of silver azide and the atomic weight of

<<--
FIG. 6.4(a) : Crystals melted in a test tube [scale -- tube outer diameter is 1.25 mm];
FIG. 6.4(b) : Molten silver azide which then decomposed [magnification: twice that in (a)]

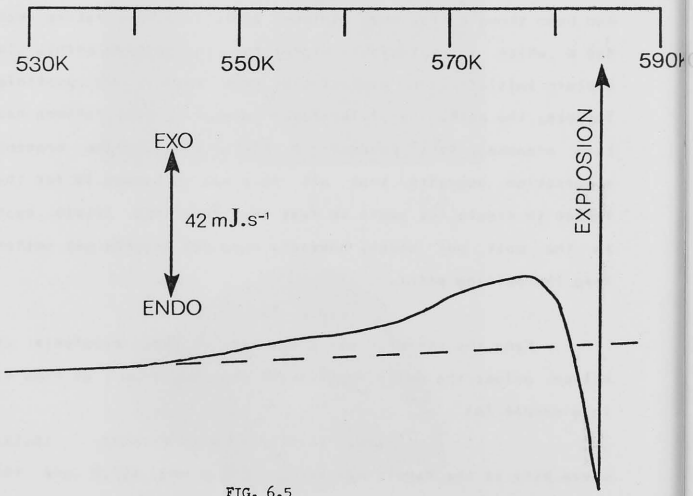

FIG. 6.5

DSC trace of Silver Azide
at a heating rate of 5 K.min^{-1}

silver, respectively. As discussed in Section 4.1, to determine the kinetics is to be able to express the molar reaction velocity as

$$da/dt = R\, f(1 - a) \qquad (6.2),$$

where R is a function of temperature. A FORTRAN program (Appendix F) reads in the W(t) data and reduces them into a(t) points. Cubic splines are then fitted to these points, so that well-behaved da/dt values can be calculated algebraically from the knots fitted. Further ananlysis in the program is according to the procedure proposed in Section 4.3.2.

In Figs. 6.6, 6.7 and 6.8 are shown the results for the cases of T = 513 K (time taken for a to reach 0.5 was 441 min), 551 K (69.2 min), and 558 K (49.4 min). The other cases were T = 520 K (227 min), 529 K (179 min), 539 K (113 min), 544 K (97.7 min), and 554 K (56.3 min). In all the eight cases, the reduced-time plots show that the a-t curves are isomorphic, indicating a unique functional form for f(1-a). The plots of log[-ln(1 - a)] vs. log(t), $0.15 < a < 0.5$, are all found to be roughly linear with a slope of ca. 1.1. This approximate value of the slope suggests that the decomposition is unimolecular or of the phase-boundary controlled type. The graphs of log(a) vs. log(1 - a) which were therefore next generated show that, up to $a = 0.9$, $f(1 - a) = (1 - a)^{1/2}$ with a correlation coefficient in no case worse than 0.9. Within the experimental range of temperatures and this range of a, therefore,

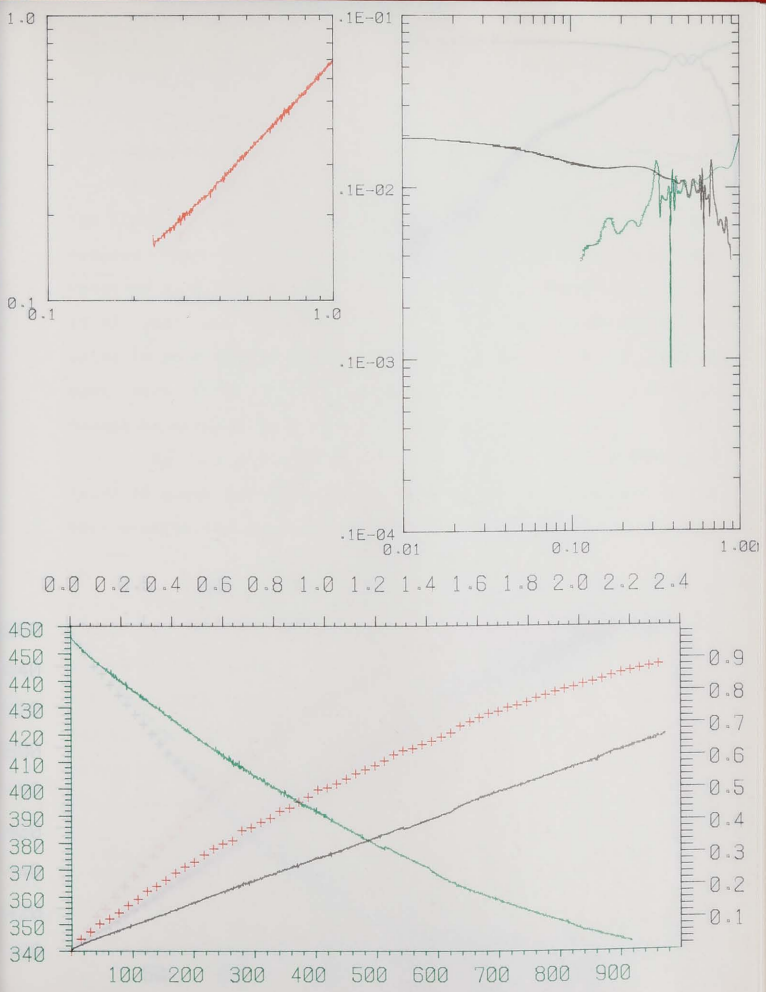
1.0
0.1
0.1
1.0
.1E-01
.1E-02
.1E-03
.1E-04
0.01
0.10
1.00
0.0 0.2 0.4 0.6 0.8 1.0 1.2 1.4 1.6 1.8 2.0 2.2 2.4
460
450
440
430
420
410
400
390
380
370
360
350
340
0.9
0.8
0.7
0.6
0.5
0.4
0.3
0.2
0.1
100 200 300 400 500 600 700 800 900

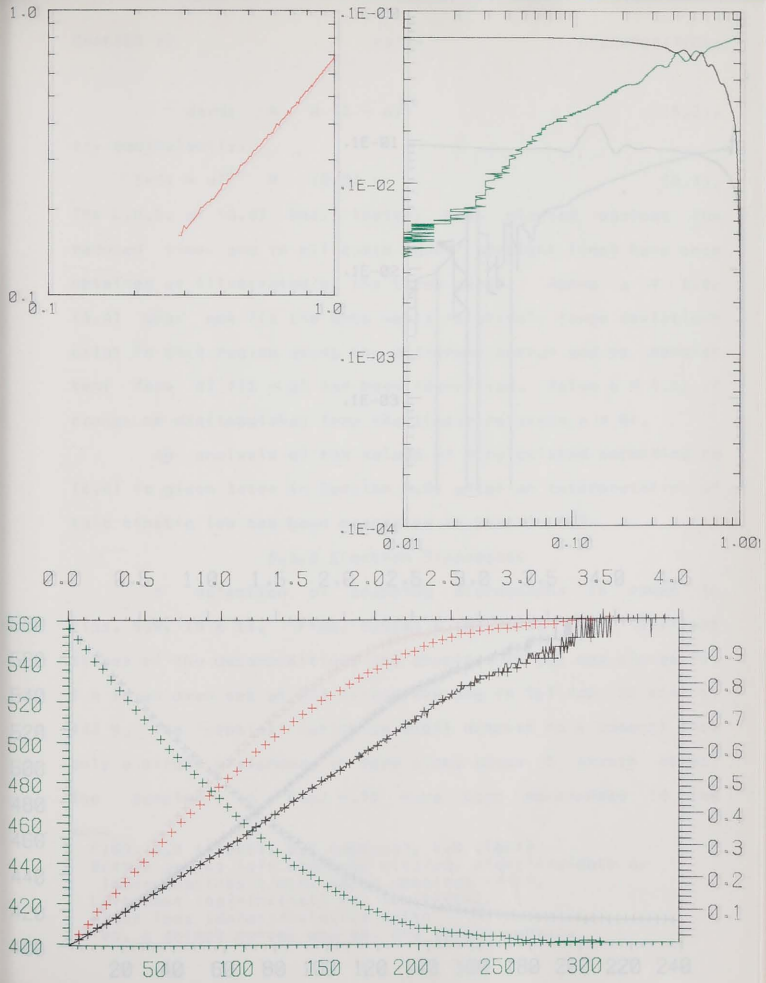
1.0
0.1
0.1
1.0
.1E-01
.1E-02
.1E-03
.1E-04
0.01
0.10
1.000
0.0
0.5
1.0
1.5
2.0
2.5
3.0
3.5
4.0
560
540
520
500
480
460
440
420
400
50
100
150
200
250
300
0.9
0.8
0.7
0.6
0.5
0.4
0.3
0.2
0.1

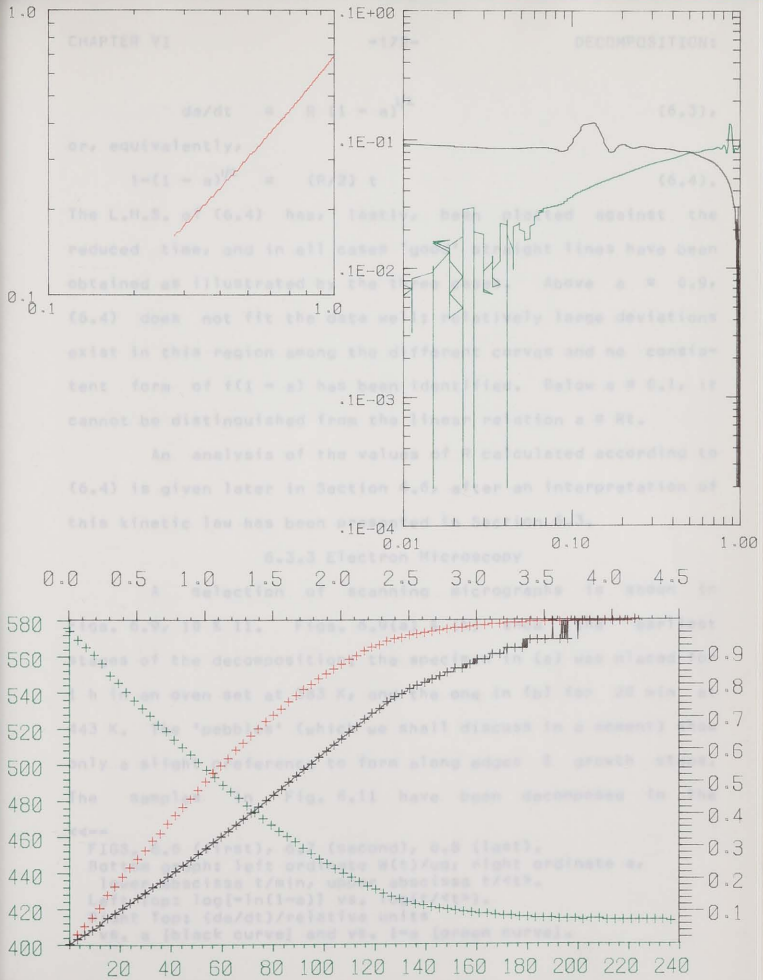
1.0
0.1
0.1
1.0
.1E+00
.1E-01
.1E-02
.1E-03
.1E-04
0.01
0.10
1.00
0.0 0.5 1.0 1.5 2.0 2.5 3.0 3.5 4.0 4.5
580
560
540
520
500
480
460
440
420
400
0.9
0.8
0.7
0.6
0.5
0.4
0.3
0.2
0.1
20 40 60 80 100 120 140 160 180 200 220 240

$$da/dt = R\,(1 - a)^{1/2} \qquad (6.3),$$

or, equivalently,

$$1-(1 - a)^{1/2} = (R/2)\,t \qquad (6.4).$$

The L.H.S. of (6.4) has, lastly, been plotted against the reduced time, and in all cases 'good' straight lines have been obtained as illustrated by the three cases. Above a = 0.9, (6.4) does not fit the data well; relatively large deviations exist in this region among the different curves and no consistent form of f(1 - a) has been identified. Below a = 0.1, it cannot be distinguished from the linear relation a = Rt.

An analysis of the values of R calculated according to (6.4) is given later in Section 6.6, after an interpretation of this kinetic law has been presented in Section 6.3.

6.3.3 Electron Microscopy

A selection of scanning micrographs is shown in Figs. 6.9, 10 & 11. Figs. 6.9(a) & (b) show the earliest stages of the decomposition; the specimen in (a) was placed for 1 h in an oven set at 383 K, and the one in (b) for 20 min at 443 K. The 'pebbles' (which we shall discuss in a moment) show only a slight preference to form along edges & growth steps. The samples in Fig. 6.11 have been decomposed in the

<<--
FIGS. 6.6 (first), 6.7 (second), 6.8 (last).
Bottom graph: left ordinate W(t)/ug, right ordinate a,
lower abscissa t/min, upper abscissa t/<t>.
Left Top: log[-ln(1-a)] vs. log(t/<t>).
Right Top: (da/dt)/relative units
vs. a [black curve] and vs. 1-a [green curve].

(a) 60

(b) 60

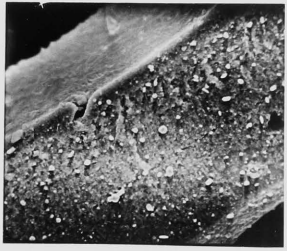

(α) 100

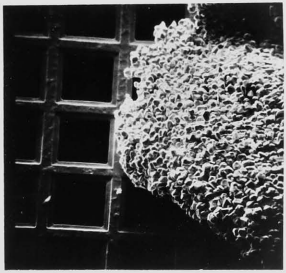

(b) 550

thermobalance. The crystal in Fig. 6.11(a) was heated at 463 K until a is 0.1, when its faces were completely covered with these pebbles. It is obvious from (b), (c) & (d), which show the same crystal after it was partially cleaved, that the formation of pebbles is a surface phenomenon: the few formed on the cleaved faces were caused by the electron beam of the micrograph. That the distribution of pebbles which are big enough to be seen has little correlation with surface imperfection is confirmed by (e) and (g), in which 'bad' crystals have been chosen as samples. There is a difference, however, in that there seem to occur some break up of the parent crystal into blocks which then decomposed. This can be deduced from the presence of cavities in some of the pebbles (see (f) which is an enlargement of (e)); the molar volume of silver is a third of that of silver azide.

During the pyrolysis, the crystal usually developed cracks on the surface as shown in Figs. 6.11(h), (i) & (j) (furnace temperature 513, 443, 443 K, and a = 0.1, 0.12, 0.14, respectively). The cracks were seen in crystals decomposed at both above and below the crystallographic transformation temperature, and generally belonged to the zone [001].

Figs. 6.11(k), and 6.10(a), 6.11(l) & 6.11(u) which

<<--
FIG. 6.9 (a), (b) -- top
FIG. 6.10(a), (b) -- bottom
Number indicates width of micrograph in um;
for description see text

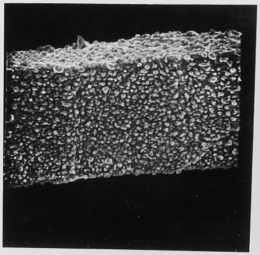

(a) 120

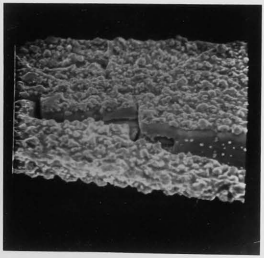

(b) 120

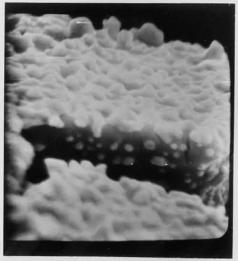

(c) 21

(d) 50

(e) 48

(f) 19

(g) 48

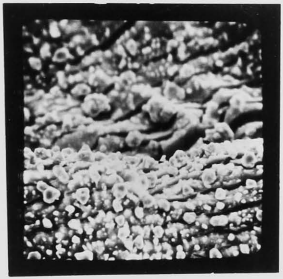

(h) 130

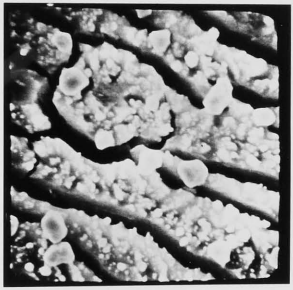

(i) 50

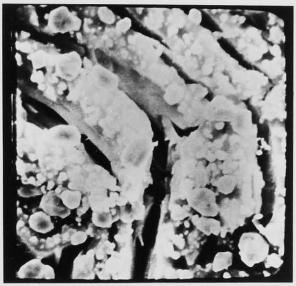

(j) 50

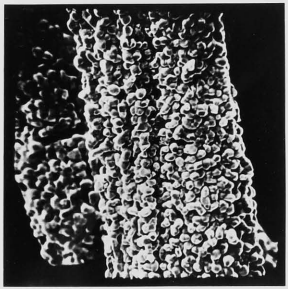

(k) 178

(l) 110

(m) 8·6

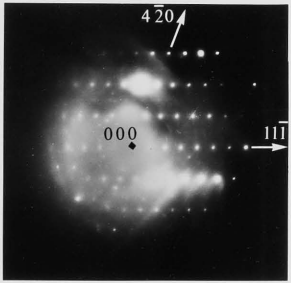

(n)

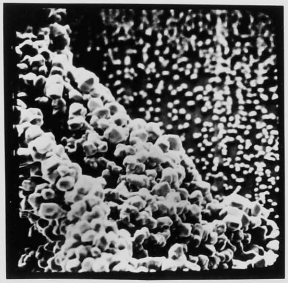

(o) 150

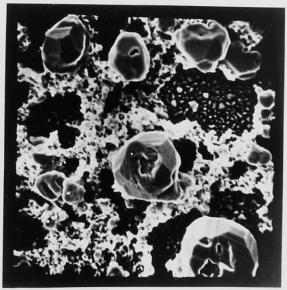

(p) 84

(q) 55

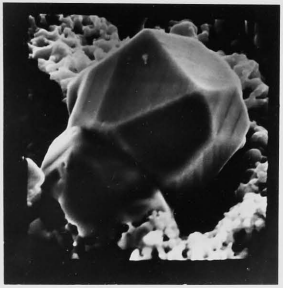

(r) 22

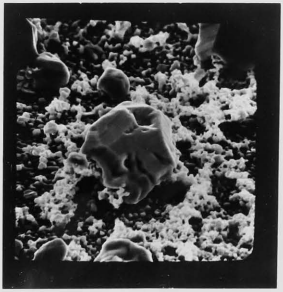

(s) 55

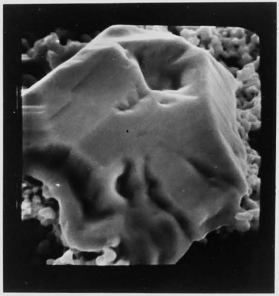

(t) 22

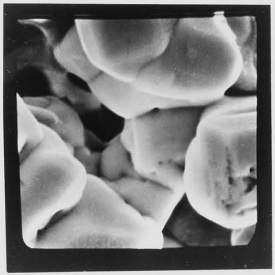

(u) 40

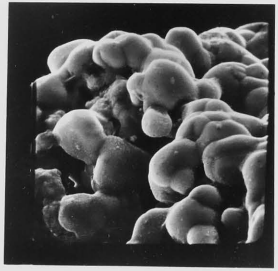

(v) 43

(w) 21

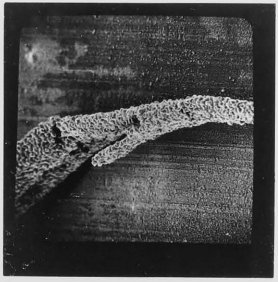

(x) 720

show the same specimen, are micrographs of crystals completely decomposed at 513 and 573 K respectively. A most striking feature of the pyrolysis of silver azide is that the end product is in the form of 'pebbles' which, as apparent from preceeding micrographs, project out from the surface of a decomposing crystal. Diffraction studies confirmed that they are metallic silver, probably in the form of single crystals (see below). A majority of them have pronounced angular shapes. This is unlike the silver particles produced in the pyrolysis of silver acetate, which are spherical. Further, in the case of a 'good' crystal decomposed at a temperature well below the melting point, most of them are free from cavities, suggesting that they are not formed by the partially decomposed crystal breaking into small blocks which then decomposed completely. Their surface density on a completely decomposed crystal is ca. 10E11 /square-m. They grow to a maximum size and then the growth stops, as indicated by the relative uniformity of their sizes in all the micrographs (except (p) to (t) -- see below). The maximum diameter apparently increases with the temperature, from ca. 7 um at 513 K to ca. 14 um at 573 K.

The pebbles have also been observed by McAuslan (1957) in his study on the slow decomposition of silver azide. He

<<--
FIGS. 6.11 (a) to (x)
Number beneath each micrograph indicates its width in um;
for description see text

decomposed single crystals on a hot stage placed inside a scanning electron microscope, at temperatures unspecified but probably just below 453 K. The pebbles in his case were ca. 200 um in diameter.

In Figs. 4.11(l) & (u) a small amount of melting has occurred, as indicated by the presence of a small patch of white film surrounding the 'crystal' (see 4.11(o), where it is resolved into spherical specks). Most of the silver azide has apparently melted before decomposing in (p) to (t) (furnace temperature 578 K), and the 'pebbles' are some three times bigger in diameter. Pebbles formed at high temperatures may contain cavities. More interestingly, if formed from molten silver azide they show distinctive faceting and their cubo-octahedral shape suggests that the f.c.c. silver has grown into over-sized Wulff polyhedra (van Hardeveld & Hartog 1969). Coalescence of pebbles is also apparent at high pyrolysis temperatures.

Occasionally, there are regions in a decomposed crystal where many of the pebbles show signs of sintering and are highly non-angular in shape. Fig. 6.11(v) is an example (furnace temperature 518 K). The reasons for this phenomenon has not been investigated. Likewise, in a specimen decomposed at 418 K and shown in (w), the pebbles were found to be different in appearance, their most remarkable property being the possession of 'wiskers'. Micrograph (x) illustrates that

sometimes the crystal bends while decomposing (there, at 548 K).

Fig. 6.11(n) is a typical HVEM diffraction pattern of a small pebble; the particular pebble concerned is arrowed in 6.11(m) and was picked up from a crystal partially decomposed at 443 K and shown in 6.10(b). Note the presence of Kikuchi lines. The diffractograms show that the pebbles, or at least the smaller ones, are essentially monocrystalline; some extra spots present may be due to twinning, double reflection, or diffraction from neighbouring ones that the beam hit.

When the aperture of the beam was increased to examine many pebbles, the pattern changed into a great number of spots superimposed on rings. That little crystallographic order exists among them is also indicated by the X-ray pictures taken of decomposed crystals as a whole, which show no structure. The displacement of the pebbles while being pressed against the carbon film and the distortion of the crystal during mounting on the goniometer have been minimised, and could not be responsible for the large degrees of randomness indicated. It seems, therefore, that the product indeed retains little or no orientation relationship to the parent crystal: the pyrolysis is not topotaxical. This is in direct contrast to the cases of thallium, lead and sodium azides (Spath 1977). Also, this appears to contradict the observation by McAuslan (1957) that, whereas copper and gold evaporated on the silver azide surface

do not aggregate with preferred orientations, evaporated silver tends to have its (110) plane parallel to the (010) growth face of the azide substrate. On the other hand, Camp (1959) stated that only in thin flakes exposed to an intence electron beam was the produced silver found to be ordered with respect to the original silver azide, and not so in crystals decomposed by a low intensity beam or by exposure to practical sources of alpha- or gamma-ray. The comment is in order, however, that as far as dielectric breakdown is concerned the disputed question of topotaxy should have no great significance.

It is of interest to compare our observations with those of Montagu-Pollock (1961, 1962) on the end products in the pyrolysis of silver cyanamide crystals of um thickness. They decompose to give metallic silver, also in the form of pebble -- or 'specks' as called there -- which in his transmission electron micrographs were seen to protrude out from the crystal surface and to be angular in shape. Using electron diffraction he showed that they are single crystals and usually of random orientation relative to the parent crystal. One difference between our and his case, however, is that the cyanimide gives another solid product, an amorphous material which is probably either cyanogen polymer or carbon.

It may also be of interest to mention that no hexagonal close-packed structure was detected in the HVEM. This structure is, according to Quarrell (1937), the stable form of

Dotted lines represent contracting surfaces during decomposition.

Cross section of AgN_3 single crystals

Fig. 6.12

silver in very thin films.

6.4 TOPOCHEMISTRY

The TG results indicate that, in the temperature range 513-558 K and for $a < 0.9$, the pyrolysis of silver azide follows (6.4). Now, the crystals are much longer in one direction than in the other two, so that as pyrolysis proceeds, the surface area of the undecomposed part of a crystal will vary approximately as the square root of the volume of this part. This kinetic law therefore suggests that at constant temperature a is proportional to the area, i.e., the phase boundary contracts at a constant speed. We demonstrate here the validity of this interpretation.

We have said in Appendix A that among the needle-form crystals we have grown the cross sections are in the shape of a hexagon. Referring to Fig. 6.12, we define g by $A/D \equiv 2-g$. This dimensionless parameter varies in different crystals, but for those in our TG samples $0 < g << 1$. Taking that the hexagonal shape is equiangular, we have $B = (1-g)\sqrt{3}D$. The linear speeds at which the decomposing front moves into the crystal along the a- and the b-axis are assumed equal, and will be denoted by U. The scanning electron micrographs have shown that the ratio of the two speeds cannot be very different from unity. The volume of silver azide still undecomposed at time t is then

$$V(t) = ABC\,(1-s)\,(1 - s[(B/A)^2+(1-D/A)^2]^{1/2} - (1-s)(A-D)/2B) \qquad (6.5),$$

where $s \equiv 2\,U\,t/B$. Therefore

$$1-a \equiv V(t) / V(0) = V(t)/(\,ABC[1-(A-D)/2A]\,) = (1-s)[\,1-3s(1-g)/(3-g)\,] \qquad (6.6).$$

The resulting quadratic equation in s is solved and, choosing the sign such that a decreases when s increases, we obtain

$$[1-g/(3-2g)]s = 1 - (1 - a[1-g^2/(3-2g)^2])^{1/2} \qquad (6.7),$$

or, to first order of $y \equiv g/(3-2g) = (2B-A)/(2A-B)$,

$$1-(1-a)^{1/2} = 2(1-y)\,U\,t/B \qquad (6.8).$$

For example, if g = 0.2, then y 0.2/3 and y 0.005 0.

In previous experiments on silver azide powder, the kinetic law found was

$$da/dt = R\,(1-a)^{2/3} \qquad (6.9),$$

in the ranges 464 to 573 K and for a between 0 or 0.3 and 0.9 (Bartlett et al. 1958; Gray & Waddington 1957; Zakharov et al. 1966). In the single-crystal work reported in Bartlett el al. (1958), the decomposition curves were analysed by an acceleratory cubic expression followed by a decay law of the same type as (6.9). Our interpretation is consistent with the validity of (6.9) for, in the case of powder, the total surface area will vary as two thirds power of 1-a.

Our understanding of the kinetics of the decomposition in silver azide as being topochemical points to either a

surface or an interfacial mechanism. The second alternative is more likely since, as argued below, the reaction is autocatalytic. Eq. (6.4) will apply if and when a coherent silver film is formed on silver azide, and before the pyrolysis has become so advanced that the simple geometry of Fig. 6.4 no longer suffices. Decomposition may of course occur at point defects and dislocations (which are probably charged) within the crystals, but the contributions of these 'internal surfaces' appear unimportant.

6.5 MECHANISM

The decomposition of an ionic metal azide consists of the generation of azide radicals which combine bimolecularly to yield nitrogen gas, and the formation of the metal atoms. The pyrolysis of silver azide follows this overall scheme, as has been mentioned in Section 2.1. The detailed mechanism, however, is still uncertain.

6.5.1 The Suggested Mechanism

Here we propose a tentative mechanism for the regime T>464 K (the lower limit of temperature in our experiments) and a > 0.1. It is based on the proposal by Mott (1939) for the pyrolysis of barium azide, a model which is an extension of the Gurney-Mott (1938) theory of the photographic development of latent images in silver halides. We assume that the rate-limiting step is the thermal emission of electrons into silver

which has already be formed, from adjacent azide ions. This redox process at the interface may alternatively be viewed as the emission of holes from the partially filled band of the product into the valence band of the reactant. The rate of decomposition is controlled by the generation of holes in the azide. The negatively charged metallic nucleus attracts interstitial silver ions and grows. The holes combine at a nearby free surface where nitrogen gas can escape. The combination results in a steady concentration gradient and thus a net diffusive flux of holes from interface to surface. Since they diffuse away before combining, there is no polarisation at the interface hindering the discharge of interstitial silver ions.

In this mechanism the electron transfer from anions to cations takes place energetically via the fermi level of silver. The elementary steps of [a] interfacial activation, [b] cation drift and discharge, [c] hole diffusion, and [d] radical combination on the surface may be represented as

[a] $N_3^- \; Ag_n \underset{\Delta'}{\overset{\Delta}{\rightleftharpoons}} N_3 \; Ag_n^-$

[b] $Ag_i^+ + Ag_n^- \longrightarrow Ag_{n+1}$

[c] $N_3 \longrightarrow N_3$ (surface)

[d] $2\,N_3 \longrightarrow 3\,N_2$

We now examine the plausibility of this model. The rate-limiting step Δ will be elaborated upon in Section 6.5. It has been shown in Section 2.3 that the interstitial cation

is the dominant defect system in silver azide in thermodynamic equilibrium. A steady-state concentration of mobile cations should thus sustain [b]. Gas'maev et al. (1976) observed the average rate of silver nuclear growth in single crystals decomposing at 433 K, and also measured the ionic conductivity at that temperature. The growth rate was seen to be adequately accounted for by the flux of silver ions towards the metallic phase calculated according to Mott & Gurney (1948:pp.232-3). No data at higher temperatures are available. However, our other investigations, discribed in Section 2.6.2, has suggested that the activation energy of the hopping process [b] is probably 0.5 eV. Concerning [c], its mean free path has been inferred to be ca. 1 um (Bowden et al. 1962) and the hole mobility, discussed in Section 3.2, probably has an activation energy of a few tenths of a eV at most. The combination step [d] is exothermic by 9.5±0.5 eV. It probably occurs as an inelastic scattering of a hole by another localised at a trap of the type which is electrically neutral when filled with an electron (Section 7.1). Its activation energy may be expected to be relatively small: less than 0.2 eV according to Thomas & Tompkins (1951).

In our picture then, as a silver azide crystal decomposes surface films of silver are formed which, when a reaches a certain value < 0.1, cover the whole crystal. Cracks open up, but few or no silver nuclei are formed on the new free

surfaces along the sides of these cracks. This may be explained by the domination of interfacial growth of silver on the uppermost faces, over the competing formation of fresh silver film elsewhere, a process which is supposed to be comparatively slow. In this connection we may mention that, when silver azide is bombarded by alpha particles or recoiling fission fragments, silver appears not along their ionisation tracks, which are ca. 10 um long, but on the original surface of the crystal (Camp 1959). The reverse case is true in uranyl oxalate (Young 1960). In a study on the decomposition, by heavy charged particles, of alkali and alkaline earth azides and of their perchlorates, Oblivantsev et al. (1966) showed that the decomposition is due to hot spots generated along the particles tracks.

The continuous production of the silver pebbles is regarded as the secondary process of accretion of atoms in each patch of film, a process in which they migrate over distances of the order 10 um. The high diffusivity of silver atoms on the surface of silver azide at room temperature and above has already been mentioned in Section 3.3.2. Sharma & Spitz (1979) have showed that, on quartz substrate, silver atoms in a sputtered film agglomerate when heated. They explain this agglomeration by surface diffusion, and by diffusion creep with thermal compressive stress as the driving force. As have also been argued in Section 3.3.2, the patches of silver films do

not grow epitaxially, explaining the absence of topotaxy. On the other hand, individual pebbles grown within each crystallographic domain of the film can be monocrystalline.

Granqvist & Buhrman (1976) studied the sizes of metal particles prepared by a variety of techniques, including the growth of islands on a substrate by single-atom transport, and concluded that the logarithm of the particle diameter has a Gaussian distribution. Although the ranges of diameter of the particles studied were in the neighbourhood of 20 nm, and the precise form of log-normal distribution will most probably not be applicable to our much larger pebbles, nevertheless, by general statistical considerations, we would have expected some broad distribution of their diameters. That they in fact have a fairly uniform size which increases with temperature is, we suggest, due to the higher surface diffusivity of silver atoms, which increases the average distance these atoms migrate before accreting. Similar phenomena have been observed only in the decomposition of a few other substances. In a study on the pyrolysis and the photolysis of silver oxalate, Boldyrev et al. (1968) found that in both cases surface nuclei of silver were formed whose growth rate rapidly decreased after reaching diameters of 2 to 5 um. Their other results suggested that the rate-limiting step is the diffusion of interstitial Ag^+ ions through the oxalate, and they explained the criticality of the nucleus size by the depletion of these ions

around the nucleus. Again, in the pyrolysis of ammonium perchorate, Herley et al. (1970) noted that there is a limiting size for the surface nuclei, but which they did not attempt to explain.

In the evaporating of gold in 10E3 Pa argon, Hansson & Tholen (1978) found that often long chains of particles were formed which were of nearly the same size. However, this phenomenon is probably not connected with the phenomena being discussed.

6.5.2. Film Formation

Let us now consider how the silver film is formed on the surface in the beginning. Although an induction period has not generally been observed in the pyrolysis of silver azide, Pai Verneker & Maycock (1968) claimed to have detected its presence. They decomposed powders at moderate temperatures in a mass spectrometer and found, in the very early stages, a rise followed by a fall in the rate of nitrogen evolution not attributed to gas desorption. After this peak the rate became constant. The initial peak decreased if the size of the crystallites was larger, and increased if they were so doped that they contained more anion vacancies and less cation vacancies. Unfortunately, no kinetic analysis of this part of the decomposition curve was given.

Nevertheless, we may suggest a probable mechanism of film formation. A hole may be generated in silver azide by the

emission of a valence electron not only into the fermi level of the metallic phase, when present, but also into its own conduction band. The mobile electron or polaron (Young 1971) thus arising can be localised at a trap. During the time interval that the trap remains filled, an interstitial silver ion may diffuse to it, or diffuse nearby and then drift towards it under the influence of electrostatic interaction if it is negatively charged when filled. (Depending on its nature, it may be positively charged when empty, and neutral when filled.) The neutral atom so formed, if in the bulk, should, unlike the ion, have very low mobility. (The ionic and atomic contact radii of silver are 0.126 and 0.16 nm respectively.) Alone, the atom will release the electron after a while due to thermal excitation. If the trap is on or sufficiently near the surface, however, the atom can diffuse away, and the trap is resetted. Moreover, migrating atoms may aggregate, and once their number exceeds a certain limit (Mott 1939), the nucleus they form will survive and itself act as an electron trap (and later as an acceptor). In this way, the surface will be rapidly covered with a coherent layer of silver atoms.

6.5.3 Alternative Mechanisms

In discussing the mechanism proposed by Mott for the pyrolysis of barium azide, Young (1966,p.178) has pointed out an apparent inconsistency that the silver nucleus would permit a positive hole to diffuse away, and yet be capable of

attracting a positive ion. It seems, however, that there is no real difficulty. The sequence of elementary steps is envisaged as :

$$\mathbb{\Delta} \rightarrow \mathbb{\Delta}' \rightarrow \mathbb{\Delta} \rightarrow \mathbb{\Delta}' \rightarrow \ldots \mathbb{\Delta} \rightarrow (b) \rightarrow (c)$$

after which another $\mathbb{\Delta}$ is possible. The nucleus in effect acts as a cation-valence electron recombination centre and makes possible a process of internal electrolysis.

Nevertheless, a possible modification of our proposed mechanism is that instead of the holes diffusing away to a free surface, they combine in the vicinity of the interface, resulting in an aggregation of F-centres. The nitrogen formed is supposed to escape through fissures along the interface, while the aggregate presumably will collapse subsequently to form (colloidal) silver. Thomas & Tompkins (1951) and Prout & Moore (1969) have proposed this different mechanism for the pyrolysis of barium and strontium azides, respectively. In sodium azide, the existence of F-centres has been confirmed (Bartram et al. 1973); and in silver halides, F-centres are known to be stable defects and to have considerable mobility through interaction with a-centres (Mitchell 1949). In the case of silver azide, however, this mechanism appears unlikely, at least unless the decomposition is such that high local concentrations of exited anions are maintained, as possibly in decomposition by strongly absorbed radiation. Indeed, although an F-band has been tentatively identified in the absorption

spectrum of crystals partially decomposed by ultra-violet light (Section 2.2), it has never been reported in thermally decomposed crystals. Secondly, Sawkill (1955, 1957) in his electron diffraction study detected no F-centre aggregates, though it was shown later that this evidence related to decomposition by the electron beam (Camp 1959, 1960). Thirdly, metallic silver formed by the collapse of F-centres aggregates is likely to be highly orientated with the parent crystal, as is the case in the photolytic and electron beam decompositions of silver halide single crystals at high temperatures (Sonoike 1956). In any case, the formation of silver from F-centre aggregate cannot explain the outward growth of the 'pebbles'.

Another different mechanism was previously used by Gray & Waddington (1957), McLaren & Rogers (1957) and Bowden et al. (1962). In place of $\angle\Delta$, the rate-limiting step is taken to be the homogeneous generation of electron-hole pairs in the bulk of silver azide. The mobile electron (or polarons) are localised at traps, which are re-set by interstitial cations. Now, homogeneous mechanisms (as distinct from surface and interfacial ones) are indeed found in solid-state reactions, an example being that of the pyrolysis of alkali perchlorates (Cordes & Ruven Smith 1968). This is unlikely to be the case for silver azide, however. The homogeneous mechanism accounts for both the formation and the growth of silver nuclei, so that no induction should have been observed. Also, in the next sec-

tion we shall argue that silver, once formed, will provide an energetically more favourable path for the generation of holes than band-to-band transitions. Thirdly, a homogeneous mechanism cannot easily explain the different catalytic actions of oxides, and of compounds containing the same metal (see again the following section). Finally, using homogeneous reaction theory and with the assumptions that the trap density is constant and that the holes have short life-times, Gray & Waddington (1957) derived a reaction order of 2/3. The present work has shown that the apparent reaction order is purely a reflection of the interfacial geometry, and it changes to 1/2 when long crystals, instead of powders, are decomposed.

The most radically different proposal is by Savel'ev and co-workers (1966,1967). They found that cathodic polarisation at an external field of 0.23 or 0.6 MV/m accelerated the pyrolysis of silver azide, while anodic polarisation retarded its rate. Based on these observations and those of the influences of additives they suggested that the rate-limiting step is in fact (d). Their argument was that the lifetime of azide radicals on the surface would be reduced by an electronic space charge, and increased by a depletion region there. The polarisation effects therefore apparently indicated that the combination of radicals was the slowest elementary step. However, the observations are also explicable by our suggested mechanism, according to which the rate-limiting step $\Delta\Delta$ occurs

similarly at a covering interface and not in the bulk. The actions of dopants are discussed in Section 6.5.2.

6.6 CORRELATION WITH ELECTRONIC STRUCTURE

6.6.1 Autocatalysis

A simple consideration suggests that the emission of electrons into silver is less expensive energywise than that into the azide conduction band. We assume correct the band structure of silver azide given in Fig. 2.7. For silver, the work functions for various crystollographic faces have been listed in Table 3.1. We take that, as far as electronic energy levels are concerned, the silver film may be treated as siver with normal bulk properties, having $Wf' = 4.64 \pm 0.10$ eV > Wf, where Wf is the work function of silver azide. By the same arguement already stated in Section 3.2, we may assign the idealistic energy diagram of Fig. 3.4 to characterise the reactant-product contact. The energy step for an electron to climb, in going from the azide band to the lowest unfilled level in silver, is $\Delta E = Eg - Wf' + X$ or (see Section 2.2) 1.1 ± 0.3 eV. Here Eg, the band gap of the high-temperature allotrope, has, as a working hypothesis, been taken to be the same as that of the low-temperature form, which value, 4.1 ± 0.2 eV, has an uncertainty of 10% anyway. (In this scheme, ΔE has in fact been equated with W[+] in Section 3.2.) The thermal energy required to promote an electron from the valence into

the conduction band of the azide is between 0.45 Eg to 0.60 Eg (Section 2.2) or 1.8 to 2.5 eV, which is higher than ΔE by an amount significant even in view of the approximate nature of our calculations.

Based on an estimation combining various theoretically calculated and experimentally measured properties, Gray (1963) has given the electron affinity (there mistakenly called the work function) of silver azide as 4.9 eV. This would put the conduction band edge below the fermi levels of silver and most other metals. However, the value we adopt here was reported as an experimental result and should thus be more reliable. Moreover, if Gray's value as well as the foregoing idealisation of the azide-metal contact were both sufficiently valid, then in electrical conduction the electrons in the cathode would have only a small energy barrier to surmount to flow into the azide. (The barrier would exist purely because of the band bending arising from the injected charges themselves.) A space charge should then be maintained in the interfacial region by the thermally injecting cathode, a situation we can reject as argued in Section 3.2.

According to Young (1964) 'colloidal' silver in silver azide provides donor levels which are ca. 0.56 eV below the conduction band edge (Section 2.2). These energy levels, if they do exist (in single crystals), are much higher than the fermi level of bulk silver. They should, therefore, have no

direct effect on the rate-limiting step, which is the generation of holes at the interface with the silver film.

6.6.2 Additives

Zakharov and co-workers (1964, 1966, 1968) studied the catalytic effects of additives in polycrystalline silver azide. Their samples were in the form of either pressed tablet or powder. In the case of oxide additives, the samples were prepared by mixing solutions of silver nitrate and sodium azide in the presence of a finely dispersed suspension of micron-size particles of the oxide concerned.

Denoting pre-exponential factors and activation energies of pyrolysis and of electrical conductivity respectively as R*, E, 6*, and E[6], we may group their findings as below (the figure in brackets after each additive represent its amount in mol%):

(1) R*, E, and E[6] are unaffected, but 6* is increased or decreased, respectively, when Ag_2CO_3 (0.1-5) or $Pb(N_3)_2$ (0.15-6) is added;

(2) no significant changes in E and E[6], but R* is increased: $Cu(N_3)_2$ (1), NiO (30), CdO (10), and ZnO (1-12);

(3) E is reduced : for Co_2O_3 and Ni_2O_3, to ca. 1 eV; for Co_3O_4, to 0.8 eV; and for CoO, to 0.5 eV (all 10).

According to Zakharov et al., these results show that the rate-limiting step in the pyrolysis is (d). However, we can offer a

qualitative explanation of most of the findings by our proposed mechanism. In Group 1, the dopants almost certainly exist in the charge state CO_3^{2-} and Pb++ (radius 0.13 nm) and in substitutional positions. The concentration of interstitial silver ions is increased and decreased, respectively, in $Ag(CO_3)_x(N_3)_{1-2x}$ and $Ag_{1-2x}Pb_xN_3$, so that 6* is changed but not E[6]. There is no effect on either R* or E, because the equilibrium constant in the rate-limiting step $\Delta\lambda$ is not coupled to the ionic concentration. In Group 3, the additives may either form solid solutions or exist as distributed heterophase impurities which, at the pyrolysis temperatures, will be chemically inert. However, even if solid solutions are originally formed, they will precipitate out continuously when the host substance decomposes. Now, the reductions in the activation energy indicate changes in the mechanism. By measuring contact potentials under the experimental conditions of pyrolysis, Zakharov et al. estimated the work functions of Ni_2O_3, CoO and Co_3O_4 to be 5.3, 5.55 and 5.65 eV respectively; i.e., all higher than that of silver. These additives therefore are electron acceptors and electron transfers can be energetically more favourable at their interfaces with silver azides, explaining the lower E observed. Note that if additives of increasing work function are introduced, a stage will be reached when some other elementary step in the reaction scheme becomes rate-limiting instead.

Consider now Group 2. Zakharov et al. quoted the work function of ZnO as 4.2 eV, and that of CdO as being smaller still. They should not, therefore, compete with the silver product in catalysing $\Delta\Delta$. The non-action of NiO is unexpected, however, its work-function being given as 5.48 eV. If this value is correct, the anomaly may be a result of effects such as some chemical reaction on the interface between NiO and silver azide (cf. Williams 1978). On the other hand, the increases in R* in all thses cases are not explained. The situation is really more complex, since the shape of the few a-time curves published by Zakharov et al. is seen to be also changed. In the case of cupric azide, an interstitial solid solution is likely to be formed with copper in the charge state Cu^{++} (radius 0.07 nm), as it is in copper-doped AgCl (Burnham & Moser 1964). By hopping to the silver-silver azide interface, it will accept an electron by changing its oxidation state to the cuprous ion Cu^{+} or to the neutral metal. This should increase R*, since the concentration of the L.H.S. in $\Delta\Delta$ is reduced but, the work function of metallic copper being less than that of silver, E is not affected.

Bartlett (see Young 1966, p.196) noted that the co-precipitation of cadmium nitrate (ca. 3%) with silver azide greatly depressed the rate for a <ca. 0.05 but the remainder of the pyrolysis was apparently unaffected, whereas after blackening by exposure to hydrogen sulphide for a few seconds

the initial rate was enhanced. The presence of Cd++, if substitutional (its radius is 0.11 nm), leads to an excess of cation vacancies in the bulk and, likewise with the surface action of hydrogen sulphide, will influence the formation of the silver film. After the rate-limiting step has become the interfacial excitation the rate is no longer affected.

On the other hand, we can offer no obvious explanation for the observation (Kurochkin et al. 1968) that certain organic dyes increase the thermal reactivity of silver azide, the trend being greater reactivity with increased molecular chain length and number of -N=N- groups. Neither is it clear why the explosion temperature is lowered in silver azide co-precipitated with silver cyanamide solution (ca. 10 and 20% in nitric acid; Gray & Waddington 1957). However, the explosion temperature is only a rough indication of the rate of pyrolysis. Moreover, it is uncertain whether CNN-- ions were incorporated in the lattice substitutionally, or the prepared powder behaved simply as a physical mixture of azide and cyanamide.

6.7 KINETIC CONSTANTS

From Eqs. (6.4) and (6.8), the speed of advance of the decomposition front is calculated as $U = R\,B/4(1 - \gamma)$, where B and γ are the averages of respective values of each of the two crystals comprising the sample in hand. In Fig. 6.13, the

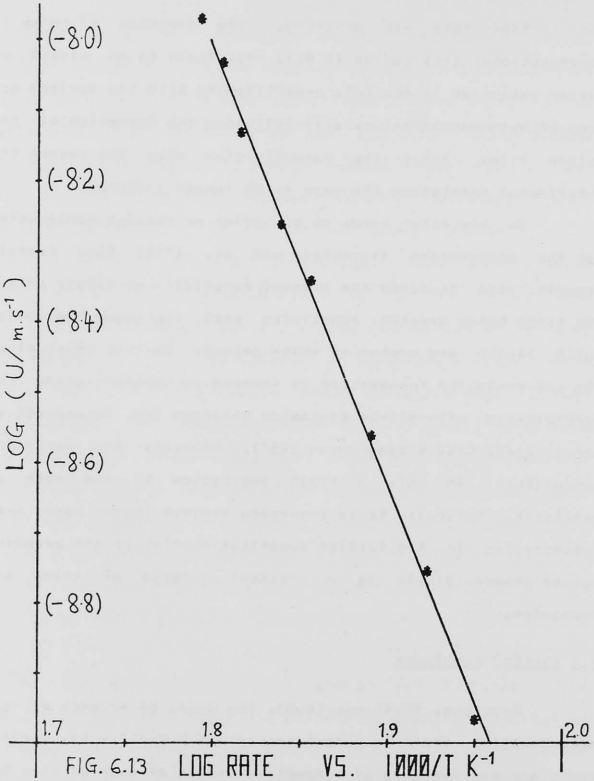

FIG. 6.13 LOG RATE VS. 1000/T K^{-1}

common logarithm of U is plotted against the reciprocal of temperature. The graph shows that, in m/s,

$$U = 10E3.1 \exp(1.23\ eV/\ kT) \qquad (6.10).$$

The standard errors in these numerical values are estimated to be much larger than are apparent from the residuals of the eight experimental points. The fractional error in the determination of R is reckoned as not appreciably larger than 2%, which is the expected inaccuracy of the thermobalance in measuring weight. Length measurements under the microscope are accurate to 5 um, so that the fractional error $\Delta U/U$ =ca. 13%. In addition, there are non-uniformity in the crystal cross-section, the ignored decomposition of the two ends of the crystal, and the approximations in taking B and γ simply as averages. Their effects on the functional form in (6.4) are unclear, but should be negligible within the straight-line section of the plot from which R was measured. Regarding T, a theoretical estimate was made of the discrepancy between the sample and the furnace temperatures. In Chaudhri & Field (1975) an equation was derived for the temperature, assumed uniform, of a reacting crystal placed in a gasous atmosphere where the flow is convective. We solved this equation, numerically by the Newton-Raphson method, using typical crystal dimensions and furnace temperature, and the calculated values of kinetic constants of the pyrolysis. The rise of crystal temperature is found to be not more than 3 K. The rise would be smaller for smaller

crystal dimensions, lower furnace temperature, smaller U* or larger E. If we take T' = 513 K, T" = 558 K, for which ln(U"/U') is ca. 2.30, the fractional error in E = T' T" k ln(U"/U')/(T"-T') is then 16%; a similar calculation of that in the pre-exponential factor U* gives 80%. Thus U* = 10E2.5 to 10E3.4 m/s, and E = 1.23±0.2 eV.

A comparison with the values of E obtained in previous works is displayed in Table 6.2.

Table 6.2 Activation Energy of Pyrolysis

Authors	Measurement	Sample	E /eV	Temp. /K
Audubert 1939	chemi-luminescence	powder?	1.7-1.9	500-560
Audubert 1952	gas evolution	powder?	1.65	511-558
Haycock (Garner 1955,p.238)	ditto	?	1.25	483-543
Gray & Waddington 1957	ditto	pellet*	1.56±0.22	503-573
Bartlett et al. 1958	ditto	powder*	1.36±0.1**	464-523
Zakharov 1964	weight	powder (a)*	1.30±0.1	470-520
Zakharov 1966	weight	powder (b)*	1.43±0.1	490-530

(a) particle size 3-9 um; (b) 1-10 um.
* Gray & Waddington, Bartlett et al., and Zakharov et al. specified that their samples were prepared from sodium azide and silver nitrate solutions.
**Bartlett et al. reported that, below the phase transition temperature, E is roughly 1.96 eV in the range 433 - 463 K.

Note that the two different choices of the functional form of f(1 - a) in (6.4) and in (6.9) affect the pre-exponential factor U*, but not E. We have not been able to deduce the

values of U* from the log(R) vs. 1/T graphs sometimes given in these previous works. The sizes of crystallites in a powder usually have an approximate Gaussian distribution (Hitchinson et al. 1973). It will be difficult to calculate U*, i.e. R* normalised to per unit area, even if the crystallites can be assumed to be all cubic in shape; in any case, the exact magnitude of the standard deviation in the distribution is unknown.

We now examine the physical significance of the macro-kinetic constants U* and E. First, they are interpretated in thermodynamic terms, so that the treatment is independent of the reaction mechanism. The advancing speed of a planar reaction interface is expected to be constant (Young 1966, pp.17-8) and is, by the modified Polanyi-Wigner equation we have discussed in Section 4.2.2 :

$$U = d(kT/h)\exp(\Delta S'/k)\exp(-\Delta H'/kT) \qquad (6.11),$$

where d =ca. 0.15 nm is the thickness of a monolayer of silver azide, and $\Delta S'$ and $\Delta H'$ are respectively the entropy and the enthalpy of activation. If the rate-limiting step is unimolecular, as Δ in our scheme is, the frequency factor kT/h may more accurately be replaced by the mean frequency of lattice vibration in silver azide. Now, the Debye temperature $\underline{I}$ is related to the velocity of sound v by the relation

$$\underline{I} = (hv/k)(4\pi V/3)$$

where V is the molecular volume. For silver azide, v has been

measured to be in the range 2.1 - 2.9 km/s (Table 1.2, Chapter 1). The unit-cell dimensions of the high-temperature form are unknown, but cannot be very different from those of the orthorhombic allotrope, so that V comes out to be 5 x 10E-29 cubic-m (Appendix A). Thus $I \leq 240$ K. At our experimental temperatures, which are all higher than I, the mean phonon frequency is therefore $kI/h = 5 \times 10E12$ Hz. From our experimental results, therefore, approximately $\Delta H' = 1.23$ eV and

$$\Delta S' = k \ln(7.5 \times 10E2 \text{ (m/s)} / U^*) = \text{ca. } 0$$

which is reasonable (Young 1966, p.44) and expected for our particular Δ which involves only the transfer of an electron.

Secondly, if our proposed mechanism is correct, the molar reaction speed is given by the rate of thermionic emission from silver azide into silver (Mott 1939). By modifying the Richardson-Dushman equation (Eq. (3.9), Chapter 3), the electronic flux density is

$$J' = P' \exp(-\Delta E/kT) \qquad (6.12),$$

where $P' = 7.5(m^*/m)10^{24} T^2$ /(s.square-m), in which q is the charge and m the mass of an electron, and m* its effective mass in silver films. The weak T dependence will, of course, not be experimentally significant. By taking an average value of T as 530 K, the pre-exponential factor comes out as 2.1(m*/m) 10E30 /(s.square-m). Further, since ΔE depends on the band gap which usually varies linearly with T (Aschroft &

Mermin 1976, p.566), $\Delta E = \Delta E (1 \pm r T)$, where r should be a few parts per 10E4 K. We assume that r has the minus sign, as was done in the case of barium azide (Mott 1939). By using the same value of V as before, the value of U* can be converted into 2.5 x 10E31 molecules/(s.square-m). This agrees with the modified pre-exponential factor derived here, P' exp(r ΔE /k), where ΔE /k is ca. 1.4x10E4 K, within expected ranges of the values of m* and r.

6.8 SUMMARY

The isothermal pyrolysis of single crystals of silver azide has been investigated in the temperature range 513 to 558 K using a thermobalance. The kinetic equation is determined as

$$1 - (1 - a)^{1/2} = t\, 4(1-\gamma)/B\, U^* \exp(E/kT)$$

where a is the molar fraction of decomposition, B the thickness of the specimen, $\gamma \ll 1$ is an aspect ratio, U* 10E2.5 to 10E3.4 m/s, and E 1.23±0.20 eV. The reaction is topochemical. The solid product (silver) has been examined with X-rays and with scanning and high voltage transmission electron microscopes. It is shown that silver aggregates in the form of 'pebbles' 7 to 14 um in diameter, which protrude out from the decomposing surface, are randomly orientated but are probably monocrystalline. A mechanism based on Mott's model is proposed, in which the reaction is autocatalytic. This as well

as its topochemical characteristics suggest that, as it proceeds, a silver film covers the crystal external surfaces.

The proposed mechanism appears to be supported by considerable evidence. The theoretical values of the activation energy E and the pre-exponential factor U* are in general agreement with the experimental results. Many effects of additives can also be explained. The mechanism may be applicable to the decompositions of some other metallic azides and, for example, silver cyanamide. Also, the work may have revealed a method of producing silver single crystals possessive of a uniform and controllabe size. Further experiments which will be interesting include studying the kinetics as well as the morphology of the pyrolysis when an electric field is applied, and to measure the effects of photons of different energies on the kinetics (cf. Jacobs et al. 1959) in different stages of the reaction.

After this investigation of slow decomposition under the action of heat, we are in a position to consider what mechanisms may together be responsible for the electrical decomposition and the dielectric breakdown of silver azide.

CHAPTER VII

MECHANISMS OF ELECTRICAL DECOMPOSITION, DIELECTRIC BREAKDOWN & EXPLOSION INITIATION

7.1 SUGGESTED MECHANISM OF ELECTRICAL DECOMPOSITION

In the last chapter we have proposed a scheme of elementary steps for the thermal decomposition of silver azide. It seems reasonable to suppose that the elementary processes responsible for the decompossition under a strong electric field bear a close similarity to those for the thermal case.

We suggest a mechanism for electrical decomposition as follows. Under the influence of a high field at the cathode, electrons are injected into the conduction band of silver azide; the process occurring in the early phase of thermal decomposition is equivalent in effect except that they are emitted from the valence band of the azide itself. The mobile electrons, or polarons, drift towards the anode. They constitute a non-equilibrium (surplus) concentration and so a net number of them may be localised at electron traps, in the interfacial regions (Section 3.2) as well as elsewhere in the bulk. An interstitial cation may then get discharged at a filled electron trap. (Cf. Section 6.5.2.) On the crystal surface, a neutral atom can migrate with a considerable speed and agglomerate, giving rise to a network of thin silver film, and to 'pebbles' which are permanent formations (Fig. 3.7 & 3.9). At very late stages, macroscopic patches of thick film are also formed (Fig. 3.9(g)). The non-uniform distribution of 'pebbles' in the form of 'trees', in contrast to the thermal case as illustrated in Fig. 6.11(a)), is consistent with the

observation by Camp (1959) that at very low rates of decomposition, caused by the action of e.g. low intensity electron beams or practical sources of alpha- or gamma-ray, silver is produced perferentially on specific areas.

In the advanced phase of thermal decomposition, electrons begin to be injected under the action of phonons into the fermi level of silver which has been produced, this process requiring less energy than the interband transition: the decomposition becomes autocatalytic. This does not happen in electrical decomposition, occurring as it is at room temperature. We do expect, however, that any silver aggregates produced will become efficient electron traps, so that new silver will have a preference to form next to existing silver. This explains the continued growth of the old 'trees' after the polarity of applied field was reversed between Figs. 3.7(f) and (g), (h) & (i).

In thermal decomposition, the emission or the thermal injection of a valence electron leaves behind a hole, which diffuses away and combines with another on a free surface of the crystal to produce nitrogen. In the electrical case, the valence electrons are extracted into the anode, in the separate process of field injection of holes. The holes drift from the anode towards the cathode, some of them combining bimolecularly on the way. A distinction, therefore, between the two cases is that in the former, the holes are generated just beneath a

surface film and they move by diffusion, while in the latter a macroscopic field is present and they drift in the bulk of the crystal. The appearance of internal factures and lines of 'dots' on the surface, found in the latter but not in the former, probably refects this difference.

The molecular rate of nitrogen evolution is generally about 0.3 of the initial rate of charge transport (Section 3.4.2). The interpretation of this observation is ambiguous, because the value 0.3 is probably accurate to only within a factor of 2, and we do not know what fraction of the charge movement is made up by holes. Nevertheless, if this fraction is constant, then an approximate proportionality of decomposition rate to conduction current seems reasonable. Consider the situation that there exist in the crystal a relatively large number of efficient hole trap (Section 3.2) and that most of the combinations take place between a localised hole and another hole that drifts slowly by. Denoting by N the trap density, presumed uniform, a, the trapping cross section, N*(x,t) the density of filled traps as a function of distance from the anode and time, w the probability per unit time that a trapped hole is thermally released, J(x) the hole flux, and c the combination cross section, we write

$$\partial N^*/\partial t = a\,(N-N^*)\,J(x) - w\,N^* - c\,N^*\,J(x) \qquad (7.1),$$

the last term representing the combination rate D(x). Hence, in the steady state $N^* = aNJ/(aJ+cJ+w) = ca.\ aN/(a+c)$, if w

is small compared to (a+c)J. This assumption is consistent with the observation that the evolution rates of nitrogen after J becomes zero is much smaller than that when the voltage is on (Section 3.4.1). On the other hand, since a steady rate of decomposition is reached in a time on the order of a minute (Figs. 3.14 & 15), w is probably not more than many seconds. (Cf. Discussions on hole trapping in Section 3.2.) Now, in the steady state N* does not change with t, so that

$$\text{div } J = -2\,D(x) \qquad (7.2),$$

where the factor of 2 accounts for the fact that each combination event remove a hole in the flux as well as reset a trap. In our one-dimensional situation, and since in the steady state N* has been shown to be not a function of x,

$$J(x) = J(0)\exp(-2\,c\,N^*\,x) \qquad (7.3).$$

The total decomposition rate is therefore

$$D = A\int_0^L D(x)\,dz = 2\,A\,c\,N^*\int_0^L J(x)\,dx$$

$$= a/(a+c)\;A\;[1-\exp(-2cNL)]\;J(0) \qquad (7.4),$$

where A is the cross sectional area and L the length of the sample. From (7.4) we see that D is proportional to J(0) or, if qJ(0)/I does not vary with I, to the measured initial current I. For samples whose A and L, and presumably N, are not very different, similar values of the proportionality factor are expected, explaining Fig. 3.16. In fact the product cN may be so large that, for L equal to a few mm, when the

cathode is reached $J(L) = J(0) \exp(-2cNL)$ is always nearly zero. This agrees with the indirect deduction (Section 3.3.2) that the combination of holes mainly occurs near the anode.

The constancy of D/I may also be explained in the situation where combinations occur mainly between mobile holes. Without repeating the mathematics, one can see that D remains proportional to J(anode)-J(cathode). Nevertheless, we suggest that the combination most probably have to take place via a trap. Its activation energy is less than 1.23 ± 0.2 eV, because it is not the rate controlling step in pyrolysis, but may still be very large compared to kT at room temperature (Section 6.5.1). On the other hand, the trap may be of the type that when filled it is neutral, so that electrostatic repulsion between two holes is avoided. Moreover, the observation that D/I greatly decreases after prolong period (Section 3.4.2) can be explained as an exhaustion of hole traps (silver formed are efficient traps of electrons only) so that $-2cNL$ becomes algebraically greater. Indeed, it will be very useful if a, c and N can be estimated so that Eq. (7.4) can be tested. Unfortunately, the kinetics experiments on pyrolysis do not yield information on these parameters, which are not involved in the rate-limiting step there.

7.2 IN SUPPORT OF SUGGESTED MECHANISM

7.2.1 Implausibility of Alternatives

In an investigation on dielectric breakdown and subsequent detonation of lead azide pellets, Sukhuskin et al. (1970) suggested that while in samples with densities not bigger than 3xE3 kg/cubic-m the breakdown occurred by microdischarges in the pores, in those with densities close to that of the single crystal (4.7xE3 kg/cubic-m, according to Federoff et al. 1960), the detonation was initiated probably not thermally, but due to the development of electron avalanches whose products reacted directly and caused decomposition. The idea was more precisely described in a later publication (Sukhushin et al. 1972), where some experimental evidence was also presented showing that decomposition takes place in silver, lead, and thallous azides at fields below 'breakdown values'; we have referred to these experiments in Section 3.3.2. They claimed that the decomposition was caused by impact ionisation (of electrons in Ag and Tl, of holes in Pb azides). The possible source of the 'hot' carriers was thought to be electrode injection, injection from space charge field, or electrostatic ionisation. The local high fields required were reckoned to be generated by space charge domains which were continually being swept across the crystal.

In this so-called avalanche-chemical model of Sukhushin et al., the fluctuating character of the current (Sections 2.5.2 & 3.2) will probably be attributed to the occurrence of discrete avalanches of electrons. To the extent that injections of non-equilibrium charge carriers are supposed to take place, the model agrees with ours. However, it will not easily explain the fact, mentioned in Section 3.4.2, that initially the decomposition rate does not increase greatly when the current rises sharply at the onset of final breakdown. Furthermore, the existence of high-field domains depends on a physical process which phenomenologically gives rise to a voltage-controlled differential negative resistance (see e.g. Sze 1969, Chapter 14), and mechanistically form thin slices of the crystal extending perpendicular to the current direction, which separate regions of low field and propagate along the crystal at carrier drift velocity. A few mechanisms do this but they are found in only a small number of semiconductors such as InP, CdTe and ZnSe. It seems unreasonable to speculates that some such mechanism operate in the three azides, in the absence of any support whether experimental or theoretical. We shall see that, in contrast, our proposed explanation of dielectric breakdown envisages the formation, due to decomposition, of high-current filaments running along the field direction.

Another mechanism was suggested by de Panafieu et al.

(1976) for the particular case of field-enhanced thermal decomposition in potassium azide. As mentioned in Section 3.3.2, it seems possible to us that the large effect they observed experimentally was merely due to electrolysis.

Their suggestion is that the application of the field greatly increases the surface field in the crystal, which in turn faciliates the dissociation of azide ions and thus the decomposition. Now, as pointed out by Lehovec (1953) and Lifshits & Geguqin (1965), an electtric double layer exists on the surface of an ionic crystal whenever the enthalpies of formation of the cation and the anion vacancies are unequal, a condition which is generally in force because of the difference in their sizes etc. The field experienced by this intrinsic dipole layer may be considerable even at room temperature; the width of the surface layer decreases at higher temperatures. It may become even more intense when an external field is applied, due to the ionic space charge set up by a partially blocking electrode. Then, the surface field is expected to lead to a proportional distortion in the azide ions: a quantitative calculation in the case of crystal field induced asymmetry in lead azide has been done by Fisher et al. (1975). Finally, it has often been proposed (Soderquist 1968; S. F. Trevino et al. 1970, unpublished, quoted by Choi in Fair & Walker 1977) that an intra-ionic polarisation reduces the stability of the ions. In all, therefore, the field effect

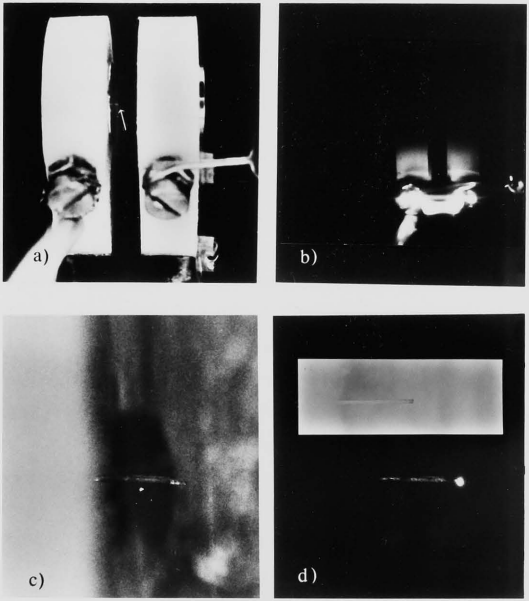
a)
b)
c)
d)

suggested by de Panafieu et al. should exist, but this is only a qualitative fact.

In silver azide, as in potassium azide at high temperatures, we think that the effect is small and not responsible for the observed decomposition. The effect is basically an electrostatic process, by which the proportionality of the decomposition rate to the current (Section 3.4.2) is hard to explain. Indeed, we have shown in a qualitative but rather dramatic experiment that, under a high field but with the current limited to a very small value, little or no electrical decomposition occurs. This is described below.

7.2.2 Corona Discharge Experiment

Two PTFE blocks were fixed on a perspex plate by screws, the separation between them being 3.3 mm (Fig. 7.1(a)). Each rigidly held a brass cylinder which was connected through a bolt to a wire. On the inside face of one was drilled a hole about 1 mm deep. Silverdag was introduced into the hole, and a silver azide crystal was slowly pushed vertically into the paint before it hardened. Fig. 7.1(c) shows one of the crystals used, whose free part is 1.35 mm long. The white arrow in (a) points to the crystal.

When a voltage of either polarity but exceeding ca. 6 kV was applied across the two cylinders, corona discharge

<<--
FIG. 7.1
For scales and descriptions see text

occurred as manifested by a steady blue light sphere surrounding the tip of the crystal (Fig. 7.1(d)), the radius of the light sphere apparently increasing with the voltage. Sometimes, glows were also found at a few spots on the surface of the opposite pole piece. After sustaining the discharge for a few minutes, the tip was observed to have turned dark (inset in (d)). If the crystal was then put into a weak ammonia solution, an insoluble brownish-colour skin could be seen to float off, the remaining crystal becoming transparent again. This surface decomposition of the crystal tip was thought to be due to heating by the corona discharge. Now, taking the crystal as a perfect insulator and ignoring edge effects, we treat the system as simply two capacitors in series and calculate the field (uniform in our approximation) in the crystal as

$$F = V/(L + el) \qquad (7.5),$$

where V is the voltage between the brass cylinders, L the length of the crystal, e its dielectric constant (= 9.5), and l = 3.3mm - L is the length of the air gap. F comes out as 250 to 350 kV/m for the different crystals we have used. The amount of decomposition observed is much smaller than that of electrical decomposition which, one expects, will be caused by fields of these magnitudes (Section 3.3.1).

When the voltage was increased beyond ca. 7 kV, an arc discharge was produced between the air gap separating the free end of the crystal and the opposite electrode cylinder,

resulting in the explosion of the crystal. Further experiments were performed with the crystal immersed in silicone oil (Edwards Vacuum, MS 705). When the oil was clean enough it could be considered as a lossless dielectric with a static relative permittivity of 2; a maximum field calculated with this assumption to be 1 MV/m was attained in a sample but no fast decomposition was initiated. Parenthetically, we should mention that, in the first experiment using oil, the oil was made to cover up to the top of the electrode cylinders only, and at 13.5 kV an arc developed across the nuts holding wires to the electrodes (Fig. 7.1(b)). The oil level was increased, but then the crystal came loose and 'danced' between the two pole pieces. It was probably charged at each contact with the electrodes and moved because of electrophoresis. Subsequent samples were, after having been inserted to the silverdag, dried in an evacuated dessicator and this procedure appeared to ensure a mechanically strong bonding.

Lastly, we note that the breakdown of lead azide has been investigated under the condition that both electrodes are insulated by mylar sheets (Leopold 1973; Avramc et al. 1976). The result obtained is similar to ours: both pressed pellets and single crystals withstand a field up to four times the value that leads to breakdown in contacted samples, for half an hour without any initiation of fast decomposition.

7.3 DIELECTRIC BREAKDOWN THEORIES

Fundamental studies on solid insulator breakdown have been going on for over a century and the subject is truly huge. One finds copious literature which includes monographs and book-length reviews (Whitehead 1951, Franz 1956, Klein 1969a, O'Dwyer 1973), dealing with a great and, sometimes, confusing variety of processes. More often than not, available data on a paticular breakdown process are still inadequate to identify its mechanism beyond reasonable doubt. Our purpose in this section will be restricted to setting out the types of mechanisms which have been proposed for the breakdown of 'thick', homogeneous ionic crystals, so that the one we shall suggest may be put in a perspective. (By 'thick' samples we mean those whose breakdown is by a bulk mechanism, rather than by an inter-electrode process such as tunnelling.)

On the basis of both experimental and theoretical evidence, dielectric breakdown has been catalogued as either thermal or 'purely electrical'. Historically, the second category has been sub-divided into intrinsic and avalanche types. However, persistent attempts to measure a unique, ultimate breakdown strength for a given material have not met with success. The trend, therefore, is to draw no distinction between the two types, which collectively may be designated 'purely electrical' in a terminology due to O'Dwyer (1973). In contrast, thermal breakdown is a simpler and quite unified

concept and, below, it will be discussed first but briefly. Furthermore, in addition to the two generally recognised classes, we wish to propose the notion of a third one, which we shall name 'secondary processes'. This category includes our suggested mechanism for silver azide and will be discussed last.

We should note at the outset, even if it may be obvious, that the actual mechanism underlying a breakdown depends not only on the substance in hand, but also on boundary conditions like temperature and the manner of voltage application. Thus, at ambients higher than roughly 500 K, the breakdown of alkali halides is thermal in general, but is purely electrical below room temperature (Konorova & Sorokina 1965). At intermediate temperatures the situation is on the whole uncertain (Hanscomb 1970). We shall suggest a mechanism for the breakdown of silver azide at room temperature. The question of how generally applicable it is to silver azide under different conditions -- and to other compounds -- will be taken up in the concluding chapter.

7.4 THERMAL BREAKDOWN

This type of breakdown, recognised by Wagner as early as in 1922, is treated as a continuation of the low field situation: considerations based on pre-breakdown conditions are assumed to apply without basic modification. That is, no

processes other than Joule heating and thermal conduction contribute to thermal balance in the dielectric. The equation governing the temperature T(r, t) at an arbitrary 'point' r in it at time t is

$$C(\partial T/\partial t) - \text{div}\,(K\ \text{grad}\ T) = \sigma F^2 \qquad (7.5),$$

where C is its 'specific' heat per unit volume, K its thermal and σ its electrical conductivities, and F the local electric field. As breakdown of the dielectric as a whole is associated with its hottest part, only T*(t), the maximum value of T at time t, needs to be looked at. The calculation of T*(t) will involve a number of boundary conditions: the temperature and thermal conductivities of the environment and of the electrodes, the explicit form of

$$\sigma = \sigma(T, F) \qquad (7.6),$$

i.e., the nature of the conduction processes (cf. Section 3.1), and that of

$$F = F(r, t) \qquad (7.7),$$

i.e., the sample geometry, electrode configuration, and waveform of applied voltage. K has been taken as constant, which is usually true, at least in comparison to $\sigma(T)$. It turns out (e.g. O'Dwyer 1973) that under a very general condition, namely that σ is an increasing function of T and hence there is a positive feedback loop, and in the case of a DC voltage applied, the solutions of T*(t) shows certain universal characteristics. The most important feature is that at low

fields T* rises with time but at a steadily decreasing rate, approaching asymtotically some finite values. However, a threshold field F* exists, corresponding to the asymtotic value Tc which often is a lower temperature than the melting point of the dielectric. F* is such that for F > F*, T* increases at first rapidly and then slows down, as for F < F*, but Tc is reached in a finite time after which T* rather suddenly 'takes off', rising without limit. The time elapsed before the current runaway happens decreases with increasing F. This time as well as the voltage-current characteristic has been calculated by Altcheh & Klein (1973) for the cases of thin-film and cylindrical samples and using several possible forms of Eq. (7.6).

Some general observations on thermal breakdown are:

[1] It is favoured at high temperatures, when δ is greater and K smaller normally. Its F* drops as the ambient temperature is raised.

[2] F* varies with the thermal properties of the surroundings and the electrodes.

[3] Also, F* has a pronounced time dependence. In practice, it takes milliseconds to seconds for a thermal breakdown to occur.

7.5 PURELY ELECTRICAL BREAKDOWN

For some materials below certain temperatures, current instability happens at fields lower than the F* dictated by preceding considerations. It is still commonly agreed (but see the proposal of Budenstein described later) that the heating effect of the current remains responsible for the ultimate disruption. However, the abrupt current rise itself cannot be of thermal origin. The generally accepted explanation is that the current runaway is due to impact ionisation, by interband transitions (an idea which was originally put forward by von Hippel (1937) who made an analogy with gas discharge) or, possibly, by ionisation from donor-like impurity levels. The primary 'hot' electrons causing the ionisation may be injected from the cathode by thermionic emission with Schottky lowering of the barrier or by thermally assisted field emission, or they may be generated by some mechanisms in the bulk (Section 3.1.1 (c)).

It should be emphasised that there does not appear to be strong direct evidence that impact ionisation is in fact a precursor of dielectric breakdown. Unlike the case in semiconductors, data on the field dependence of ionisation coefficients in insulators are scarce. Nevertheless, the multiplication of charge carriers by collision ionisation is generally accepted as the central process in both cases (O'Dwyer, p.13 -- but see end of this section). One

difference, however, is that in semiconductors two-carrier ionisation operates, but in insulators, whose band gaps are wide, impact ionisation is thought to be feasible by electrons only, owing to the deep trapping in general of holes which therefore have very low mobilities (in silver azide: Section 3.2).

As we have mentioned in the introduction, some older theories envisaged that for each material there is an ultimate breakdown field. In these 'intrinsic' breakdowns, the free electrons in the bulk of the materials are accelerated by the electric field but retarded through scattering by the crystal lattice. The field exceeds the breakdown value when the average energy gain becomes greater than the possible energy loss, so that a steady state can no longer be maintained. The critical electron energy value is usually taken as the interband ionisation energy: Frohlich's (1937) high energy criterion. Available theoretical predictions from this physical picture have been calculated either by staying at the one-electron approximation level or, if the collective energy distribution among carriers is taken into account, by (Frohlich & Paranjape 1956) assuming that Maxwellian statistics apply, with the 'hot' electrons assigned a temperature which is greater than the lattice temperature. However, with the accumulation of experimental data, the intrinsic theories appeared more and more unsatisfactory. No unique breakdown

strength could be determined for any of the substance studied in even the most carefully prepared samples, as reviewed in (Cooper 1966) and (Klein 1969a). The breakdown criterion of 'the onset of ionisation' was also doubted, since copious ionisation without breakdown occurring can be observed in semiconductors (the most common examples being Zener diodes operating in the avalanching range) or during the anodic growth of aluminium oxide (van Geel et al. 1957).

'Intrinsic' theories picture the multiplication of the carrier number as an abrupt change from the steady state, and identify impact ionisation as the onset of breakdown. In contradistinction, 'avalanche' breakdown theories view it as a gradually building up process with increasing field strengths, during which the collision ionisation is balanced by the inverse process of recombination, until the Joule heating of the current reaches the critical magnitude leading to melting or, in exothermic substances, to decomposition which is self-sustained.

The basic concept that equates the high temperature resulting from the build up of electron avalanches to dielectric breakdown is simple, but to devise a complete mechanism is complicated and has been done in many ways. In the so-called forty-generation theory, Seitz (1949) considers single electrons injected from the cathode. He shows by an order-of-magnitude calculation that criticality is reached if

on average there are 40 ionising collisions along the length of the crystal. Forlani & Minnaja (1964) include the origin of the injected electrons into consideration by taking it to be field emission ([c] in Section 3.1.2).

The above theories are based on many simplifying assumptions, the most objectionable of which being probably the neglect of space charges. With this assumption, a sharp value of the threshold breakdown field is predicted, below which no electrical failure takes place, but at which it will occur in a few ns, the time required for the avalanche to reach the new size. However, space charges are bound to arise, because the holes generated in the pair productions are usually immobile relative to the electrons. The earliest theory which allows for the non-uniformity of the field due to space charges is due to O'Dwyer (1967) and has been further developed by the same author (1969a, b). In it, the positive charges enhance the cathode field and thus the electron injection, but this positive feedback action is opposed by the drifting away of the positive charges. A balance is no longer possible when the applied field exceeds a threshold value, the cathode field rises sharply, and current instability results. DiStefano & Shatzkes (1974) and Klein & Solomon (1976) have recently treated the case in which the feedback is opposed by electron-hole recombination. This situation applies when all the holes are trapped so deep that their drift can totally be ignored.

Another model, proposed by Klein (1972) for the case of insulating films, is particularly interesting. In this picture, an electron injected into the conduction band of the dielectric is the initial event. It causes impact ionisation, producing a finite avalanche of free electrons and leaving behind nearly (but not quite) immobile positive charges. The electrons are quickly swept to the anode while the positive charges slowly drift to the cathode. The positive charges prevent the formation of large, destructive avalanches in the bulk but enhance the field at the cathode. In most cases the positive charge clusters leave the insulator without further effects. However, the enhancement of the field at the cathode greatly increases the local injection rate of electrons, so there is a finite probability that an injected electron will hit the tiny charge cluster during its transit through the insulator. When this happens, there is further avalanching with its accompanying field enhancement and increase in the chance for successor avalanches. When this build up results in certainty of electron injection during the transit time of positive charges, local instability with current runaway arises. According to this model, the breakdown event takes on a statistical character. The disruption occurs at a spot random in space, and over a range of fields, the time to breakdown decreasing smoothly as some exponential function of increasing field.

The basic assumption in all the above theories and models is that the formation of electron avalanches is the prime agent of non-thermal breakdowns. Its validity, although commonly accepted (the case is particularly strong in thin films: Forlani & Minnaja 1969), has not been unchallenged. From their work on Al-SiO-Al capacitors, Budenstein & Hayes (1967) proposed that the breakdown occurs due to the breaking of chemical bonds by high local fields which polarised the ions in SiO. A similar mechanism was suggested by Harari (1977) for the breakdown of thermally grown SiO_2 films, maintaining that no trapping of holes was observed in his samples.

Shousha et al. (1972) proposed a model of 'avalanche-thermal' breakdown where the thermal runaway follows a nondestructive electronic avalanche, which raises the temperature of the filamentary channel and thus its conductivity. In this model, the time to breakdown is expected to be on the order of seconds and the breakdown field will be lower than that required to cause either thermal or purely electrical breakdown. The model may serve as an interpretation of the experimental results of Budenstein & Hays (1969) who, contradicting Klein (1969b, & Gafni 1966, & Burstein 1967, & Levanon 1967), argued that the thermal breakdown of thin-film capacitors is localised rather than over their whole area.

The most novel idea has been advanced by Budenstein and students (Budenstein 1973, Lloyd & Budenstein 1977). According

to them, when the density of excess charge in a local region of a dielectric exceeds a critical value, chemical bonds are broken. This produces a gaseous plasma containing excited atoms, ions, and free electrons. If the process is self-sustained, the plasma grows to a gaseous channel bridging the electrodes. (We note that chemical decomposition caused by energetic electrons injected or extracted from an electrode and culminating in the formation of a hollow discharge channel has recently been used to explain long induction time breakdown in polymers: Tanaka & Greenwood 1977.) The distinguishing features of this model is that the source of the excess charge may be a number of means and not necessarily impact ionisation, and that the gaseous channel grows prior to the attainment of the high conductance characteristic of breakdown. (In both thermal and avalanche theories, the discharge channel which constitutes the structural and compositional disruption is considered to form after the breakdown event, arising as it is out of the Joule heating of the high current density supported.) Experimental evidence which Budenstein has cited in support of his model includes:

[1] Cooper & Elliott (1966) were able to detect light emission 20 ns before voltage collapse in KBr;

[2] in a continuation of their investigation of pre-breakdown light emission, Cooper & Elliott (1968) showed that the discharge channel is in the direction of current instability,

which is not necessarily in the direction of applied field; and [3] in SiO_2, the chemical composition of the products from a breakdown channel is not explicable in terms of thermal decomposition, but is so if the material is broken down into its separate atoms which subsequently react (Ridley 1975).

Another empirical result we have noticed and which also contradicts the occurrence of avalanches is that, in boron, Klein (1968) found for the concentration of carriers an increase only by a factor of 10 at the onset of breakdown.

None of the models alternative to the avalanche theories is well-developed, remaining essentially speculative.

7.6 'SECONDARY PROCESSES' BREAKDOWN

With the exception of the novel models of Shousha et al., Klein and Rudenstein, the purely electrical theories described in the last section share two common characteristics. Their breakdowns have no time dependence down to a microsecond or less. In fact, an experimental observation on a given substance under certain conditions that the breakdown field stength is not a function of the voltage waveform from DC to single-shot impulses with milliseconds rise times will be taken as strongly pointing to an avalanche mechanism. Secondly, for homogeneous materials of widely different structures and compositions the same orders of magnitude are predicted for the breakdown field at room temperature, namely 100 and 1000 MV/m.

The main reason is that the electron ionisation coefficient is generally small until a field of these magnitudes is approached. Although in Budenstein's model there is no quantitative prediction of the breakdown field, we think that there will predictably be a large spread above an absolute lower limit, the time to breakdown decreasing with an increasing field in that range. This feature is explicitly stated by Klein for his model.

In this section we consider mechanisms by which long times to breakdown can be explained and the fields necessitated in some of which are much less than 100 MV/m. All of them involve the operation of certain processes in addition to conduction, Joule heating and sometimes electron avalanching, hence our proposed terminology of 'secondary processes' breakdowns. The processes are not, however, chemical degradation or other ageing effects under the action of thermal or other evironmental factors. These effects have been studied extensively in polymers; strictly speaking, they are not breakdown phenomena. The mechanisms we have in mind depend primarily on the action of an electric field only and are found in crystalline insulators. Moreover, only the action of the field on the insulator proper is considered relevant; thus excluded is 'tracking' (Whitehead 1951, pp. 223 - 233), or a discharge in the ambient gas but along the insulator surface because of surface conductance or local enhancement of the

electric field (see, however, the concluding chapter)

The earliest secondary processes breakdown discussed in the literature involves the occurrence of some electrochemical processes. In the paper which first put forward the idea of explaining the breakdown of alkali halides by electron avalanches, von Hippel (1937) also reported that in NaCl and NaCl doped with 0.1 % AgCl at the temperature of 800 K, when the breakdown field is approached a dendrite was seen to grow out of the cathode toward the anode. He ascribed the phenomenon to the discharge of sodium and silver ions by electrons. These electrons were produced in avalanches, subsequently slowed down by the positive space charges left behind, and trapped by the cations. At the same time, he thought that the cathode injected electrons due to the field enhancement, again resulting in the formation of metal atoms. The atoms coagulated, originating the metallic elongation of the cathode. A similar mechanism, the growth of conducting bridges due to electrode-oxide reaction, was envisaged by Chou & Eldridge (1970) in the breakdown of silicon dioxide at high temperatures. Organic dielectrics, on the other hand, may suffer breakdown through the classical process of electrolysis (Whitehead 1951, Chapter 5).

The next type of mechanisms involve the drift of ions. In silica films formed by ion implantation, Dylewski & Joshi (1977) observed that when the metal electrode was negative, the

counter electrode being the silicon bulk, the dielectric strength was ca. 1000MV/m, and no breakdown occurred if the applied field was slightly lower. When the metal electrode was positive, however, lower fields still caused breakdowns but with longer delays, e.g. 30 s at 600 MV/m. The authors identified this time dependence with that of the formation of a positive space charge at the silicon-silicon dioxide interface. The space charge arose from the presence of impurity ions such as Na^+, and it enhanced the local field until the 'breakdown strength' was exceeded. In his work on the same system, Ridley (1975) put forward a more specific model for the breakdown, after arguing that the introduction of some unobservable electronic process like impact ionisation was entirely unnecessary. In this model, field emission at the cathode led to filamentary current and Joule heating; an additional process was postulated that resulted in a positive feedback loop, namely, the activation of impurity ions like Na^+ and H^+ which drifted towards the cathode and enhanced the field there. The processes of bi-polar injection, filamentary current because of inhomogeneities in the material, the positive feedback action due to trappings of holes at the cathode and electrons at the anode, and finally thermal runaway have also been suggested as responsible for the breakdown of silicon (Barnett & Milnes 1966), but instability by such a mechanism has not been verified in other semiconductors nor in any insulator.

In alkali halides, it is still uncertain whether the enhancement of the cathodic field by an ionic space charge can be important. At temperatures less than ca. 800 K these substances conduct by ionic transport. Alger & von Hippel (1949) suggested ionic polarisation as a plausible explanation of the sharp decrease in breakdown strength which they found for KBr above 473 K. Recent work by Cooper & Pulfrey (1971) claimed, however, that ionic drift plays no significant role in the breakdown of KBr between 223 and 300 K, and that field enhancement arose only from the accumulation of positive space charge generated by electron impact ionisation. On the other hand, Watson & Heyes (1970) observed that, in NaCl at 573 K and at 623 K, the time to breakdown varies between <1 to 150 us and inversely proportional to the field. This observation they interpretated in terms of the time dependent accumulation of cations in front of the cathode.

Finally, we come to breakdowns which can have induction times as long as an hour and more. The proposal of Thoma (1975, 1976) has already been discussed in Section 2.5.2: he attributed the breakdown very generally to the growth of conduction filaments due to the dislocation structure of the insulator. Very recently (December 1978), Narayan et al. reported that breakdown in single crystals of MgO at 1300 K occurred under an applied field of 100 kV/m after over 100 hours. They suggested that during the induction time ('incuba-

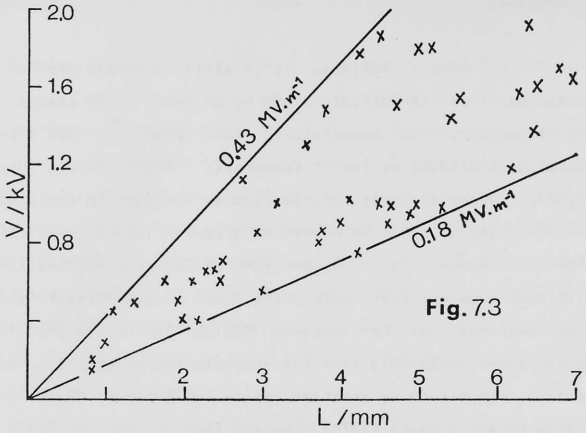
2.0
1.6
1.2
0.8
V / kV
0.43 MV.m⁻¹
0.18 MV.m⁻¹
2
3
4
5
6
7
L / mm

Fig. 7.3

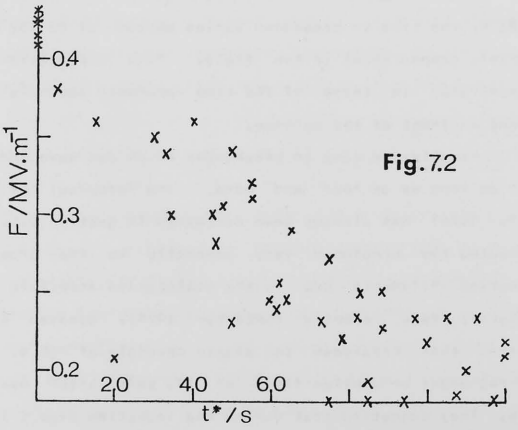
0.4
0.3
0.2
F / MV.m⁻¹
2.0
4.0
6.0
t* / s

Fig. 7.2

tion period') the properties of the material in the vicinity of dislocations and small-angle grain boundaries changed. The changes increased the conductance along these pathways, leading to current filaments, local heating, and thus dielectric breakdown. They stated that no evidence was found for metal-precipitate formation either of impurities or of Mg, but that small interstitial clusters were observed indicating some contribution of interstitial conductivity to the breakdown process. They did not specify the nature of the structural and electrical changes any further, nor their mechanisms.

Below we shall, after discussing the experimental observations, put forward a mechanistic model for the breakdown of silver azide. The suggested mechanism belongs to what we have called the 'secondary processes' type and, in fact, shares some common features with all the models described above.

7.7 OBSERVED CHARACTERISTICS OF DIELECTRIC BREAKDOWN OF SILVER AZIDE

Our model is put forward by consideration of the known facts about the breakdown of silver azide.

[1] It occurs whenever the field F is strong enough to cause electrical decomposition, although the induction time t* may be many hours (Section 3.3.1). Fig. 7.2 summarises our measurements on samples with silverdag painted electrodes; cases where t* > 2 min have been arbitrarily excluded. F has been

calculated as applied voltage V divided by inter-electrode distance L, and their values are given in Fig. 7.3. We did not notice any apparent correlation between L and t*. (The longest sample we have used had L=25.1 mm, V=3 kV, t*=250 s, and explosion was initiated at the anode.)

[2] The probability of breakdown under an AC field rapidly decreases with the frequency (Bowden & McLaren 1958). We have repeated the experiment and found that at 50 Hz under fields of 0.6±0.1 MV/m peak-to-peak, t* are 10±5 s, while at 2 kHz no breakdown occurs even up to 30 min at 1.2 MV/m. An AC field gives rise to little or no ionic polarisations (Appendix B), and any electrical decomposition is greatly reduced (Section 3.3.1). Further, no breakdown can be brought about if the field is applied through one insulated electrode (Section 7.2), when again no electrical decomposition can take place.

[3] During the induction time, an appreciable current flows that gradually increases. The existence of a large current precursor before the final breakdown, the fact that t* can be vastly in excess of a microsecond, and the moderate values of the breakdown field combine to rule out all purely electrical mechanisms.

[4] In particular, our observation (see Section 7.7 below) concerning the location of subsequent explosion initiations are against the Seitz (1949) and the O'Dwyer (1967) models, in which most of the energy of impact-generated carriers is at the

exit electrode, as well as the DiStefano & Shatzkes and the Klein & Solomon (1976) models, in which it is at the injecting electrode.

[5] The unusually long t* points to either a thermal breakdown or a process involving the build up of space charges. However, it may be seen that the initail value of the current when the field is first applied corresponds to a power density which, however non-uniform, is insufficient to cause the gradual increase of the current by local temperature rise; cf. the solutions of Eq. (7.5) for a planar geometry by Ridley (1973), and for a cylindrical geometry by Down et al. (1975) using Green's function. The relaxation time of ionic space charges is 10E3 s or shorter (Section 2.5.2), and by itself not long enough to explain t* which can be up to hours.

[6] Using a transient digitiser to record the current, we found that the final stage of the breakdown is completed in ca. 1 us, after which the low resistance path between the electrodes is maintained for some tens of us by the detonating crystal and resulting plasma. Just before this final breakdown the currents, which till then vary slowly enough to be read on a galvanometer, are 50±25 uA in all samples tested and appear quite uncorrelated with their cross sectional areas. Zakharov et al. (1964) measured the 'pre-breakdown current' in pellets of 8 mm diameter, and obtained approximately the same value of 70 uA at the different temperatures of 353 and 378 K. We have

also made the measurement at 273.2 K for three crystals, and found the value of 40±10 uA.

[7] The subsequent initiation of fast decomposition is thermal; this will be discussed in Section 7.9.

We have shown that when a moderate field is applied to silver azide through conducting electrodes, decomposition takes place prior to the eventual breakdown. To explain the breakdown, we regard it unnecessary to postulate new processes, in particular the avalanching of electrons which many mechanisms such as that of Klein (1972) require, nor to make use of any novel speculative model, like that due to Budenstein (1973). Moreover, these theories cannot easily be made consistent with the thermal nature of explosion initiation. It seems entirely adequate to accept electrical decomposition as the only group of secondary processes that is involved in the breakdown. Bowden & McLaren (1958) observed in single crystals an increase in breakdown strength as the temperature was lowered, and the results on pellets given in (Zakharov et al. 1964) and (Zakharov & Savel'ev 1966) show the same correlation. We exploded three crystals at 273.2 K, and obtained $F*=0.6\pm0.1$ MV/m at $t*=20\pm5$ s. Our hypothesis is consistent with this empirical evidence, since at lower temperature smaller ionic space charges will be formed at the electrodes, so that higher fields need to be applied to get the same charge injection rates and thus the same decomposition rate. On the

other hand, the near constancy of the current at the onset of the final breakdown, independent of the sample area and, approximately, also of the temperature, suggests that the immediate cause of the breakdown is localised thermal runaway at certain structures formed in, or on, the crystal (or crystallites) whose individual dimensions are thereby unrelated to the bulk geometry and whose conductivity is quite temperature independent.

7.8 PROPOSED BREAKDOWN MECHANISM

In the mechanism we envisage, the electrical decomposition gives rise to a filament-like patches of thin silver film on the crystal surface, as in pyrolysis. The growth of these patches in number and in size leads to paths of increasing conductance between the electrodes. The fraction of the current going through these paths and, more importantly, the total current, both become greater. At sufficiently high local current density, 'hot spots' are formed where thermal decomposition occurs. The thermal decomposition usually results in the discontinuity of the particular conduction filament concerned, because of the removal of material, on the surface. If the filament is thick enough, however, the thermal decomposition is sustained, the current rises without limit, until fast decomposition is initiated at the hot spot.

The sharp bursts of nitrogen evolution which were

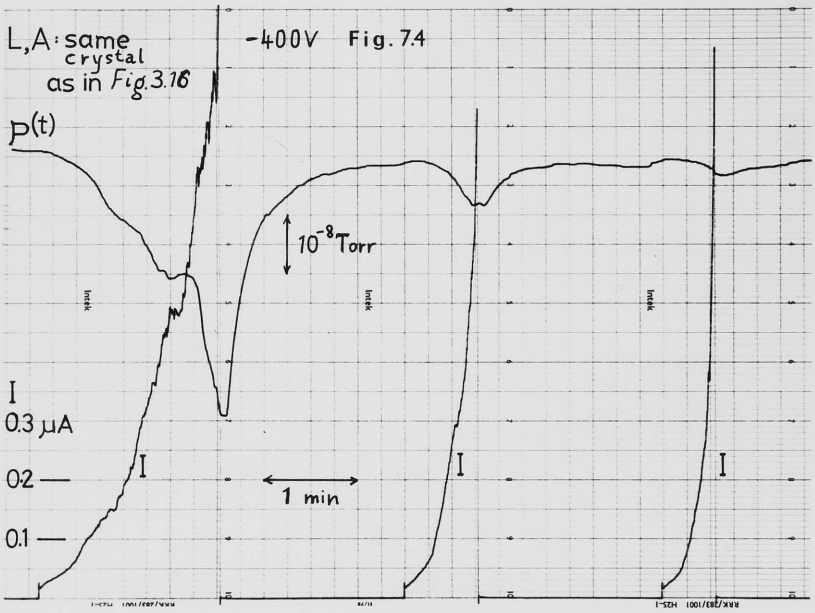
L,A: same crystal as in Fig. 3.16
-400V Fig. 7.4
p(t)
10^{-8} Torr
Inlek
I
0.3 μA
0.2
0.1
1 min

observed superimposed on the continuous electrical decomposition are interpreted in our model as manifestations of the thermal decomposition, which is localised both in space and time. Their increases in magnitude and frequency reflect the growth of conduction filaments. The onset of the final breakdown should be accompained by the largest evolution of nitrogen but, for reasons already stated in Section 3.4.2, its observation is thwarted by considerable experimental difficulties, and has not yet been made.

On the other hand, the gradual build-up of the current during the induction time should not be correlated with a proportional increase of the electrical decomposition, as the additional current is not injected but is conducted by metallic filaments. This rationalises the following observation, which appeared at first very surprising. We have mentioned in Section 2.5.2 the pre-breakdown 'memory effect'. Fig. 7.4 illustrates this phenomenon, namely, that a repeated application of the field gives the same initial current but whose rate of rise is faster. The investigation was carried out in the time-of-flight spectrometer (Section 3.4.2). The apparent paradox was observed that the evolution of nitrogen increased initially at the same rate as before, and therefore lagged behind the change in the current.

In our proposal, the network of this silver films is not permanent owing to the diffusion and accretion of silver

atoms and, less importantly in the present case, their oxidation and gas absorption (cf. Meiksin 1975). The diffusion and accretion result in 'pebbles' and coherent thick films, which are stable, but the former are zero-dimensional structures and do not constitute a continuous conduction path, while the latter cannot form till very late stages. The current rise is therefore reversible. The memory effect is explained as caused by the presence of silver atoms which have not yet aggregated, so that the growth of conduction filaments is faster. This suggestion predicted that the 'activation energy' of the memory effect is related to that of the surface diffusivity of silver.

We have not attempted to develop our phenomenological model into a quantitative theory, because many of the parameters involved remain completely unknown, in particular those pertaining to the silver filaments whose growth represents the first stage. This is unfortunate, since the general theories of conduction by ultra thin quasi-continuous metal films have been worked out in considerable detail (Hill 1969; Campbell & Morley 1971 -- a review not the most recent but one of the best and incidentally also covering dielectric and cermet films). At least, however, it has been shown (Coutts & Hopewell 1971, using computer simulation) that a randomly growing metallic network does conduct a current which on the whole rises at increasing rates. Empirically, we have estimated by mass spectrometry that the total amount of silver

atoms produced before the final breakdown was nearly reached, in a fresh crystal, was ca. 0.05 monolayer averaged over the whole of its surface. This result has been obtained from only one sample and should therefore be regarded as tentative; the induction time lasted 82 s and 250 kV/m was applied.

During the last microsecond or so constituting the final breakdown (see [6], Section 7.7), electrical decomposition should be unimportant. We visualise the development of a quantitative model for this late stage, in which the calculation will artificially but conveniently be split into two parts. Heat balance equation (7.5) is solved for the conduction filament; when a chosen temperature of an appropriate magnitude is reached, its right-hand side representing Joule heating is replaced by the exothermicity due to thermal decomposition, and its solution sought. The theoretical results may then be compared with experimental observations such as the statistical variation of t^* with F, and the current-time behaviour including the current waveform within a few microseconds before explosion initiation. Incidentally, a patent (Schulz 1974) has been taken out on a form of silver azide which explodes under the application of extremely low fields. The composition, prepared by the reduction of silver nitrate dissolved in an aqueous suspension, is an intimate mixture of finely divided silver and the azide. This product corresponds to silver azide permanently conditioned, according

to our model, at the final stage of the decomposition-induced breakdown.

7.9 INITIATION OF FAST DECOMPOSITION

In the paper which initiated the study of electric field induced explosion in silver azide, Bowden & McLaren (1958) have speculated on the cause of the explosion. They believed that the azide conducted by electrons derived form impurities. The immobile positive charges left behind enhanced the field at the cathode, leading to the injection of electrons, impact ionisation and decomposition. The heat of decomposition at the local points of contact between the crystal and the cathode, when high enough, gave rise to self-heating. The process is similar to that visualised by Bowden and Yoffe (1958) for initiation of silver azide by a high intensity light flash.

This model has considerable difficulties. The conduction mechanism presumed is untenable, and there is no evidence that the cathode is 'exclusive' (Parrott 1974) while the anode is 'extracting' to electrons: they are more likely to be field-injecting. These points are less important, since a space charge may still be formed: by ionic polarisation as we have argued. More crucially, it is improbable that the interfacial field remains intense enough over a sufficiently long distance as to induce impact ionisation. Moreover, though the

decomposition is highly exothermic, its rate appears not to be high enough to initiate an explosion at the cathode even if it indeed occurs; in our own model, the injection of holes at the anode is not supposed to do this either. This proposition has both deductive and inductive supports. The bi-molecular combination of two azide radicals generates a 'thermal spike', i.e., a region to which an overall temperature higher than the ambient may be assigned. Its minimum diameter is something like 30 lattice spacings (Thompson 1969, pp. 246-7) so that, with the energy released being 9.5 ± 0.5 eV, the averaged temperature rise is of the order 10 K, too low to be responsible for the self-heating at room temperature. We can ignore cooperative heating: the probability of a second combination occurring in the same region within a few lattice vibrational periods may easily be seen to be negligible given a reasonable value of the current density. Further support comes from the empirical observation that the site at which explosion is set off is found to be fairly random and not necessarily at either the cathode or the anode.

Before discussing initiation locality, for completeness we mention here the mechanisms which have been suggested for breakdown induced initiation of detonation in other azides. Zakharov & Sukhushin (1970) mentioned, for the case of thallous and cupric azides, that shock waves generated by the current discharge channel may be responsible. Fair et al. (1973)

argued that in explosives electronically excited states can have different decomposition activation energies. In their conception, sufficiently intense electronic excitations lead to a very small or zero activation energy, when normal atomic vibrations will at once cause explosion initiation (cf. the model of Budenstein described in Section 7.5).

To lend empirical basis for this novel idea, Fair et al. carried out some photo-electric initiation experiments on lead azide single crystals. Initiation was achieved at a field of approximately half the 'dark' breakdown strength, when the crystal was irradiated by light (400 nm) of intensity some 10E6 times smaller than that required for initiation by light alone. They estimated that the thermal energy density caused by the degradation of absorbed light into heat, and the Joule heating of the photocurrent, were unlikely to be sufficient to give rise to initiation.

However, the mechanism we have suggested can explain this reduction of breakdown field as due to the generation, by light, of mobile electrons (from impurities perhaps) which drift towards the cathode. The resulting electronic space charges at the cathode (accumulation) and the anode (depletion) enhancing the ionic polarisation, so that a greater rate of injection is achieved for the same applied field. Furthermore, in our case at least all these alternative ideas appear to be inconsistent with the thermal nature of the initiation of post-

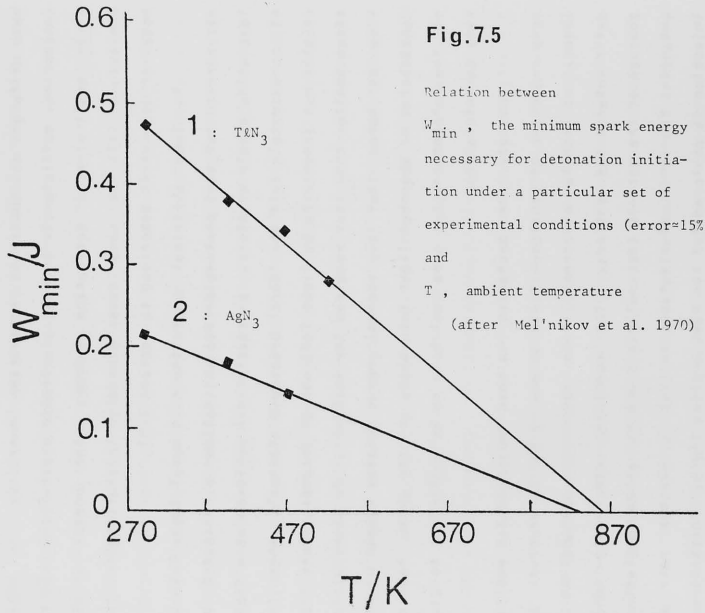

Fig. 7.5

Relation between

W_{min} , the minimum spark energy necessary for detonation initiation under a particular set of experimental conditions (error≈15%)

and

T , ambient temperature

(after Mel'nikov et al. 1970)

breakdown explosion. Firstly, we have mentioned in Section 3.3.1 that if the crystal is in series with a large resistance then on breakdown it can conduct a large current without exploding, when the voltage drop across it and thus the heating effect of the current diminish automatically. Secondly, Mel'nikov et al. (1970) applied pulses of rise time ca. 5 us and 4.5 kV to 0.1 mm-thick pellets of silver and thallous azides. By monitoring the voltage and current waveforms, and the exact instant of explosion, they showed that for it to initiate the energy dissipated had to exceed a threshold value, which decreased linearly as the temperature was increased (Fig. 7.5). With the use of a voltage cut-off circuit, they claimed to be able to estimate the size of the discharge channel. From its calculated mass and the reported value of the critical energy for initiation at room temperature, we can work out its average temperature to be ca. 640 K, a highly plausible figure.

We now come back to our evidence relating to the locality of explosion initiation. It has been established in the following series of experiments. Firstly, we took single shot photographs of crystals mounted on microscope slides in the following way. A current differentiator circuit of conventional design was connected in series with the sample under investigation, so that an output pulse of suitable shape and magnitude was obtained when the sample resistance

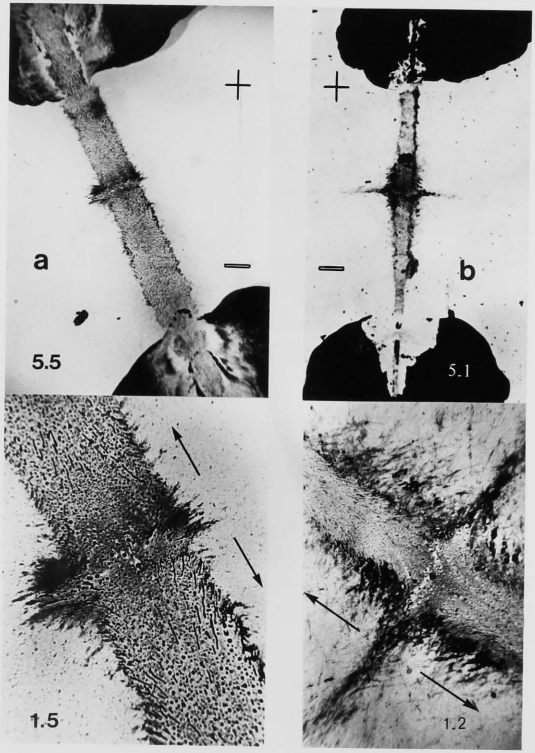
a
5.5
b
5.1
1.5
1.2

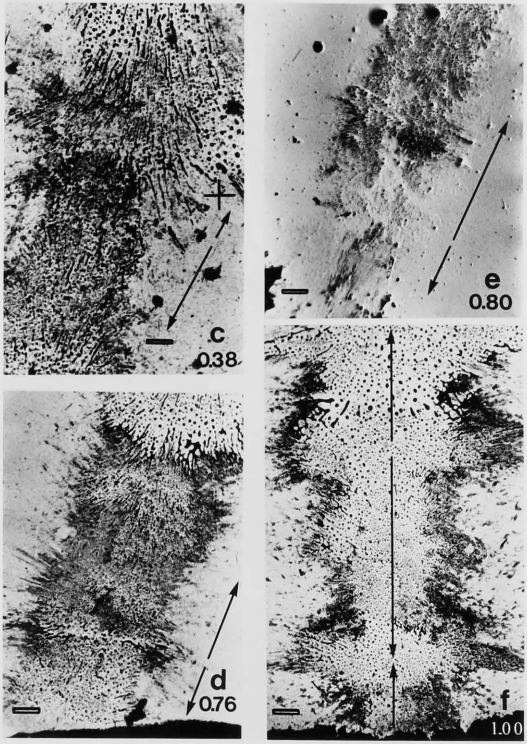
c
0.38
e
0.80
d
0.76
f
1.00

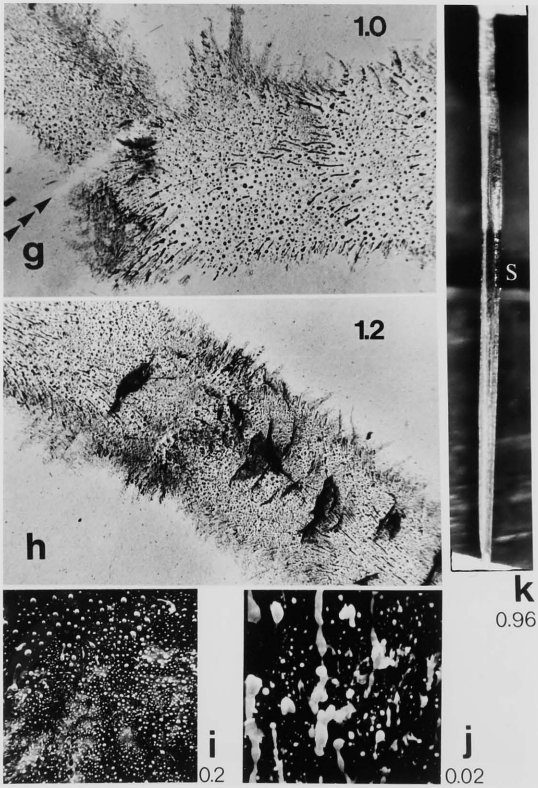
1.0
g
1.2
h
S
k
0.96
i
0.2
j
0.02

collapsed. The pulse triggered a Beckman & Whitley Model 501 delay unit which in turn fired a Model 5401 point light source, of rise time 100 ns nominal and duration 150 ns. The experiments were made in the dark, with an open shutter polaroid camera mounted in line with the sample and the light source. Transmission photographs, an example of which will be shown in Fig. 8.1(b), were obtained showing the earliest stage of the detonation in most cases, the delay being set at 0.5 us.

During the course of these experiments we discovered a more convenient, certain and informative method of deciding on the initiation sites, namely, by inspection of the residue left on the slide after the explosion. Fig. 7.6 (a), where the electrodes are of carbon-dag, and (b), where they are of silverdag (as are in following micrographs), illustrate the 'bulge' and the change of 'flow lines' at locations which the corresponding high speed photograph have shown to be the initiation centres. The second feature is more reliable, as shown in (c) to (f). In (e), the initiation was from the cathode. This was also true in (f), but in this case it occurred also at another site, and there first, as deduced from the longer distance over which the detonation front from there travelled before meeting that from the cathode site. We have

<<--
FIGS. 7.6 (a) to (k)
Number on or near micrograph indicates its width in mm;
arrows show directions of explosion propagation

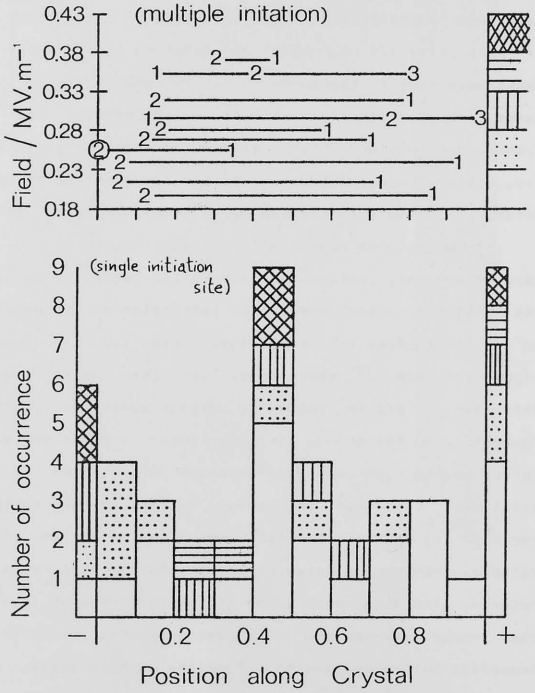
(multiple initation)
Field / MV.m⁻¹
0.43
0.38
0.33
0.28
0.23
0.18
(single initiation site)
Number of occurrence
9
8
7
6
5
4
3
2
1
−
0.2
0.4
0.6
0.8
+
Position along Crystal

Fig. 7.7

confirmed the correspondence of the 'flow lines' pattern with propagation direction by two sets of tests. In one, a crystal was covered by two 200 um slits ca. 4 mm apart. A Q-switched Ruby laser beam (1J 20ns) then simultaneously irradiated the crystal through these slits. The intensity of the beam was high enough to cause initiation at both sites. In the other set of experiments the initiation was achieved by placing a fine wire on the crystal, and high current pulsed along the wire to heat it.

Our results are given in Fig. 7.7. The samples totalled 58, among which 8 had two initiation sites and 2 had three; the numbers in the diagram represent the deduced order in time. Initiation seems to take place usually on the anode side first. In the single site cases, there is an apparent preference for locations very near the middle, at the anode, or at the cathode. These results are from samples with silverdag electrodes. Those with carbon-dag electrodes behaved in a similar way: initiation near the middle 4 cases, at the anode 3, near the cathode 1, and no multiple initiations were found. Our proposed mechanism is not yet detailed enough to explain these characteristics, though the fact that in the middle of the crystal heat conductance to the metallic electrodes is minimum may be of significance. Nevertheless, a distribution of initiation locality is not inconsistent with our model. Multiple initiations may simply be explained by the

multiplicity of hot spots.

In one of the 'hot wire test' runs, we deduced that the crystal apparently melted and twisted beforee exploding (Fig. 7.6(g): arrows indicate position of wire). This agrees with the statement by Bowden & Yoffe (1958, p.142: cf. Fig. 79 there). Another incidental observation is that if, and only if, the explosion is confined by just a piece of paper covering the crystal, cracks are found afterwards on the glass slide ((h)). Scanning electron micrographs of the residues are shown in (i) and (j), and these condensations have been confirmed to be silver by energy dispersive X-ray analysis.

We have taken three crystals and decomposed a small section of each through a fine slit (S in Fig. 7.6(k)) under a Hg lamp. The time taken for the current in each to rise to 5 uA under 0.22 MV/m (170, 100, and 110 s respectively) was unchanged before and (1 day) after the photolysis. The initiation site was subsequently found to be not situated at the decomposed region. In the previous samples we have also noticed that the site was not necessarily where the crystal was narrowest in cross section. A broad silver film leads to small Joule heating and the width of a filament bears no direct relation to the dimensions of the 'host', so both observations are explicable on our model.

CHAPTER VIII

ELECTROMECHANICAL PROPERTIES

It appears that considerable mechanical stress is set up in a silver azide subjected to a strong electric field, because occasionally cracks are observed. Fig. 8.1(a) shows a crystal 8.75 mm long. It exploded 45 s after 2.4 kV were applied to it, and (b) is the single shot photograph obtained in the way described in Section 7.9. It is seen to have broken near the middle where there was originally an abrupt change in the crystal cross section. As shown by the trace left on the glass slide, the mechanical disruption occurred before the

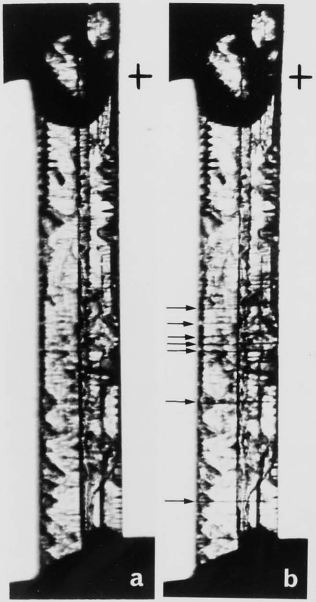

8.1

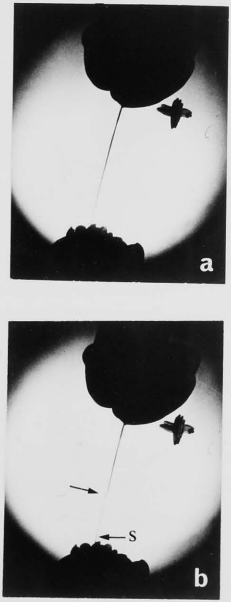

8.2

original initiation of explosion (marked S in (b)) but at this fracture point a second initiation also took place. This judgment is consistent with the observation illustrated in Fig. 8.2. The sample in (a) was 0.740 mm in length, and (b) shows it 5 min after the application of 110 V. The voltage was subsequently changed to 85 V, and it did not explode until ca. 30 min afterwards. Similar transverse fractures were seen in two other samples, and in all cases they tended to be on the cathode side. Six other crystals examined did not crack in this fashion, however (see Figs. 3.7 & 9).

Electrochemical breakdowns have been proposed for soft compressible polymer sheets: by Stark & Garton (1955) for irradiated polyethylene, and by Lawson (1966) and Blok & LeGrand (1968) for polythene. Such mechanisms, by which mechanical collapse is caused by the electrostatic effect of the field, are unlikely in our case because of the form of samples used. Nevertheless, considering its crystal structure we do expect silver azide to deform when in an electric field (the reverse piezoelectric effect). Various processes can then conceivably lead to breakdown. When the elastic limit is exceeded, plastic deformation occurs, and in many alkali halides [1] the conductivity increases owing to the generation of excess electrons or interstitial ions or owning to the drift

<<--
FIGS. 8.1 & 2
For scales and descriptions see text.

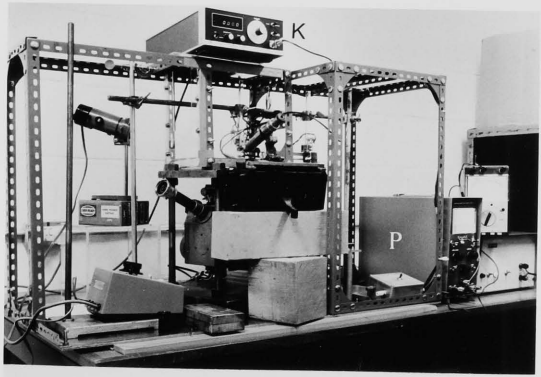

Fig. 8.3

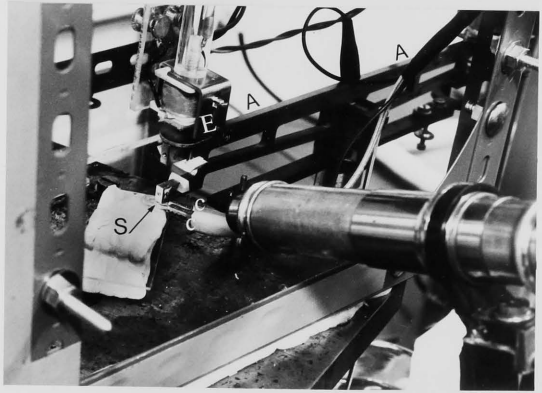

of charged dislocations (see the review of Whitworth 1975), or [2] high local fields may be produced by the motion of ionic vacancies (Kornfeld 1979). [3] The last possibility may also be realised when the conditions are such that fractures appear (Kornfeld 1978).

Two preliminary measurements have been carried out to gauge the significance, if any, of electromechanical effects to the breakdown. In the first, three samples were in turn subjected to known small compressive forces along their b-axes, and the differential charges produced on the two surfaces monitored. Fig. 8.3 shows the apparatus used, in which the downward force on the crystals was controlled by the currents supplied by P through the electromagnets E attracting the two arms A of the balance. The net charge produced was measured through cables (c) by a Keithley 616 acting as a coulombmeter (K). The values obtained of the piezoelectric constant defined as (charge density / stress) are 1.5 ± 1 10E-14 C/N. In the second experiment, a very low field was applied to a crystal placed under the indentor of a Leitz microindentation hardness testing apparatus. The indentor was of the Vickers diamond (pyramid shaped) type. Four samples have been tested, and the loading was 12 g. When the indentor was pressed down and left there, the current was seen to rise rapidly at first and then fall back to a constant level which was a few tens of percents higher than the value before indentation. (Fracture may also

be induced, resulting sometimes in open circuit.) If the indentor was then raised, the current decayed to a level which was perhaps still slightly larger than this original value. Because of the uncertainty of the underlying mechanism and the complication of any calculation (cf. Whitworth 1975), no attempt has been made to derive quantitative results.

The piezoelectric constant obtained is not for the c-axis and the degree of anisotropy of silver azide is unknown. Moreover, the mechanical properties of the substance are also largely unknown, so that we cannot predict its mechanical response when subjected to an electric field. The second experiment shows that plastic deformation and/or the creation of defects cause electrical variation, and therefore there may be positive feedback effects. However, although our results are not conclusive, it does seem that a model in which they are responsible entirely for the dielectric breakdown will be far stretched. Nevertheless, they may have modifying influences on the electrical initiation of explosion -- and indeed possibly also on mechanical initiation by impact or shock waves. The experimental investigation on electrochemical properties may therefore merit further efforts.

CHAPTER IX

CONCLUDING DISCUSSION

Let us first summarise the results given in the previous chapters. The breakdown of single crystals of heavy metal azides has been investigated. A variety of experiments were made and a new model for the dielectric breakdown of one of the heavy-metal azides has been proposed.

In silver azide, the low-field conduction is by mobile interstitial cations and their enthalpies of formation and hopping have been determined from the Arrhenius plot of the conductivity. Based on AC conductivity measurements and the observed time dependence of the current, it is shown that ionic polarisation occurs at the electrode interfaces. With fields

higher than 15 kV/m (for silver or carbon electrodes) bipolar field injection is thought to take place. These fields can lead to dielectric breakdown, although the incubation period may last up to several days - but less than a second if the field is 0.4 MV/m or higher. Evolution of nitrogen has been measured by mass spectrometry under this condition. Based on a comparison with the thermal decomposition of silver azide, the following mechanism is proposed for the 'electrical decomposition'. Holes injected from the anode combine bi-molecularly via traps and produce nitrogen gas. Some of the electrons from the cathode are localised at impurity centres or defects. The discharge of mobile Ag^+ at the electron traps results in silver atoms which if formed on the surface, may migrate as well as aggregate because of their high diffusivity even at room temperature. By optical and electron microscopy silver nuclei have been detected on the surface of a crystal to which a strong field is applied through conducting contacts. It has also been observed that post-breakdown disruption in the form of an explosion occurs. The breakdown is explained as due to the formation on the crystal surface of filamentlike silver films, and the initiation of deflagration and subsequent detonation, to the appearance along the metallic conduction path of 'hot spots' arising from Joule heating and leading to thermal decomposition and self-heating. This explanation is supported by evidence such as initiation locality.

In the comprehensive study on the thermal decomposition of silver azide, new methods have also been suggested for the analysis of kinetic data, both isothermal and dynamic, from solid state reactions.

It is obvious that more work is needed to elucidate the details of the model, in particular the stage concerning the growth of the silver films. Further experiments are required to establish the mechamisms more firmly. Subsequently, the range of temperature over which they remain valid will have to be investigated.

Variables such as the strength and the rise-time of the applied field may also be significant. In our model, impact ionisation by injected electrons is not responsible for the dielectric breakdown. Whether this still holds when fast rising fields of the order of 10 MV/m or more are applied remains to be seen. However, an affirmative answer is not contradicted by an observation of Chaudhri (1973), who subjected single crystals (0.6 to 1.2 mm in length and submerged in transformer oil) to 10 kV pulses of rise times less than 0.5 us. By high-speed photography he showed that the explosion following the breakdown, which took place within a fraction of 1 us, initiated at points which could be away from the electrodes. Although in so short a time any diffusion of surface silver atoms is likely to be ineffective, our breakdown model may still apply, if the number of them produced is so

great that conduction filaments are still formed. Chaudhri noted that on occasions the voltage pulse was applied many times before fast decomposition was initiated; this we may explain as their progressive accumulation on the surface.

Under intense fields and in an ambient of air, the crystals would probably explode by a different mechanism: most likely by the heating effect of 'tracking' or 'surface' ('creeping') sparks, i.e., gaseous discharges along the azide-air interface (Section 7.6).

Besides the 'in-depth' development of the proposed model, a very fruitful work will be to explore its 'breadth', that is, to see whether mechanisms which are similar to greater or lesser extents operate in other substances of interest.

We have carried out some experiments on single-crystals of thallous and lead azides. The results may be briefly mentioned here. The field strengths at which dielectric breakdown and explosion initiation occur nearly instantaneously in them have been listed in Table 1.1. (N.B. The dielectric strength of lead azide powder pressed to a porosity of 0.4 was given in (Stenqach 1975) as ca. 20 MV/m, which is considerably higher than our single crystal value.) We have established that, under lower fields, the events still occur but the times to breakdown are much larger. Also, their I-V characteristics are ohmic initially and then (for F > 400 and 800 kV/m in thallous and lead azides respectively) become supralinear, in

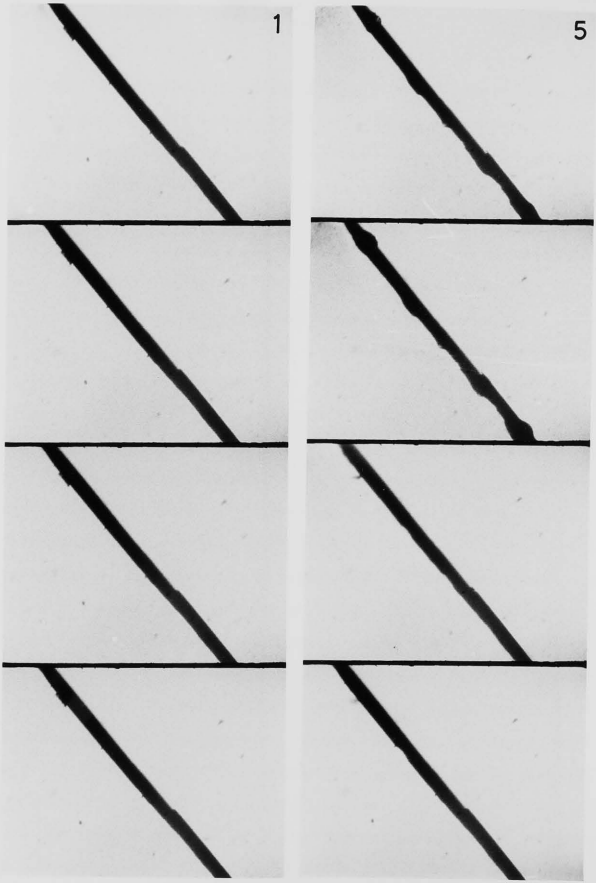
1
5

which regimes the 'memory effect' is apparent. A crystal of the lead compound was put into the quadrupole mass spectrometer and evolution of nitrogen detected when a moderate field was applied. In thallous azide, an explosion initiated does not propagate to all parts unless the sample is confined, e.g. in oil. Fig. 9.1 is a photographic sequence of one in air; the voltage was removed by a relay triggered when the voltage across the sample collapsed. Frames 5 & 6 show initiations at a number of sites along the crystal, none of which propagated very far, and all of which were away from the electrodes. The 'lumps' at these sites 'collapsed' in frames 7 & 8, but a jet of gas or particles remained visible at a spot on the upper end. Post-breakdown examination revealed droplets of thallium metal deposited on the underneath of the crystal surface at the sites. In all, these preliminary results suggest that the other two heavy metal azides have breakdown and explosion initiation mechanisms similar to silver azide.

More ambitiously, we regard it a distinct possibility that dielectric breakdown of long incubation periods can be brought about by analogous 'electrical decomposition' processes in some metal halides, oxides, hydrides, alkali azides and other ionic metal compounds, although in substances which are

<<--
FIG. 9.1
Breakdown-induced fast decomposition of a thallous azide crystal (diameter 210 um); frames run from top to bottom and then from left to right; inter-frame time is 15.6 ms

not highly exothermic no explosion will follow the breakdown. If true, this will open up a vast new field of research on a general and important phenomenon which has hitherto received scant attention. We have looked at one crystal of sodium azide and found that, for $F < 200$ kV/m, the current was very nearly proportional to the voltage but decreased slowly with time. At higher fields, the current fluctuated, and after a prolonged period, parts of the crystal turned into an amorphous mass, suggesting decomposition (the experiment was in laboratory air). It looks promising to pursue the investigation on these and other insulating metal compounds. The best approach should be, if our experience with silver azide may serve as a guide, to study low-field processes and to find out if chemical reactivity is in action leading to the formation of the metal phase. The work on MgO by Narayan et al. (1978), already mentioned in Section 7.6, is interesting, although they claimed that no metallic precipitation was observed.

We said in Section 1.3 that ironically, the ionicity of the heavy metal azides makes them less sensitive in many ways (Section 2.1) but less stable electrically, they having lower breakdown field strengths than the covalent azides. Our model explains this remarkable fact, since the injection of non-ionising charge carriers into a covalent azide should not cause decomposition, for no mobile ions are present. Moreover, even if it decomposes only the metal nitride is produced (Sec-

tion 2.1) which remains a bad conductor, so that the mechanism of breakdown by metallic filaments cannot operate. In cupric azide, the dielectric strength increases with temperature, contrary to its behaviour in thallous azide (Zakharov & Sukhushin 1970), which is the same as that in silver azide and which is the expected behaviour in our model (Section 7.7).

To conclude, it appears not impossible that the dielectric breakdown of ionic azides has, for the first time, been given an explanation which is correct in broad outline. (We may perhaps add that their optical, photochemical and thermochemical properties have in fact been first elucidated also by previous members in the same 'Cambridge School' of Bowden and Yoffe.) Schematically, the mechanisms proposed are:-

(ionic polarisation of electrodes) -> injection -> 'electrical decomposition' -> metallic films -> DIELECTRIC BREAKDOWN;
[in exothermic substance:] -> hot spots -> thermal decomposition -> EXPLOSION INITIATION.

APPENDIX A

PREPARATION & CHARACTERISATION OF SILVER AZIDE

In all the experiments on silver azide described in this thesis, needle-shape single crystals were used. We have prepared stoichiometric silver azide by mixing filtered equimolar solutions of silver nitrate (analytical reagent grade) and sodium azide (laboratory reagent grade). The sodium azide used had not been recrystallised from water, since impurities soluble in water would co-crystallise with the azide and therefore not be removed; the hydrolytic decompostion of the azide might even introduce additional impurities. The precipitate was washed free of ions, dissolved in ammonium hydroxide solution and filtered. All operations were performed under subdued light which was strongly attenuated below 500 nm by a Kodak Wratten '00' glass plate.

The growth solution was in the approximate proportions of 1 g silver azide to 15 ml of 0.35 ammonia plus 40 ml of de-ionised water: the strength of the solution influenced the habit of the crystals grown. Slow re-crystallisation in the dark proceeded in a stainless steel bowl which had been cleaned with concentrated nitric acid and then rinsed with distilled water. The bowl was placed inside a glass container, which had a restricted outlet to the atmosphere and rested on a vibration-absorbing platform. A light-tight cabin was spe-

cially built to house the glass containers, where they were separated fom one another by welded steel plates, to reduce the danger of spontaneous explosions. To collect the crystals grown after a few days, a drop of 0.35 ammonia was added to the bowl before the glass cover was removed. This was done to prevent any trace of silver azide still in the solution from crystallising non-uniformly onto the crystals surfaces, as the remaininhg ammonia escaped. The crystals were then filtered off in a funnel, washed with enthanol, dried, and then stored in evacuated desicators housed in the light-tight cabin.

In this way, crystals were obtained which were of needle shape, 50 to 200 um in thickness and up to 10 mm in length. They were used as the samples in nearly all our experiments, and their typical micrographs are shown in Figs. A(a), (b) & (c). If the glass container had been surrounded by watertice, the crystals grown could then be as long as 5 cm (see photograph (d)). A few of our experiments had used them. On the other hand, if a container -- in our case, a 'desicator' with the cock left open -- was employed, plates were obtained after about two weeks: see Figs. A(e) & (g).

The major metallic impurity was determined by atomic absorption to be iron (70±20 ppm). By exploding a small crystal in a continously pumped ultrahigh vacuum system and operating the attached quadrupole mass spectrometer in a fast scanning mode, we did not detect in the residue gas (nitrogen

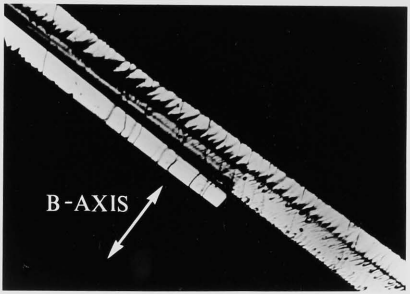

(a)

1·8

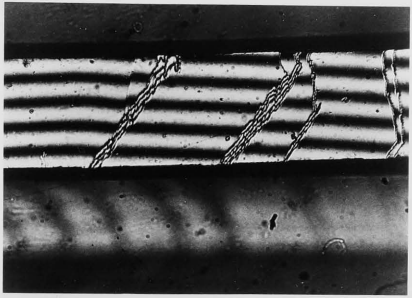

(b)

0·25

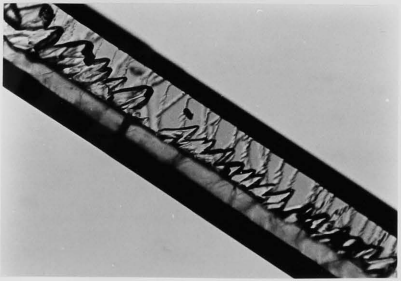

(c)

1·0

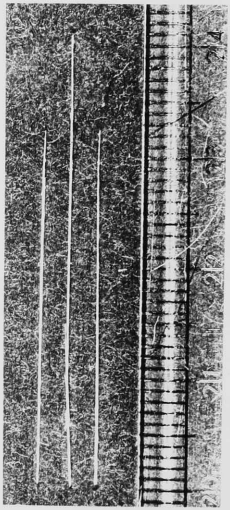

(d)
19·2

(g)
12·7

(h)
1·40

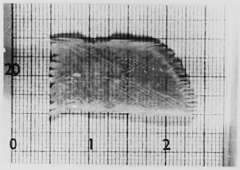

(e) 61

(f) 1·3

(i)
0.85

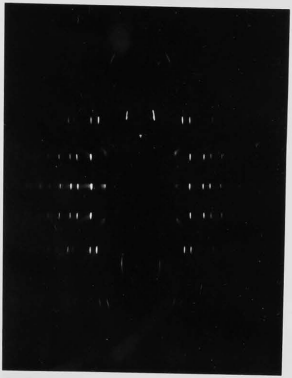

(j)

69.0

(k)
0.13

at a peak pressure of 10E-4 torr) any impurities (ammonia for example) within the mass range of 1 to 250 a.m.u. at a partial pressure sensitivity of 10E-7 torr, though there might have been some water at a lower partial pressure.

Photo-microscope examinations showed that the cross-sections of both needle types of crystals were in the form of a hexagon, two sides of which were usually slightly wider than the other four (Figs. A(i) & 6.12). The crystals appeared to be monocrystalline when viewed under a polarising microscope. This was confirmed by X-ray oscillation patterns (Fig. A(j)), which further showed that the longer diagonal in the cross-section is the a-axis; normal to it is the b-axis, while the c-axis is along the length of the crystal. The 'inclined' faces are identified as the $\{120\}$ planes. (The crystallographic structure can be found in Pfeiffer 1948 and Morv &

<<--

FIG. A (number near each frame indicates its width in mm)
(a) crystal cleaved along (100) under cross polarised light, showing that all parts have the same extinction angle;
(b) interferometric (Na line) micrograph of a crystal face showing growth steps;
(c) crystal showing another and rarer type of surface steps - its face on the under side may be seen to have growth steps of the type in (b);
(d) long crystals grown from solution maintained at 273 K;
(e) plate-type crystal;
(f) surface details of crystal in (e);
(g) another plate, under cross polarised light;
(h) surface details of (g);
(i) end of a needle-type crystal in reflected light;
(j) X-ray diffractogram of a needle: oscillation 40° about c-axis, wavelength 0.07093 nm (Mo α_1 KL_{III}), camera radius 28.65 mm;
(k) scanning electron micrograph of growth steps

Stanford 1962; one unit cell contains 4 molecules and the size is 0.56 x 0.59 x 0.60 nm^3.) The crystal surfaces have growth steps (Figs. A(b) & (k)) but are otherwise perfect.

Silver azide undergoes a phase transition at 461±2 K (Section 6.3.1). The exact structure of the high-temperature allotrope has not been determined.

The plate-type crystals were found to be polycrystalline under the polarising microscope and have not been used. This was unfortunate, since their geometry and dimensions would have faciliated many measurements.

Lastly but not least importantly, we should mention the safety aspects in the handling of silver azide. Its explosion hazard is severe when iniation agents (Section 1.5) are present. We have tested that an exploding needle crystal, confined between two microscope slides, could send glass fragments up to a meter away, although little or no fracture of the slide occurred if the other side was open air. A less commonly recognised danger is the fact that, in common with other siver compounds, it can lead to the absorption of silver through the skin or, on explosion in its particular case, through inhalation. Long-term health problems will then result, such as the condition called 'argyria' or a greyish pigmentation of the skin. With care and scientific common sense, however, we have had no accident.

APPENDIX B

AC CONDUCTIVITY OF IONIC CRYSTALS

Consider a capacitor comprising a slab of dielectric of relative permittivity (or dielectric constant) e and thickness d, between two metal plates of area A. Its reactance at an angular frequency w of the applied voltage is $1/jw(eC)$. Here C is the geometrical (vacuum) capacitance of the conducting plates alone and is given by $C=e^*A/d$, in which e^* is the permittivity of free space.

To include into consideration the inevitable loss in the 'insulating' slab, one can for convenience write analogously that

$$\text{impedance} = 1/jw(\underline{e}C) \qquad (B.1),$$

if $\underline{e}$ is now a complex quantity representing $e'-je''$. Under the applied voltage $V \sin(wt)$, the dielectric carries a current

$$\underline{I} = jw(e'-je'')\, C\, V \sin(t) \qquad (B.2).$$

The imaginary part of $\underline{I}$ is the usual displacement current in the capacitor. The real part, whose peak-to-peak value is $we''CV$, is in-phase with the voltage and represents the dielectric loss. This dissipation corresponds to an AC conductivity of

$$\sigma = (we''CV/A) / (V/d) = w\, e''\, e^* \qquad (B.3).$$

When the dielectric is an ionic solid, several processes can contribute to its AC conduvtivity. One is the

drift of mobile ions, as happens in DC ionic conduction. Other scattering or 'frictional' processes, with different relaxation times, may also be important. They give rise to resonances, i.e., the dielectric loss peaks at frequency bands corresponding to inverses of the relaxation times. The more important of these processes are usually the re-orientation of dipoles formed by ion-vacancy complexes and, at VHF frequencies, that of permanent dipoles of molecules (in silver azide: see Section 2.1).

Ionic conduction can also introduce frequency-dependence into ϵ, through the mechanism of interfacial electrical polarisation. The ions may not be able to discharge at an electrode or to enter the crystal from the electrode as fast as they can drift in the bulk of the crystal. An ionic accumulation in front of the electrode repels approaching carriers of the same sign or retards departing carriers of the opposite sign; a depletion region behaves as a space charge of the inverse polarity. The result is a decrease of the apparent conductivity. This effect, one may expect, decreases with an increase in the frequency of the applied voltage. Although no microscopic theory yet exists for the current transport at an interface between a metal and a solid electrolyte, phenomenological models are available which can predict the form of the frequency dependence. Outlined below is a treatment due to Friauf (1954), which we have adapted for the spe-

cial case of silver azide.

As shown in Section 2.3, in the case of silver azide the conduction is unipolar: only the cations are mobile, by hopping between interstitial sites. In our calculation, these ionic defects are reduced to point charges in a continuous medium with static dielectric constant e. The Einstein relation u/D = q/kT between mobility and diffusion coefficient is assumed valid. We shall also neglect the generation of mobile cations and their recombination with cation vacancies, i.e., the cations have infinite lifetime in the bulk. The cation vacancy density N is therefore constant and, furthermore, will be taken as uniform. The concentration P of mobile cations, as a function of time t and distance x along the crystal, is then determined by their drift under the local electric field F(t,x) and by their diffusion due to concentration gradient:

$$\partial P/\partial t = -u\,\partial(PF)/\partial x + D\,\partial^2 P/\partial x^2 \qquad (B.4a)$$

supplemented by Poisson's equation

$$-\partial F/\partial x = -q(P-N)/e(e^*) \qquad (B.4b)$$

Considering that the nonlinear dependence of P on the applied voltage is insignificant, we seek a solution of the form $P(t,x) = P^*(x) + p\sin(\omega t)$, where $p \equiv p(x)$. It will be further taken that the static space charge layer next to the electrodes, when no voltage is applied, can be ignored in comparison with the polarisation layer arising from the alternating voltage; this condition is a strong assumption,

but without this the mathematics is intractable. Then $P^*(x) = N$, $I^*(x) = 0$, and $F^*(x) = 0$ for all x. The linear, homogeneous equations which result can now be solved analytically:

$$jwp = -uN\, dF/dx + D\, d^2p/dx^2 \qquad (B.5a)$$

where $$dF/dx = qp/e(e^*) \qquad (B.5b)$$

The variable F is normalised by the condition

$$\frac{1}{V}\int_{-L}^{L} F(x)dx = 1 \qquad (B.5c)$$

where the origin has been placed at the middle of the sample of assigned length 2L. The boundary conditions are chosen to be in the form:

$$I(t,\pm L) = \pm\, r(qD/L)p\, \sin(wt) \qquad (B.5d),$$

in which the dimensionless constant r parametrises the degree of blocking at either of the electrodes. In the case of complete blocking, $r = 0$, and (B.5d) becomes

$$I(t,\pm L) = 0 \qquad (B.6),$$

while if completely free passage of the cations is allowed, $r \dashrightarrow \infty$, and

$$p(t,\pm L) = 0 \qquad (B.7).$$

The degrees of blocking at the anode and at the cathode have been assumed equal. Silver ions have to leave the anode and dissolve in the crystal or, in the case of a chemically inert anode, azide ions have to be discharged (i.e., hole injection). At the cathode, the interstitial cations in the crystal have to

discharge.

The general solution of (B.5), obtained after considerable simplification of the situation, are still extremely lengthy in their algebraic forms (Friauf 1954: Eqs.(8), (11) and (16)). They will not be discussed here; the frequency dependence cannot be directly deduced from them. Nevertheless, the theoretical curves generated by numerical calculation for a model substance show that when w is raised δ increases or, at its weakest dependence, stays constant (ibid., Fig.8). On the other hand, the particular cases of $r = 0$ and $r \dashrightarrow \infty$ have uncomplicated solutions. If the electrodes are completely blocking, then from (B.5a,b) and (B.6)

$$\delta = G\, w^2\langle t\rangle^2/(1+w^2\langle t\rangle^2) \qquad (B.8),$$

where G is the high-frequency limiting conductivity, and the relaxation time $\langle t\rangle = 2L/(D \times$ the Debye-Huckel screening constant for Ag^+ in silver azide). In the case of complete absence of blocking,

$$\delta = \text{constant} \qquad (B.9),$$

a result which is expected. Note that a monotonic increase of δ with w is predicted by (B.8), even if $\langle t\rangle$ has a sharp value and not a broad distribution of values.

APPENDIX C

RELATIONS BETWEEN HEATING RATE & PEAK QUANTITIES

Consider a solid state reaction which is allowed to proceed under a number of heating rates $H \equiv dT/dt$. The cases studied will be those in which the temperature T rises linearly with the time t, i.e., in each individual case H is a constant. We wish to predict how the value of a at peak reaction rate, a*, varies with H; it will be seen, also, that our calculations may be easily adapted to give the variation of T*. Here $a \equiv a(t)$ is the molecular fraction of conversion of the reactant, and the superscript * denotes 'peak' quantities, as in Chapter 5. At a = a*: from (5.4),

$$\int_0^{a^*} \frac{da}{f(1-a)} - \frac{R^*}{H} \int_{T(0)}^{T^*} dT \exp(-E/kT)$$

$$\equiv F(a^*, H, T^*) = 0 \qquad \text{(C.1)},$$

and from the fact that $d a/dt = 0$

$$f'(1-a^*) - \frac{E}{k}\,\frac{H}{T^*}\,\frac{\exp(E/kT^*)}{R^*}$$

$$\equiv G(a^*, H, T^*) = 0 \qquad \text{(C.2)}.$$

Solving the simultaneous equation dF = 0 and dG = 0, we find

$$\frac{da^*}{dH} = \left(\frac{DF}{DH}\frac{DG}{DT^*} - \frac{DF}{DT^*}\frac{DG}{DH}\right) \Big/ \left(\frac{DF}{DT^*}\frac{DG}{Da^*} - \frac{DF}{Da^*}\frac{DG}{DT^*}\right) \qquad \text{(C.3)},$$

where D denotes partial differentiation. Defining the dimensionless quantities $P \equiv E/kT^*$, $Q \equiv H/R^*T^*$, and

$I(a*) \equiv \int_0^{a*} da/f(1 - a)$, we have the followings:

$$\frac{dF}{da*} = \frac{1}{f(1 - a*)},$$

$$\frac{dF}{dH} = \frac{R*}{H}\int_{T(0)}^{T*} dT \exp(-P) = \frac{I(a*)}{H},$$

$$\frac{dF}{dT*} = \frac{1}{Q \exp(P)\, T*}$$

$$\frac{dG}{da*} = -f''(1 - a*),$$

$$\frac{dG}{dH} = \frac{PQ}{H} \exp(P),$$

$$\frac{dG}{dT*} = \frac{PQ(2 + P)}{T*} \exp(P)$$

Thus
$$\frac{da*}{dH} = -\frac{P}{H}\,\frac{S(2 + P)I(a*) - 1}{SP(2 + P)/f(1 - a*) - f''(1 - a*)/S} \qquad (C.4),$$

where $S \equiv Q \exp(P)$. $dT*/dH$ can be derived in a similar way.

The only case we find reported in the literature, in which $a*$ is apparently independent of H, is the primary recrystallisation of pre-compressed copper (Lucci & Tamanini 1957), where $a* \equiv 0.5$. In all other cases, experiments give changing $a*$. We have made a rough check on (C.4) by taking the case of the pyrolysis of the explosive RDX (Rogers & Smith

1970), for which the Roger and Morris method gives E = 2.10 eV and R* = 10E18.4/s. The reaction is complex, but these representative values are chosen because they correspond to an assumed kinetic equation in which f(1 - a) = 1. We thus have very simply I(a*) = a* and f"(1 - a*) = 0. For H = 0.167 K/s, a* is given as 0.62 and T* as 512 K; our calculation shows da*/dH =ca. -0.1 s/K, a value which compares well with the experimental indication that $\Delta a^*/\Delta H$ = (0.60 - 0.62)/(0.333 - 0.167) s/K.

APPENDIX D

```
1    SUBMIT %H+
2    JOB T6T1 <P$<PROJECT$<%PROJECT$*>
3    SAVE
4    LIMSTORE 98K
5    COMP 3
6    PRIORITY 240
7    TURNAROUND NUM OR NON
8    // EXEC FTG1CLG,REGC=98K
9    C ------------------------------------------------
10   C  Program written by I.B. lang to generate
11   C log(ln) plots of theoretical Isothermal Data
12   C ------------------------------------------------
13         DIMENSION W(300),X(300)
14         CALL CRTPLT(8,300.)
15         CALL GPETYP(0,64)
16          DO 10 N=1,3
17         R=FLOAT(N+1)
18         P=0.5/(200.**R)
19         J=0
20         DO 1 I=1,300
21         W(I)=R*(FLOAT(I)**P)
22   C  Values of constants & form of W(I)
23   C  above to be changed for other TSD.
24         IF (W(I).GT.  1.) W(I)=1.
25         IF (W(I).LE.0.15)   J =1
26    1    CONTINUE
27         CALL PEN(N)
28    9    K=300
29         T1=5.E-3
30         T2=1.5
31         CALL PLIMIT(20.,170.,30.,130.)
32         CALL DELTIT(T1,T2,0.,1.)
33         CALL PLTGR (0,K,T1,12)
34         CALL LOGCHP(0.7,W(140),0)
35         PRTIF(8,900) R
36         IF (J.LT.1) STOP
37         IF (N.GE.1) GO TO 2
38         CALL ANFRE0(3,6,5,5)
39         CALL AXEXY('(F3.1)',(F3.1)')
40    2    K=200-J
```

```
41            DO 5 I=1,K
42            L=I+J
43            W(I)=-ALOG(1.-R(L))
44      3     X(I)=FLOAT(L)/200.
45            CALL PLIMIT(35.,150.,150.,260.)
46            IF (N.GT.1) GO TO 4
47            CALL ULIMIT(0.,0.,0.,0.)
48            CALL PLIGLL(X,W,K)
49            CALL GWLIM (X1,X2,Y1,Y2)
50            CALL BOXLL (0,0)
51            GO TO 5
52      4     CALL ULIMIT(X1,X2,Y1,Y2)
53            CALL PLIGLL(X,W,K)
54      5     CALL LOGCOR(ALOG10(X(1)),ALOG10(W(1)),0)
55     10     WRITE(6,800) N
56            IF (N.GE.5) STOP
57            IF (N.EQ.4) GO TO 8

58            N=4
59            R=ALOG(0.5/0.12)/(200.-20.)
60            C=0.12/EXP(R*20.)
61            J=0
62      6     DO 7 I=1,300
63            W(I)=C*EXP(R*FLOAT(I))
64      C  See comment above.
65            IF (N.EQ.5) R(I)=W(I)/(1.+W(I))
66            IF (W(I).GT.   1.) W(I)=1.
67            IF (W(I).LE.0.15)   J =I
68      7     CONTINUE
69            CALL PEN(2)
70            GO TO 9
71      8     N=5
72            R=-ALOG(C)/200.
73      C  See comments above.
74            CALL PEN(1)
75            GO TO 6
76     800  FORMAT('+',I1)
77      C  Output is out on disc file; if to be plotted
78      C  straightaway change DSN=( ).PLOT,DISP=SHR to
79      C  SYSOUT=P
80            END
81      /*
82      //LKED.SYSLIB    DD
83      //                DD   DSN=GRAPHDEV.PLOTLIB,DISP=SHR
84      //GO.FT08F001     DD   DSN=TBT1.PLOT,DISP=SHR
85      /*EOF
86      +
```

APPENDIX E

BT1.J at 13.15 on 17 Mar 1978
ember IC91

```
1     REQUEST ' ACTIVATION ENERGY (eV)' E$1,
2     REQUEST ' TEMPERATURE RANGE (*LE.140)' L$135
3     REQUEST ' ..MINS/,BY HHHH,/OVERNIGHT ' T$NOW
4     SUBMIT %H*
5     JOB TBT1 4008 ' TEST
6     TURNROUND <T> OR OVERNIGHT
7     ROUTE PRINTER DUMMY
8     COMP 10
9     //  EXEC FTGICLG<LIST*,>REGG=100K
10    //SYSIN     DD   *
11    C ------------------------------------------------------------------
12    C       Program written by T.B.Tang to feed artificial data
13    C into activation energy plot for 4 different kinetic equations.
14    C ------------------------------------------------------------------
```

```
      EXTERNAL INTEGRAL
      DIMENSION X(<L>),XN(60),FN(60),GN(60),DN(60),R(<L>),W(<L>),
     1THETA(60),WS(1986),WT(<L>)
      COMMON PEF,E
C     1eV=9.6487*E7 J/kmole=96.487/4.1868 or 23.046 kcal/mole
        E = <E>*1.E5/8.6171
        X1 = 180. + 273.15
        X2 = X1 + FLOAT(<L>)
C     use NAG quadrature subroutine D01ABF to generate data
        ACC= 1. E-2
        MAX= 128
        IFAIL = 1
        CALL D01ABF (X1,X2,INTEGRAL,ACC,MAX,N,W(<L>),IFAIL)
        PEF= PEF/W(<L>)
         L = <L>-1
        DO 2 I=1,L
        X(I)  =  X1 + FLOAT(I)
        IFAIL = 1
 2      CALL D01ABF (X1,X(I),INTEGRAL,ACC,MAX,N,W(I),IFAIL)
        W(<L>)=W(L)
          L   = <L>
        X(L)  = X2
        CALL GRFTYP(0,0)
        CALL PLIMIT(30.,170.,50.,120.)
        CALL GRFLT( 0., 130.)
        CALL PLTGY (W,L,X1,X2)
        CALL AXEXY (0,0)
        DO 6 I=1,L
        WT(I) =100.
        IF (W(I).GT.0.99) WT(I)=1.
 6      CONTINUE
        K = 100
        CALL VC03A (L,K,X,W,WT,R,XN,FN,GN,DN,THETA,0,WS)
C     reconstruct by -TG01E and plot spine-fit A-t curve
C     at the same time, calculate and plot R(I)=dA/dt(N)
        DO 7 I=1,L
             J=I-2
         R(I) = DERIV (I,X,XN,FN,GN)
        WT(I) = TG01B (J,K,XN,FN,GN,X(I))
        W (I) = 1.- WT(I)
        IF (R(I).LT.0.) R(I)=0.
 7      CONTINUE
        IF (R(1).LE.0.) R(1)=0.00002

        CALL PEN(2)
        CALL PLTGY(WT,L,X1,X2)
        CALL ULIMIT(0.0,0.0,0.0,0.0)
        CALL PEN(3)
        CALL PLTGY (R,L,X1,X2)
        CALL ULIMIT(30.,170.,50.,120.)
        CALL PEN(1)
        CALL LOCCHR(45.,100.,0)
        WRITE (8,700)
 700    FORMAT('+RED-TG01B FIT; GREEN-DERIVATIVE')
C     Plot on a new graph  log(1/N)((1-A)**(1/N-1))(dA/dt)
C     vs.1000/T for N=2,3; log is to base e,T in abs scale
C     and whence E(activation) = -slope *8.5171*E(-5+3) eV
             Q=2./3.
          X(1)=1000./X(1)
          WT(1)=ALOG(AES(R(1)/3.))
             DO 8 I=2,L
             IF (W(I).LT.0.01.OR.R(I).LT.0.00002) GO TO 18
             WT(I)=ALOG((R(I)/3.)/W(I)**Q)
             GO TO 8
 18          J=I-1
             WT(I)=WT(J)
  8          X(I)=1000./X(I)
             WT(L)=WT(L)
```

```
82              CALL BRKPLT(8,400.)
83              CALL PLIMIT(30.,170.,10.,150.)
84              CALL BCXGXY (X,WT,L)
85              CALL PEN(2)
86              CALL MOVETO (X(10),WT(10))
87              CALL PLTCHR (241)
88              DO 9 I=2,L
89              IF (W(I).LT.0.01.OR.R(I).LT.0.00002) GO TO 19
90              WT(I)=ALOG((R(I)/2.)/W(I)**0.5)
91              GO TO 9
92        19    J=I-1
93              WT(I)=WT(J)
94         9    CONTINUE
95              CALL PEN(3)
96              CALL PLTGXY(X,WT,L)
97              CALL MOVETO(X(10),WT(10))
98              CALL PLTCHR(242)
99            P=1./3.
100           Q=((3.1416/6.)**P)*3.
101            W(1)=WT(1)
102           DO 12 I=2,L
103           IF (R(I).LT.0.00002) GO TO 22
104           WT(I)=ALOG(R(I))
105           WW    =1.-W(I)
106           IF (WW.LT.0.01) WW=0.01
107           W (I)=ALOG((R(I)/Q)/(WW**WW)**P)
108           GO TO 12
109       22  J=I-1
110           WT(I)=WT(J)
111           W (I)=W (J)
112       12  CONTINUE
113           CALL PEN(1)
114           CALL PLTGXY(X,WT,L)
115           CALL PLTGXY(X,W ,L)
116           CALL MOVETO(X(10),WT(10))
117           CALL PLTCHR(243)
118           CALL MOVETO(X(10),W (10))
119           CALL PLTCHR(244)
120           CALL ULIMIT(30.,170.,10.,150.)
121           CALL LOCCHR(30.,135.,0)
122           WRITE (3,120)
123           CALL LOCCHR(40.,130.,0)
124           WRITE (3,280)
125       120 FORMAT('+LOG N*(1-A)**(N-1)*DA/DT : 1(N=1/3), 2(=1/2)')
126       280 FORMAT('+N-DIMENSIONAL GROWTH :  3(N=1), 4(=3)')
127             STOP
128             END
129   C
130             FUNCTION INTEGRAL(X)
131           COMMON PEF,E
132           INTEGRAL = PEF * EXP(-E/X)
133           RETURN
134             END
135   C
136             FUNCTION DERIV(I,X,XN,FN,GN)
137           DIMENSION X(65),XN(60),FN(60),GN(60)
138           IF(I.LT.2) J=2
139       1   IF(X(I).LE.XN(J))GOTO 2
140             J = J+1
141           GOTO 1
142       2     M = J-1
143             H = XN(J)-XN(M)
144             XX =( X(I)-XN(M) )/H
145             C =3.*(FN(J)-FN(M))/H-2.*GN(M)-GN(J)
146             D =2.*(FN(M)-FN(J))/H+GN(M)+GN(J)
147           DERIV=GN(M)+(2.*C+3.*D*XX)*XX
148           RETURN
149             END
150   C
```

```
151   C  N.B. This program makes use of subroutines
152   C  from several software libaries named below.
153   /*
154   //LKED.SYSLIB    DD
155   //               DD DSN=SYS2.FORTLIB,DISP=SHR
156   //               DD DSN=SYS2.CAMLIB,DISP=SHR
157   //               DD DSN=NAG.FORTLIB,DISP=SHR
158   //               DD DSN=GRAPHDEV.PLOTLIB,DISP=SHR
159   //GO.FT08F001    DD DSN=TBT1.PLOT,DISP=SHR
160   /*EOF
161   +
```

APPENDIX F

TBT1.d at 14.20 on 23 Mar 1978
Member E

```
    1   REQUEST ' FILE ?  ' FILE
    2   REQUEST ' START WEIGHT ?' WO
    3   REQUEST ' L = NO. OF POINT ?' L
    4   REQUEST ' EACH ? MINUTES:=' TU
    5   REQUEST ' LOG LOG PLOT ?: D/DT 1: FOT, FIT 0' I
    6   REQUEST ' TF 1   K(<<IF1X(L/2))=' K$1 '7L+9K+6=' M$1
    7   REQUEST ' TF 0   N=' N$2 ' DECAY PERIOD? 9 IF YES' J$1
    8   REQUEST 'TURNROUND?..MINS/"BY HHMM"/OVERNIGHT 'I$NOW
    9   SUBMIT &H+
   10   JOB TBT1 4008 ' <FILE> ISOTHERMAL
   11   TURNROUND <I> OR OVERNIGHT
   12   ROUTE PRINTER DUMMY
   13   LIMSTORE 180K
   14   COMP 10
   15   //   EXEC FTG1CLG,REGG=180K
   16   //SYSIN     DD  *
   17   C     ------------------------------------------
   18   C       Program written by T.B.Tang, to find out
   19   C     which kinetic equation best fits isothermal
   20   C     TG data (read-in from disc file .S(FILE?));
   21   C     I=2 for most general but less definite scan
   22   C     then if appropriate I=1, lastly I=0 to con-
   23   C     firm chosen equation (form used in the pro-
   24   C     gram changed as required) where a separate
   25   C     plot for the decay period is optional. 7779
   26   CC    Return I=5 when plots are produced for use
   27   CC    in thesis; all three graphs will be plotted
   28   CC    in reduced scale and 'logically' positioned
   29   CC    together in one quarto-size window.    7873
   30   C     ------------------------------------------
   31         DIMENSION DW(<K>),THETA(<K>),WS(<K>)
   32         COMMON/DRV/X(<L>),XN(<K>),FN(<K>),GN(<K>)
   33         COMMON I,J,JDE,JCAY,K,L,RN,W(<L>),WT(<L>),R(<L>)
   34         L  = <L>
   35         TU = <TU>
   36   C     <K> estimated number of knots in curve fit
   37   C     <M> calculated size of working space reqd.
   38   C   read in data
   39         DO 1 I=1,L
   40    1    CALL BREAD(W(I),&2,&2,&3)
   41    3    TLAST = FLOAT(L)*TU
   42           CALL  CPTPLT(8, 300.)
   43   C   plot  weight loss  curve
   44   CC  following values originally 30.,230.,30.,190.
   45         CALL PLIMIT(20.,170.,30.,110.)
   46         CALL PEN(3)
   47         CALL GPETYP(-10,'+')
   48         CALL PLTGY (W,L,TU,TLAST)
   49         CALL ANSIZE(2.,1.,2.,1.)
   50         CALL AXEXY('(I3)','(I3)')
```

```
CC  callANSIZE only for thesis
C   plot  alpha  time  curve
      JDE    =  0
      JCAY   =  0
      J      =  0
      DO 4 I=1,L
      W(I)   = 3.567*(1.-W(I)/<W0>)

      IF (JCAY.GE.1) GO TO 4
      IF (W(I).GE.0.8) JCAY= I
      IF (JDE .GE.1) GO TO 4
      IF (W(I).GE.0.6) JDE = I
      IF (J.GE.1) GO TO 4
      IF (W(I).GE.0.5) J=I
 4    CONTINUE
      WJ = W(J)
      TJ = FLOAT(J)*TU
      TU = TU/TJ
      TLAST = TLAST/TJ
      CALL PLIMIT(170.,20.,110.,30.)
      CALL RANGE (TLAST,TU,10,XST,XSP,V)
C   e/TLAST/4./ if 'standard' width of 4*t(0.5) required
      XST= XST+1E-5
      XSP= XSP+1E-5
      CALL ULIMIT(XST,XSP,1.,1E-5)
      CALL PEN(2)
      CALL PLTGY (W,L,TU,TLAST)
      CALL PEN(1)
      CALL ANSIZE(-3.,-1.,-4.,-2.)
      CALL AXEXY (0,0)
      CALL ANSIZE(3.,1.5,4.,2.)
      IF (<I>.EQ.1) GO TO  5
      IF (<I>.EQ.2) GO TO 23
      IF (<I>.EQ.9) GO TO  7
C
C   fit equation  1-(1-alpha)**(1/N) = kt
C   (form of equation changed as required)
 5    RN = 1./FLOAT(<N>)
      DO 6 I=1,L
      IF (W(I).GT.1.) W(I)=1.
      WT(I) =  1.-(1.-W(I))**RN
 6    CONTINUE
      CALL GRFTYP(10,'+')
      CALL PLTGY (WT,L,TU,TLAST)
      IF (<I>.EQ.5) GO TO 23
      GO TO 7
C
C   plot d(alpha)/d(t) curves
C   first, a cubic spine fit to alpha-time by a Harwell
C   subroutine  ( derivatives at knots returned in GN )
 8    DO 9 I=1,L
      X(I)   = FLOAT(I)*<TU>
 9    WT(I) =1.
      K     = <K>
      CALL VC03A(L,K,X,W,WT,R,XN,FN,GN,DN,THETA,0,WS)
      IF (K.LT.1) GO TO 7
C   if -VC03a requires K larger, K is returned negative
C   second, reconstruct (using Harwell -TG01B) and plot
C   the fitted alpha-time (curve red on plotter output)
      DO 10I=1,L
                J=I-2
 10   R(I)   = TG01B(J,K,XN,FN,GN,X(1))
      CALL PEN(1)
      CALL PPTY(R,L,TU,TLAST)
C   third, calculate and plot normalised differences
```

```
C    and spline-fit derivatives ; + = deriv's at knots
C    NOW NO DIFFERENCE PLOT 2 statements below made C
          RN  =  4.*<TH>
              J=L-4
          DO 11I=1,J
          R(I)  =( W(I+4) - W(I) )/ RN
C         if (R(I).LT. 1E-5) R(I)=1E-5
   11     CONTINUE
          R(L-2)= 1E-5
          R(L-1)= 1E-5
          R(L)  = 1E-5
          RMAX  = R(J)
          DO 12I=6,L
              J=14L-I
            RN  = R(J)
          IF ( RN.GT.RMAX) RMAX=RN
   12     R(J+2)= RN
C         r(2)  = r(1)
          CALL PINTI(XSI,XSP,RMAX,1E-5,0.)
C         call prty(r,l,fu,tlast)
          DO 13I=1,L
   13     R(I)  = DERIV(I)
          CALL PLTARY(GN,K,TU,TLAST,-1,78)
          CALL PLTARY( R,L,TH,TLAST, 0,64)
          GO TO 7
C    On a new graph: ln(R) vs. ln(alpha) and vs. ln(1-a')
C    (ln -to base 10) first curve being req, second green
C    and in addition black + plotted from knot deriv's GN
   14     PX1= 90.
          PX2=230.
          PY1= 20.
          PY2=260.
  144         I=0
   15         I=I+1
          IF (W(I).GE.0.01) GO TO 155
            W(I) = 0.01
          GO TO 15
  155     IF (<I>.EQ.5) GO TO 16
          CALL SRMARL(W,P,L,0,64,'RED:LOG A; GREEN:LOG 1-A',24)
          GO TO 166
   16     CALL PEN(2)
          CALL PLIMIT(102.,185.,133.,260.)
          CALL WLIMIT(-2.,0.,0.,0.)
          CALL PLTGLL(W,P,L)
          IF (<I>.EQ.5) GO TO 211
          CALL PEN(1)
  166     DO 17I=1,K
          IF (GN(I).LT.1.5E-5) GN(I)=1.5E-5
   17     CONTINUE
              I=0
   18         I=I+1
          IF (FN(I).GE.0.01) GO TO 19
            FN(I)=0.01
          GO TO 18
   19     CALL PLTARL(FN,GN,K,-1,78)
          DO 20I=1,K
            FN(I)=1.-FN(I)

          IF (FN(I).LT.0.01) FN(I)=0.01
   20     CONTINUE
          CALL PLTARL(FN,GN,K,-1,78)
  211     DO 21I=1,L
            WT(I)=1.-W(I)
          IF (WT(I).LT.0.01) WT(I)=0.01
   21     CONTINUE
          CALL PEN(3)
          CALL PLTGLL(WT,R,L)
          CALL PEN(1)
          CALL BOXLL (0,'(F0.1)')
            STOP
C
```

```
C
C   plot log(-log*(1-a)) vs. log(t/t(0.5))
C   for 0.15<a<0.5  log* is to base e
 23       K  = 0
          DO 25 I=1,J
          IF (  K .GT. 0  ) GO TO 24
          IF (W(I).LT.0.15) GO TO 25
 24         K  = K+1
          WT(K) =-ALOG(1.-W(I))
           X(K) = FLOAT(I)*TU
 25       CONTINUE
          IF (<I>.EQ.5) GO TO 26
           PX1 = 50.
           PX2 =230.
           PY1 = 20.
           PY2 =200.
          CALL DRWARL(X,WT,K,0,64,'LOG LOG PLOT',12)
            STOP
CC  below for thesis, plotting also LOG10(P) curves
 26       CALL SCLCHR(0.8,0.7)
          CALL GPFTYP(0,0)
          CALL PLIMIT(15.,85.,190.,260.)
          CALL BOXGLL(X,WT,K)
          DO 27 I=1,L
          WT(I) =1.
 27         X(I) = FLOAT(I)*<TU>
            K  = <K>
          CALL VC03A(L,K,X,W,WT,R,XN,FN,GN,DN,THETA,0,WS)
          DO 28 I=1,L
 28         R(I) = DERIV(T)
          GO TO 144
C
C   name the curves at top of 1st graph
  7       CALL PLOTT(230.,30.,200.,40.,0.)
          CALL LOCCHR(101.,218.,0)
          CALL PEN(3)
          WRITE (6,100)
          CALL LOCCHR(101.,224.,0)
          CALL PEN (2)
          WRITE (6,101)
          CALL LOCCHR( 50.,236.,0)
          WRITE (6,103) L
          CALL LOCCHR( 77.,230.,0)
          CALL PEN(1)
          IF (<I>.EQ.1) GO TO 22
```

IBT1,J at 14.20 on 23 Mar 1978
Member F_____contd

```
          WRITE (6,102) WJ,TJ
          IF (<J>.GT.5) CALL DECAY
            STOP
 22       WRITE (6, 99) K
          IF (K.LT.1)  STOP
          GO TO 14
 99       FORMAT('+CUBIC SPLINE FIT: NO.OF KNOTS IS',I4)
100       FORMAT('+GREEK: WEIGHT LOSS CURVE')
101       FORMAT('+ REF : ALPHA  TIME CURVE')
102       FORMAT(
         2'+BLACK:1-(1-ALPHA)**(1/<N>)  T(',F5.3,')=',F6.2)
103       FORMAT(
         3'+START WT. <.0>',I8,' POINTS:EACH <TU> MINUTES')
            END
C
```

```
C
      FUNCTION DERIV(I)
C   to calculate d/dx a+b(x)+c(x**2)+d(x**3)
      COMMON/DRV/X(<L>),XN(<K>),FN(<K>),GN(<K>)
      IF (I.LT.2) J=2
    1 IF (X(I).LE.XN(J)) GO TO 2
      J = J+1
      GO TO 1
    2   M = J-1
        H = XN(J)-XN(M)
        XX =( X(I)-XN(M) )/H
        C =3.*(FN(J)-FN(M))/H - 2.*GN(M) - GN(J)
        D =2.*(FN(M)-FN(J))/H + GN(M) + GN(J)
      DERIV=GN(M) + XX*(2.*C + 3.*XX*D)
      IF (DERIV.LT. 2E-5) DERIV=2E-5
      RETURN
      END
C
      SUBROUTINE DECAY
C   plot NEW-reduced time for N= 3 and 2, alpha=[0.0,1]
C   1-(1-(A-A(0.6)))**(1/d)  vs. (t-t(0.5))/(t-t(0.8))
      COMMON I,J,JDE,JCAY,K,L,RN,X(<L>),WT(<L>),R(<L>)
      COMMON/PSETUP/TNIT,PX1,PX2,PY1,PY2
      IF (JCAY.LE.1) RETURN
      RN=1./3.
      J = I-JDE+1
      WDE   =W(JDE)
      WCAY  =W(JCAY)
      DO 1 I=1,L
        K  =I+JDE-1
      W(I)  =  W(K)-WDE
      R(I)  =1.-W(I)
      WT(I) =1.-R(I)**RN
    1 R(I)  =1.-R(I)**0.5
      PX1= 30.
      PX2=200.
      PY1= 50.
      PY2=135.
      TU = 0.
      TTT= 8.
      CALL BRKPLT (8,300.)
      CALL RANGE(TU,TTT,10,XST,XSP,V)
      CALL PTNIT(XST,XSP,0.,0.4,0.)
```

```
286           YSP= FLOAT(L-JDE)/FLOAT(JDAY-JDE)
287           CALL PPTY (D ,J,0.,YSP)
288           CALL PAXESA (0,0)
289           CALL PEN(2)
290           CALL PPTY (WT,J,0.,YSP)
291           CALL PEN(3)
292           CALL PPTY(R ,J,0.,YSP)
293     C  name the curves at bottom of graph
294           CALL PLMIT(30.,200.,50.,135.,0.)
295           CALL LOCCHR (60.,33.,0)
296           WRITE (8,100) DCAY,RDE
297           CALL LOCCHR (60.,27.,0)
298           WRITE (8,200)
299      100  FORMAT('+DECAY PERIOD :  ',F5.3,')-I(',F5.3,')')
300      200  FORMAT('+RED:1-(1-A)**1/3; GREEN:I-(1-A)**1/2')
301           RETURN
302     C    Output destinated to ForTran unit 08 is put onto
303     C    disc file user.PLOT; if you desire output to be
304     C    sent to the plotter straightaway change below
305     C    DSN=(your userID).PLOT,DISP=SHR to  SYSOUT=P
306     CC   TBT1.PRIVLIB contains compiled PLTARY,PPTY,etc.
307          END
308     /*
309     //LKED.SYSLIB    DD
310     //                DD   DSN=GRAPHDEV.PLOTLIB,DISP=SHR
311     //                DD   DSN=TBT1.PRIVLIB,DISP=SHR
312     //                DD   DSN=SYS2.FORTLIB,DISP=SHR
313     //                DD   DSN=SYS2.CARLIB,DISP=SHR
314     //GO.FT08F001     DD   DSN=TBT1.PLOT,DISP=SHR
315     //FFIN            DD   DSN=TBT1.G(<FILE>),DISP=SHR
316     /*EOF
317     +
```

APPENDIX G

DYNAMIC TG DATA FROM THE PYROLYSIS OF SILVER AZIDE

Dynamic thermogravimetric measurements were carried out using basically the same system as described in Section 6.2. The programmer incorporated in the Stanton Redcroft thermobalance was set so that the furnace temperature T' rose linearly with time t. All experimental runs have been performed at the same (nominal) heating rate dT'/dt.

Several calibration tests were carried out to compare

the displayed temperature T' with that indicated by a fine thermocouple junction attached to an empty pan, T, which was taken to be the temperature of the sample when it was in the pan. During the tests, it was ensured that the downward force on the pan by the thermocouple remained positive and within the scale of the the balance, so that the pan should stay in virtually the same position. Between 490 and 600 K and for the particular length of the sample pan suspension wire used, the following numerical relation was found valid: $T/T' = 0.91 \pm 0.03$, where T and T' were in deg.C. The sample heating rate $dT/dt \equiv H$ was thus determined to be 1.2 ± 0.3 K/minute.

Separate empty-pan runs showed that an apparent decrease of sample weight accompanied the rise of T'. Correction for this effect, which was probably due to increasing convection, was established for our instrument to be adequately given by +15 ug/(100 K).

The TG data obtained were analysed by the approach suggested in Section 5.4. The weight readings recorded on tape at regular intervals were converted into a ('alpha') values, the molar fractions of decomposition, and da/dt calculated by numerical differentiation of a smoothed a(T) curve. By plotting against (10E3)/T the logarithm of (da/dT)/f(1 - a), we should then be able to obtain E/k(10E3) from the slope and R*/H from the y-intercept. These analyses have been done by

the computer program listed overleaf. In it, four forms of $f(1 - a)$ were tried: $(1 - a)^{2/3}$, $(1 - a)^{1/2}$, 1 (i.e. $a = R(T)\,t$ or one-dimensional growth of nuclei), and $a^{-2/3}$ (i.e. $a^{1/3} = R(T)\,t$ or three-dimensional growth); according to Section 6.3.2 the first form is the correct one. However, the two sets of typical results shown in the graphs following the computer listing illustrate the situation encountered in all the results, that no straight lines were generated in the Arrhenius plots with any form of $f(1 - a)$ used.

The advantages and disadvantages of the dynamic method in studying reaction kinetics have been mentioned in Section 5.1; the special difficulty arising out of temperature gradients is discussed in Section 5.2. In the present case we tentatively conclude that, the pyrolysis of silver azide being strongly exothermic, the arrangement in our thermobalance is inadequate to maintain a sufficiently uniform temperature in the large single crystals used as samples. This explains the failure to obtain E and R* from the dynamic data.

```
T8T1.J at 10.45 on 28 Mar 1979
Member 3

    1   REQUEST ' FILE? ' FILE  'START WEIGHT? ' WC
    2   REQUEST ' TEMPERATURE RANGE L=' L*100
    3   REQUEST ' -- CORRECTION FACTOR' T$0.91
    4   REQUEST ' INPUT HERE 7*L+4906 =' N$1606
    5   REQUEST ' **MINS/,EY RRRR,/OVERNIGHT 'T$JUM
    6   SUBMIT *R+
    7   JOB T8T1 4008 ' <FILL><FILL>
    8   TURNROUND <T> OR OVERNIGHT
    9   ROUTE PRINTER DUMMY
   10   LIMSTORE 180K
   11   COMP 10
   12   // EXEC FTG1CLG,<LIST3,>REGG=180K
   13   //SYSIN    DD     *
```

```
C ------------------------------------------------------------
C Solid-State Thermal Decomposition
C Kinetics determination
C Program number two --- Dynamic analysis:
C   Program written by T.daTang  to obtain from TG data
C alpha-time curve, DTG curve, and activation energy plot
C                        Program in the Fortran language, for
C                        implementation on IBM 370/165 which
C                        read-in the job by Phoenix language.
C ------------------------------------------------------------
      EXTERNAL XX,YY
      DIMENSION X(<L>),XN(100),FN(100),GN(100),
     1DN(100),THETA(100),WS(<N>),WT(<L>)
      COMMON IJK,LMN,P,Q,R(<L>),W(<L>)
      CALL GRETYP(C,D)
      M = 242
      L = <L>
C   read in data from file
C     do 1 I=1,M
C1    call AREAD(WNIL,&2,&2,&3)
C   new data 1 to 241 deleted in file
    3   DO 4 I=1,L
    4     CALL AREAD(X(I),&2,&2,&5)
C   plot weight vs. temp.(time)
    5     CALL PLIMIT(20.,175.,45.,125.)
          X1 = <T>*FLOAT(M)
          X2 = <T>*FLOAT(M+L)
          CALL CRTPLT (0,200.)
          CALL PLTCV   (M,L,X1,X2)
          CALL AXEXY (C,D)
          TX=0.6*X1+0.2*X2
          TY=0.5*<XC>
          CALL LOCCHR(TX,TY,0)
          WRITE (6,500)
  500   FORMAT('+WEIGHT (MICROGRAM) VS TEMP. (C)')
C   convert weight into alpha (A) , which is plotted
C  on a new graph and cubic spline fitted by -VC00A
          DO 6 I=1,L
          X(I)= <T>*FLOAT(M+I)
          W(I) =3.557*(1.-W(I)/<XC>)
          WT(I) =20.
          IF (W(I).GT.0.99) WT(I)=1.
    6     CONTINUE
          CALL ULIMIT(0.0,0.0,0.0,0.0)


          CALL BRKPLT(6,300.)
          CALL PLTCV (M,L,X1,X2)
          CALL AXEXY (C,D)
          CALL LOCCHR(TX,0.7,0)
          WRITE (6,600)
  600     FORMAT('+BLACK-ALPHA,RED-SMOOTHED,GREEN-D/DT')
          K = 100
          CALL VC00A (L,K,X,W,WT,R,XN,FN,GN,DN,THETA,0,WS)
C     reconstruct by -TG01B and plot spine-fit A-t curve
C     Meanwhile, calculate(DERIV) and plot(normalised) dA/dt
          DO 7 I=1,L
             J=I-2
          R(1) = DERIV (1,X,XN,FN,GN)
          WT(I) = TG01B (J,K,XN,FN,GN,X(I))
          W (1) = 1.- WT(I)
          IF (R(I).LT.0.) R(I)=0.
    7     CONTINUE
          IF (R(1).LE.0.) R(1)=0.00002
          CALL PEN(2)
          CALL PLTCV(WT,L,X1,X2)
          CALL ULIMIT(0.0,0.0,0.0,0.0)
          CALL PEN(3)
          CALL PLTCV( R,L,X1,X2)
```

```
C     heating rate gl/dt determines unit for deriv
C       (and thus unit of pre-exponential factor)
C
C     Plot on a new 'page' log(1/N)((1-A)**(1/K-1))(dA/dt)
C     vs.1000/T for N=2,3; log is to base e,T in abs scale
          IF (X(1).LE.1.) GO TO 34
          XSCL=25.*((1./(273.15+X1))-1./(273.15+X2))
          CALL SCALE(XSCL,20.)
          CALL ORIGIN(-1./(273.15+X2),16.)
          DO 11 N=2,3
C       drawing Y=YY=log( )  for given n  vs. XX=1/T
          CALL PEN(N)
          P = 1./FLOAT(N)
          Q = 1.-P
          CALL MOVETO(XX(1),YY(1))
          CALL LOGCHR(0.,0.,1)
          WRITE (6,100) N
  100     FORMAT('+',I1)
          IJK=1
          LMN=3
          DO 11 I = 2,L
          Y = YY(I)
          IF ( IJK.EQ.2 .AND. LMN.EQ.2 ) GO TO 10
          CALL DRAWTO(XX(I),Y)
          GO TO 11
   10     CALL MOVETO(XX(I),Y)
   11     CONTINUE
          CALL LOG(L,XSCL,XX,YY)
            STOP
C
   28       D=2./3.
C          WRITE(6,150) X
C150       FORMAT(10(2X,10F8.2/))
           X(1)=1000./(273.16+X(1))
           WT(1)=ALOG(ABS(R(1)/3.))
             DO 6 I=2,L
             IF (R(I).LT.0.01.OR.R(I).LT.0.00002) GO TO 15
             WT(I)=ALOG((R(I)/3.)/W(I)**D)
             GO TO 6
    15       J=I-1
             WT(I)=WT(J)
      8      X(I)=1000./(273.16+X(I))
             WT(L)=WT(L)+1.
C          forgot X(1); 1 hour spent to discover mistake!
C          WRITE(6,160) X
C160       FORMAT(10(4X,10F8.2/))
             CALL ERRPLT(8)
             CALL PLINIT(30.,.175,.75,.285.)
             CALL ANVALS(0.1,0.1,.0)
             CALL EXGXY(X,WT,L)
             CALL PEN(2)
             CALL MOVETO (X(10),WT(10))
             CALL PLTCHR (241)
C     adding T-ticks (TX deg.C) and identifying the 2 curves
          CALL SCTCHR(1.5708)
          DO 29 I=10,L,20
          TX=1000./X(I)-273.15
          CALL MOVETO(X(I),-2.)
          CALL DRAWBY(0.,0.4)
          CALL LOGCHR(0.,0.1,1)
   29     WRITE (6,350) TX
  350     FORMAT(1X,F5.1)
          CALL SCTCHR(-1.5708)
             DO 5 I=3,L
             IF ( (I).LT.0.01.OR.R(I).LT.0.00002) GO TO 19
             WT(I)=ALOG((R(I)/3.)/W(I)**0.5)
             GO TO 9
    19       J=I-1
             WT(I)=WT(J)
      9      CONTINUE
```

```
151             CALL PEN(3)
152             CALL PLTGXY(X,WT,L)
153             CALL MOVETO(X(10),WT(10))
154             CALL PLTCHR(242)
155           P=1./3.
156           Q=((3.1+10/6.)**P)*3.
157            W(1)=WT(1)
158           DO 12 I=3,L
159           IF (R(I).LT.0.00002) GO TO 22
160           WT(I)=ALOG(R(I))
161           WW    =1.-R(I)
162           IF (WW.LT.0.01) WW=0.01
163           W (I)=ALOG((R(I)/Q)/(WW**WW)**P)
164           GO TO 12
165    22     J=I-1
166           WT(I)=WT(J)
167           W (I)=W (J)
168    12     CONTINUE
169           CALL PEN(1)
170           CALL PLTGXY(X,WT,L)
171           CALL PLTGXY(X,W ,L)
172    C    identifying the 2 accod curves;
173    C    then name all 4 at top of graph
174           CALL MOVETO(X(10),WT(10))
175           CALL PLTCHR(243)
176           CALL MOVETO(X(10),W (10))
177           CALL PLTCHR(244)
178           CALL ULIMIT(30.,175.,75.,255.)
179           CALL LOCCHR(40.,260.,0)
180           WRITE (3,120)
181           CALL LOCCHR(50.,255.,0)
182           WRITE (3,280)
183    120    FORMAT('+LOG N*(1-A)**(N-1)*DA/DT : 1(N=1/3), 2(=1/3)')
184    280    FORMAT('+N-DIMENSIONAL GROWTH :  3(=1), +(=3)')
185    2      STOP
186           END
187    C
188            FUNCTION XX(I)
189           XX = 1./(273.16+FLOAT(I+M)*CT)
190           RETURN
191           END
192    C
193            FUNCTION YY(I)
194           COMMON IJK,LMN,P,Q,R(<L>),W(<L>)
195    C    no plot where 1-A or d(A)/dt is too small
196             IF (W(I).LT.0.01 .OR. R(I).LT.0.0002) GO TO 1
197           YY = ALOG(P*R(I)/W(I)**Q)
198           LMN=3
199            IF (IJK .EQ. 2) LMN=2
200           IJK=1
201           RETURN
202    1      IJK=2
203           RETURN
204           END
205    C
206           FUNCTION DERIV(I,X,XN,FN,GN)
207           DIMENSION X(<L>),XN(100),FN(100),GN(100)
208    C    to calculate d/dx( a+b(x)+c(x**2)+d(x**3))
209             IF(I.LT.2) J=2
210    1      IF(X(I).LE.XN(J))GOTO 2
211                J = J+1
212           GOTO 1
213    2         M = J-1
214              H = XN(J)-XN(M)
215             XX =( X(I)-XN(M) )/H
216              C =3.*(FN(J)-FN(M))/H-2.*GN(M)-GN(J)
217              D =2.*(FN(M)-FN(J))/H+GN(M)+GN(J)
218           DERIV=GN(M)+(2.*C+3.*D*XX)*XX
219           RETURN
220           END
```

FORTRAN UNIT NUMBER 8

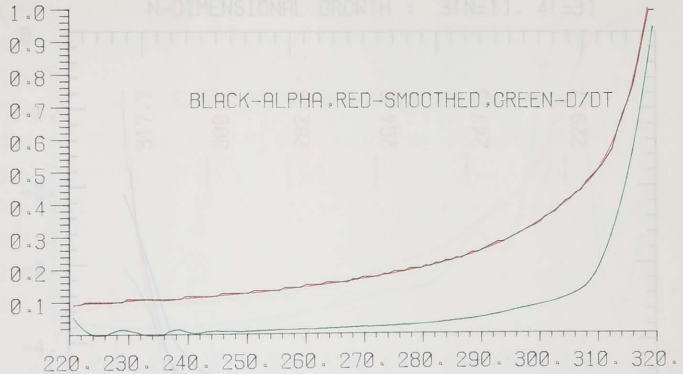

FORTRAN UNIT NUMBER 8

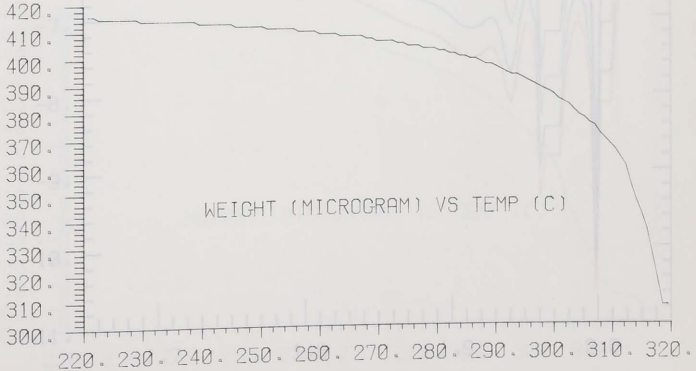

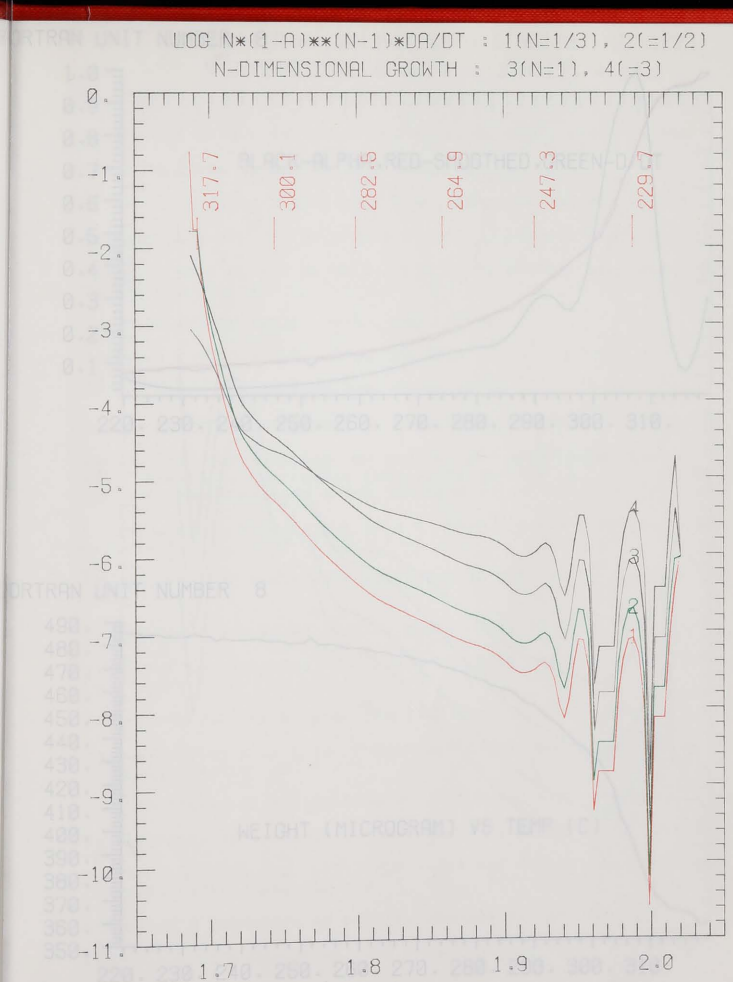
LOG N*(1-A)**(N-1)*DA/DT : 1(N=1/3), 2(=1/2)
N-DIMENSIONAL GROWTH : 3(N=1), 4(=3)
0.
-1.
-2.
-3.
-4.
-5.
-6.
-7.
-8.
-9.
-10.
-11.
317.7
300.1
282.5
264.9
247.3
229.7
1
2
3
4
1.7
1.8
1.9
2.0

FORTRAN UNIT NUMBER 8

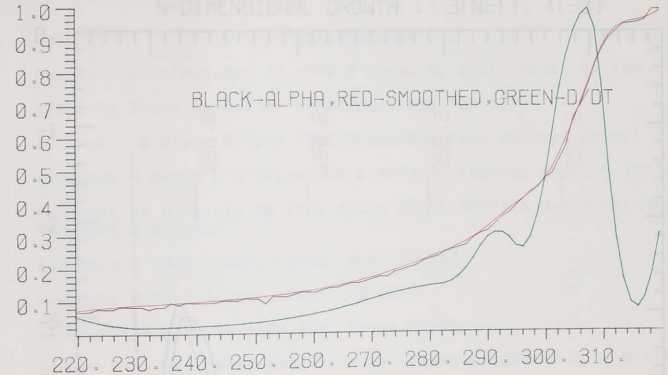

FORTRAN UNIT NUMBER 8

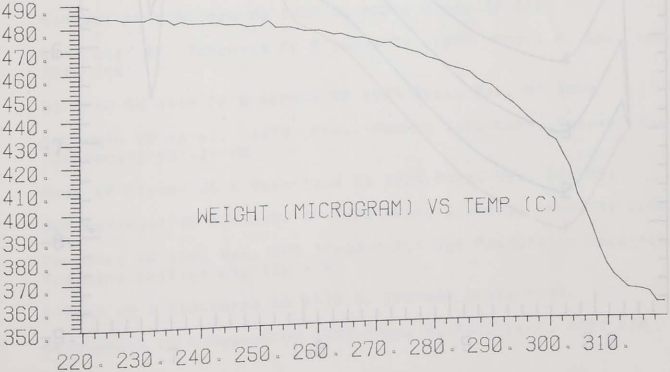

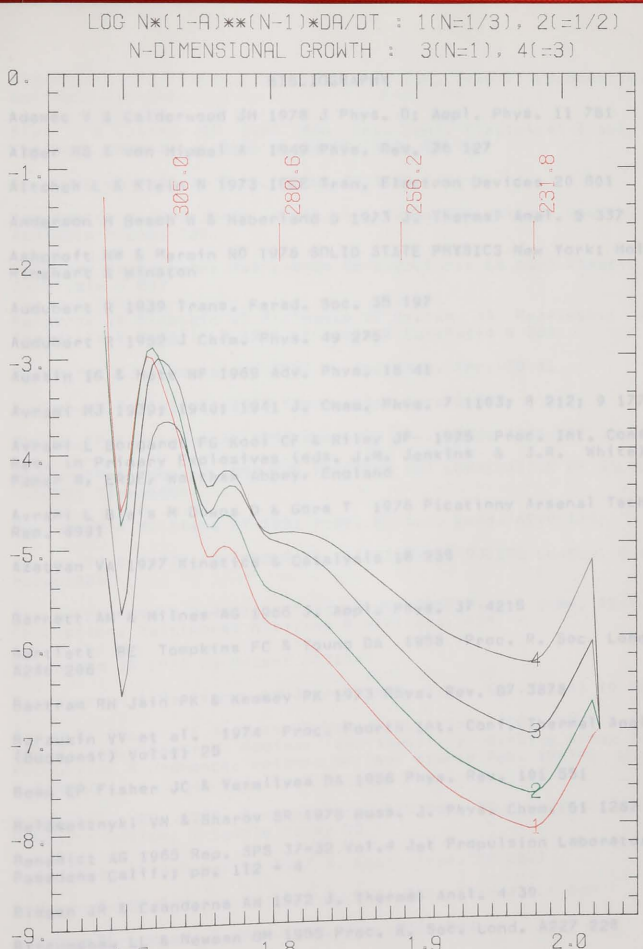
LOG N*(1-A)**(N-1)*DA/DT : 1(N=1/3), 2(=1/2)
N-DIMENSIONAL GROWTH : 3(N=1), 4(=3)
0.
-1.
-2.
-3.
-4.
-5.
-6.
-7.
-8.
-9.
1.7
1.8
1.9
2.0
305.0
280.6
256.2
231.8
1
2
3
4

BIBLIOGRAPHY

Adamec V & Calderwood JH 1978 J Phys. D: Appl. Phys. 11 781

Alger RS & von Hippel A 1949 Phys. Rev. 76 127

Altcheh L & Klein N 1973 IEEE Tran. Electron Devices 20 801

Anderson H Besch W & Haberland D 1973 J. Thermal Anal. 5 337

Ashcroft NW & Mermin ND 1976 SOLID STATE PHYSICS New York: Holt Rinehart & Winston

Audubert R 1939 Trans. Farad. Soc. 35 197

Audubert R 1952 J Chim. Phys. 49 275

Austin IG & Mott NF 1969 Adv. Phys. 18 41

Avrami MJ 1939; 1940; 1941 J. Chem. Phys. 7 1103; 8 212; 9 177

Avrami L Borgardt FG Kooi CF & Riley JF 1975 Proc. Int. Conf. Res. in Primary Explosives (eds. J.M. Jenkins & J.R. White), Paper 8, ERDE, Waltham Abbey, England

Avrami L Blais M Downs D & Gora T 1976 Picatinny Arsenal Tech. Rep. 4991

Azatyan VA 1977 Kinetics & Catalysis 18 235

Barnett AM & Milnes AG 1966 J. Appl. Phys. 37 4215

Bartlett BE Tompkins FC & Young DA 1958 Proc. R. Soc. Lond. A246 206

Bartram RH Jain PK & Kemmey PK 1973 Phys. Rev. B7 3878

Barzukin VV et al. 1974 Proc. Fourth Int. Conf. Thermal Anal. (Budapest) Vol.1; 25

Bean CP Fisher JC & Vermilyea DA 1956 Phys. Rev. 101 551

Belomestnykl VN & Sharov SR 1978 Russ. J. Phys. Chem. 51 1262

Benedict AG 1965 Rep. SPS 37-32 Vol.4 Jet Propulsion Laboratory Pasadena Calif.; pp. 112 - 4

Biegen JR & Czanderna AW 1972 J. Thermal Anal. 4 39

Bircumshaw LL & Newman BH 1955 Proc. R. Soc. Lond. A227 228

Blazek A 1973 THERMAL ANALYSIS (tr. J.F. Tyson) London: Van Nostrand Reinhold

Blok J & LeGrand DG 1968 Ann. Rep. Conf. Electrical Insul. & Dielect. Phenomena, Washington DC: NAS; 53

Blumberg AA 1959 J. Phys. Chem. 63 1129

Boddington T 1963 Proc. Ninth Int. Symp. Combustion, New York: Academic Press; 287

Boldyrev VV Zakharov YuA Lykhin VM & Votinova LA 1963 Kinetic & Catalysis 4 587

Boldyrev VV Eroshkin VI Pis'menko VI Ryzhak IA Medvinskii AA Shmidt IV & Kefeli LM 1968 Kinetics & Catalysis 9 260

Borchardt HJ & Daniels F 1957 J. Am. Chem. Soc. 79 41

Borham BM & Olson FA 1973 Thermochim. Acta 6 345

Bowden FP & McLaren AC 1958 Proc. R. Soc. Lond. A246 197

Bowden FP & Tabor D 1954 THE FRICTION AND LUBRICATION OF SOLIDS Oxford: Clarendon

Bowden FP & Williams HT 1951 Proc. R. Soc. Lond. A208 176

Bowden FP & Yoffe AD 1958 FAST REACTIONS IN SOLIDS London: Butterworths

Bowden FP Camp M & Montagu-Pollock HM 1962 Eighth Symp. (Int.) Combustion, Baltimore: Williams & Williams; 836

Breazeale JD 1976 US Patent 3931040

Brockway LO & Pauling L 1933 Proc. Nat. Acad. Sci. (USA) 19 860

Brown NE Grover JE Hartman DL Mangan DL & Scott CG 1973 Proc. Third Ann. Meeting Nuclear Survivability Working Group for Propulsion & Ordnance, Defense Nuclear Agency Rep. 1987P, LMSC - 030983

Budenstein PP 1973 Contract Rep. DAHC04 - 72 - 0001, US Army Research Office, Triangle Park, NC

Budenstein PP & Hayes PJ 1967 J. Appl. Phys. 38 2837

Budenstein PP & Hayes PJ 1969 J. Vac. Sci. Technol. 6 602

Burnham DC & Moser F 1964 Phys. Rev. 136 A744

Butcher PN & Hayden KJ 1977 Proc. Seventh Int. Conf. Amorphous & Liquid Semiconductors, Edinburgh, England; 2

Cagle FN & Eyring H 1953 J. Phys. Chem. 57 942

Camp M 1959 Ph. D Thesis, University of Cambridge

Camp M 1960 Fourth Int. Conf. Electron Microscopy, Berlin: Springer-Verlag; 134

Campbell DS & Morley AR 1971 Rep. Prog. Phys. 34 283 - 368

Carl LR 1940 J. Franklin Inst. 230 355

Caserta G Rispoli B & Serra A 1969 Phys. Status Solidi 35 237

Chaudhri MM 1969 Ph. D Thesis, University of Cambridge

Chaudhri MM 1973 Nature (Phys. Sci.) 242 110

Chaudhri MM & Field JE 1970 Proc. Fifth Symp. (Int.) Detonation, Pasadena, Calif.; pp. 245 - 253

Chaudhri MM & Field JE 1975 J. Solid State Chem. 12 72

Chaudhri MM Garrett WL Sandus O & Slagg N 1977 Propellants & Explosives 2 91

Chen DTY & Fong PH 1977 Thermochim. Acta 18 161

Coats AW & Redfearn JP 1964 Nature 201 68

Constable FH 1925 Proc. R. Soc. Lond. A108 355

Cook MA & Abegg MT 1956 Ind. Eng. Chem. 48 1090

Cooper R 1966 Brit. J. appl. Phys. 17 149

Cooper R & Elliott CT 1966 Brit. J. appl. Phys. 17 481

Cooper R & Elliott CT 1968 J. Phys. D: Appl. Phys. 1 121

Cooper R & Pulfrey DL 1971 J. Phys. D: Appl. Phys. 4 292

Cordes HF & Ruven Smith S 1968 J. Phys. Chem. 72 2189

Cornelis CC 1974 Tech. Rep. 226, Mason & Hanger-Silas Mason Co., Inc. (Burlington, Iowa, USA)

Coutts TJ & Hopewell B 1971 Thin Solid Films 9 37

Das Gupta DK & Brockley RS 1977 Ann. Rep. Conf. Electrical Insul. & Dielect. Phenomena, Washington DC: NAS; 197

David PK & Zelenyanszki F 1973 J. Thermal Anal. 5 337

Deb SK 1961 J. Chem. Phys. 35 2122

Deb SK 1967 Trans. Faraday Soc. 59 1423

Deb SK & Yoffe AD 1960 Proc. R. Soc. Lond. A256 514

DiStefano TH & Shatzkes M 1974 Appl. Phys. Lett. 25 685

Dickens B & Flynn JH 1976 Proc.First Europ. Symp. Thermal Anal. (ed. D. Dollimore); 15

Doelman A Greggas AR & Barall EM 1978 IBM J. Res.Develop. 22 81

Dogonadze RR Kuznetsoo AM & Chernenko AA 1965 Russ. Chem. Rev. 34 759

Downs DS Gora T Blais M & Garrett WL 1975 Picatinny Arsenal Tech. Rep. 4874

Doyle DC 1961 J. Appl. Polymer Sci. 5 285

Draper AL & Steum LK 1970 Thermochim. Acta 1 345

Dubovitskii AV Prokhorin EV Yakovlev VV & Manelis GB 1976 High Energy Chemistry 10 49

Dweydari AW & Mee CHB 1973; 1975 Phys. Status Solidi 17 247; 27 223

Dylewski J & Joshi MC 1977 Thin Solid Films 42 227

Evans BL & Yoffe AD 1957;59 Proc.R.Soc.Lond. A238 568; A250 346

Evofeev BV 1946 Compt. Rend. Acad. Sci. (USSR) 52 511

Fair HD & Downs DS 1971 Bull. Am. Phys. Soc. 16 519

Fair HD & Forsyth AC 1969 J. Phys. Chem. Solids 30 2559

Fair HD & Walker RF (eds.) 1977 ENERGETIC MATERIALS Vol.1 New York: Plenum

Fair HD Downs DS Forsyth AC Garrett W Blais M Gora TF & Williams FE 1973 Picartiny Arsenal Tech. Rep. 4607

Fedoroff BT Aaronson HA Sheffield OE Reese EF & Clift GD 1960 ENCYCLOPEDIA OF EXPLOSIVES AND RELATED ITEMS Vol.1 Picatinny Arsenal, Dover, NJ, USA

Felder RM & Stahel EP 1970 Nature 228 1085

Fiechowicz T 1974 French Patent 2132910

Fisher CR Bartraux RJ & Kemmey PJ 1975 Bull.Am.Phys.Soc. 20 487

Fong PH & Chen DTY 1977 Thermochim. Acta 18 273

Forlani F & Minneja N 1964 Phys. Status Solidi 4 311

Forlani F & Minnaja N 1969 J. Vacuum Sci. Technol. 6 518

Fox PG 1970 J. Solid State Chem. 2 491

Franklin JL Dibeler VH Reese RM & Krauss M 1958 J. Am. Chem. Soc. 80 298

Franz W 1956 Handbuck der Physik 17 155 - 263

Freeman ES & Carroll B 1958 Anal. Chem. 62 394

Frenkel J 1938 Phys. Rev. 54 647

Frianf RJ 1954 J. Chem. Phys. 22 1329

Friedmann HL 1967 J. Macromol. Sci. Chem. 1 57

Fripait JJ & Toussaint F 1963 J. Phys. Chem. 67 30

Frohlich H 1937 Proc. R. Soc. Lond. A160 230

Frohlich H & Paranjape BV 1956 Proc. Phys. Soc. Lond. B69 21

Galway AK & Jacobs PWM 1960 Proc. R. Soc. Lond. A254 455

Gangulee A & d'Heurle FM 1975 Thin Solid Films 25 317

Garn PD 1974 Proc. Fourth Int. Conf. Thermal Anal. (Budapest) Vol.1; 25

Garn PD 1976 J. Thermal Anal. 9 295

Garner WE & Marke DJB 1936 J. Chem. Soc. 657

Garner WE 1939 Nature 144 287

Garner WE & Rees LW 1954 Trans. Farad. Soc. 50 254

Garner WE (ed.) 1955 CHEMISTRY OF THE SOLID STATE London: Butterworths

Gas'maev VK & Zakharov YuA 1972 Russ. J. Phys. Chem. 46 1695

Gas'maev VK Zakharov YuA & Meshkov VA 1976 Russ. J. Phys. Chem. 50 1015

van Geel WCh Pistorius AC & Bouma BC 1957 Philips Res.Rep. 12 6

Ginstling AM & Brounshtein BI 1950 J. Appl.Chem. (USSR) 23 1327

Gora T 1971 J. Phys. Chem. Solids 32 529

Gorbatcher VM & Logvinenko VA 1972 J. Thermal Anal. 4 475

Gordy W & Thomas WJO 1956 J. Chem. Phys. 24 439

Granqvist CG & Buhrman RA 1976 J. Appl. Phys. 47 2200; 2220

Gray P 1963 Quarterly Rev. Chem. Soc. Lond. 17 441

Gray P & Waddington TC 1956; 1957 Proc. R. Soc. Lond. A235 481; A241, 110

Grigorovici R Croitoru N & Devenyi A 1961 Rev. Roum. Phys. 6 49

Guarini GGT Spinicci R Carlini FM & Donati D 1973 J. Thermal Anal. 5 307

Gurney RW & Mott NF 1938 Proc. R. Soc. Lond. A164 151

Hailes HR 1933 Trans. Farad. Soc. 29 544

Hancock JD & Sharp JH 1972 J. Am. Ceram. Soc. 49 379

Hanscomb JR 1970 J. Appl. Phys. 41 3597

Hansson I & Tholen A 1978 Phil. Mag. 37A 535

Harari E 1977 Appl. Phys. Lett. 30 601

Harris LB 1968 J. Appl. Phys. 39 4871

Harrison LG 1969 COMPREHENSIVE CHEMICAL KINETICS (eds. C.H. Bamford & C.F.H. Tipper) Vol.2, Amsterdam: Elsevier; pp.377-462

van Hartdeveld R & Hartog F 1969 Surface Sci. 15 189

Hauser HM 1977 Ph. D. Thesis, University of Cambridge

Hauser HM & Field JE 1978 Thermochim. Acta 27 1

Haynes RM & Young DA 1961 Disc. Farad. Soc. 31 229

Hays SD & Seay GE 1976 Proc. Fifth Symp. Nuclear Survivability of Propulsion & Ordnance Systems, Menlo Park, Calif.: Stanford Research Inst.

Hendricks SB & Pauling L 1925 J. Amer. Chem. Soc. 47 2904

Herber RH & Cheng HS 1969 Inorg. Chem. 8 2145

Herley PJ Jacobs PWM & Levy PW 1970 Proc. R.Soc. Lond. A318 197

Heuchamps C & Duval X 1966 Carbon 4 243

Hill RAW 1958 Trans. Farad. Soc. 54 685

Hill RM 1969 Proc. R. Soc. Lond. A309 377; 397

Hill RM 1971 Phil. Mag. 23 59

von Hippel A 1937 J. Appl. Phys. 8 815

von Hippel A Gross E Jelatis J & Geller M 1953 Phys.Rev. 91 568

Hitch AR 1918 J. Amer. Chem. Soc. 40 1195

Hitchinson RW Kleinberg S & Stein FP 1973 J. Phys. Chem. 77 870

Hold JB Cutler IB & Wadsworth ME 1962 J. Am. Ceram. Soc. 45 133

Horowitz HH & Metzger G 1963 Anal. Chem. 35 1464

Idea M Sawa G & Kato S 1971 J. Appl. Phys. 42 3737

Ishii T Furuichi R & Hara Y 1977 J. Thermal Anal. 11 71

Jacobs PWM & Kureishy ART 1962 Trans. Farad. Soc. 58 551

Jacobs PWM & Tompkins FC 1952 Proc. R. Soc. Lond. A215 265

Jacobs PWM Tompkins FC & Young DA 1959 Disc. Farad. Soc. 234

Jander W 1927 Z. Anorg. Allgem. Chem. 163 1

Jonscher AK 1967 Thin Solid Films 1 213

Kissinger HE 1957 Anal. Chem. 29 1702

Klein N 1969a Adv. Electron. Electron Phys. 26 309

Klein N 1969b J. Electrochem. Soc. 116 963

Klein N 1978 Thin Solid Films 50 223

Klein N & Purstein E 1967 Ann. Rep. Conf. Electrical Insul. & Dielect. Phenomena, Washington DC: NAS; 108

Klein N & Gafni H 1966 IEEE Trans. Electron Devices 13 281

Klein N & Levanon N 1967 J. Appl. Phys. 38 3721

Klein N & Solomon P 1976 J. Appl. Phys. 47 4364

Klein W 1968 J. Appl. Phys. 39 5797

Konorova EA & Sorokina LA 1965 Soviet Phys.- Solid State 7 1186

Kornfeld MI 1978; 1979 J. Phys. D: Appl. Phys. 11 1295; 12 279

van Krevelen DW van Herden C & Huntjens FJ 1951 Fuel 30 253

Krien G 1973 Proc. Third Symp. Chem. Problems Stability Explosives Ystad 33

Krug D 1977 Thermochim. Acta 20 53

Kurochkin ES Savel'yev GG Zakharov YuA & Chizhikova OI 1968 Zh. Vses. Khim. Obshchest. 13 466

Kurtin S McGill TC & Mead CA 1969 Phys. Rev. Lett. 22 1433

Lampert MA & Mark P 1970 CURRENT INJECTION IN SOLIDS New York: Academic Press

Lawson WG 1966 Proc. I.E.E. 113 197

Lehovec K 1953 J. Chem. Phys. 21 1123

Leopold HS 1973 Naval Ordnance Laboratory Tech. Rep. 73 - 125

Lewis TJ 1966 Trans. Farad. Soc. 62 889

Lifshits IM & Geguzin YaE 1965 Sov. Phys.- Solid State 7 44

Lloyd JM Jr. & Budenstein PP 1977 Ann. Rep. Conf. Electrical Insul. & Dielect. Phenomena, Washington DC: NAS; 339

Lucci A & Tamanini M 1975 Thermochim. Acta 13 147

McAuslan JHL 1957 Ph. D. Thesis, University of Cambridge

McCarty M Maycock JN & Pai Verneker VP 1968 J.Phys.Chem.72 4009

MacCallum JR 1971 Nature (Phys. Sci.) 232 41

MacCallum JR & Tanner J 1970 Nature 225 1127

MacDonald JY & Hinshelwood CN 1925 J. Chem. Soc. 127 2764

MacKenzie KJD 1973 J. Thermal Anal. 5 5; 5 19; 5 363

MacKenzie KJD & Banerjee RK 1978 Trans. Brit. Ceram. Soc. 77 88

McLaren AC & Rogers GT 1957; 1958 Proc. R. Soc. Lond. A240 484; A246 250

Madelung O 1978 INTRODUCTION TO SOLID-STATE THEORY (tr. B.C. Taylor) Berlin: Springer

Marcu V & Segal E 1978 Thermochim. Acta 24 178

Marcus RA 1956 J. Chem. Phys. 24 966

Mark P & Gora T 1974 J. Solid State Chem. 15 79

Marr HE III & Stanford RH Jr. 1962 Acta Cryst. 15 1313

Maycock JN & Pai Vernecker VR 1968 Proc. R. Soc. Lond. A307 303

Maycock JN & Pai Vernecker VR 1969 J. Appl. Phys. 40 5015

Maycock JN & Pai Vernecker VR 1970 Thermochim. Acta 1 191

Meiksin ZH 1975 Physics of Thin Films 8 99

Mel'nikov MA Gavrilin AI Dimova NI & Kalashnikov AL 1970 Russian J. Phys. Chem. 44 1314

Mitchell JW 1949 Phil. Mag. 40 249

Montagu-Pollock HM 1961 Ph. D. Thesis, Univ. of Cambridge

Montagu-Pollock HM 1962 Proc. R. Soc. Lond. A269 219

Monteith LK & Hauser JR 1967 J. Appl. Phys. 38 5355

Moore PWJ 1958 Proc. R. Soc. Lond. A246 195

Mott NF 1939 Proc. R. Soc. Lond. A172 325

Mott NF & Gurney RW 1948 ELECTRONIC PROCESSES IN IONIC CRYSTALS 2nd ed., Oxford: Clarendon

Mulliken RS 1934; 1935 J. Chem. Phys. 2 782; 3 573

Murant M Fevre A & Comel C 1976 Proc.First Europ. Symp. Thermal Anal. (ed. D. Dollimore); 98

Murant M Fevre A & Comel C 1977 J. Thermal Anal. 12 429

Murgatroyd PN 1971 Phys. Status Solidi (a) 8 259

Narayan J Weeks RA & Sonder E 1978 J. Appl. Phys. 49 5977

Ng WL 1975 Aust. J. Chem. 28 1169

Nolan PS & Lemay HE 1973 Thermochim. Acta 6 179

Norwisz J 1978 Thermochim. Acta 25 123

O'Dwyer JJ 1967 J. Phys. Chem. Solids 28 1137

O'Dwyer JJ 1969a J. Electrochem. Soc. 116 239

O'Dwyer JJ 1969b Ann. Rep. Conf. Electrical Insul. & Dielect. Phenomena, Washington DC: NAS

O'Dwyer JJ 1973 THE THEORY OF ELECTRICAL CONDUCTION AND BREAK-DOWN IN SOLID DIELECTRICS Oxford: Clarendon

Oblivantsev AN Boldyrev VV Eremin LI & Lykhin VM 1966 Kinetics & Catalysis 7 872

Ozawa T 1965 Bull. Chem. Soc. Jap. 38 1881

Ozawa T 1975; 1976 J. Thermal Anal. 7 601; 9 217

Pai Verneker VR & Maycock JN 1968 Explosivstoffe 9 193

de Panafieu A Royce BSH & Russell T 1976 J. Chem. Phys. 64 1473

Parrott JE 1974 METAL-SEMICONDUCTOR CONTACTS London: Inst. of Phys.; 20 - 6

Patai S (ed.) 1971 THE CHEMISTRY OF THE AZIDO GROUP New York: Wiley-Interscience

Patel RG 1978 Ph. D. Thesis, University of Cambridge

Patel RG & Chaudhri MM 1977 Proc. Fourth Symp. Chem. Problems Stability Explosives (ed. J. Hansson); 347 - 70

Patel RG & Chaudhri MM 1978 Thermochim. Acta 25 247

Pauling L 1960 THE NATURE OF THE CHEMICAL BOND 3rd ed., Ithaca: Cornell Univ. Press

Petty HR Arakawa ET & Baird JK 1977 J. Thermal Anal. 11 417

Pfieffer HG 1948 Ph. D. Thesis, Calif. Inst. Tech.

Phillips JC 1970 Rev. Mod. Phys. 42 317 - 56

Pollack SR 1963 J. Appl. Phys. 34 877

Pollak M 1971 Phil. Mag. 23 519

Pollak M & Knotek ML 1979 HOPPING CONDUCTION (to be published)

Pollock BD 1974 Proc. 16th Explosives Safety Seminar, Hollywood Florida USA

Poole HH 1916; 1917 Phil. Mag. 32 112; 34 195

Protopopov Mikheeva Shreinberg & Shappe 1966 Fiz. Tverdogo Tela 8 1140

Prout EG & Tompkins FC 1944 Trans. Farad. Soc. 40 488

Quarrell AG 1937 Proc. Phys. Soc. Lond. 49 279

Redhead PA 1962 Vacuum 12 203

Reed RL Weber L & Gottfried BS 1965 Ind. Eng. Chem. Fundamentals 4 38

Ridley BK 1975 J. Appl. Phys. 46 998

Roberts GG & Polanco JI 1970 Phys. Status Solidi (a) 1 409

Robrieux B Faure R & Dussaulcy JP 1974 C.R. Acad. Sci. B278 659

Rogers RN & Morris ED 1966 Anal. Chem. 38 412

Rogers RN & Smith LC 1970 Thermochim. Acta 1 1

Roginsky S & Schulz E 1928 Z. Phys. Chem. A138 21

Rose A 1955 Phys. Rev. 97 1538

Rouquerol J 1973 J. Thermal Anal. 5 203

Rozenband VI & Makarova EA 1977 Combustion Expl. Shock Waves 12 601

Ruppel W Rose A & Gerritsen HJ 1957 Helv. Phys. Acta 30 238

Savel'ev GG & Greben VP 1967 Izv. VUZ. Fiz. 10 38

Savel'ev GG Zakharov YuA & Spitsa VB 1965 Russian J. Phys. Chem. 39 1500

Savel'ev GG Zakharov YuA & Spitsa VB 1966 Izv. Tomskogo Politekh. Inst. 151 32

Savel'ev GG Zakharov YuA & Shechkov GT 1967 Russ. J. Phys. Chem. 41 904

Sawkill J 1955 Proc. R. Soc. Lond. A229 135

Sawkill J 1957 'The Decomposition of Silver Azide: an investigation using optical microscopy, electron microscopy and X-ray diffraction', PCS Rep., Cavendish Laboratory, unpublished

Schaffert RM 1967 US Patent 3316088; UK Patent 1056135

Schmalzried A 1974 SOLID STATE REACTIONS (tr. A.D. Pelton) New York: Academic Press

Schottky W 1938 Naturwiss. 26 843

Schulz WE 1974 US Patent 3806384

Schuttevaer JW 1969 Netherland Patent 6902804

Segal E & Fatu D 1976 J. Thermal Anal. 9 65

Sestak J & Kratochvil J 1973 J. Thermal Anal. 5 193

Seitz F 1949 Phys. Rev. 76 1376

Seiwatz H & Brophy JJ 1965 Ann. Rept. Conf. Electrical Insul. & Dielect. Phenomena, Washington DC: NAS; 1

Shannon RD 1964 Trans. Farad. Soc. 60 1902

Sharma J & Laskar AL 1973 J. Phys. Chem. Solids 34 989

Sharma J Wiegand DA Garrett WL & DiBona P 1975 Proc. Int. Conf. Res. in Primary Explosives (eds. J.M. Jenkins & J.R. White), Paper 23(i), ERDE, Waltham Abbey, England

Sharma SK & Spitz J 1979 Thin Solid Films 56 L17

Sharp JH Brindley CW & Narahari Achar BN 1966 J. Am. Ceram. Soc. 49 379

Sharp JH & Wentworth SA 1969 Anal. Chem. 41 2060

Shechkov GT & Zakharov YuA 1969 Izv. Tomskogo Politekh. Inst. 199 68

Shousha AHM Pulfrey DL & Young L 1972 J. Appl. Phys. 43 15

Simmons EL & Wendlandt WW 1972 Thermochim. Acta 3 498

Simmons JG 1968 Phys. Rev. 166 912

Simon J 1973 J. Thermal Anal. 5 271

Simon J & Debreczeny E 1971 J. Thermal Anal. 2 460

Skramovsky S 1932 Chem. Listy. 26 521

Skvara F Sestak J & Sestak V 1974 Proc. Fourth Int. Conf. Thermal Anal. (Budapest) Vol.1: 105

Soderquist R 1968 Proc. First Symp. Chemical Problems Connected with Stability of Explosives (ed. J. Hanssen)

Sonder E Kelton KF Pigg JC & Weeks RA 1978 J.Appl.Phys. 49 5971

Sonoike S 1956 PHOTOGRAPHIC SENSITIVITY (ed. H. Fujisawa) Vol.1, Tokyo: Maruzen; 59

Soria Ruiz J 1968 Ph. D. Thesis, University of Cambridge

Sosnovsky HMC 1959 J. Phys. Chem. Solids 10 304

Spath HJ 1977 REACTIVITY OF SOLIDS (eds. J. Wood et al.) New York: Plenum; 319

Stark KH & Garton CG 1955 Nature 176 1225

Stengach VV 1972a Fiz. Goreniya Vzr. Nauka Sib. Otdel. Novosib. 6 113

Stengach VV 1972b Zh. Prikladnoi Mekh. Tekhnich. Fiz. 1 128

Stengach VV 1975 Zh. Prikladnoi Mekh. Tekhnich. Fiz. 6 128

Street RA Davies G & Yoffe AD 1971 J. Non-Crystalline Solids 5 276

Sukhushin YuN Zakharov YuA Pappord GA 1970 Izv. Tomskogo Politeckh. Inst. 251 219

Sukhushin YuN Zakharov YuA Ivanov FI 1973 High Energy Chem. 7 231

Sze SM 1969 PHYSICS OF SEMICONDUCTOR DEVICES New York: Wiley-Interscience

Tanaka T & Greenwood A 1977 Ann. Rep. Conf. Electrical Insul. & Dielect. Phenomena, Washington DC: NAS; 309

Tang TB 1978 Laboratory Practice 27 289

Tantraporn W 1964 Solid-State Electron. 7 81

Taylor CA & Rinkenback WH 1925 US Army Ordnance 5 824

Taylor GWC 1957 UK Patent 781440

Taylor W & Weale A 1938 Trans. Farad. Soc. 34 995

Thoma P 1975 Rep. PTB - E - 5 Physik.-Tech. Bundesanstalt Braunschweig and Berlin

Thoma P 1976 J. Appl. Phys. 47 5304

Thompson MW 1969 DEFECTS & RADIATION DAMAGE IN METALS Cambridge: Univ. Press

Thomas JGN & Tompkins FC 1951 Proc. R. Soc. Lond. A210 111

Tokar K & Herzog GW 1966 Monatsh. Chem. 97 765; 1215

Ubbelohde AR 1948 Phil. Trans. R. Soc. Lond. A241 200; 280

Wagner KW 1922 Trans. Am. Inst. Electr. Eng. 41 288

Walker RF 1967 Ph. D. Thesis, University of Cambridge

Walker RF Gane N & Bowden FP 1966 Proc. R. Soc. Lond. 294 417

Watson DR & Heyes W 1970 J. Phys. Chem. Solids 31 2531

Weast RC (ed.) 1974 HANDBOOK OF CHEMISTRY AND PHYSICS 55th ed., CRC Press

Whitehead S 1951 DIELECTRIC BREAKDOWN OF SOLIDS Oxf.: Clarendon

Whitworth RW 1975 Adv. Phys. 24 203

Williams RH Montgomery V & Varma RR 1978 J. Phys. C: Solid State Phys. 11 L735

Yoffe AD 1966 DEVELOPMENTS IN INORGANIC NITROGEN CHEMISTRY (ed. C.B. Colburn) Vol.1, Amsterdam: Elsevier; pp. 72 - 149

Yoganarasimhan SR 1976 Proc. Symp. Chem. & Phys. Surface of Metals & Their Oxides, Reactor Research Centre, Kalpakkam, India; 18 - 43

Young DA 1960 J. Chem. Soc. Lond. 4533

Young DA 1964 Brit. J. appl. Phys. 15 499

Young DA 1966 DECOMPOSITION OF SOLIDS Oxford: Pergamon

Young DA 1971 PROGRESS IN SOLID STATE CHEMISTRY (ed. H. Reiss) Vol.5, Oxford: Pergamon; pp. 401 - 29

Young L 1961 ANODIC OXIDE FILMS New York: Academic Press

Yuill AM 1953 Ph. D. Thesis, University of Cambridge

Zakharov YuA & Kabanov AA 1964 Russ. J. Phys. Chem. 38 1567

Zakharov YuA & Kurochkin ES 1968 Russ. J. Inorg. Chem. 13 919

Zakharov YuA & Savel'ev GG 1966 Kinetics & Catalysis 7 46

Zakharov YuA & Sukhushin YuN 1970 Izv. Tomskogo Politekh. Inst. 251 213

Zakharov YuA Savel'ev GG Boldyrev VV & Votinova LA 1964 Kinetics & Catalysis 5 709

Zakharov YuA et al. 1965 Kinetics & Catalysis 6 364; 546

Zakharov YuA Kurochkin ES Savel'ev GG & Rufov YuN 1966 Kinetics & Catalysis 7 377

Zakharov YuA Kolesnikov LV Charkashin AE & Kashcheev SP 1975 Izv. Vys. Ucheb. Zaved. Fiz. 6 44

Zakharov YuA Gas'maev VK & Kolesnikov LV 1976 Russ. J. Phys. Chem. 50 1009

Zhuze VP 1955 Zh. Tekh. Fiz. 25 2079

Zimmerschied A & Davies F 1974 Rep. T2 - 4096 - 1 The Boeing Co., USA

Zsako J 1970;1973 J. Thermal Anal. 2 460; 5 239

* * * * *